

**JOINT NUMERICAL MODELS AND HYDROCHEMICAL STUDIES OF FLOW
AND TRANSPORT PROCESSES AT BASIN-SCALE**
*BY EXAMPLE OF THE NORTH EAST GERMAN BASIN AND THE WESTERN
ANATOLIA GEOTHERMAL SYSTEM*

SUBMITTED BY

FABIEN MAGRI

DEPARTMENT OF EARTH SCIENCES

FREIE UNIVERSITÄT BERLIN

PREFACE

The main theme of this research is the application of numerical models and hydrochemical data to study the occurrence of environmental anomalies in sedimentary basins, such as salty springs, upsurge of thermal waters or seawater intrusions. This is done through the selection of seven peer-reviewed articles (first author) based on two real study cases: the North East German Basin (NEGB) and the Seferihisar-Balçova Geothermal system (SBG), western Turkey. A numerical white paper in the Appendix explains the methodology applied to model variable fluid density in a wide range of temperatures and concentrations. Major emphasis will be given to the coupled nature of different hydrologic regimes and the impact of controlling factors, like hydraulic permeability heterogeneities and variable fluid properties. The expression “*fluid transport process*”, often used throughout the papers, refers to the central role of groundwater in transferring energy (i.e. heat) and mass (i.e. solutes) over basin-scales and geological time periods.

The studies presented here were carried out within two research programs funded by the German Research Foundation DFG, from 2002 to 2011. During those nine years of research, the results have been published in different international journals and presented in a variety of international conferences (see enclosed CV).

- (1) The first project “Deep reaching fluid-flow in the Central European Basin System” was carried out within the SPP1135 program “Dynamics of sedimentary basins (Ba 796/10)”, from 2002 to 2008. The main goal was to understand the major transport processes responsible for the formation of several salty springs in the North East German Basin (NEGB), highlighting the role of deep groundwater flow near salt diapirs. This project allowed me to obtain a Ph.D. degree within the first three years of research. This was the starting point of my teaching experience and student supervision at the Freie Universität Berlin, in the modeling course of Prof. Ulf Bayer.
- (2) From 2008 to 2011, the DFG granted an additional three years research funds for a project I wrote, entitled “Thermohaline modeling of hot geothermal fluid systems in coastal environment: the Seferihisar- Balçova Area example (Turkey) – Ma4450/1”. This project addressed further issues of coupled fluid transport processes not comprised in the NEGB case, such as geothermal heat migration, the impact of faults and seawater intrusions.

At present, the DFG accepted a new project I submitted entitled “Hydrogeological and hydrochemical modeling of density-driven flow in the Tiberias Basin – Ma4450/2”. The new years of research will allow three dimensional studies of deep fluid processes and their interactions with the waters of the Tiberias Lake (Israel).

This work is organized following the chronological order of the two research projects. The introduction in **chapter 1** recalls the applied methods and the different types of coupled flow processes at basin-scale. In this chapter, *slanted words* refer to particular expressions used in the field of hydrology. A brief explanation of these words can be found in the glossary. The main findings of fluid transport processes in the NEGB are given in **chapter 2**, whereas **chapter 3** is dedicated to the SBG case. These two chapters are the core of the research. The sorting of the articles within the two chapters reflects the type of coupled flow regime and the studied controlling factors, as follows:

In chapter 2, basin-scale models of groundwater flow are presented for two scenarios, (i) deep and (ii) shallow salt structures.

- (i) Deep salt structures are studied in chapters 2.1 and 2.2. In 2.1, a first paper highlights the role of deep seated salt diapirs in coupling both heat and solute migration. An additional paper investigates the effects of permeability distributions related to stratigraphy. The paper in chapter 2.2 focuses on the impact of local heterogeneities caused by Rupelian Clay, Muschelkalk and variable thermal conductivity of deeply buried salt diapirs.
- (ii) The second scenario concerns brine migration in shallow salt structures and the additional dynamics effects related to shallow salt dissolution. The findings are illustrated by two papers, one in chapter 2.3 and a second in chapter 2.4. In chapter 2.3, particular attention is given to the impact of young geological features such as Pleistocene channels and sand units in controlling shallow salinity patterns. The twofold effects of variable fluid viscosity in triggering or slowing brine flow are investigated in chapter 2.4.

Chapter 3 comprises two papers which address additional issues not investigated in the NEGB. These are geothermal fluid flow within faults (chapter 3.1) and naturally induced seawater intrusions (chapter 3.2). In chapter 3.1, it is shown how highly permeable conduits strongly perturb the temperature field at different depths, by allowing both inflow of cold recharge water and upward migration of hot thermal waters. The findings in 3.2 also highlight the role of faults in determining pressure distribution and consequently inducing seawater encroachment.

All papers are reformatted in order to present this manuscript with a layout style as homogeneous as possible. Only the paper headings are in their original journal style. All references are collected in a common list at the end to avoid repetitions of frequently cited papers.

The concluding **chapter 4** summarizes the main findings of the whole research and delineates the possible future challenges related to the importance of additional coupling of groundwater flow with deformation and reactive solute transport.

The author of this work is also the lead author of all selected papers. Besides the supervision of Prof. Bayer and Prof. Pekdeger, the co-authors intensively contributed to the preparation of the manuscripts by providing interpreted hydrochemical and geological data.

All simulations have been carried out using the commercial software FEFLOW (DHI-WASY GmbH). The mathematical formulation can be found in the **Appendix**. It includes the original C++ code developed during my Ph.D in order to expand FEFLOW capabilities to simulate deep transport processes in a wide range of temperature and pressure. This methodology is accepted and published by WASY.

ACKNOWLEDGMENTS

These years of research and publications would not have been possible without the continuous support of the German Science Foundation (DFG). I would like to express my deep gratitude to Prof. Ulf Bayer for his encouragements and fundamental critiques in writing this habilitation thesis and keeping me on schedule. I thank Prof. Michael Schneider (Freie Universität Berlin) for his strong support, trust and for always providing excellent facilities that allowed me teaching at the FU Berlin. My grateful thanks are also extended to all colleagues who helped me during these years of research and to all project partners for their technical assistance in software tools and hydrochemical analyses, particularly Prof. Peter Möller (GFZ, Potsdam).

My last thought goes to Prof. Asaf Pekdeger for sharing with me his unique flair for enjoying life and for always encouraging me in submitting a habilitation thesis.

DANKSAGUNG

Die Jahre der Forschung und des Publizierens ären nicht möglich gewesen ohne die kontinuierliche Förderung der Deutschen Forschungsgemeinschaft (DFG). Ich möchte meine tief Dankbarkeit gegenüber Prof Ulf Bayer für seine Anregungen und fundamentale Kritiken beim Verfassen der vorliegenden Habilitation aussprechen. Ich bedanke mich bei Prof. Michael Schneider (Freie Universität Berlin) für seine stete Unterstützung, Vertrauen, und Bereitstellung von hervorragenden Möglichkeiten, die mir eine Lehrtätigkeit an der FU Berlin ermöglichten. Mein Dank erstreckt sich auch auf alle Kollegen, die mir in all den Jahren behilflich waren, und auf alle Projektteilnehmer für ihre technische Hilfeleistungen bei der Erstellung von software tools und hydrochemischen Analysen, insbesondere Prof. Peter Möller (GFZ Potsdam).

Mein letzter Gedanke wendet sich an Prof. Asaf Pekdeger, der mich an seinem einzigartigen Spürsinn für Lebensfreude teilhaben ließ und mich wiederholt ermunterte meine Habilitationsarbeit einzureichen.

VORWORT

Das Hauptthema dieser Forschung ist die Anwendung von numerischen Modellen und hydrochemischen Daten um das Vorkommen von Umweltanomalien in Sedimentbecken wie zum Beispiel von Solequellen, Aufstieg von Thermalwasser oder Seewasser zu studieren. Dies wird aufgezeigt anhand von 7 *peer-reviewed* Artikeln über 2 Fallstudien: das Nord-Ost Deutsche Becken (NEGB) und des Seferihisar-Balcova Geothermalsystems (SBG), West-Türkei. Ein..... im Appendix erläutert die Methodologie die bei der Modellierung von variabler Flüssigkeitsdichte in einem weiten Bereich von Temperatur und Konzentration. Besonderes Augenmerk wird auf die Kopplung von verschiedener hydrologischer Regime und variablen Flüssigkeitseigenschaften gelegt. Der Ausdruck „Fluid transport process“, häufig erwähnt in dieser Arbeit, verweist auf die zentrale Bedeutung von Grundwasser beim Transport von Energie (z.B. Wärme) und Masse (z.B. Lösungsfracht) über geologische und Beckenbildungszeiten.

Die hier angeführten Studien wurden im Rahmen von 2 Forschungsprogrammen durchgeführt, die von der Deutschen Forschungsgemeinschaft DFG im Zeitraum 2002-2011 unterstützt wurden. Während dieser 9 Forschungsjahre wurden diese Ergebnisse in verschiedenen Internationalen Zeitschriften publiziert und auf verschiedenen internationalen Konferenzen vorgestellt (siehe beigefügtes CV).

- (1) Das erste Projekt „Deep reaching fluid-flow in the Central European Basin System“ wurde im Rahmen des SPP1135 Programm „Dynamics of Sedimentary Basins (Ba 796/10)“ von 2002 bis 2008 durchgeführt. Das Hauptziel war das Verständnis der wichtigen Transportprozesse, die zur Bildung von Solequellen im Norddeutschen Becken (NEGB) geführt haben, das Herausarbeiten der Rolle von tiefem Grundwasserfluss in der Nähe von Salzdiapiren. In den ersten drei Jahren habe ich meine Dissertation abschließen. Dies war auch der Beginn meiner Lehrtätigkeit und Studentenanleitung im Rahmen des Modellier-Kurses von Prof. Dr. Ulf Bayer an der Freien Universität Berlin.
- (2) Von 2008 bis 2011 förderte die DFG mein Forschungsvorhaben „ Thermohaline modeling of hot geothermal fluid systems in coastal environment: The Seferihisar-Balcova Area example (Turkey)-MA4459/1“. Diese Projekt behandelte weitergehende Aspekte von gekoppeltem Fluid Transport Prozessen, die nicht Teil des NEGB Projekt waren, wie z.B. geothermaler Wärmefluss unter Beeinflussung von tektonischen Störungen und Intrusion von Seewasser.

Zur Zeit fördert die DFG mein Forschungsvorhaben „Hydrogeological and hydrochemical modelling of density-driven flow in the Tiberias Basin – MA4450/2“. Die kommenden Jahre ermöglichen mir 3-dimensional Studien von tiefen Fluid Prozessen und deren Wechselwirkung mit dem Wasser des See Genezareth (Lake Tiberias) durchzuführen.

Die vorgelegte Arbeit ist chronologisch entsprechend den 2 abgeschlossenen Forschungsvorhaben gegliedert. Die Einführung in Kapitel 1 wiederholt die angewandten Methoden und verschiedene Arten von gekoppelten Fluss Prozessen in Beckenmaßstab. Kursiv geschriebene Wörter entsprechen Fachausdrücken im Bereich der Hydrologie. Eine Erläuterung dieser Begriffe ist im *Glossary* gegeben. Die Hauptergebnisse zum Fluid-Transport im NEGB werden in Kapitel 2 gegeben. Kapitel 3 widmet sich den

Ergebnissen in SGB. Diese beiden Kapitel sind das Herzstück. Das Sortieren der Beiträge innerhalb der beiden Kapitel entsprechen dem Typ des gekoppelten Fluss Regimes und der untersuchten Kontrollfaktoren wie folgt:

In Kapitel 2 wird der Grundwasserfluss für 2 Szenarien, (i) tief und (ii) flache Salzstrukturen im Becken Maßstab vorgestellt.

- (i) Tiefe Salzstrukturen werden Kapitel 2.1 und 2.2 untersucht. In 2.1 beleuchtet die erste Arbeit die Rolle von tief-sitzenden Salz Diapiren in gekoppelter Wärme und Masse Migration. Die zusätzliche Arbeit untersucht den Einfluss der Verteilung von Permeabilität im Hinblick auf die Stratigraphie. Die Arbeit in Kapitel 2.2 betrachtet den Einfluß lokaler Heterogenitäten bedingt durch Vorkommen von Rupelton, Muschelkalk und variablen thermischer Wärmeleitfähigkeit bedingt durch tiefliegenden Salz-Diapire.
- (ii) Das zweite Szenario beleuchtet Solewanderung in flachen Salzstrukturen. Die Ergebnisse sind in 2 Arbeiten wiedergegeben, eine in Kapitel 2.3 und die zweite in Kapitel 2.4. In Kapitel 2.3 wird besondere Aufmerksamkeit auf den Einfluss junger geologischer Strukturen wie z.B. Pleistozäne Rinnen und Sandablagerungen, die die Verteilung von flachen Solen kontrollieren. Der zweifache Effekt von variabler Fluidviskosität, die den Fluidfluß anstößt oder aber verlangsamt, wird in Kapitel 2.4 behandelt.

Kapitel 3 fasst 2 Arbeiten zusammen, in denen zusätzliche Parameter behandelt werden, die nicht im Rahmen des NEGB bearbeitet wurden. Dies sind die Fluidbewegungen auf tektonischen Störungen (Kapitel 3.1) und natürliche Seewasser –Intrusion (Kapitel 3.2). In Kapitel 3.1 wird gezeigt, wie hoch permeable Zonen das Temperaturfeld durch Zufluss von kaltem Recharge Wasser und Aufwärtswanderung von Thermalwasser in verschiedenen Teufenlagen stören. Die Ergebnisse in 3.2 beleuchten die Rolle von Störungen bei der Bestimmung der Druckverteilung und folglich der Einbeziehung von Seewasser.

Alle Arbeiten wurden dem Stil des vorliegenden Manuskriptes angepasst, um es so einheitlich wie möglich zu gestalten. Nur die Titel der Arbeiten entsprechen dem Original. Alle Zitate wurden in einer gemeinsamen Liste zusammengefasst, um häufig zitierte Arbeiten nicht wiederholen zu müssen.

Das abschließende Kapitel fasst die wichtigsten Ergebnisse zusammen und verweist auf zukünftige Themen, die mit der Bedeutung zusätzlicher Wechselwirkung von Grundwasserbewegung, Deformation und reaktivem Masse Transport.

Alle Simulationen wurden anhand der käuflichen software FEFLOW (DHI-WASY GmbH) durchgeführt. Die mathematische Behandlung wird im Appendix wiedergegeben. Das Appendix beinhaltet auch den originalen C++ Code, der in 2002 programmiert wurde, um FEFLOW dahingehend zu erweitern, tiefe Transport Prozesse in einem weiten Temperatur- und Druckfeld zu simulieren.

ABSTRACT

The North East German Basin (NEGB) and the Seferihisar Balçova Geothermal system (SBG) serve as examples to investigate the central role of deep groundwater flow in transferring energy (i.e. heat) and mass (i.e. solutes) over geological time periods. The methodology applied is numerical modeling supported by hydrochemical investigations.

The NEGB hosts several salt structures at different depths and young geological features such as shallow sand units and cutting Pleistocene channels. The geothermal field of the SBG is characterized by active fault systems. The different structural and geophysical characteristics of these two basins allow studying the interaction of different hydrologic regimes and the subsequent enforced flow dynamics. To some extent, the simulations further highlight the impact of controlling factors on fluid transport processes.

In the NEGB, hydrochemical data indicate that the salinity of several springs originates from the dissolution of deep and shallow salt structures. In the case of deep salt diapirs, the modeling results suggest that the disturbed temperature field around the salt domes can generate upward flow of brines. This thermally-induced convective flow is controlled by the spatial heterogeneity of both thickness and permeability of the units. The numerical studies mainly focused on the hydraulic conductivity within the Cenozoic unit and Middle Triassic. The results reveal that Rupelian clay does not prevent brackish water from reaching the surface. Locally more permeable Cenozoic sediments allow dilution of salty waters with freshwater rather than enhancing an outflow of brines. Sensitivity analyses in deeper units indicate that salinity concentrations are controlled by the Middle Triassic sediments. Furthermore, higher thermal conductivity contrasts can enhance thermally driven brine flow around deep salt diapirs. Additional simulations indicated the role of hydrostatical forces from the surrounding highlands in determining near-surface salinity patterns.

Another scenario for salt dissolution is provided by shallow salt structures (i.e. -500 m). In this case, the results suggest that different flow regimes can coexist. Shallow brine migration is strongly controlled by the geological features of the basin such as glacial channels, sand layers and transition zones. Furthermore, shallow salt dissolution is the major cause for brines to sink into the underlying aquifers. This source of salinization from above leads to the formation of instable salinity profiles at 2 km depth by generating fluid density inversion. Permeable units located near shallow salt structures further enhance downward brine flow. By contrast, the presence of a less permeable transition zone in direct contact with the salt reduces the flow velocity of groundwater near the salt flank. As less dissolved halite enters the flow system, groundwater recharge within the sedimentary rock remains more dilute. Upward thermally-driven flow persists within thick permeable areas far from shallow salt structures. Effects of variable viscosity are also investigated. The results indicate that by neglecting viscosity changes

in a variable-density flow system, salinity gradients are likely to be overestimated. Variable brine viscosity hinders the sinking of cold heavy brine plumes at the regional- (i.e., km-) scale. When both transition-zone and viscosity effects are included in the simulations, calculated concentrations are in better agreement with available mass trends.

The second study case concerns the SBG, a geothermal system characterized by complex temperature and hydrochemical anomalies due to faults and seawater encroachment. The available data suggest that the hydrothermal phenomena of the SBG result from deep groundwater circulation in highly permeable faults. Isotopic analyses also indicate strong interactions between inflows of colder recharge water from the horsts, upwelling hot fluids from depth and seawater mixing. The numerical results support the hypothesis derived from interpreted hydrochemical data: Faults act as the major pathways for outflow of thermal water even from basement depths. When recharge processes are weak, the convective patterns in the faults can expand to surrounding reservoir units or below the seafloor. Additional simulations which couple salt transport and groundwater flow show that the fault-induced convection cells can induce seawater intrusions. At fault intersections, seawater mixes with rising hot thermal waters. The resulting saline fluids ascend to the surface along the fault, driven by buoyant forces. In Balçova, thick alluvium, minor faults and regional flow prevent ascending salty water from spreading at the surface, whereas the weak recharge flow in the thin alluvium of the southern SBG is not sufficient to flush the ascending hot salty waters.

From a numerical point of view, the papers also offer a solution for implementing a general equation of state reproducing variable brine density in a wide range of temperatures and pressures.

The manuscript ends with a discussion about the challenges of large-scale modeling that need to be addressed by future research. These mainly concern the detailed study of coupled processes in three dimensions and the impact of physical property variations induced by chemical reactions. While the study of these new effects are currently being improved and are not addressed in this work, the two real case examples provided here nicely describe the occurrences and dynamics of natural fluid processes at basin-scale.

CONTENT

PREFACE		III
ACKNOWLEDGMENTS / DANKSAGUNG		V
VORWORT		VII
ABSTRACT		IX
LIST OF ABBREVIATIONS		XII
GLOSSARY		XII
1. INTRODUCTION		1
1.1 The methods		1
1.2 Brief description of driving forces in large-scale groundwater flow systems		4
1.3 Coupled processes		7
1.4 Controlling factors		10
1.5 The main examples		13
2. BRINE MIGRATION FROM DEEP AND SHALLOW SALT DOMES: THE NORTH EAST GERMAN BASIN (NEGB)		15
2.1 Deep salt domes	<i>2 papers</i>	18
2.2 Impact of hydraulic and heat conductivity distribution	<i>1 paper</i>	57
2.3 Shallow salt structures and Pleistocene channels	<i>1 paper</i>	76
2.4 Transition zones and variable viscosity	<i>1 paper</i>	96
3. GEOTHERMAL ENERGY MIGRATION IN FAULTED AREAS: THE SEFERIHISAR BALCOVA GEOTHERMAL SYSTEM (SBG)		111
3.1 The impact of faults	<i>1 paper</i>	114
3.2 Thermally induced seawater intrusions	<i>1 paper</i>	140
4. DISCUSSIONS AND CHALLENGES		163
REFERENCES		171
APPENDIX: FEFLOW FORMULATION AND BRINE DENSITY EOS	<i>1 white paper</i>	191

LIST OF ABBREVIATIONS

- EOS:** Equation of State
- NEGB:** North East German Basin
- REE:** Rare Earth Elements
- REY:** Rare- earth elements and yttrium
- SBG:** Seferihisar-Balçova Geothermal
- THMC:** Thermal-Hydrological-Mechanical-Chemical processes

GLOSSARY

Basin-scale: length scale referring to hydrogeologic systems which extend laterally for hundreds of kilometres and to depth of several kilometres

Counter-rotating cells: convective cells rotating in opposite directions

Coupled processes: fluid processes involving different interacting driving forces giving rise to new effects and new hydrogeologic regimes

Coupling: see coupled processes

Density driven flow: see gravity driven flow

Fluid transport process: refers to the central role of groundwater in transferring energy (i.e. heat) and mass (i.e. solutes)

Forced convection: groundwater flow driven by water table gradients. In case the head mimics topographical variations, forced convection is also referred to as topography driven flow

Free convection: groundwater flow driven by density difference (buoyant forces) due to temperature variations

Geological forcing: any geological process than can alter hydrostatic conditions and induce a groundwater flow (e.g. sediment compaction, hydrocarbon generation, degassing from magma)

Gravity driven flow: groundwater flow driven by density difference (buoyant forces) due to variations of solute concentration

Hydrogeologic regimes: the driving forces of groundwater flow that contribute to the transfer of mass (solutes) and energy (heat)

Mixed convection: hydrologic regime resulting from the interaction between forced and free convection

Topography driven flow: see forced convection

Thermally driven flow: see free convection

Transient behavior: the time-dependent or dynamic nature of fluid processes

Transition zone: A sedimentary unit along the flanks of piercing salt diapirs which is presumably characterized by intermixing of salt and fragments of sedimentary rock

INTRODUCTION

1. INTRODUCTION

Contents

1.1	The methods	1
1.2	The driving forces	4
1.3	Coupled processes	7
1.4	Controlling factors	10
1.5	The main examples	13

Groundwater flow can be studied at length scales ranging from the pore size to aquifers (few km) or basin systems (hundreds of km). These papers focus on groundwater flow and transport processes (heat and solute) at *basin-scale*. The length scale refers to hydrogeologic systems which extend laterally for hundreds of kilometres and to depth of several kilometres.

1.1 The methods: numerical modeling and hydrochemistry, two complementary tools for the study of groundwater flow processes

Mathematical models can represent transport processes at very slow rates over basin length scales and therefore became a frequently used tool to study a wide variety of hydrogeological conditions. In the late sixties, the first studies of large-scale groundwater flow mainly focused on water-supply and water-quality problems in order to predict the movement of contaminants through the subsurface environment on small drainage systems (e.g. Pinder et al., 1968).

The rapidly increasing computer power and the development of user-friendly modeling software allows nowadays to simulate groundwater flow and transport processes in the scale of sedimentary basins (i.e. hundreds of km) and geologic time periods (i.e. thousands to millions of years). In the last two decades, numerical modeling has been applied to study the *transient behavior* of temperature and mineral migration in sedimentary basins and to elucidate the controlling role of hydraulic permeability distributions, as illustrated by example in figure 1.1.

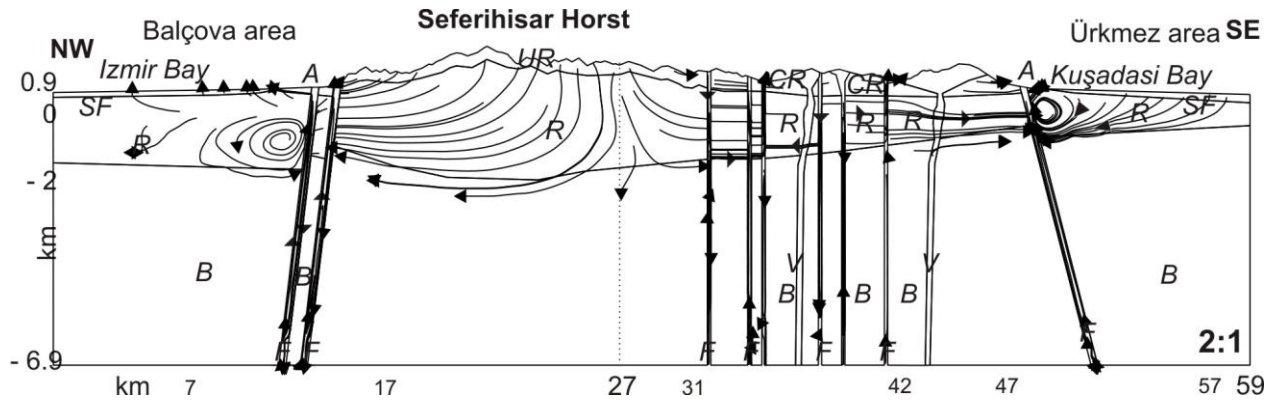


Fig. 1.1: Example of computed flow lines along a representative cross-section of the Seferihisar-Balçova geothermal basin, Turkey (Magri et al., 2010). The model is used to clarify the possible fluid dynamics and flow directions (vectors) within the different units as explained in details in Chapter 3. The dashed line locates the natural groundwater divide. *Legend:* SF: sea floor; A: alluvium; R: reservoir unit Bornova Mélange; UR: Upper Reservoir; CR: Cap Rock; V Volcanic intrusions; B: basement.

Comprehensive reviews of numerical modeling of regional groundwater flow can be found in Bear et al. (1987), Anderson et al. (1992), Garven (1995), Konikow et al. (2006), and Zhou et al. (2011). The most recent examples are numerical simulations of mid-ocean ridge hydrothermal systems. Numerical studies of these systems are particularly difficult because of the multi-phases involved (solid/liquid/gas) and the reactive nature of the chemical transport processes, as highlighted by Ingebritsen et al. (2009). These challenging aspects of numerical modeling will be explained in more details in Chapter 4.

Although numerical modeling provides a powerful tool to increase our understanding of hydrogeologic systems, the interpretations of large-scale flow patterns often requires additional methodologies to be applied. As pointed out by Fairley et al. (2004), basin-scale studies have demonstrated the importance of spring hydrochemistry in understanding interactions between different flow paths. Standard chemical data (major cations and anions) are used to assess fluid flow and water-rock interactions. Analyses of standard chemical data allow identifying source rocks and mixing of different groundwater sources. Radioactive isotopes can be used to evaluate groundwater age and the heights of recharge systems. Isotopes provide insights into circulation time and mixing of fossil groundwater with young meteoric groundwater, thermal waters or seawater (e.g. Fig.1.2).

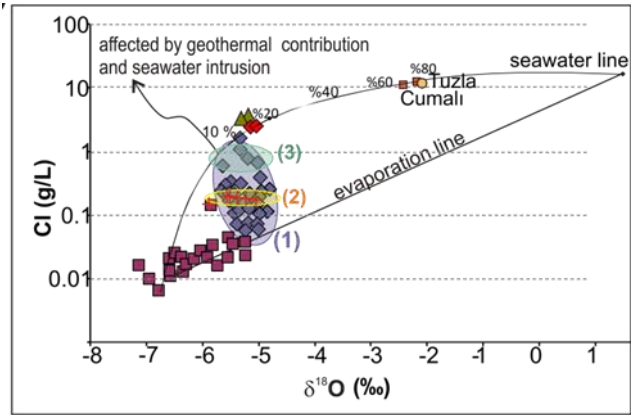


Fig.1.2: Example of isotope data used to infer water types in the Seferihisar-Balcova area, Turkey (Magri et al., 2012). Chloride content of sampled waters as function of $\delta^{18}\text{O}$. Seawater amounts are in percentages on the mixing line. Group 1 waters have both thermal water (group 2) and seawater (group 3) fingerprints. For more details, refer to Chapter 3.

Accordingly, the integrated use of both numerical modeling and hydrochemistry are nowadays fundamental tools for testing conceptual models of fluid migration, heat flow and chemical transport. In this regard, the joint use of these methodologies demonstrated that groundwater flow is the major control in many geologic processes at basin-scale such as mineral deposits (Walshe et al., 1996), formation of evaporites (Hardie, 1991), sedimentary basin evolution (Etheridge et al., 1983), diagenesis (Wood et al., 1984), seismicity (Saar et al., 2003), oil and brine migration (Tòth, 1980) and geothermal heat transport (O'Sullivan, 2009). Joint numerical and hydrochemical investigations of *fluid transport processes* within sedimentary basins all over the world are published at rates of dozens per year.

This manuscript is a collection of peer-reviewed papers aimed to provide two additional real-case examples in which the above described methodologies are applied to study transport processes at basin-scale. The first set of papers (chapter 2) focuses on the origin and migration of brines from deep and shallow salt structures of the North East German Basin (NEGB). The second field example (chapter 3) concerns the occurrence of geothermal springs in the faulted systems of the Seferihisar-Balcova Geothermal system (SBG), Western Anatolia and their interaction with seawater. In the last chapter (chapter 4), the key research challenges of numerical studies at basin-scale are discussed. In the appendix the mathematical formulation of coupled flow is given together with the Equation Of State (EOS) specifically developed for these two examples in order to reproduce brine density in a wide range of temperature, pressure and solute concentration.

A brief description of the driving forces, causing basin-scale flow, is given in paragraph 1.2 in order to better highlight how transport processes are controlled by groundwater flow. Emphasis will be given to topography-driven flow, thermal convection, density-driven flow and their *coupling*, or in other words, the fact that in nature different driving forces interact giving rise to new dynamical effects.

1.2 Brief description of driving forces in large-scale groundwater flow systems

In sedimentary basins, different driving forces contribute to the transfer of mass and heat. These are often referred to as *hydrogeologic regimes*. Flow, transport and reaction at the scale of sedimentary basins are in most cases slow processes. However, over the scale of geologic time, their effects are of great importance as they can generate important energy resources.

Topography driven flow (forced convection) (Fig. 1.3) is the dominant regional-scale groundwater flow in uplifted sedimentary basins, both in the shallow and deep sub-surface (Freeze et al., 1967).

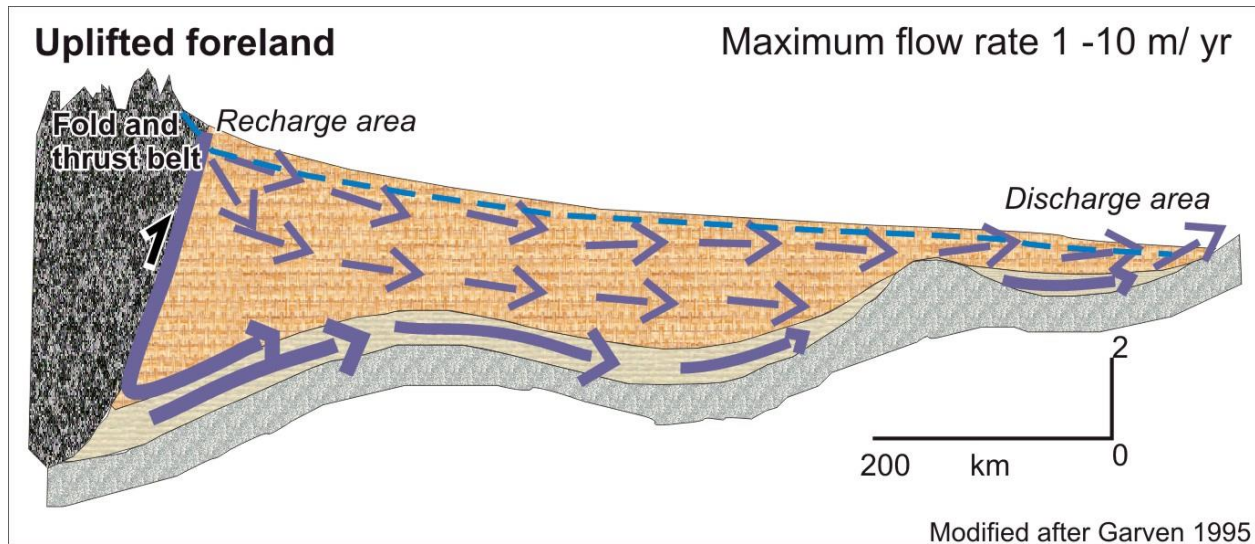


Fig. 1.3: *Topography driven flow (forced convection)* in an uplifted sedimentary basin. The dashed line illustrates the water-table that is a replica of the landscape. Vectors indicate the flow field. Stronger flow (thicker vector) occurs in more permeable units (m/yr: meter per year).

Usually, in a foreland basin the water table mimics the topographic relief (blue dashed lines in Fig. 1.3). A regional flow is induced because of the differences in the hydrostatic head that drive fluid from high-elevation recharge areas to low-elevation discharge areas. In general, groundwater flow is called *forced convection* when it is driven by water table gradients.

Flow lines (bold vectors in Fig. 1.3) and rates depend on several factors as the geometry of the aquifers (e.g variable thickness) and their physical properties (e.g., hydraulic permeability). For instance, vigorous recharge flow can be observed within the fault as well as in the adjacent thin and highly permeable sand unit. Pleistocene channels (not displayed in Fig. 1.3) are also important geological features that strongly impact the velocity field and flow patterns. Almost no flow occurs in the bottom unit (e.g. impervious clay). Accordingly, typical maximum flow rates can strongly vary, ranging from 1 to 10 m year⁻¹.

1.2 Brief description of driving forces in large-scale groundwater flow systems

Thermally driven flow (free convection). In sedimentary basins, the presence of a geothermal field induces fluid-density variations which in turn drive groundwater flow. Fluid motion caused by density difference due to temperature variations is called *free convection* (Fig. 1.4).

Most commonly, heating of groundwater in a geothermal system is provided by a heat source located at depths. In a porous media heated from below, the warmer fluid (i.e. less dense) starts to ascend. During this upward migration, the fluid loses its heat. Therefore buoyancy forces weaken and the fluid starts to sink again. The resulting flow path is called convective cell. Convective patterns are mainly controlled by the hydraulic permeability and the thickness of the units. Stronger convective flows are expected to take place in thick and permeable stratigraphic units whereas thin aquitards prevent the formation of any free convective motion. In highly permeable faults, a multi-cellular regime can develop and drive hot fluids to shallow depths. In the surroundings of faults, pressure and temperature patterns are strongly perturbed and differ from linear hydrostatic and conductive regimes. The impact of faults and less permeable units on geothermal energy migration is illustrated for the Western Anatolia example in chapter 3.

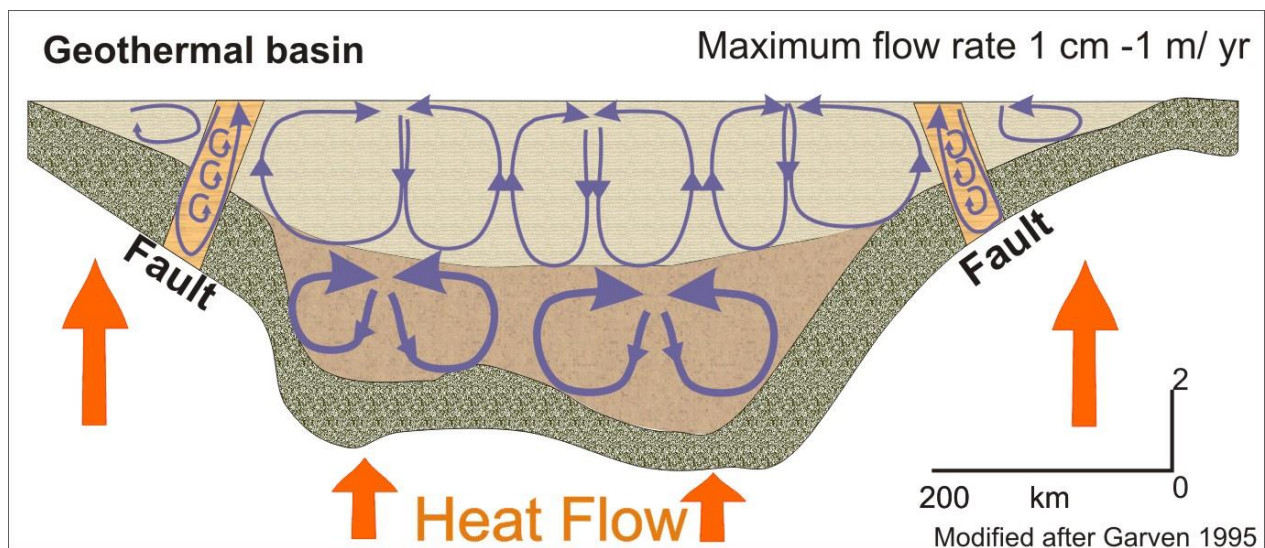


Fig. 1.4: Thermally driven flow (free convection) in a geothermal basin. Vectors illustrate the convective cells. Stronger convective flow (thicker vector) occurs in more permeable units. Near the faults, cells pattern are elongated toward the faults indicating that these units act as preferential pathways for fluid migration. (m/yr: meter per year).

In this regard, dimensionless studies based on Rayleigh and Prandtl numbers, as well as the evaluation of the buoyancy ratio, have been developed to determine the onset of convection in systems having a given thickness and constant physical parameters (Nield, 1968). However, in sedimentary basins, these conditions rarely, if ever, occur. Therefore, determining the onset of thermal convection by dimensionless analysis of the basin system is often not practical (Simmons et al., 2001). Flow rates in convection cells may vary from few centimeters per year up to a meter per year.

1.2 Brief description of driving forces in large-scale groundwater flow systems

Gravity driven flow (or density driven flow) is the term used when the convective currents are induced by density differences due to variations of solute concentration. A favorable scenario for gravitational convection is the presence of large salt bodies extending into shallow units (Fig. 1.5). The formation of dense brines by dissolution at the base of these salt sheets destabilizes the hydrostatic equilibrium within the underlying sediments.

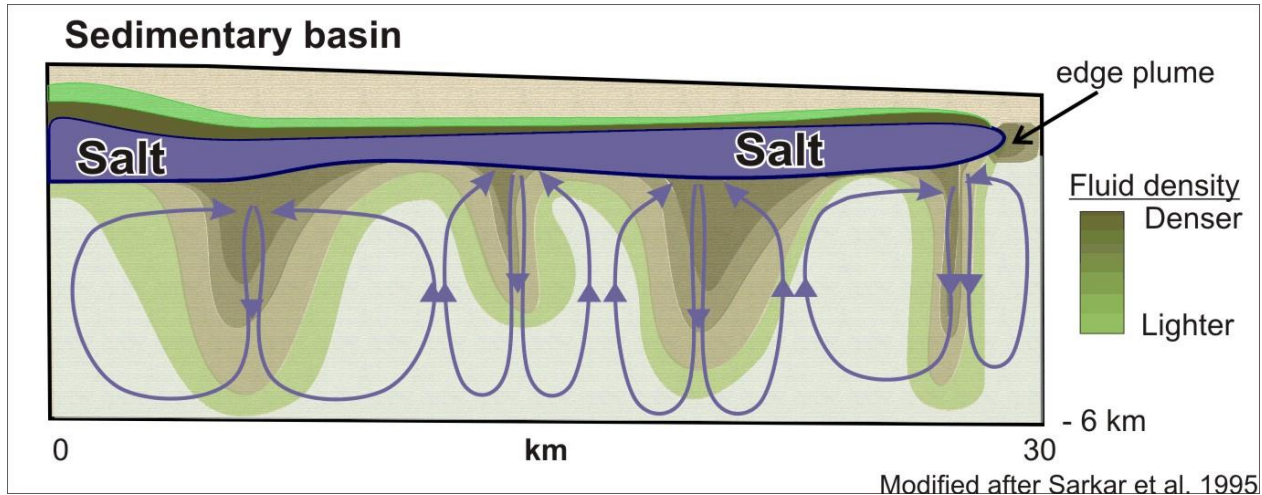


Fig. 1.5: Gravitational convection in a geothermal basin. Vectors illustrate the convective cells. (m/yr: meter per year)

Gravity instability beneath the base of the salt sheet manifests itself in the form of several incipient downwelling plumes in addition to the edge plume (Fig. 1.5). The solute plumes descend toward the base of the underlying sedimentary sequence. The resulting horizontal density gradients between the plumes give rise to orderly *counter-rotating* convection cells. This phenomenon can also be observed along the flanks of deep seated salt domes. However, in this case, the geothermal gradient also plays a role in inducing density variations and new effects might arise. These effects will be explained later in paragraph 1.3.

Ongoing geological processes such as sediment compaction, hydrocarbon generation or degassing of magma can also generate significant fluid flow at different velocity rates. These hydrologic regimes, also called *geological forcing* (Neuzil, 1995), are not considered in this work. Compactionally driven pore-water flow rates are usually very slow, in the order of 10^{-6} to 10^{-3} m year⁻¹, while tectonic compression can induce flow rates of 0.5 m year⁻¹ (Garven, 1995). A thorough review can be found in Garven (1995).

Although the above mentioned driving forces have been described separately, in nature large-scale processes often occur together so that they cannot be regarded independently.

1.3 Coupled processes

Over the large spatial scales encountered in sedimentary basins, temperature and solute concentration vary strongly and basin deformations are often substantial. Therefore the driving forces of groundwater flow can interact leading to new hydrologic regimes. Depending on the characteristics of the basin (e.g. heat source, presence of minerals, ongoing compaction), the “combination” of all or some of the previously described driving forces will determine the hydrological behavior of the basin. In other words, the synergy between the different processes is referred to as *coupling* (Tsang, 1991; Bedeohofat and Norton, 1990). As Chen et al. (1990, p. 104) notes, “*Although we tend to think of a single process it often happens that a variety of processes are coupled so strongly that qualitatively new effects and system behaviors arise because of this coupling*”

Thermohaline convection: the coupling of density-driven flow: The archetypal example for sedimentary basins is the coupling of heat and dissolved halite by controlling fluid density: the resulting regime is then called *thermohaline convection* (Nield and Bejan 1999). Since in geothermal basins the temperature gradients increase with depth, heat acts as a destabilizing potential. Thermohaline convection can develop cells at rates approaching 1 m yr^{-1} (Evans and Nunn, 1989; Garven, 1995) which are strong enough to control temperature and concentration fields. Excellent examples of thermohaline convection in a salt dome environment are the Gulf of Mexico (Evans and Nunn, 1989) and the NEGB which is thoroughly described in chapter 2. Two major scenarios for thermohaline convection to occur can be distinguished:

- (1) Salt concentration increases with depth, as for instance in the surroundings of deep-seated salt structures (Fig. 1.6).

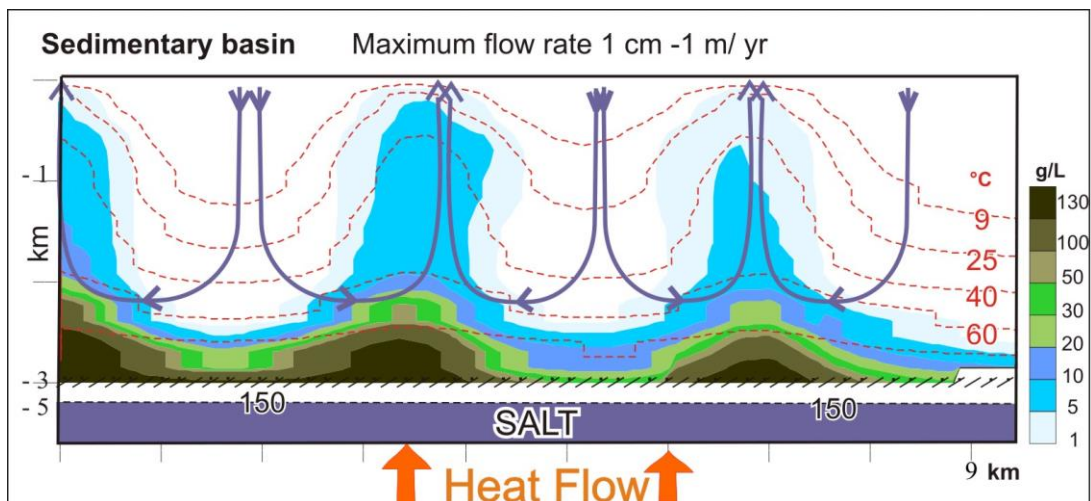


Fig. 1.6: Thermohaline convection above a deep salt structure, results from numerical simulations. Bold vectors illustrate the direction of the convective flow. The isotherms (red dashed lines) show typical convective multi-cellular regime. Picture modified after Magri et al. (2005). m/yr: meter per year

1.3 Coupled processes

In this case, the salinity gradient acts as stabilizing force. The deeper brines are heated from below and become less dense: an upward flow will be triggered when thermal induced buoyant forces will overcome gravity, leading to the formation of salty plumes. As the plumes keep rising, the brines will cool off quickly while losing little salt because of the different rates of diffusion (heat diffuses faster than salt). Buoyancy forces will therefore weaken and brine will start sinking. The chapters 2.1 and 2.2 provide examples of thermally driven flow around deep-seated salt domes.

(2) Another possible scenario arises when salinity gradients act as destabilizing factors. This can happen when brine forms in shallow areas of the basin (e.g., from shallow salt layers, Fig. 1.7). The denser fluid will therefore sink into the deeper sediments of the basin, depressing the isotherms. At the same time, lighter and hotter fluids will move upward owing to the thermally induced buoyant forces. Consequently, brine lenses and convection cells form.

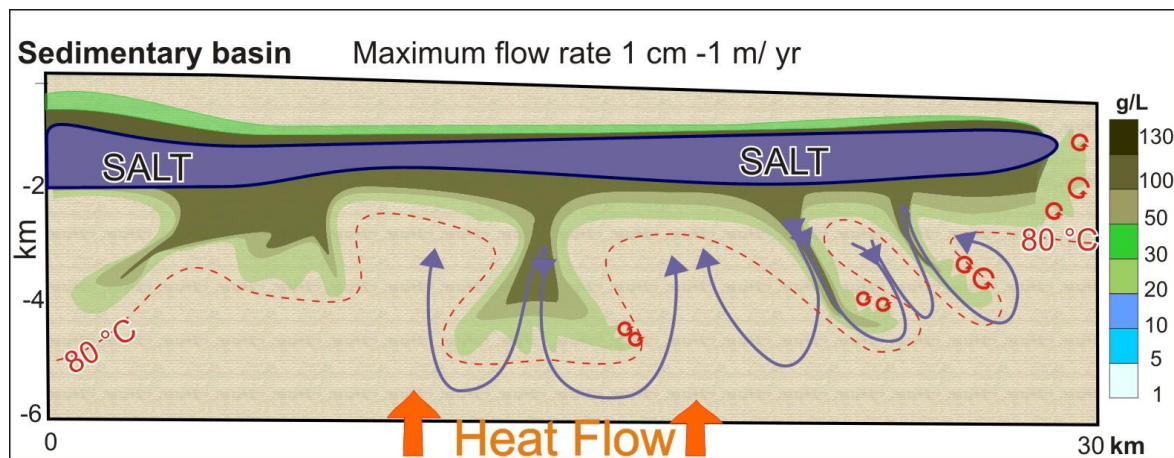


Fig. 1.7: *Gravitational convection* in a geothermal basin, results from numerical simulations. Bold vectors illustrate the direction of the convective flow. Smaller cells (red circles) can develop at the plume tips. Sinking brines decrease the temperature at depths (concave isotherms, red dashed lines). M/yr: meter per year

At the tips of both the sinking plumes and the edge plume, temperature oscillations can develop in a free-convective regime (red circles in Fig. 1.7), generating small brine fingers. This case is nicely illustrated for the Schleswig-Holstein shallow salt dome, in chapters 2.3 and 2.4

Mixed convection: the coupling of free and forced convection

When an external factor such as head-driven groundwater flow (forced convection) is imposed on a free thermohaline system the resulting regime is referred to as *mixed convection*. In sedimentary basins, it can happen that thermally-induced and topography-driven flows coexist

(Raffensperger and Garven, 1995a; Thornton and Wilson, 2007). Under such mixed condition, the regional flow affects the shape of thermally induced flow patterns and brine plumes: the short wavelengths of the temperature oscillations and the elongated brine plumes characterizing the free thermohaline regime can merge in bigger cells (Fig. 1.8).

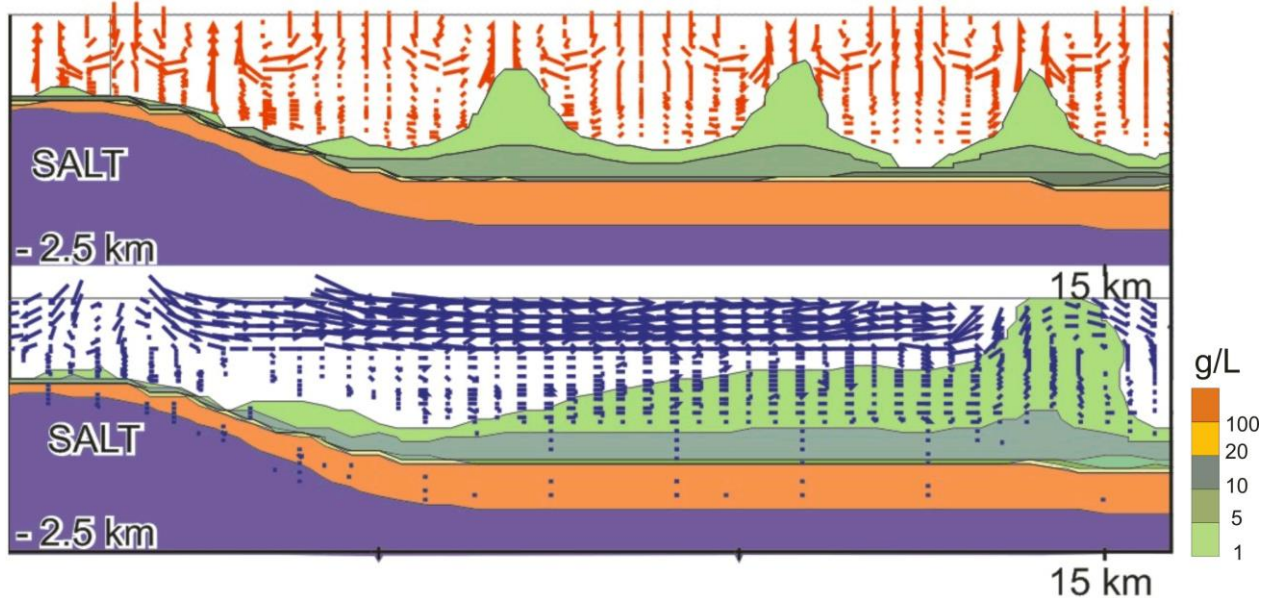


Fig. 1.8: *Mixed convection* near a salt dome, results from numerical simulations. Free thermohaline regime (top) compared to a mixed convective regime (bottom). The topography driven flow (blue vectors) overwhelms the thermohaline cells that would develop in a free regime (red vectors). In the mixed convective regime, only one larger brine finger reaches the surface. Modified after Magri et al. (2005)

On the other hand, vigorous topographically-driven groundwater flow can overwhelm free convection and modify the thermal structure of the basin. Precisely, it causes cooling and solute dilution in recharge areas whereas it increases heat flow and brine migration in discharge areas. In the NEGB (Chap 2), temperature and solute concentration differences can be observed between recharge and discharge areas reaching values of few degrees and few g/L, respectively. In active geothermal basins these differences can reach 50°C and several g/L (Ingebritsen and Sanford, 1998). An example of the strong impact of mixed convection on heat and solute transport is the Western Anatolia area, illustrated in chapter 3.

Other coupled processes

Additional effects that contribute to the coupling of hydrologic regimes have mechanical or chemical origins, such as dissolution or mineral precipitation that respectively increase or reduce both the porosity and permeability of rocks. These processes modify the spatial distribution of the physical properties and accordingly boost dramatically the complexity of the coupling effects. Hydromechanical and reactive transport coupling at basin-scale is the state of

1.3 Coupled processes

the art of numerical and mathematical studies, and require further research, as discussed in the concluding chapter 4.

However, in a basin system the dominant hydrologic regime is the result of a complex interplay between the relative strength of the existing driving forces and other controlling factors. As it will be explained in paragraph 1.4, these controlling factors are related to the spatial distribution of the rock properties (e.g. hydraulic conductivity) and the fluid properties (density and viscosity).

1.4 Controlling factors

The primary coupling between groundwater flow, mass and heat transport processes is through the Darcy law. This can be easily inferred by looking at the mathematical formulation of the coupled fluid flow equations (Appendix): the Darcy flow rate \mathbf{q} in equation 2 (Appendix) controls the rate of heat and mass convected through the media (equations 3 and 4 Appendix) and is also a function of fluid density and dynamic viscosity, which are both related on temperature, solute concentration and pressure by the respective EOS (equation 5 Appendix).

Therefore coupled fluid flow processes are intrinsically controlled by (1) the hydraulic permeability distribution and (2) fluid properties appearing in the Darcy law. In other words, the interplay of both solid and fluid properties determines the distribution of fluid pressure, flow rates, heat and solute migration.

(1) Since sedimentation processes occurred over geological time-scale, hydraulic conductivity can exhibit a wide range of values in the vertical direction. The heterogeneity of hydraulic conductivity is also evident in the surroundings of piercing salt domes (quasi-impervious), Pleistocene channels (highly permeable) and faults (permeable/impervious depending on the core properties). For instance, in-situ measured permeability data in fractured crystalline rocks can display variations of several orders of magnitude (Ingebristen and Sanford, 1998). Furthermore compositionally identical rocks can have different permeability at different depths because of consolidation and temperature effects.

When building a numerical model of fluid flow at basin-scale, the basin is usually divided in hydrostratigraphic units to represent hydraulically similar rock units within a hydrogeologic model (Bitzer et al., 2001). Depending on the type of transport modeled, the rock properties can also include heat conductivity, porosity, and dispersivity which dissipates density driven flow. Because of the difficulty in representing the spatial and temporal variations of these properties, the general approach is to give an average or equivalent value of the physical rock properties to each hydrostratigraphic units. Therefore, the critical issues of basin-scale modeling are the accuracy of the hydrogeologic model, the spatial discretization of the different units and the associated equivalent properties. Several techniques exist to estimate equivalent hydraulic conductivity as summarized in Zhang et al. (2006).

1.4 Controlling factors

Here, the classical approach of representing the sedimentary deposits by a series of homogeneous hydrogeologic units is used. In the NEGB case (chapter 2), the impact of permeability distribution on heat and brine migration is illustrated with respect to the different stratigraphic units. Particular attention will be given to young geological features as sands and Pleistocene channels (chapter 2.2 and 2.3). The role of highly permeable faults is investigated in the Western Anatolia example (chapter 3).

(2) The major fluid properties involved in fluid flow coupling are density and viscosity. On one hand, density variations must be accounted in the Darcy formulation to correctly calculate buoyant driving forces, in addition to the pressure gradient (equation 2, Appendix). On the other hand, as fluid viscosity appears in the denominator of the hydraulic conductivity formula (equation 6, Appendix), small viscosity variations will highly impact the effective hydraulic conductivity and consequently the flow rates. Equations of States (EOS) are needed to correctly describe temperature, pressure and concentration dependences of density and viscosity. One approach is to fit the available fluid data with polynomial expressions (Sorey 1976). Other modeling techniques involve the use of look-up tables. Here, polynomial EOS are used. One of the challenges of the simulations presented here was the implementation of a suitable EOS of the fluid density into FEFLOW. A detailed description of the used equation and its C++ code are given in the Appendix.

As fluid properties strongly depend on temperature and concentration, any effect which causes a significant variation in temperature and concentration will play a fundamental role in controlling groundwater flow. As mentioned in paragraph 1.3, salt diapirs strongly influence the concentration of dissolved solids. Furthermore, salt diapirs also perturb the temperature field because of their high thermal conductivity which is two to four times greater than that of the surrounding sediments. In this regard, one can say that salt diapirs are a unique geological environment controlling coupled fluid flow processes, which is the core of the researched carried out in the NEGB (Chapter 2).

Near salt domes, the impact of fluid viscosity is twofold: In a colder and highly saline environment, such as a shallow salt-dome crest, it retards brine flow by decreasing the effective hydraulic conductivity. In a warmer and less saline environment, variable fluid viscosity enhances thermally induced flow. In chapter 2.4, the effects of variable viscosity on density-driven flow are illustrated for a shallow salt dome of the NEGB.

1.4 Controlling factors

The following flowchart (Fig. 1.9) illustrates the major steps needed to build numerical models suitable to study the impact of the controlling factors. The steps include the pre-processing by which the available geological and hydrochemical data are transformed into a format appropriate for the numerical software. The model runs refers to the numerical calculations. The calibration is the process of modifying the input parameters until the output from the numerical results matches an observed set of data. Owing to the huge number of unknowns and simplifying assumptions of basin-scale models, the numerical results are calibrated with respect to regional trends of pressure, salinity or temperature rather than a set of observation points.

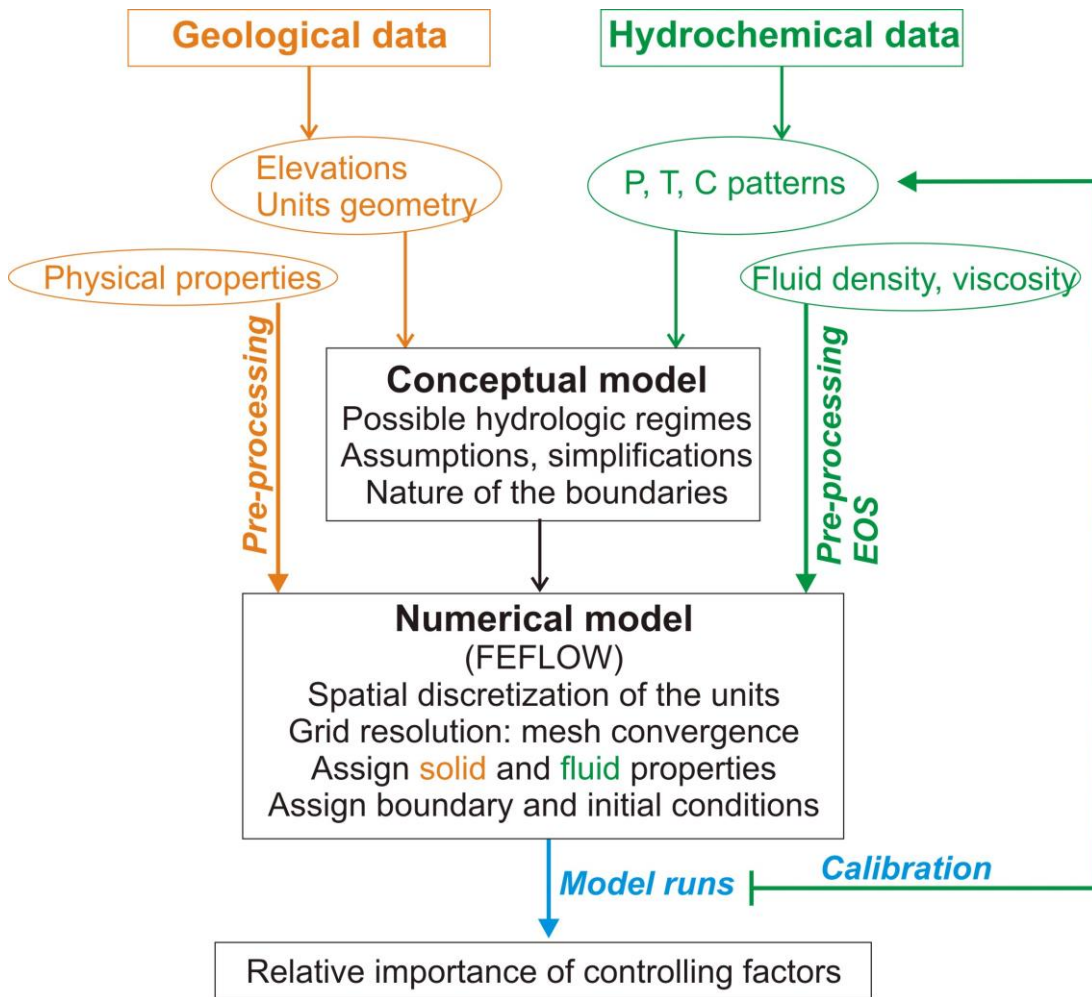


Fig. 1.9: Flowchart: steps taken in order to build numerical models suitable for assessing the impact of the controlling factors. (Legend. EOS: Equation Of States, P: pressure, T: temperature, C: concentration)

A very important numerical aspect related to the simulations of fluid transport processes is the grid resolution. The usual attempt is to subsequently refine the grid until the calculated patterns are qualitatively similar. This type of analysis is called mesh convergence (Fig. 1.9). It enables

1.4 Controlling factors

obtaining an accurate solution with a mesh that is sufficiently dense and at the same time maintaining computational times reasonable.

1.5 The main examples

Here, the North East German Basin (NEGB) and the Seferihisar-Balçova Geothermal (SBG) area, Western Anatolia, serve as research sites whereby numerical models and hydrochemical studies have been applied to investigate hypotheses of (i) thermally-induced brine migration (NEGB-chapter 2) and (ii) geothermal activity (SBG- chapter 3). This is done through a selection of eight peer-reviewed articles which combine numerical modeling and hydrochemistry.

The major criteria of grouping and sorting are as follows: (i) all papers based on the NEGB form chapter two whereas the SBG is the topic of chapter three (ii) the sorting within each chapter is done with respect to the type of coupling and controlling factor: In chapter 2.1, particular emphasis will be given to thermohaline convection near deep-seated salt domes and the impact of permeability distribution related to stratigraphy. An example investigating the impact of local heterogeneity, as the presence of Rupelian clay, is given in chapter 2.2 The shallow salt structure scenario illustrated in chapter 1.3 will be examined in details in chapter 2.3, in order to gain insights into the interaction between gravitational convection, thermally driven flow and young geological features such as Pleistocene and sand channels. Chapter 2.4 focuses on the importance of variable fluid viscosity in controlling density-driven flow in a shallow salt diapir. In general, chapter 2 will show how salt domes play a central role in controlling deep fluid flow at basin-scale. These coupled processes could be responsible for the temperature and concentration anomalies observed in several area of Germany.

As explained previously, the triggering factors for the onset of thermal convection are hydraulic permeability and unit thickness. In this regard, faults are geological features that strongly affect the permeability distributions and the structures of the sedimentary units. An example of thermally induced flow in a faulted geothermal system is given in chapter 3. It will be shown that convection is not only bounded within the fault but can also extend to surrounding units, strongly impacting pressure and flow patterns as well as the temperature field (chapter 3.1). An additional coupling with salinity from the neighboring seacoast is given in chapter 3.2, providing possible explanations for the observed seawater intrusions.

In all chapters, mixed convection will appear as the strongest coupling effect occurring in nature.

All simulations are supported by hydrochemical and isotopic investigations. These investigations were used as (i) additional tool to assess the validity of the modeling results and (ii) as a fundamental dataset to calibrate the models and correctly derive the EOS of fluid density, as

1.5 The main examples

illustrated in the flowchart 1.9. The reader can refer to the FEFLOW formulation summarized in the appendix for further mathematical details.

The following papers are reformatted in order to present the manuscript with a layout style as homogeneous as possible. Only the paper headings are in their original journal style. All references can be found in a common list at the end to avoid repetitions of frequently cited papers.

CHAPTER 2

2. BRINE MIGRATION FROM DEEP AND SHALLOW SALT DOMES: THE NORTH EAST GERMAN BASIN (NEGB)

Contents

2.1	Deep salt domes	18
2.2	Impact of hydraulic and heat conductivity distribution	57
2.3	Shallow salt structures and Pleistocene channels	76
2.4	Transition zones and variable viscosity	96

In some areas of the NEGB, groundwater is anomalously salty. This is witnessed by the presence of several saline springs. Further evidence of saline waters is given by plants commonly found along sea beaches or in salty soils, such as seashore salt grass, which grow in different areas of the basin. The figure below illustrates two species of these plants (Sea Milkwort, Strand-Milchkraut and Sea Arrowgrass, Strand-Dreizack) which have been photographed during a field trip in 2004 in Gröben, 50 km south of Berlin.



Fig. 2.1: Sea Milkwort, Strand-Milchkraut and Sea Arrowgrass, Strand-Dreizack in the Gröben area, 50 km south of Berlin.

The spontaneous growth of seashore grass far from the Baltic Sea coast is unusual and signals the existence of highly salty soils in the inner part of the basin.

Although these phenomena are observed since two centuries, the origin and mechanisms driving salt in the NEGB aquifer are not fully understood. The hydrochemical analyses indicate that the main source of salinization is dissolution of evaporites at different depths. However, Heck (1932) and Johannsen (1980) listed various locations of saltwater occurrences which

CHAPTER 2

cannot be related to any shallow salt deposits or salt domes. Therefore driving forces exceeding the gravity field must exist to allow heavy brines to migrate and reach the surface. As explained in the introduction, salt structures are a unique geological environment controlling density-driven fluid flow processes (chapter 1.3). Here numerical models of thermohaline convection in both deep and shallow salt structures of the NEGB are presented in order to investigate the role of the different forces and controlling factors of brine migration.

The two papers in **chapter 2.1** focus on brine migration near deep salt domes. The simulations indicate that the interaction between buoyant forces and regional flow (i.e. mixed convection (left figure, or Fig. 1.8) is the dominant hydrologic regime. While the resulting flows are slow, they are still sufficient to produce convection at basin scale and to drive brine up to the surface.

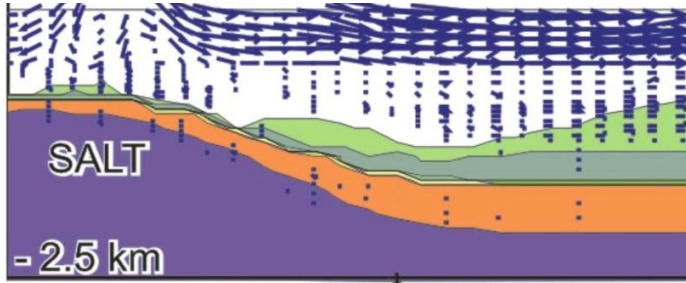


Fig. 2.2: Mixed convection near a deep salt dome. Refer to picture 1.8 in the for more details.

Chapter 2.2 is entirely dedicated to sensitivity analyses of the hydraulic permeability of the Cenozoic and the Muschelkalk, as well as the heat conductivity of the Zechstein salt. With a homogeneous Cenozoic, thermally induced brine plumes develop vertically. Lower value of the hydraulic conductivity within the Cenozoic due to the presence of Rupelian clay led to the formation of large brine patterns. In areas where the clay is thin or cut by channels, inflow of freshwater reaches the Pre-Rupelian aquifer, which is showed by the geochemical investigations as well. The Middle Triassic is a key unit controlling the salinity distribution throughout the profile: by increasing the hydraulic permeability of this unit more dissolved halite fills the sediment and the mass stratification is layered. Increased heat conductivity of the salt diapirs has also an impact on the calculated gradients by enhancing conduction and convection.

Brine migration from the shallow salt structures of the NEGB is the topic of **chapter 2.3**.

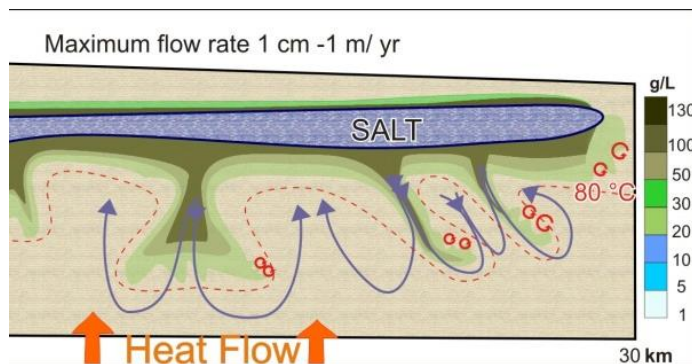


Fig. 2.3: Fig. 1.7: Gravitational convection below shallow salt structure. See the Introduction, picture 1.7 for more details.

In this scenario, gravitational convection interacts with thermal buoyant forces, as explained in chapter 1.3 (left figure, or Fig. 1.7).

Brine plumes sinking into permeable units can generate gravitational convection and overwhelm thermally induced flow. Particular attention will be given to young geological features such as Pleistocene

CHAPTER 2

channels and sand units. Quaternary channels located in discharge areas provide preferential conduits for brine outflow. Brines can migrate within interbedded sand units over several km and discharge far from the salt diapirs where they formed. These structural effects strongly perturb the fluid density throughout the whole basin. **Chapter 2.4** investigates the role of permeable transition zones along the salt flank and variable fluid viscosity. The presence of a transition zone between the salt flank and the adjacent units delays gravitational convection. It turned out that variable viscosity has a twofold effects in controlling mass and temperature patterns by reducing or increasing the effective hydraulic conductivity of the units in colder or warmer parts of the basin, respectively.

Based on the results presented here, it is apparent that the geological characteristics of salt diapirs and surrounding sediments, as well as the physical properties of brines (such as variable density and viscosity), strongly control the regional-scale behavior of thermohaline flow.

2.1 Deep salt domes



Available online at www.sciencedirect.com

SCIENCE @ DIRECT®

Tectonophysics 397 (2005) 5–20

TECTONOPHYSICS

www.elsevier.com/locate/tecto

Deep reaching fluid flow close to convective instability in the NE German basin—results from water chemistry and numerical modelling

F. Magri^a, U. Bayer^{a,*}, V. Clausnitzer^b, C. Jahnke^c, H.-J. Diersch^b, J. Fuhrmann^d,
P. Möller^c, A. Pekdeger^e, M. Tesmer^c, H. Voigt^c

^aGeoforschungszentrum Potsdam 4.3, Telegrafenberg, 14473 Potsdam, Germany

^bWASY GmbH, Waltersdorfer Str. 105, 12526 Berlin, Germany

^cBrandenburg University of Technology Cottbus (BTU), Environmental Geology, E. Weinert Str. 1, 03046 Cottbus, Germany

^dWeierstrass Institute for Applied Analysis and Stochastics, Mohrenstr. 39, 10117 Berlin, Germany

^eFreie Universität Berlin, Institut of Geological Sciences, Geochemistry, Hydrology, Mineralogy, Malteserstr. 74-100, 12249 Berlin, Germany

Received 28 October 2003; accepted 19 October 2004

Available online 28 December 2004

ABSTRACT

In several areas of the North German Basin salinar brines reach the surface locally. An evaluation of the available data of pore fluids indicates an instable stratification in terms of fluid densities. In order to study the possible physical causes, numerical simulations of coupled fluid, heat and mass flow were carried out at the basin scale. Modeling results suggest a possible presence of thermally induced free convection controlled by spatial heterogeneity in sedimentary-layer thickness and permeability. Specifically, the results point to a situation where the subsurface fluids are generally close to convective instability, with presence of free convection in those regions where a sufficient, vertically continuous permeability exists. Scenarios that allow for a local presence of free convection may be needed to understand the mechanism behind numerous previously unexplained field observations of deep-groundwater occurrences near the basin surface. The potential presence of large-scale convection cells has implications both for the fundamental understanding of basin processes and socio-economic issues.

Keywords: Salinar brines, instable stratification, free convection, heterogeneity, permeability, sedimentary basins, numerical modeling of fluid flow.

INTRODUCTION

Density-driven, or 'free', convection in sedimentary basins is well documented for cases where a denser (e.g., saline) fluid originates above a less dense fluid and subsequently sinks, thereby displacing the latter. For example, Fan et al. (1997) compiled field studies that indicate the presence of free groundwater convection underneath saline lakes for various hydrologically closed sedimentary basins in North America and Australia. This flow regime is inherently instable with small perturbations increasing in magnitude rather than dissipating. In contrast, a source of salinity located underneath the groundwater body provides a hydrodynamically stabilizing influence. A typical case is a salt layer that to the fluid within the overlying sediments represents both an impermeable boundary and, via dissolution, a source of salinity. Results from deep drilling confirm that large portions of the crust are likely fluid-saturated. As saline waters have been observed to rise to the surface, forces must be present that exceed the gravitational effect of the saline contribution to the fluid density. Generally, forced hydraulic convection in conjunction with vertically corresponding high-permeability pathways is assumed in these cases. However, thermally-induced free fluid convection originating even in the deeper, low-porosity and low-permeability subsurface is conceivable given a geothermal gradient of sufficient strength. Besides the implications for diagenesis and other geologic processes, an understanding of these phenomena is important for geothermal applications, hydrocarbon migration and assessing long-term behaviour of pollutants.

Here we present an example from the NE German Basin where both geochemical data and modeling results point to an active convective system controlled by interaction between the thermal field, locally modified by salt domes, and the associated inhomogeneous distribution of high-density salt brines. The main points will be:

1. Observations from water chemistry based on data collected over several decades by various institutions;
2. 2D-numerical modeling using Finite-Volume (FV) and Finite Element (FE) methods.

Concerning the possible causes which may cause upwelling of salinar brines we concentrate at thermal driven convection but also include hydraulic heads (Bjørlykke et al., 1988). Compaction driven flow can almost with certainty be excluded because there are no over pressure sediments. Based on the regional level, man-made discharge appears to be minor although there is evidence that it locally may affect the process in the upper most layers.

DATA

Extensive evidence for rising saline waters is available on a regional (10^4 -m) scale for sedimentary basins in northern Germany. Specifically, more than 100 locations of saline springs have been documented. A common characteristic of these springs is their instability. Strong positional fluctuations have been recorded and approximately one tenth of the springs are known only from historical accounts and presently cannot be observed. A map based on the references compiled by Schirrmeister (1996) for the North-East German Basin is shown in Fig. 1.

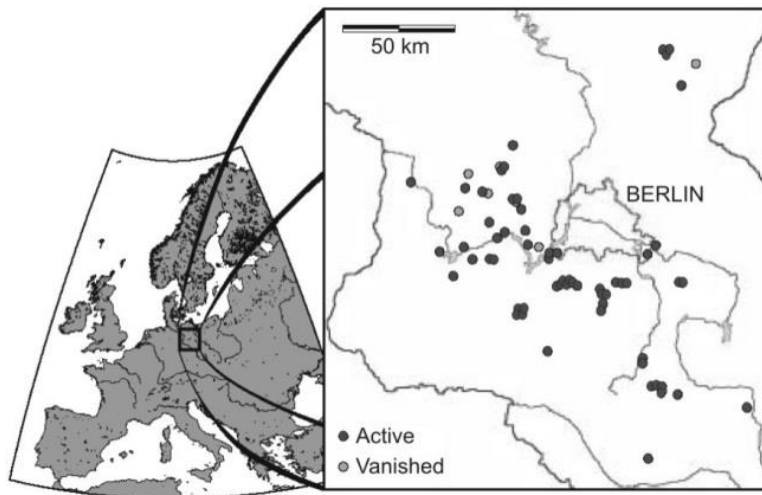


Fig. 1: Location map of saline springs in the North-East German Basin.

For the adjacent Schleswig-Holstein basin, Heck (1932) lists various locations of saltwater presence at or near the surface which cannot be explained as originating from any shallow salt deposits and whose cause remains unknown. A lack of explanation is also noted by Johannsen (1980) for observed steep vertical plumes of saline fluids that reach near-surface levels. Specifically, there is no indication of corresponding fault-related or other high-permeability conduits. Even assuming that such preferential pathways do exist, the physical driving force for the upward flow of saline fluids remains to be identified. Noting that chemical analysis strongly indicates salty layers and residual brines as the source of the salinization, Hannemann & Schirrmeister (1998) hypothesize that high-permeability pathways exist and that ultimately long-term fluctuations of the sea level are responsible for vertical exchange of saline and fresh water by affecting the hydraulic pressure gradients within the basin. However, the difficulties for a forced-convection scenario alone to explain all of the observed phenomena suggest the presence of a more complex physical system. The steep rising plumes in particular point to possibly significant temperature effects on the fluid density in addition to any forced convection present.

2.1 Brine migration: deep salt domes

The hydrochemistry of deep saline waters in the Northern German Basin was investigated by, among others, Glander & Schirrmeister (1975), Hannemann & Schirrmeister (1998), Hoth et al. (1997), Huenges (2002), Kühn (1997), Lehmann (1974a, 1974b), Loehnert et al. (1986), Müller & Papendiek (1975), Naumann (2000), Neumann (1975), Rockel et al. (1997), Rutter (1988), Thomas (1994), Trettin et al. (1990, 1997), Voigt (1972, 1975, 1977). These studies focussed on subjects such as geochemistry, geothermal energy, oil field waters, isotopes, and environmental aspects and thus will not be discussed in detail here.

In order to improve the data base, the 'grey' (unpublished) literature existing at the Geological Surveys of the federal districts of Germany and at commercial companies has been evaluated and organized in a digital database. This data base contains lithological and petrophysical data, hydro-chemical, hydraulic, and geothermal data from about 500 deep boreholes within the study area from Cretaceous to Permian/Carboniferous and several thousand datasets from superficial Cainozoic aquifers. The data originate mostly from the 1960s to the 1980s. The available data for fluid chemistry and dynamics are mainly clustered at the centres of the former oil and gas prospection and exploration activities but still represent a relatively good sampling distribution over the entire study area.

In addition, new investigations of brine chemistry have been performed. At each location samples for anions and cations, Rare Earth Elements and yttrium, $\delta^{18}\text{O}$, δD , and SiO_2 -geothermometer were sampled. Where no former analyses for $^{34}\text{S}/^{32}\text{S}$ -, $^{13}\text{C}/^{12}\text{C}$ - and $^3\text{He}/^4\text{He}$ – isotope ratio and tritium existed, samples for these isotopes were also taken. Samples were stored at 4°C and full water analysis was generally performed as soon as possible.

Based on these data a hydrological, hydrodynamic/thermal model was developed. This includes

- a model for the spatial aquifer characteristics ("aquifer model") - geometry, lithologies, porosities, permeabilities, heat conductivity and heat capacity based on the existing three dimensional structure model (Scheck, 1997, Scheck & Bayer, 1999),
- a model for the chemical and physical fluid characteristics and their spatial distribution ("fluid-model") - salt content, density, temperature, pressure, viscosity, heat capacity and heat conductivity,
- determination of the boundary and initial conditions.

The state and the processes of fluid migration in the NE German Sedimentary Basin will be described on the basis of these models in order to yield a regional picture of the dominating processes and to derive input data and control parameters for the numerical simulation.

2.1 Brine migration: deep salt domes

The geological input data are derived from a three-dimensional structural model of the North-East German Basin (Scheck, 1997, Scheck & Bayer, 1999). The area covered by the model is approximately 230 x 330 km in the horizontal extension and 30 km in the vertical direction which consists of 13 layers (from the Top Cainozoic down to the Top Moho). The physical parameters assigned to each sedimentary layer were those given by Scheck (1997) (Table.1). Within each layer it was assumed that the physical properties are constant. This first rough aquifer model differentiates only the stratigraphic layers of the model without any spatial variation. The development of a detailed aquifer model with spatial variations of porosities, permeabilities, etc., corresponding to the collected petrophysical data is the aim of further research.

Table. 1 Physical parameters assigned to the stratigraphic layers.

Layer	Abbreviations	Permeability [m ²]	Porosity [--]	Rho_s [kg/m ³]	Bulk properties	
					Heat capacity [J/(kg*K)]	Heat conductivity [J/(K*m*s)]
Cenozoic	Cz	1.e-12	0.23	2670	1180	1.5
Upper Cretaceous	K ₁	1.e-13	0.10	2400	1000	1.9
Lower Cretaceous	K ₂	1.e-13	0.13	2700	1180	2
Jurassic	J	1.e-13	0.13	2700	1180	2
Upper Triassic	T ₂₋₃	1.e-14	0.06	2700	1180	2.3
Middle Triassic	T ₂	1.e-18	0.00	2400	1000	1.85
Lower Triassic	T ₁	1.e-14	0.04	2670	1180	2
Zechstein (Salt)		1.e-30	~0.0	2160	840	3.5
Elbe Group		1.e-14	0.03	2670	1000	1.84
Mirrow Formation		1.e-14	0.03	2670	1000	2.13
Volcanics		1.e-14	0.03	2670	1000	2.4
Top basement		1.e-30	~0.0	2650	930	2.5
Top mantle		1.e-30	~0.0	2700	1000	2.65

Fluid-Model (p-T-x-density)

In contrast to normal groundwater models for freshwater, large scale simulation of thermohaline flow and transport processes requires a proper fluid model. This is necessary because the strong spatial variability of the physical and chemical fluid characteristics (for example salt content, temperature, density) in sedimentary basins have a strong influence on the dynamic system in addition to the aquifer parameters. The collected data include

- salt content and species of salts,
- density, laboratory-measured or derived from the salt content,
- in-situ temperature,
- hydraulic heads and in situ fluid pressures.

For the fluid model and the spatial distribution of the parameters some corrections of these data were necessary. Especially, the influence of temperature and pressure on the density is important and was neglected in former investigations of this area. Fig. 2 illustrates the density/depth relation in the different pre-Cainozoic aquifers. The density values are obtained from laboratory analyses (left picture) and approximated in-situ densities (right picture).

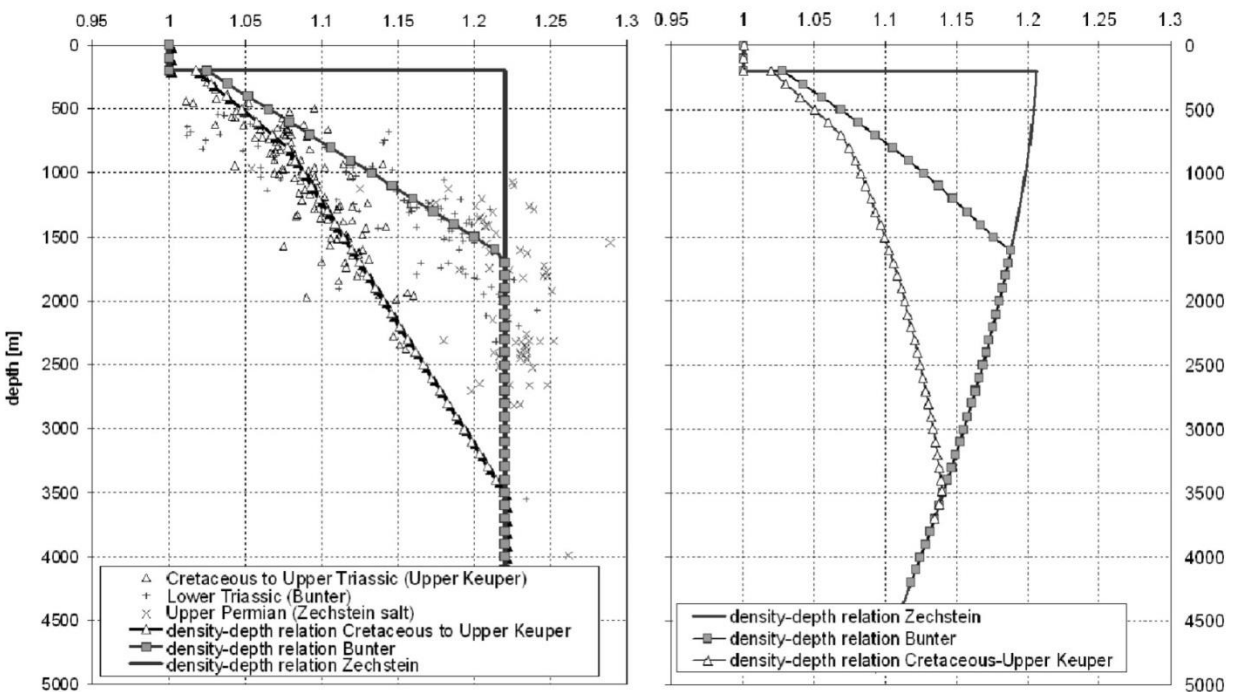


Fig. 2: Left: Depth density relations at 20°C for various stratigraphic layers within the Northeast German Basin. Right: T,p-corrected in-situ brine densities for the sediments above the Zechstein salt.

2.1 Brine migration: deep salt domes

The laboratory values show a general increase of the fluid density with depth. Once NaCl saturation is reached the densities remain nearly constant (about 1.22 g/cm³). The NaCl saturation in the stratigraphic layers is reached at different depths. Approximate density/depth relations were fitted to the experimental data for the Cretaceous to Keuper, Buntsandstein and Zechstein. For the determination of the in-situ densities a temperature and pressure correction of the laboratory data was performed. For this purpose an iteration procedure was carried out. Based on the assumption of a simple temperature model and hydrostatic conditions, temperature-corrected densities and pressures were calculated. The temperature model considers only a depth dependency of the temperature (no spatial variations). A thermal gradient of 35 °C/km was assumed for the Mesozoic strata corresponding to experimental data (Hurtig 1994). Further it was assumed that the brines are pure NaCl-solutions. For the brines within the Mesozoic strata this assumption provides a sufficient approximation.

Fig. 2 (right) shows the corrected density/depth relations for the different strata. A remarkable result is the inversion of the density-depth trend following NaCl saturation in the Buntsandstein and Zechstein due to thermal expansion of the fluids. Below the inversion depth a decrease of the density with increasing depth is observed. That means that at greater depth lighter brines occur than at lower depth and uplift pressures exist at least on local scales. Within the Cretaceous to Keuper these effect may exist at depths below 3500 m.

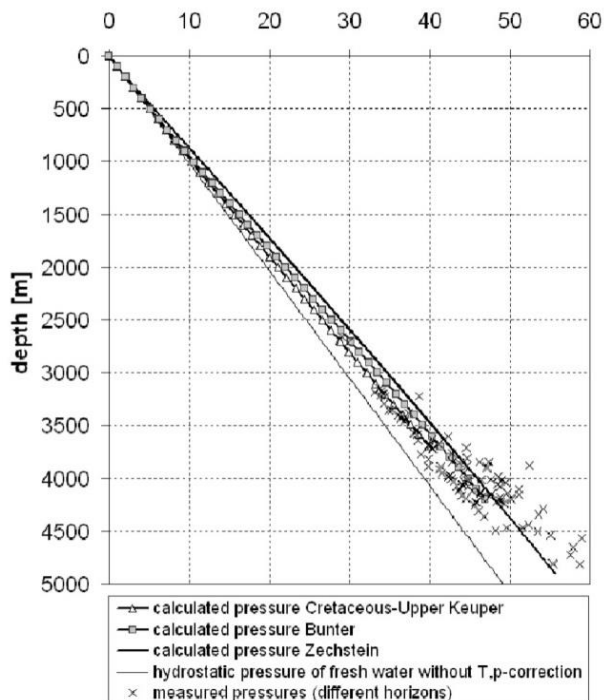


Fig. 3: Calculated hydrostatic pressures and measured pore-pressure.

Fig. 3 illustrates the calculated corrected pressures and the measured pressures from different horizons. The pressures are hydrostatic. Pressures above the hydrostatic level occur only in the Zechstein and some local zones in the Rotliegend (Voigt, 1975). The derived pressures and

gradients correspond well to experimentally obtained data from hydraulic tests (Voigt, 1975, Neumann, 1975, Rutter, 1988).

Spatial density model

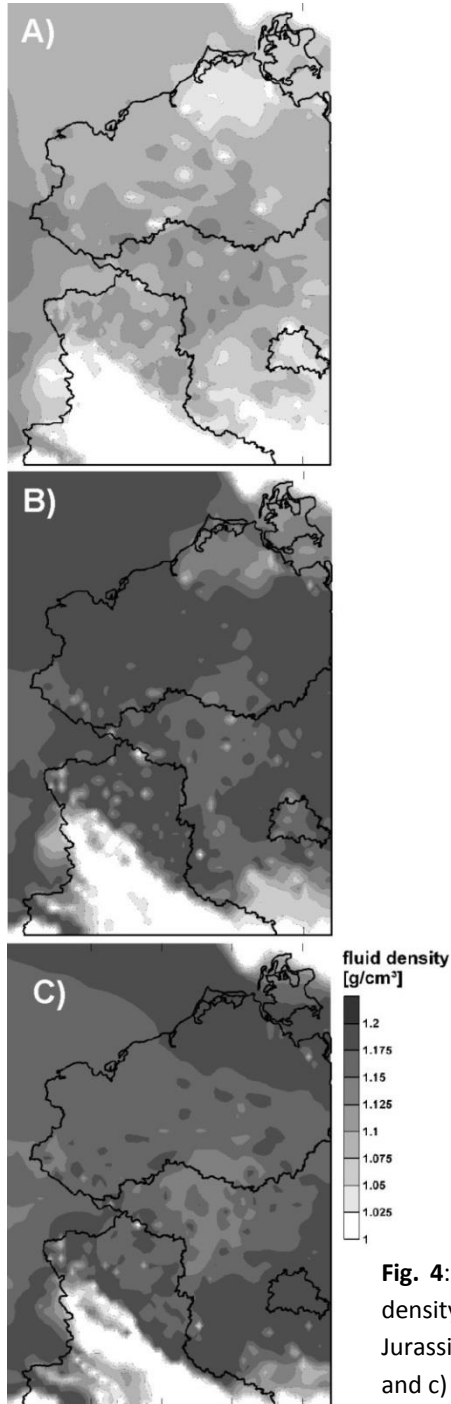


Fig. 4 provides an overview of the spatial distribution of the density in some subsurface aquifers. For the Cretaceous to Keuper the density increases from the borders of the basin towards its centre, paralleling depth. Spatial deviations exist due to salt diapirs. The Buntsandstein, however, shows a very different behaviour. At lower depth the density increases from the border to the centre due to an increase of salt content. Once NaCl saturation is reached, the density decreases according to the temperature effect. Therefore, the centre of the basin contains fluids with lower density surrounded by a ring of denser waters (Fig. 4b). This effect becomes stronger with depth and it is more distinctive at the base of the Buntsandstein (Fig. 4c).

This regionally variable density stratification is unstable and can lead to vertical fluid migration movement (convection cells) depending on the permeabilities of the aquifers. It is notable that the saliniferous springs (Voigt, 1976) occur predominantly in areas with mixed density stratification. This may indicate that these flow regimes have an influence on the water dynamics up to the surface

Fig. 4: Spatial distribution of fluid density within a) the base of Jurassic, b) the top Buntsandstein, and c) the base Buntsandstein.

MODELING APPROACH

Previously, basic studies concerning convective flow in porous media have been carried out, for example, by Curtis & Pruess (1998), Mineyuki (1998) and Nield (1968, 1991). Here we attempt to model large-scale cross sections through the basin area by use of two slightly different approaches. First we provide basic tests by use of a Finite-Volume model (Fuhrmann and Langmach, 2001, Bayer et al., 2002, Fuhrmann, 2002) which includes full nonlinear coupling of fluid and heat transport, as well as a practical method to generate detailed grids. A limitation is given by the fact that it cannot yet handle the mass transfer related to variable salt contents of the fluid. Secondly we apply a commercial Finite-Element program (FEFLOW®) which is capable of handling the full problem of coupled flow, heat, and mass transfer. Here, however, the vertical grid structure of 2D models is less flexible and not as easily adapted to the variable physical parameters of the different layers, which in combination with the grid define the effective topology and thereby the wavelength of the smallest observable convective structures. Especially the density function becomes rather complex and provides a strong nonlinear coupling term (s. Appendix).

Another problem is the well-known fact that it is rather difficult to define a stable initial distribution of the various variables interconnected in a non-linear manner. For comparability, we start with a simple conductive model and then switch on the non-linear interaction. The model then is run for about 200,000 years, a timespace where the model typically stabilizes in a rather general sense (dependent on permeabilities, which means either stable convection cells or continuously shifting cell patterns).

Presently, we do not consider the changes in surface temperature which occurred throughout the Quaternary. In contrast, we rely on the question whether free thermal driven convection may be a major source for the observed anomalous distribution of salt brines within the basin, without attempting to reproduce the observations in detail.

Finite-Volume Method

The feasibility of thermally-induced free convection in a sedimentary basin was investigated by numerically simulating the coupled flow of heat and fluid. The flow process is mathematically expressed by the flux and conservation laws for mass and energy, coupled by the dependence of the fluid density on temperature. In contrast to the usually invoked Boussinesq (1903) approximation, changes in the liquid-phase density related to pressure and temperature were considered fully, i.e., were not limited to the gravity term.

For the numerical solution, the use of unstructured meshes was necessitated specifically by the irregularity of the internal subdomain (layer) interfaces, with the related heterogeneity in physical parameters posing further requirements for the mesh to enable a numerical solution. Using Shewchuk's (1996) 'TRIANGLE' code, additional grid points are introduced that together with the employed finite-volume scheme guarantee that the numerical approximation scheme

never introduces artefacts of the type that could eventually give rise to nonphysical predicted values (e.g., negative temperature). This increase in nodal density can raise the computational expense by an order of magnitude for a two-dimensional problem of the type considered here. In return, a combination of geometric flexibility and mathematical rigor is achieved that appears to be essential for simulation of density-driven flow in porous media with natural heterogeneity (Fuhrman & Langmach, 2001). Grid convergence was established by verifying that key solutions characteristics such as number, magnitude and rate of lateral migration of convection cells do not change as the grid is further refined while always honouring the pre-described layer interfaces.

Specifically, vertical cross sections through the North-German Basin were considered based on structural data by Scheck & Bayer (1999). Temperature values at the upper and lower boundaries were fixed so as to correspond to the vertical geothermal gradient of 35 K/km prevalent in this area, with 283.15 K applied at the surface in all cases. The fluid pressure at the surface was fixed at the value given by the barometric equation and all other domain boundaries were defined as impermeable.

A snapshot of isotherms typical for the long-term behaviour of this system is shown in Fig 5. The north-south oriented, 230 km long and eight km deep cross section includes the approximate basin centre. A dominant structural feature of the basin is a thick salt layer with salt domes. This layer, located at approximately the centre in the vertical direction, is impermeable to fluid flow but allows conductive heat transport, thereby providing a well-defined boundary for the modeling problem above the salt. The physical parameters assigned to each sedimentary layer were those given by Scheck (1997). Specifically, the permeability values used for the layers above the salt, starting with the youngest are those given in Table 1.

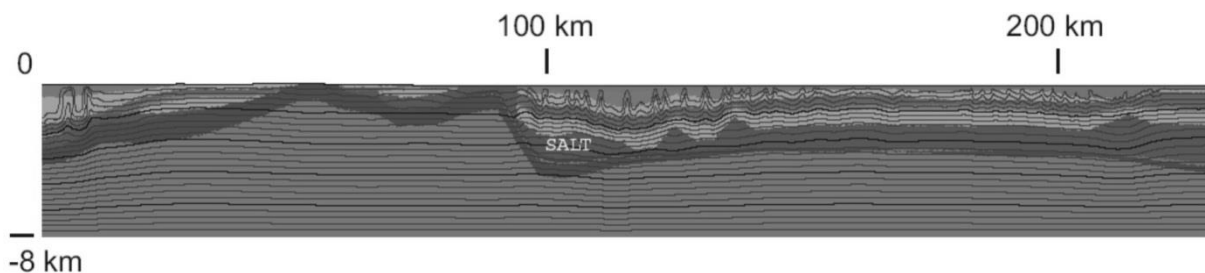
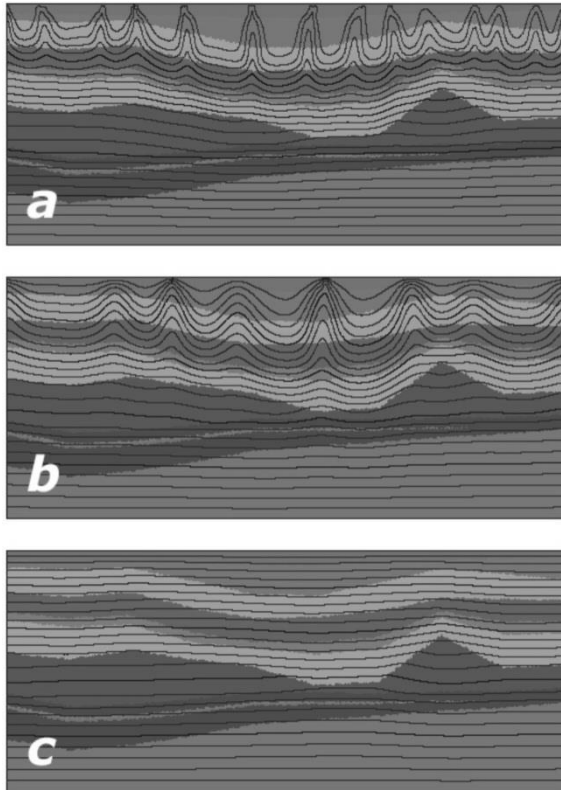


Fig. 5: Typical long-term isotherm pattern (solid lines, contour intervals of 11.2 K) obtained along a N-S cross section of the North-East German Basin by the Finite Volume method without density variations by brines. Sedimentary layers are distinguished by gray scales.

Rayleigh's (1916) theory, applied to porous media flow, predicts that free convection is favoured for a given layer as vertical permeability, layer thickness and vertical thermal gradient increase. Indeed, free-convection phenomena are observed in the simulations where the uppermost, most permeable layers have sufficient vertical thickness (Fig. 5). Specifically, new convection cells originate by splitting of existing cells near the centre of the basin in the area of

maximum thickness with a period of approximately 71 ka. Cells then migrate toward the basin perimeter where they recombine into stationary cells. As they migrate outward from the centre, the cells diminish in vertical size, corresponding to the decreasing vertical extent of the most permeable top layers. Where these layers are too thin for free convection to occur, heat transfer is purely conductive as indicated by essentially flat isotherms. The controlling effect of layer thickness regarding the locally dominant heat transfer mode (convective vs. conductive) is clearly demonstrated in Fig. 5.



While individual sedimentary layers were considered homogeneous in the simulation, in reality they are themselves subject to many sources of spatial heterogeneity in the physical flow parameters, with facies of a given layer possibly differing, for example, in permeability by several orders of magnitude. To identify the threshold in permeability below which free convection cannot be established, the permeability values assigned to the top four layers were incrementally reduced (Fig. 6).

A decrease by an order of magnitude noticeably slowed the convection process, corresponding to an increase in the period to one Ma, while a reduction of the original values by two orders of magnitude, still well within the physically reasonable range, led to a purely

Fig. 6: Effect of cross-section (Fig. 5) permeability on temperature regime for a 35 km long and six km deep subsection: permeability of top four layers (a) as in Fig. 1, Table 1, (b) lowered by one order of magnitude, (c) lowered by two orders of magnitude. Isotherms are depicted as solid lines with contour intervals of 8.4 K.

conductive heat-flow regime. With permeability conditions thus found rather close to the limit for the onset of free convection, the significance of facies heterogeneity is further emphasized.

The results of the modeling study are suggestive of a natural subsurface fluid system near a bifurcation point where the dominant mode of heat transfer shifts between conductive and convective. Under such conditions, relatively small variations in layer thickness (Fig. 4) and permeability (Fig. 6) can determine the presence or absence of free convection. Consequently, both spatial distribution and extent of convection phenomena are potentially controlled by effects of physical heterogeneity.

Free convection at the scale observed in the simulations would be expected to lift deep groundwater to near-surface levels in specific locations of limited area with likely fluctuations due to the instable nature of the physical flow process. While this is indeed in excellent agreement with the observations cited above, the modeling results need to be qualified by recognizing that solute effects on fluid density have been ignored. In physical reality, the thermal and salinity effects counteract above the salt layer, resulting in reduced buoyancy forces. Rosenberg & Spera (1992) found that the long-term behaviour will change from a convective to a conductive regime when the change in fluid density due to salinity approaches or exceeds the (negative) change due to thermal fluid expansibility. Considering the temperature range across the largest convection cells in the current study, corresponding critical concentration values of approximately 15 g/l are obtained. As concentrations exceeding this value have indeed been reported for several of the listed near-surface occurrences of saline water, it is apparent that free convection cannot, by itself, explain all of the observed saline uprising phenomena. Concerning a homogeneous density distribution within the basin fluids, free convection provides a reasonable process. To what extent free convection may still be active, concerning more realistic density distributions will now be examined by the Finite Element Method which, however, provides less spatial resolution at the current state.

Finite Elements

The commercial program FEFLOW[®] provides the possibility of a full integration of all nonlinearly coupled processes. The density model has been incorporated via a programmable interface as detailed in the appendix. The boundary and initial conditions used are:

Zero pressure at the surface (i.e., the head is set to the local topographical elevation), a constant temperature of 8°C, and zero mass concentration at the surface. 8°C represents the current average temperature for the area under consideration; past fluctuations have not yet been considered. The zero-mass condition at the upper boundary is sufficient to localize those zones where deep groundwater may rise to near-surface levels although it is recognized that this condition will not allow saline water to reach the surface itself. At the top of the salt, the brine solution is set to its saturation concentration, i.e., 345.2 g/l. At the lower boundary the temperature is set to 150 °C, a value that corresponds to a linear vertical gradient of 30 K/km. The lateral boundaries are closed to fluid, heat, or mass flow. Initial pressure and temperature conditions are obtained from steady-state solutions for fluid flow and heat transport, respectively. Using initial conditions derived from a steady-state solution of the considered problem guarantees a higher stability of the simulations and increases the rate of convergence of the coupled problem. In order to ensure stability with regard to the selected grid and parameters, two different initial mass distributions were used: first, the salt concentration was set to zero everywhere above the Buntsandstein; second, a depth-dependent initial density was derived as given above, except that the interpolation was performed between the surface and

the top of Buntsandstein. Two-dimensional thermohaline flow in a vertical cross section was simulated over a period of 200,000 years.

Fig. 7a illustrates the geological setting along a 230 km long W-E section, the calculated velocity field after 200 ka (Fig. 7b) as well as the initial mass distribution (Fig. 7c) derived from Fig. 2 and the final mass distribution at 200 ka (Fig. 7d). This particular west-east section was selected because there is almost no topographical variation along this line, so there is little influence of hydrostatically driven flow and it intersects the previous studied N-S cross-section in the basin center. It was found that the introduction of salt and its related density gradient within the basin fluids did not prevent free convection; however, the observed convection patterns differed from those obtained by the Finite-Volume model where only thermal effects on the fluid density were considered. While the spacing of convection cells in Fig. 6 corresponds to a wavelength of about four to five kilometers, this length is now approximately 15 km and more irregular. In addition, the Finite-Volume model with thermally-controlled fluid density predicted fluctuating convection cells while convection seems to approach a stable pattern in the Finite Element thermohaline model.

2.1 Brine migration: deep salt domes

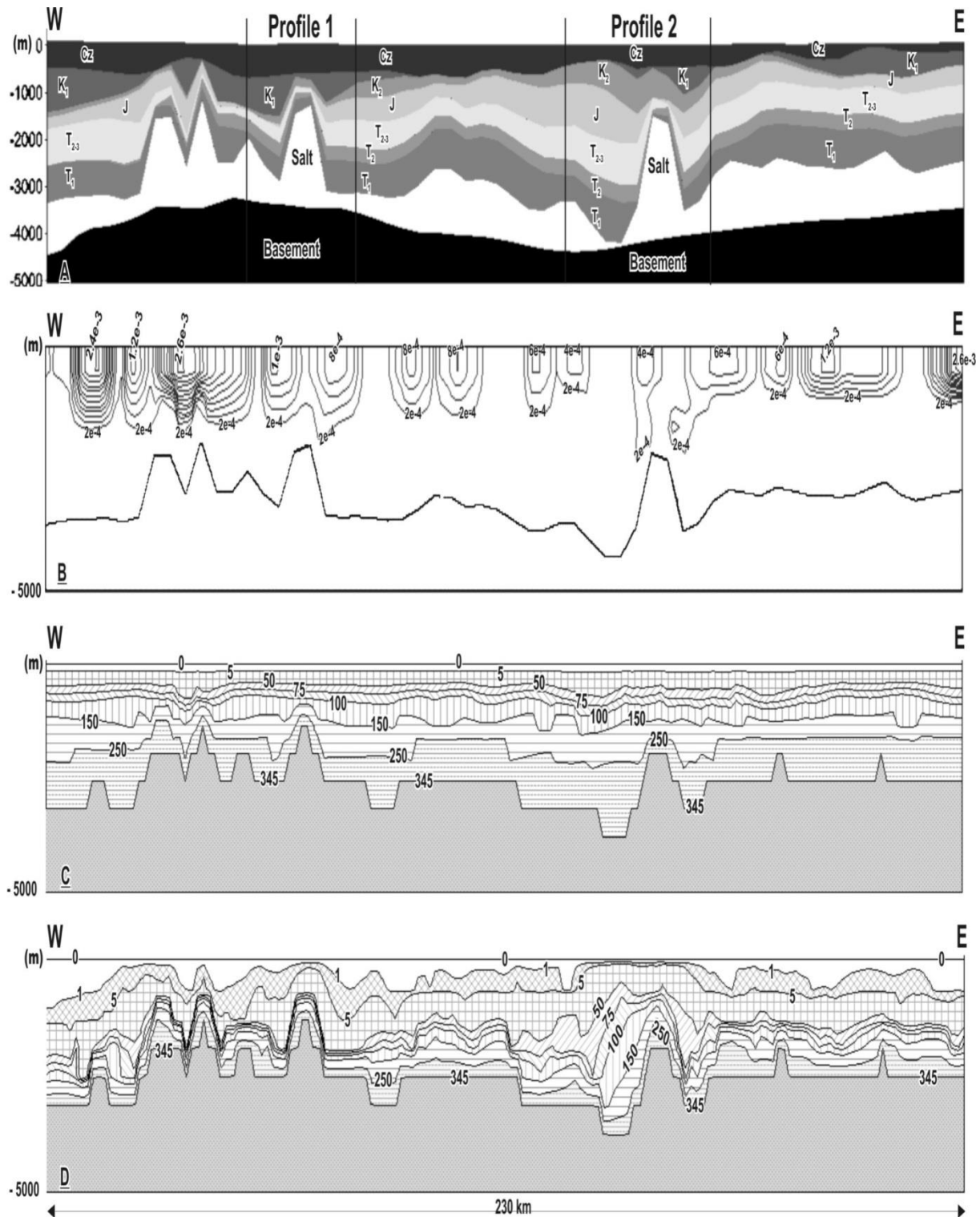


Fig. 7: Finite element model of fluid flow including density variations by NaCl-content of the pore fluid. A) geological section (abbreviations given in Table. 1), B) flow velocity in m/day, C) initial NaCl distribution derived from Fig. 2, D) mass distribution after 200 ka computing time.

2.1 Brine migration: deep salt domes

Figures 8 and 9 provide details of the entire section indicated in Fig. 7 as Profile 1 and Profile 2. Figs. 8a and 9a show the initial mass distribution based on the observed field data and Fig. 8b and 9b the resulting mass distribution at the end of the simulation run. Although the flow rates are only on the order of 10^{-1} mm/day (Figs. 8c, 9c), or about 10 to 20 cm per year, the mass distribution is effectively deformed. The flow fields and flow vectors are given in Figs. 8c and 9c. In these cases the convection cells seem to be influenced by the salt structures as they develop more or less symmetrically around the salt domes. On the other hand, there are also convection cells which are not obviously related to salt structures as elucidated by Fig. 7. Originally we expected that downward flow of dense fluids along the salt-dome shoulders would become the dominating driving force. However, the simulation indicates that the main driving force results from the temperature-field disturbances caused by the high thermal conductivity of the salt domes. This is in agreement with the density inversion model derived above from the field data and is further backed by the observation that the velocity fields for fluids of constant density are of similar magnitude. The disturbed temperature field prevents a stable stratification of the fluids.

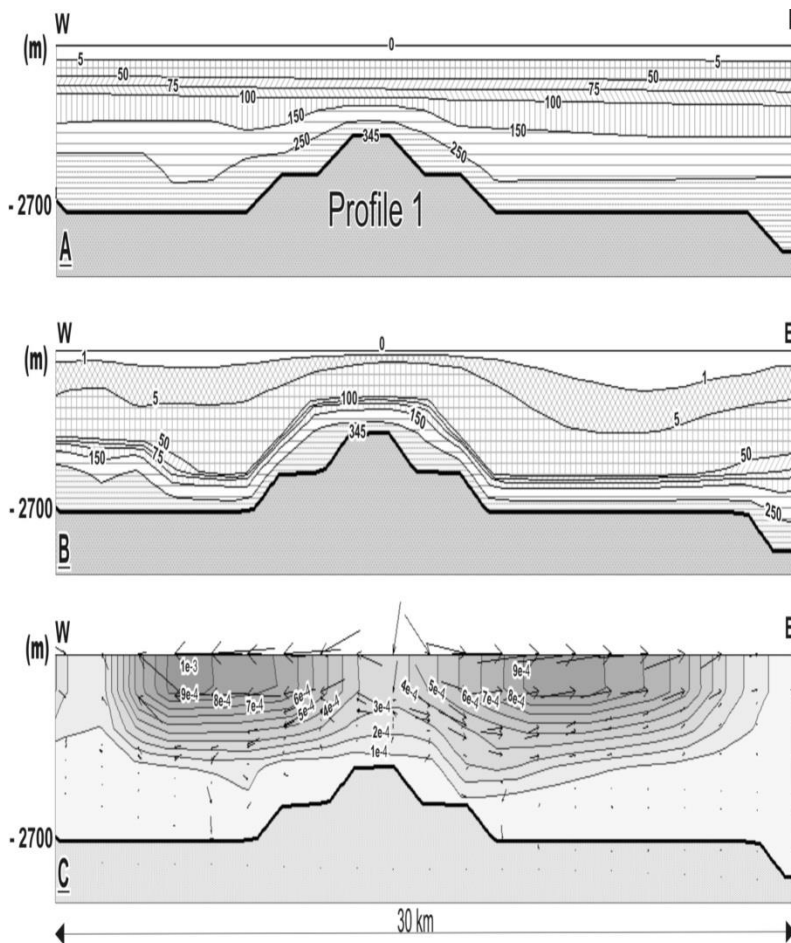


Fig. 8: Detail from Fig. 7 indicated there as Profile 1. A) Initial mass distribution, B) final mass distribution, C) convection pattern with contoured velocities (m/day) and flow arrows.

2.1 Brine migration: deep salt domes

Within the present modeling scenario the dense, highly saline fluids cannot reach the surface because of the simplified upper boundary. However, fluids can leave and enter the model at the upper boundary due to hydrostatic forces caused by the topography. This is a limitation which currently limits the program in terms of true salt brines reaching the surface as observed in the natural system. In addition, the cell size used within the model is a critical factor; however, in combination with the physical parameters like permeability and conductivity attached to the strata. The observed size and form of convective cells may depend on these parameters to some extent but anyway, a convective system is by theory never predictable in all details. The numerical models given here should be taken as indications that convective flow is a highly probable structure to explain the observed data but not as the true solution allowing local predictions.

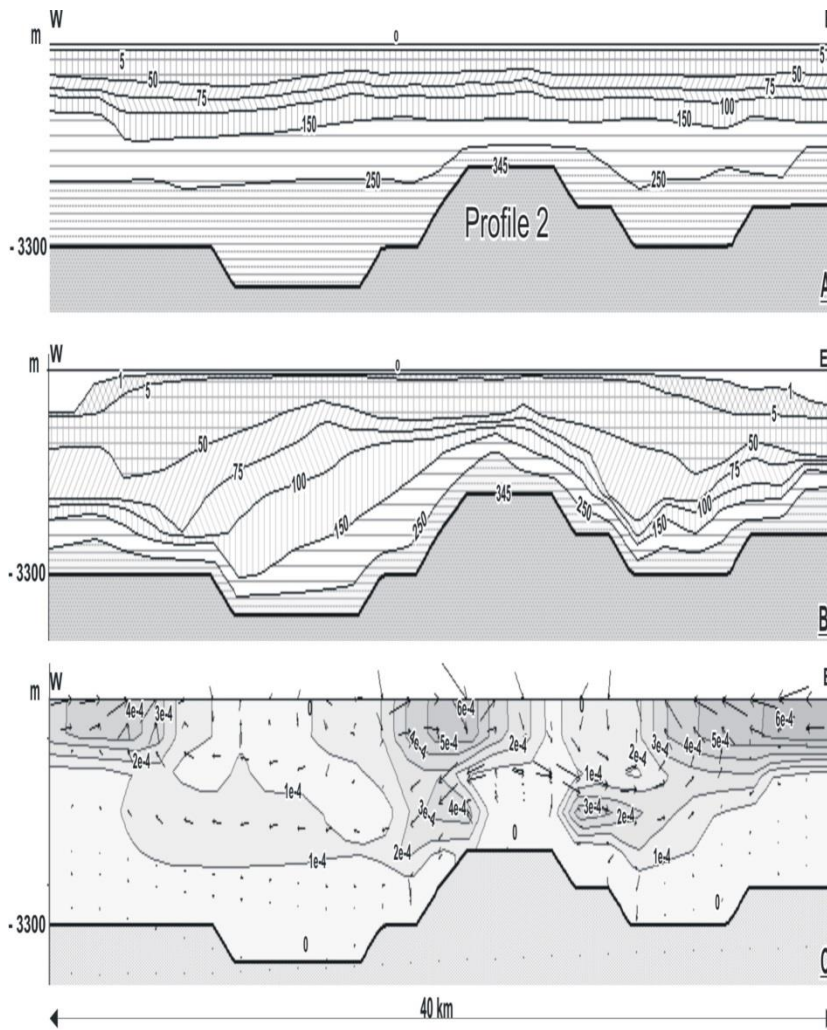


Fig. 9: Detail from Fig. 7 indicated there as Profile 2. A) Initial mass distribution, B) final mass distribution, C) convection pattern with contoured velocities (m/day) and flow arrows.

CONCLUSIONS

The NE German Basin as well as some other areas of the North German Basin are characterized by an inhomogeneous distribution of salt content within the pore water. The available data indicate a hydrostatically instable distribution causing density-driven basin-internal flows. In addition, the data provide evidence for an inversion of the fluid density at greater depth caused by increasing temperature while the fluids are already saturated with salt. In summary, the data point toward possible convective flow in the sedimentary column. 2D-numerical models support this viewpoint, even though relatively low average permeabilities have been chosen for the different strata. While the resulting flows are slow, about 1 to 2 km per 10 ka, they are still sufficient to produce convection on the regional scale considered here and to deform the density stratification. Even if the initial conditions start from homogeneous fluid density throughout the basin, free convection develops and a strong depth gradient in salt content is generated. 3D-models are under progress, however the strong non-linear interaction between temperature, fluid flow and density gradients requires additional efforts in program developments. The results derived so far show that the convection pattern in general are stable, details derived in the convective roles derived from the 2D simulations, however, are modified.

Free temperature-driven convection should therefore be considered among the major factors currently affecting parts of the North German Basin, perhaps even causing salt brines to reach the surface in certain areas. Certainly, convection is not the only driving force. Even in the North German flatland there is some topography inducing hydrostatically driven flows which then interact with the temperature-driven flow. To some extent this interaction has been realized in the numerical models. Furthermore, the different strata are not homogeneous, the physical parameters are laterally varying due to facies differences and diagenetic differences, and the entire sequence may be disturbed locally by faults. There is also evidence that groundwater abstraction provides localized additional effects, however these effects are minor with regard to the area under consideration and the observed and modeled patterns. While these additional effects need to be studied in detail, there is already a very strong indication that temperature-driven convective flow plays an important role in the area under consideration.

ACKNOWLEDGMENTS

This project is supported by the German Science Foundation (DFG) as part of the SPP 1135 “Dynamics of Sedimentary Systems under varying Stress Conditions by Example of the Central European Basin System”. Partly it also has been financially supported by the GFZ-Potsdam with regard to the Finite Volume studies, which have been carried out in a co-operation with the WIAS Berlin. We also acknowledge the help of the “Geologische Landesämter” Berlin (SenStadt Berlin), Brandenburg (LGRB), Schleswig-Holstein (LANU), and the oil and gas company EEG for providing chemical data of subsurface fluids. Last but not least, we thank H.Verweij and anonymous reviewer for their critical comments which helped to improve the manuscript.

Fabien Magri · Ulf Bayer · Christoph Jahnke
V. Clausnitzer · H. J. Diersch · J. Fuhrman
P. Möller · A. Pekdeger · M. Tesmer · H. J. Voigt

Fluid-dynamics driving saline water in the North East German Basin

ABSTRACT

In several areas of the North German Basin saline water comes close to or even reaches the surface. Available data from wells indicate that brine stratification is under unstable conditions in the deeper underground. In order to analyse the possible transport mechanisms 3D thermohaline simulations have been carried out for two different scenarios. The 3D regional model (230x330 km) indicates that salty water is driven to the surface by hydrostatical forces from the surrounding highlands. In addition a smaller scale model (10x10 km) has been constructed with a grid resolution accounting for possible convective flow. The results indicate that convective flow may play a dominant role in areas with minor topography. In summary, the complex pattern of near surface occurrences of saline water probably results from the interaction of hydrostatic and thermal forces.

Keywords

3D thermohaline modeling, regional flow, convective flow, salt springs and pots, sedimentary basins, North German Basin

INTRODUCTION

Solute transport in aquifers is studied for its relevance in socio-ecological issues such as energy self-sufficiency and pollution of the environment. An example is the migration of dissolved halite released by salt structures which are commonly found in many geological formations. In some discharge areas, brackish water reaches the surface. This phenomenon is manifested through the occurrence of salty springs or pools.

Several mechanisms may be responsible for driving the heavier saline water up to the surface. Generally, forced hydraulic convection in combination with high-permeability pathways is assumed in these cases. On the other hand, many studies based on geothermal systems have demonstrated that temperature effects on liquid density can play an important role in driving salt water flow over long distances. This process is often referred to as thermohaline convection (Nield 1968). However the origin of the saline groundwater is still not fully understood.

An interesting example illustrating the fluid dynamics driving saline water in an aquifer is provided by the North-East German Basin (NEGB). During the last two centuries, extensive evidence for rising hot saline waters has been gathered in different regions of this basin. An unsolved feature of these saline springs is their temporal and spatial instability. The locations of the known saline springs in the NEGB (Fig.1, Schirrmeister 1996) correlate with the occurrence of saline groundwater at shallow levels between 0 and 300 m (Grube et al. 2000). In Fig.1 the northern and southern basin margins are also depicted.

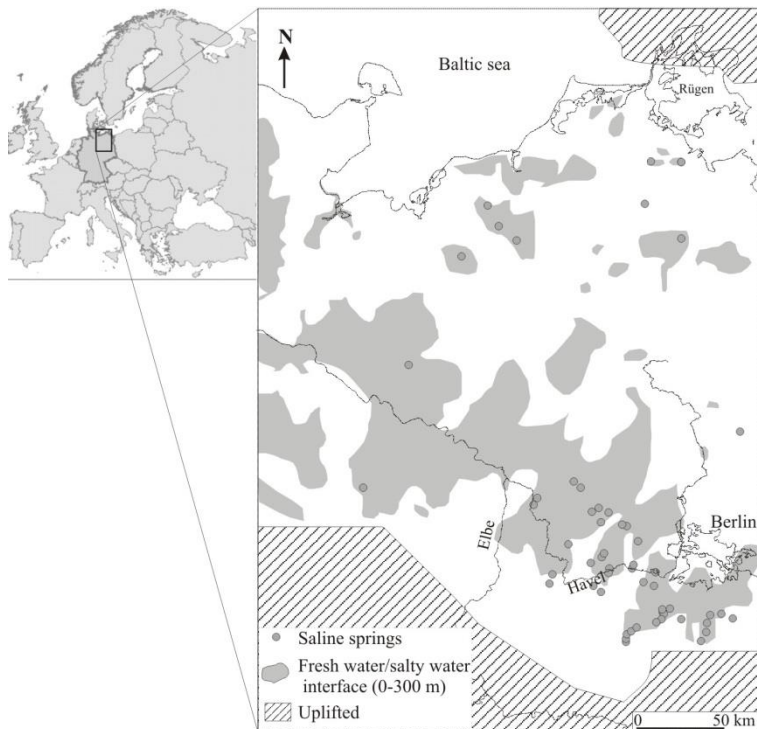


Fig. 1: Study area, location of the observed springs (Schirrmeister 1996) and salty groundwater

In a previous paper (Magri et al. in press), simulations of coupled fluid flow, heat and mass transfer in a cross section through the NEGB indicated the possibility of regional scale

convective flow throughout the basin. The results have revealed that subsurface flow can be driven by thermally induced convection even in the presence of salt dissolution. However, it remained unclear whether the convective regime will be stable in three dimensions and to which degree the convection cells are directly related to salt structures.

Here, a three-dimensional analysis will be carried out in order to clarify which mechanisms underlie salt transport in the NEGB. Indeed, the observed solute distribution at the surface cannot be inferred from two-dimensional analysis alone.

Therefore, the main goal of this paper is to illustrate results obtained from three-dimensional thermohaline simulations in order to delineate the types of fluid-dynamics occurring in the NEGB. Studies of this kind are of fundamental importance for understanding the causes which eventually could supply the observed saline springs.

DATA

Fluid density and physical parameter variations play a primary role in affecting large scale flow in geothermal systems (Straus and Schubert 1977; Wood and Hewett 1982; Rosenberg and Spera 1990; Person et al. 1996). Specifically, wide temperature differences and fluctuations in chemical composition are often encountered, giving rise to different dynamic system scenarios. Furthermore, the geological strata provide in itself an inhomogeneous system in terms of physical parameters and chemical composition. Therefore, reliable simulations of coupled fluid flow, heat and solute transport in sedimentary basins require the integration of:

- reliable fluid density data,
- geological input data including the spatial aquifer characteristics as well as the physical flow parameters for each layer of the basin (porosities, permeabilities, heat conductivity and heat capacity).

The fluid density model for the NEGB is based on a collection of data which include in-situ measurements of temperature and fluid pressures, as well as laboratory measurements of solute and salt content. Effects of temperature and pressure variations on the fluid density are also taken into account (Bayer et al. in press).

Fig.2 illustrates the topography of the top Zechstein Salt which has been derived from the geological input data (Scheck 1997) and the distribution of saline groundwater (depicted with shaded patterns) as shown in Grube et al. (2000). Grey filled circles locate the position of the observed springs (Schirrmeister 1996). The main brine pattern slants across the study area stretching from the western part to the south-eastern area near Berlin. In addition, isolated brine formations can be observed in the northern and western part of the study area.

2.1 Brine migration: deep salt domes

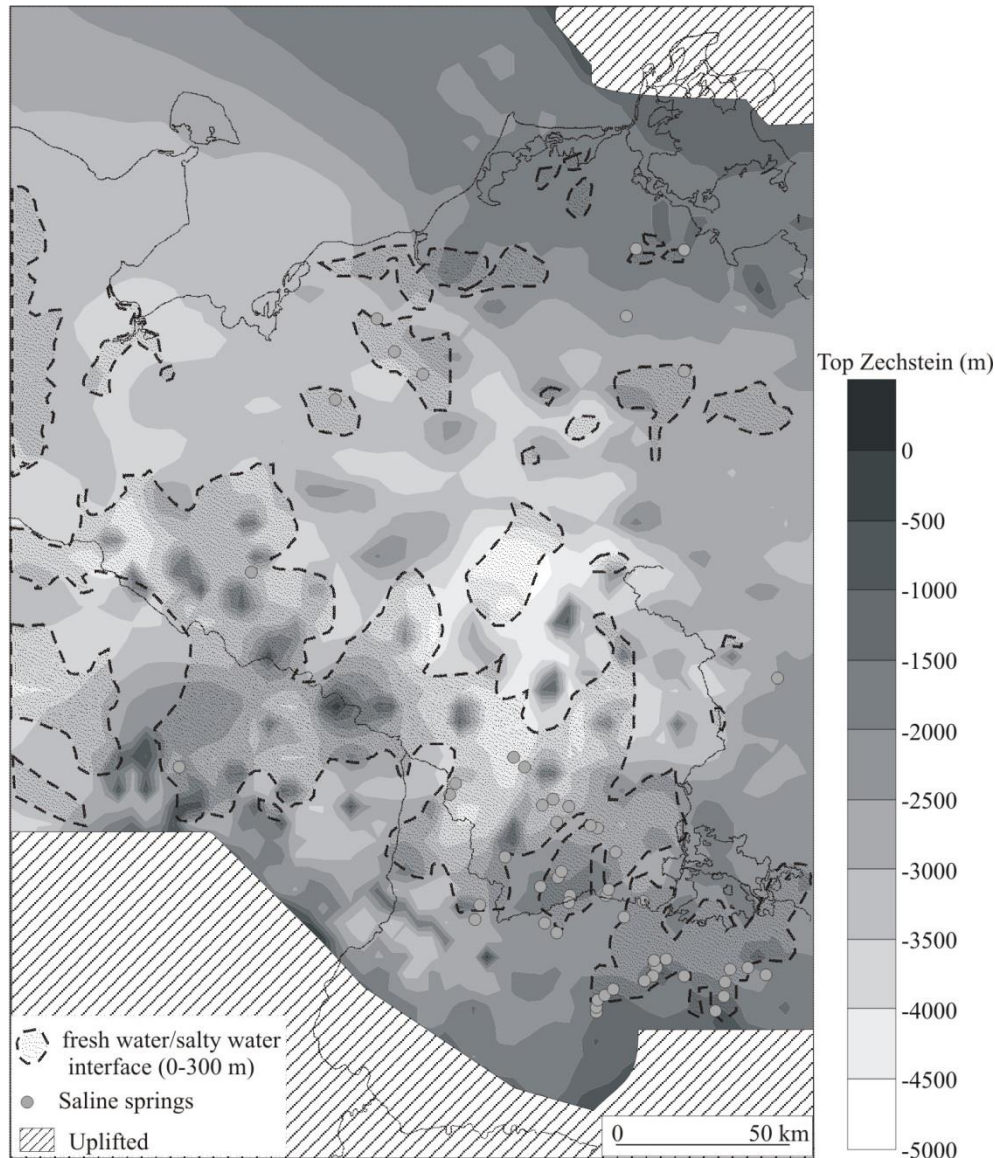


Fig.2: Top Zechstein depth map (Scheck 1997), location of the observed springs (Schirrmeyer 1996) and salty groundwater interface (Feyerabend et al. 2000).

In Fig.2, dark patches show the occurrence of salt domes while light grey areas are associated with salt pillows. It can be seen that in numerous areas of the NEGB salt diapirs have penetrated upward through the sediment fill. It appears that no obvious spatial correlation can be inferred between salt structures and near surface salt occurrences. Brine patterns are also found far away from salt dome crests. This observation suggests that the regional groundwater flow plays an important role in driving solute. The discharge area of brackish waters is concentrated in the south-eastern part of the NEGB. In fact, the majority of the saline springs are observed in the neighbourhood of the Havel river and to the south of Berlin. Only few are encountered far from these locations.

2.1 Brine migration: deep salt domes

In this paper, the brines are assumed to be pure NaCl-solutions. For the brines within the Mesozoic strata this assumption provides a sufficient approximation. Fig.3 illustrates the density/depth relation in the Buntsandstein. The square dots represent the density values obtained from laboratory analysis measured at room temperature. The interpolated average trend is illustrated by the grey line, while the approximated in-situ density is distinguished by the bold black line.

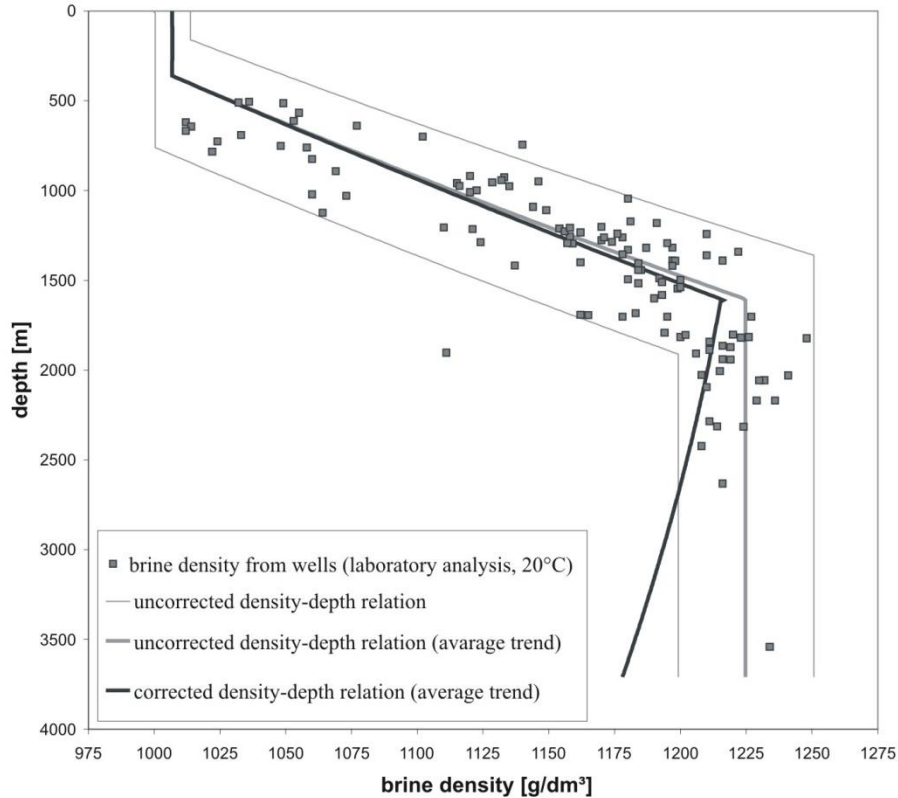


Fig. 3: T-p corrected in-situ brine densities for the Buntsandstein (modified from Bayer et al. in press).

In average, the fluid density increases linearly with depth, although with some scatter. At approximately 1.5 km depth the NaCl saturation is reached and the density remains close to 1220 g/dm³. For the determination of the in-situ densities a temperature and pressure correction of the laboratory data was performed. For this purpose an iteration procedure was carried out. Based on the assumption of a simple temperature model and hydrostatic conditions, temperature-corrected densities and pressures were calculated. The temperature model considers only a depth dependency of the temperature (no spatial variations). A thermal gradient of 35 °C/km was assumed for the Mesozoic strata in agreement with geothermal data (Hurtig 1994). In order to obtain the complete fluid density model, the technique illustrated above was applied to each layer of the basin.

In Fig.3 the corrected density/depth temperature relation indicates that the density decreases with increasing depth after saturation has been reached. The inversion of the density/depth

2.1 Brine migration: deep salt domes

trend is due to the thermal expansion of the fluid. At depth of mass saturation, temperature effects dominate and increase the brine volume, leading to a decrease of density.

As shown in Bayer et al. (in press), the NaCl saturation (i.e. the inversion point) in the stratigraphic layers is reached at different depths. Within the Cretaceous to the Keuper this effect occurs at depths below 3.500 m. That means that in greater depth lighter brines occur than in lower depth and convective flow are likely favoured at least on local scales. Moreover it was also found that the centre of the basin contains fluids with lower density surrounded by a ring of denser waters. This effect becomes stronger with depth and it is more distinctive at the base of the Buntsandstein.

Summarizing, the data point toward a profile sensitive to temperature variations which will be highly unstable in the deepest stratigraphic units. Consequently, it is reasonable to presume that thermal buoyant effects are among the major driving forces eventually generating convective cells. Whether this particular fluid-dynamics is the only one characterizing upward solute transport in the NEGB will be investigated in our numerical simulations by incorporating the density features just described.

The incorporated geological input data are derived from a three-dimensional structural model of the NEGB (Scheck 1997; Scheck and Bayer 1999). The area covered by the model is approximately 230 x 330 km in the horizontal extension and 30 km in the vertical direction which consists of 13 layers of the sedimentary fill. The physical parameters assigned to each sedimentary layer were those given by Scheck (1997, Tab.1). The physical properties considered within each layer are constant. This first rough aquifer model differentiates only the stratigraphic layers of the model without any spatial variation. The development of a detailed aquifer model with spatial variations of porosities, permeabilities, etc., corresponding to the collected petrophysical data is the aim of further research. Furthermore, local faults are not included.

Since the study of convective flow beneath the Zechstein Salt layer is not the purpose of this paper, the implemented model comprises the top eight layers of the NEGB (from Top Cainozoic down to the bottom Zechstein Salt) and of an additional impermeable basement layer located at 5 km of depth acting as the model basement. Nevertheless, results derived from geologically realistic simulations (Sarkar et al. 1995) showed that free thermohaline convection beneath salt sheets can also be considered a significant mechanism for salt dissolution.

By comparing the hydraulic permeability of the Middle Triassic (Muschelkalk) with those of the above sediments, (Tab.1) it turns out that the value is five orders less than the average. Therefore it can be inferred that this stratigraphic formation behaves as a quasi-impervious unit. The Muschelkalk is mainly dominated by fine grained carbonates. Particularly, in the central part of the basin, it contains evaporitic layers of salt rock up to some decametres with very low permeabilities. This impervious unit leads to a separation of the Post-Permian strata in two

aquifer systems with different hydrochemical and hydrodynamical characteristics (Lower Triassic and from upper most Middle Triassic to Cretaceous) which can also influence the fluid-dynamics within the basin.

MODELING APPROACH

The governing equations of thermohaline convection in a saturated porous media are derived from the conservation principles for linear momentum, mass and energy (e.g. Bear 1991; Kolditz et al. 1998; Nield and Bejan 1999). The resulting system is fully implemented in FEFLOW® and is briefly reported here by the following set of differential equations:

$$S_0 \frac{\partial \varphi}{\partial t} + \text{div}(\mathbf{q}) = Q_{\text{Boussinesq}} \quad (1)$$

$$\mathbf{q} = -\mathbf{K} \left[\mathbf{grad}(\varphi) + \frac{\rho_f - \rho_{0f}}{\rho_{0f}} \right] \quad (2)$$

$$\frac{\partial \phi C}{\partial t} + \text{div}(\mathbf{q}C) - \text{div}(\mathbf{D} \mathbf{grad}(C)) = Q_c \quad (3)$$

$$\frac{\partial}{\partial t} \left((\phi \rho_f c_f + (1 - \phi) \rho_s c_s) T \right) + \text{div}(\rho_f c_f T \mathbf{q}) - \text{div}(\lambda \mathbf{grad}(T)) = Q^T \quad (4)$$

Eq.(1) is the equation of fluid mass conservation. S_0 is the medium storativity, φ is the hydraulic head. \mathbf{q} is the Darcy (or volumetric flux density) velocity defining the specific discharge of the fluid. $Q_{\text{Boussinesq}}$ is the Boussinesq term which incorporates first order derivatives of mass-dependent and temperature dependent compression effects. The Darcy's law is expressed by Eq.(2) where \mathbf{K} is the hydraulic conductivity tensor. Eq.(3) is the equation of solute mass conservation where ϕ is the porosity of the porous medium, C is the mass concentration, \mathbf{D} is the tensor of hydrodynamic dispersion and Q^c is a mass supply. Eq.(4) is the energy balance equation of the fluid and the porous media. c_f and c_s is the heat capacity of the fluid and solid respectively, T is the temperature, λ is the thermal conductivity of the saturated porous medium as a whole.

Constitutive and phenomenological relations of the different physical parameters involved in the equations are needed to close this coupled system. Here the hydraulic conductivity relation and the Equation Of State (EOS) for the fluid density are recalled:

$$\mathbf{K} = \frac{\mathbf{k} \rho_{0f} g}{\mu_f(C, T)} \quad (5)$$

2.1 Brine migration: deep salt domes

$$\rho^f = \rho_0^f \left(1 - \bar{\beta}(T, p)(T - T_0) + \bar{\gamma}(T, p)(p - p_0) + \frac{\bar{\alpha}}{C_s - C_0}(C - C_0) \right) \quad (6)$$

The hydraulic conductivity tensor \mathbf{K} is related to the reference fluid density ρ_{0f} , g is the gravitational acceleration, \mathbf{k} is the tensor of permeability, $\mu_f(C, T)$ takes into account the fluid viscosity effects due to temperature and concentration variations. The EOS for the fluid density (Eq.(6)) is related to the reference temperature T_0 , pressure p_0 and concentration C_0 . $\bar{\alpha}$ is the mass concentration ratio, $\bar{\beta}(T, p)$ is the coefficient of thermal expansion and $\bar{\gamma}(T, p)$ is the coefficient of compressibility.

The flow and transport equations (Eq.(2), Eq.(3), Eq.(4)) for thermohaline convection are non-linear and strongly coupled since temperature and salinity control the fluid density ρ^f and dynamic viscosity μ_f . The variation of fluid density is essential for the modeling of thermohaline convection because of its primary importance for calculating the correct buoyant force included in the equation of motion (i.e. generalized Darcy's law Eq.(2)). Fitted polynomial expressions are commonly used for temperature, pressure and salinity dependences of the fluid density (Sorey 1976). In order to reproduce the density model, all the mentioned dependences are accounted for FEFLOW. For this purpose, two polynomial expressions which accurately represents the coefficient of thermal expansion $\bar{\beta}(T, p)$ and compressibility $\bar{\gamma}(T, p)$ for the fluid density (Eq.(6)) have been derived and coded as an extension to the simulation program. A detailed description of these polynomial functions and the implemented code is reported in Magri (2004). The density of the saturated brine is 1220g/L. The fluid density ρ_f^0 is referred to freshwater conditions and set equal to 1000 g/L. Therefore the density ratio $\bar{\alpha} = \frac{\rho_f^s - \rho_f^0}{\rho_f^0}$

appearing in Eq.(6) is set equal to 0.22.

A fully implicit scheme is used to advance the system of partial differential equations in time. In order to gain insights into the evolution of the studied system, a reasonable computing time interval has to be set. For the problem considered here, such an interval is strictly artificial, having no relation to any geological timescale. Based on the specific model settings, the 3D thermohaline steady state solutions are achieved at approximately 200 ka. Indeed, long term calculations did not indicate a significant variation in the calculated patterns. Therefore, a computing time period of 200 ka can be considered large enough for an evolution analysis of the system. When a time scale will be mentioned in the description of the results, it will be referred to as computing time with no regard to a particular geological timescale.

Two model scenarios are illustrated: first, a thermohaline simulation for the whole study is presented and then, due to specific cell resolution requirements, the domain of interest has been restricted to a square box of approximately 10 km length. An analysis of the interaction

between temperature and mass field derived from the simulations will suggest potential causes for the development of brine plumes even in those areas where no salt domes are present. Evolution analysis of the calculated mass, temperature and velocity field have also been derived by extracting a profile crossing the area.

General assumptions

Since our main goal is to understand convective flow in the system, a number of simplifying assumptions are required:

It is assumed that the dispersive flux of solute is governed by the Fickian law without mechanical dispersion, i.e. the coefficient of hydrodynamic dispersion is equal to the molecular diffusivity of solute in the saturated porous medium. Such a simplification may introduce differences in the resulting solute field (Nield 1974; Rubin 1975), but it does not affect the basic character of the fluid dynamics of the system (Rosenberg and Spera 1992a).

The variation of fluid properties is essential for hydrothermal convection because of its primary importance for calculating the correct buoyant force included in Darcy's law. Indeed, Straus and Schubert (1977) proved that thermal convection within a saturated porous medium is much more unstable than it would be if the fluid is considered having constant properties. Fitted polynomial expressions are commonly used for temperature, pressure and salinity dependences of the fluid properties (Sorey 1976). In order to reproduce the spatial density model, the dependences are incorporated by a polynomial expression which accurately represents the equation of state. A detailed description of the implemented equation can be found in Bayer et al. (in press) and Magri (2004).

At the present state, other fluid properties such as heat capacity and viscosity are considered constant. Since an increase in temperature leads to a decrease in viscosity, it follows from Rayleigh's theory that viscosity will enhance thermal convection especially in the deeper layers of the system where high temperatures are expected. On the other hand, all the layers of our model have overcritical Rayleigh numbers. Therefore, by neglecting fluid viscosity variations, the magnitude of the flow regime will not be affected.

Boundary and initial conditions

In earlier simulations (Bayer et al. in press), a zero mass concentration boundary was imposed on the topography, thereby preventing dissolved solute from reaching the surface. Here thermohaline fluid flow simulations are carried out with a surface permeable to solute and heat transport (natural boundary conditions).

The boundary and initial conditions used for both model scenarios (large and square box model scenario) are the following:

- At the surface, head, solute and temperature boundaries are prescribed. The head is fixed to the local topographical elevation, except in the sea area where its value is set

2.1 Brine migration: deep salt domes

equal to the water depth. The solute is allowed to reach the surface by prescribing a Cauchy boundary condition. Because sea water intrusions into the aquifer are not of primary interest, no salinity conditions are taken into account in the sea area. However, observed data (Grube et al. 2000) show that sea water intrusions locally influence the coastal aquifer. Concerning the temperature, at the surface a Cauchy boundary condition is used as well. Both solute and temperature boundary conditions at the surface are discussed in more details afterwards.

- At the basement a constant temperature boundary condition is defined. The value is set to 150 °C. In contrast to the fluid density model (Fig.3), this value corresponds to a linear vertical gradient of only 30 °C/km. This gradient provides a lower limit for instable stratification.
- In the model, the top of the salt layer is considered impervious to solute flux, and the brine concentration is set to 345.2 g/l, an approximate value for halite saturation at the depth of interest. Even though salt dissolves with time and produces brine, the shape of the salt layer does not change. Ranganathan and Hanor (1988) made a similar assumption for salt domes.
- The lateral boundaries are closed to fluid, heat, or mass flow.

In the NEGB the advected solute can flow out of the basin through the upper surface. For that reason, an open boundary condition allowing solute outflow (i.e. permeable) is needed at the top surface of the model domain. This boundary condition, referred to as Cauchy type boundary condition, is defined by the following relation:

$$\mathbf{q}_c(t) = -\Phi_c(C^* - C)\mathbf{n} \quad (7)$$

where \mathbf{q}_c is the solute flux, Φ_c is a mass transfer coefficient, C^* is the prescribed boundary condition value for the solute concentration C at the surface, and \mathbf{n} is the vector normal to the top surface of the domain. By setting a natural boundary condition for the solute at the top slice of the model, the concentration C is solved at each node of the boundary: a solute flow through top surface of the domain is computed. The transfer coefficient Φ_c appearing in Eq.(7) can be regarded as a leaching parameter which governs the mass flux through the boundary. The mass transfer is a numerical coefficient allowing the definition of an open boundary condition in the form of Eq.(7) rather than a real measurable parameter. Nevertheless a reasonable value of the mass transfer coefficient can be estimated by rewriting Eq.(7) in a Fickian form, viz.:

$$q_c(t) \approx -D_{\text{leak}} \frac{C^* - C}{d} \quad (8)$$

2.1 Brine migration: deep salt domes

where d is the thickness of a thin stratum in contact with the top surface of the domain through which the solute leaches. The mass transfer coefficient then becomes:

$$\Phi_c \approx \frac{D_{\text{leak}}}{d} \quad \text{in } [m s^{-1}] \quad (9)$$

where D_{leak} is a representative molecular diffusion coefficient of the thin stratum. D_{leak} can be considered more or less equal to the molecular diffusivity of the bordering stratigraphic unit (i.e. Cenozoic, $D_{\text{leak}} \approx 2 \times 10^{-9} m s^{-2}$). A stratum thickness in the range of a meter can be regarded as relatively thin with respect to the basin scale. Hence from Eq.(9) $\Phi_c \approx 2 \times 10^{-9} m s^{-1}$. The prescribed surface boundary condition c^* has been set equal to the reference concentration value, i.e. freshwater, $c^* = 0 \text{ g/L}$.

Since in thermohaline convection solute and thermal effects are strongly dependent, an open boundary condition allowing heat outflow trough the domain surface has to be defined in analogy to the mass outflow (Eq.(7)):

$$\mathbf{q}_T(t) = -\Phi_T(T^* - T)\mathbf{n} \quad (10)$$

where \mathbf{q}_T is the heat flux, Φ_T is a heat transfer coefficient, T^* is the prescribed boundary condition value for the temperature T at the surface, and \mathbf{n} is the vector normal to the top surface of the domain. As for the mass transfer coefficient (Eq.(9)), the heat transfer coefficient Φ_T can be estimated by rewriting Eq.(10) in a Fourier form, viz.:

$$q_T(t) \approx -\lambda_{\text{tr}} \frac{T^* - T}{d} \quad (11)$$

where d is the thickness of the heat transition layer. The heat transfer coefficient becomes:

$$\Phi_T \approx \frac{\lambda_{\text{tr}}}{d} \quad \text{in } [J m^2 s^{-1} K^{-1}] \quad (12)$$

where λ_{tr} represents a heat conduction coefficient of a thin transition stratum. λ_{tr} can be considered more or less equal to the thermal conductivity of the bordering stratigraphic unit (i.e. Cenozoic, $\lambda_{\text{tr}} \approx 1.5 J m s^{-1} K^{-1}$, Table 1.1). Assuming that surface heat and mass transfer occurs in the same thin stratum in contact with the top surface, $d \sim 1 \text{ m}$. Hence from Eq.(12) it results $1.5 J m^2 s^{-1} K^{-1}$. The prescribed surface boundary condition T^* has been set equal to the reference temperature value at the surface, i.e. $T^* = 8 \text{ }^\circ\text{C}$.

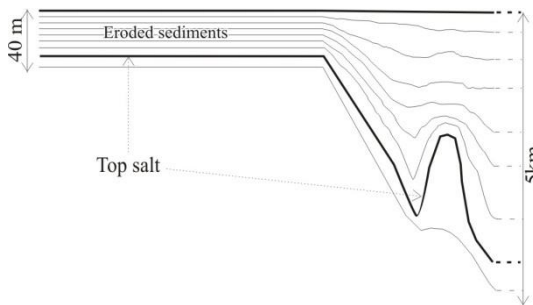
The simulation of transient flow requires the knowledge of a physically meaningful initial condition which can be obtained from a steady-state calculation. Furthermore, using initial conditions derived from steady-state solutions of the considered problem guarantees a higher stability of the simulations and increases the rate of convergence of the coupled equations.

Therefore, initial pressure and temperature conditions of the model are obtained from steady-state solutions for fluid flow and heat transport, respectively. On the other hand, the initial salt concentration was set to zero everywhere above the Zechstein.

LARGE SCALE MODEL SCENARIO

The study area covers 230 x 330 km in the horizontal and 5 km in the vertical direction. The model scenario has been subdivided into a 3D finite-element mesh composed of triangular prisms. The defined grid provides an horizontal cell resolution of approximately 2.5 x 2.5 km while the vertical resolution is variable depending on the thickness of the layers. Specifically 340,000 nodal grid points are used to discretize the balance equations of the numerical model. The mesh allows to incorporate the provided geological model into the FEFLOW database. Furthermore, the resolution ensures to keep computational time at a reasonable level.

The choice of triangular cells has been dictated by the need for adapting the grid to the irregular shape of the natural boundary conditions imposed by the northern coast line and the basin margins. Especially at the southern margin the sedimentary fill does not exceed a total thickness of 40 m as shown schematically in Fig. 4.



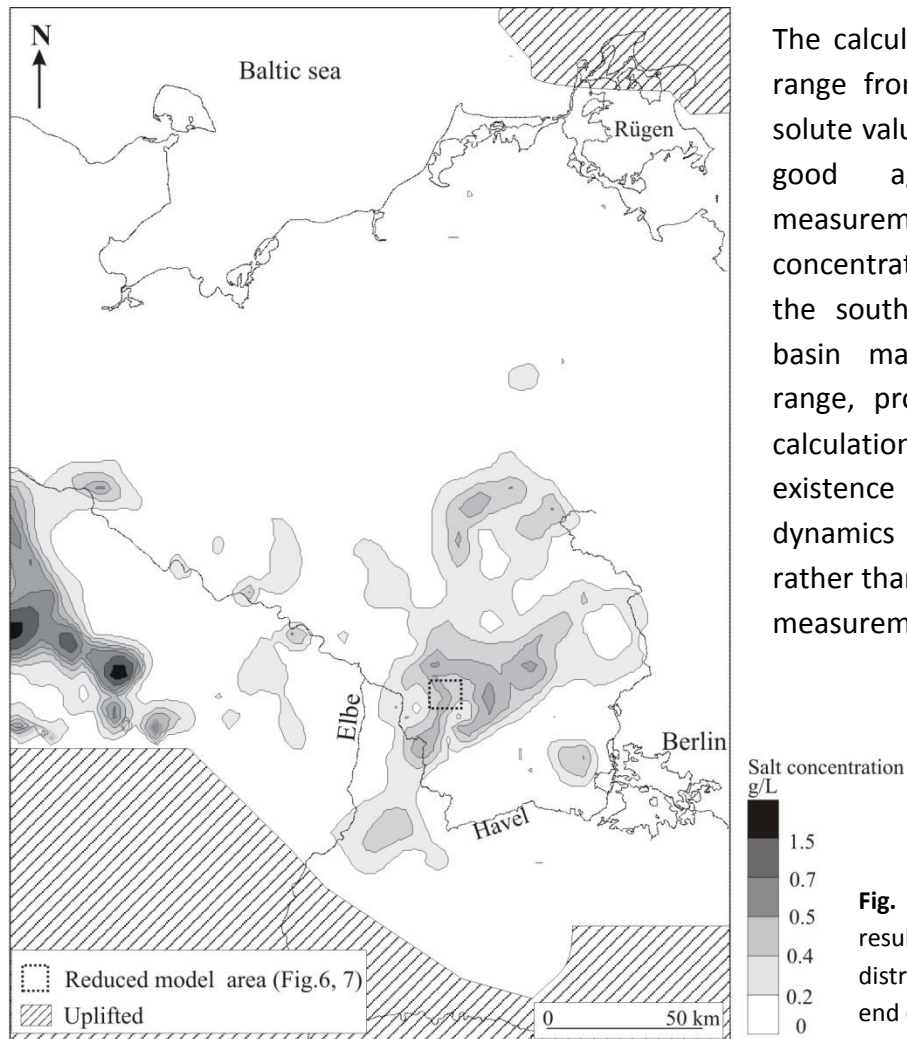
These regions are uplifted: fluid flow and mass transport play a minor role. In order to represent these no-flow zones in our numerical model and to preserve the 3D geological structure, as well as the natural boundary conditions, very low permeability and diffusivity values (close to zero)

Fig. 4: Sketch of the geological structure near the uplifted layers area.

are assigned throughout the uplifted areas. Hence, the calculated flow rates are almost equal to zero in these areas.

Fig.5 shows the calculated salinity of the pore water reaching the surface at the end of the simulation run. The results indicate two wide areas where dissolved halite reaches the surface. A first plume extends over 100 km approximately, from the western limit of the study area to the southern basin margin while the other develops west of Berlin stretching over 140 km in the north-south direction. Few isolated and smaller patterns of salty water reaching the surface (of the order of 10 km length) can also be observed along the Elbe river between the two main plumes and close to Berlin.

2.1 Brine migration: deep salt domes



The calculated mass concentrations range from fresh water (0 g/l) to solute values of 1.5 g/l, which are in good agreement with field measurements. The highest salt concentrations can be observed in the south-western area, near the basin margin. The concentration range, provided by the numerical calculations, points towards the existence of intrinsic system dynamics (i.e. upward brine flow) rather than calibrated results solving measurements.

Fig. 5: Large scale model scenario results. Calculated mass distribution at the surface at the end of the simulation run.

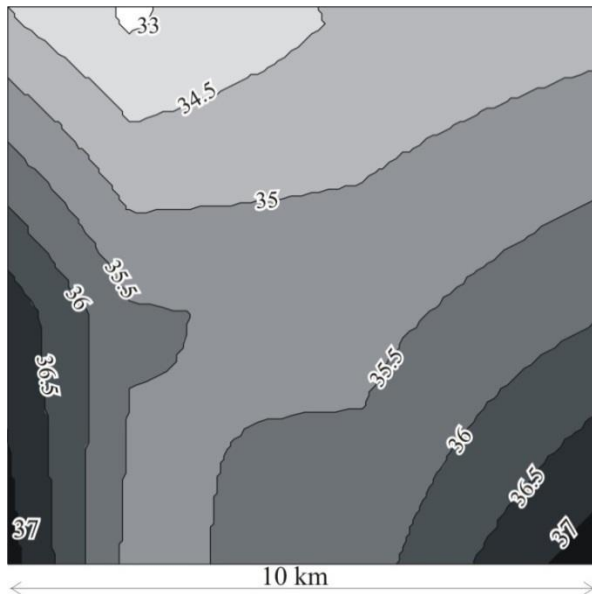
A comparison of Fig.5 with Fig.1 reveals similarities between the calculated salinity plumes at the surface (Fig.5) and the saline groundwater distribution as compiled by Grube et al. (2000) from field data, (Fig.1). In particular, in the south-western area (from the Elbe river to the basin margin) and in the central part of the basin the calculated brine patterns (Fig.5) are in agreement with the observed data (Fig.1). The data compiled by Grube et al. (2000) account for groundwater salinity profiles from the surface to a depth of 300 m whereas the numerical model provides solute distribution at the surface. Therefore the areas of Fig.5, which do not compare favourably with observations (Fig.1), likely correspond to the occurrence of brines at deeper levels. Observations as well as modeling results indicate that hydrostatic flow probably provides the dominant mechanism in the lowlands along the Elbe river.

Simulations of coupled fluid flow and solute transport, without temperature input, provide the same surface brine patterns as obtained from the thermohaline simulation. The reason is that the selected grid resolution is not fine enough to account for thermohaline effects. In order to quantify temperature effects, a higher cell resolution is required. Further mesh refinements

have revealed a dramatical increase in computational time for the bulk calculations of the numerical balance equations. Therefore within the given modeling framework, a higher density of active nodes cannot be realised for the large scale model together with long time simulations. Consequently, it is necessary to reduce the area of the study model in order to define a highly refined grid adapted to thermohaline convective flow.

SQUARE BOX MODEL SCENARIO

The location of the detailed model is indicated in Fig.5. The area covers a square box of 10 km length. The location has been chosen because it is situated within one of the identified brine plumes reaching the surface, as shown in Fig.5. Moreover, in this site, no diapir is enclosed. Fig.6 illustrates the topography of the study area without significant variation. Consequently, local hydrostatically driven flow should not be the primary force. Moreover, owing to the closed lateral boundary conditions, the supra-regional flow resulting from the “large scale model scenario” is not taken into account. Therefore, the simulation results of the square box model are indicative for temperature effects (free thermohaline convection).



The domain has been subdivided into a rectangular mesh containing 34 x 34 grid points, resulting in a cell resolution of 290 m. Both initial and boundary conditions are those used in the previous model scenario.

In order to provide an evolution analysis, solutions of the coupled balance equations will be shown at a computing time of 30 ka and at the end of the simulation run (200 ka).

Fig. 6: Topography (m) of the reduced model scenario.

Within the computing time interval, the onset of convective flows arises approximately at $t = 30$ ka while a stationary regime is approached at 200 ka. At this point it is worth recalling that these time steps are not referred to any geological timescales but present computing time steps.

Fig.7 shows the calculated solute (g/L) and temperature ($^{\circ}\text{C}$) distribution at the surface of the model area at $t = 30$ ka (a) and at the end of the simulation run (b). Solute and thermal plumes occur at the surface occupying identical regions. As time progresses, the plumes persist, however, they stretch over a longer distance. High salt concentrations correlate with increased surface temperature.

2.1 Brine migration: deep salt domes

These simulations highlight two significant aspects of the flow regime:

- If the temperature input is removed from the numerical calculations, no saline water reaches the surface.
- The peak concentration calculated at the end of the simulation run is two times higher than the concentration observed at the onset of the process. The temperatures span approximately the same range.

These two features of the system can be explained as follows. Without temperature input no solute plumes develop, therefore, it can be inferred that thermal effects on fluid density generate buoyant forces strong enough to overcome the gravity field that keeps heavy brine close to the salt layer.

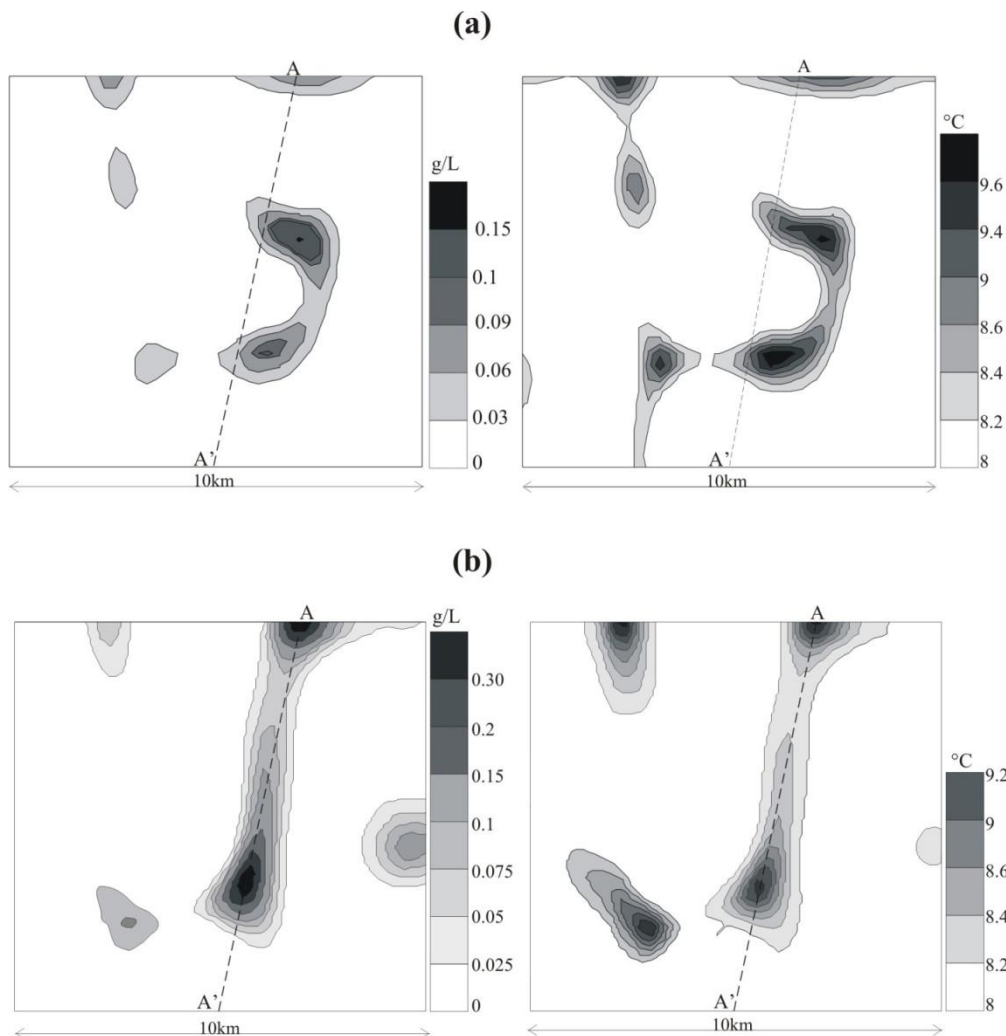


Fig. 7: Reduced model scenario results. (a) Calculated patterns at the surface at t = 30 ka. Left: salt distribution (g/L). Right: temperature (°C) distribution at the surface. (b) Calculated patterns at the surface at t = 200 ka. Left: salt distribution (g/L). Right: temperature (°C) distribution at the surface. Dotted lines indicate the location of the selected cross-section A-A'.

2.1 Brine migration: deep salt domes

Consequently, as time progresses, the brine undergoes a continuous salt replenishment from below by upward solute transport induced by the temperature gradient. Eventually, this process leads to higher concentrations at the surface at the end of the simulation run, partly a result of the closed lateral boundary conditions which prevent outflow. In summary, these results indicate that the deep-seated brine can locally reach the surface driven by induced free thermohaline convective flows.

In order to emphasize the mechanisms driving solute up to the surface, the calculated concentration, temperature and velocity field are extracted at each computing time step along a cross-section (denoted by A-A' in Fig.7). The section of approximately 9,5 km length slices the main brine and temperature pattern obtained at the surface at the end of the 3D simulation run (Fig.7b). In Fig.8a the geological structure along A-A' as well as the finite element mesh are shown. Fig.8b shows the initial temperature profile obtained from a 3D steady state heat transport simulation.

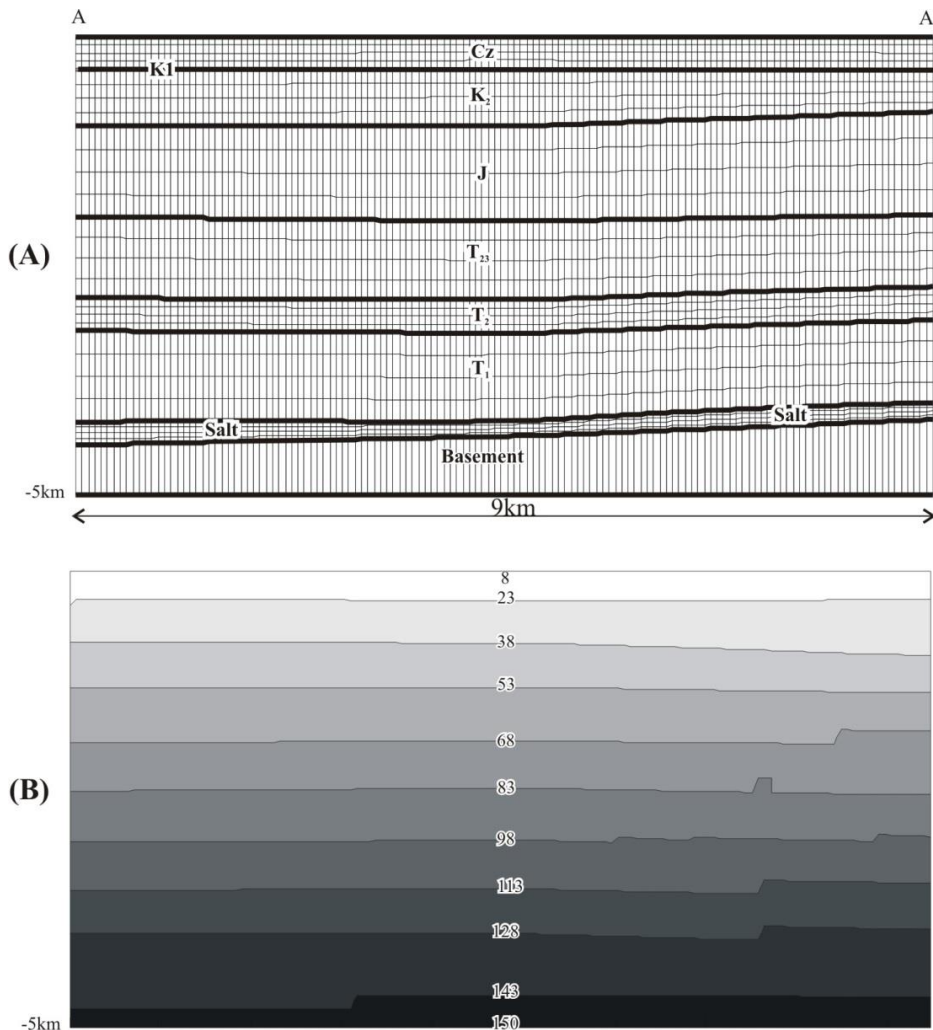


Fig. 8: a) Geological structure (abbreviations given in Table.1) and b) finite element mesh of the selected cross-section as shown in Fig.7.

2.1 Brine migration: deep salt domes

Fig. 9a, b, c respectively illustrate the calculated mass (g/L), temperature (°C) and velocity (m/d) distribution at a computing time of 30 ka. The flow dynamics, thereby, separate into two subsystems (Fig.9a):

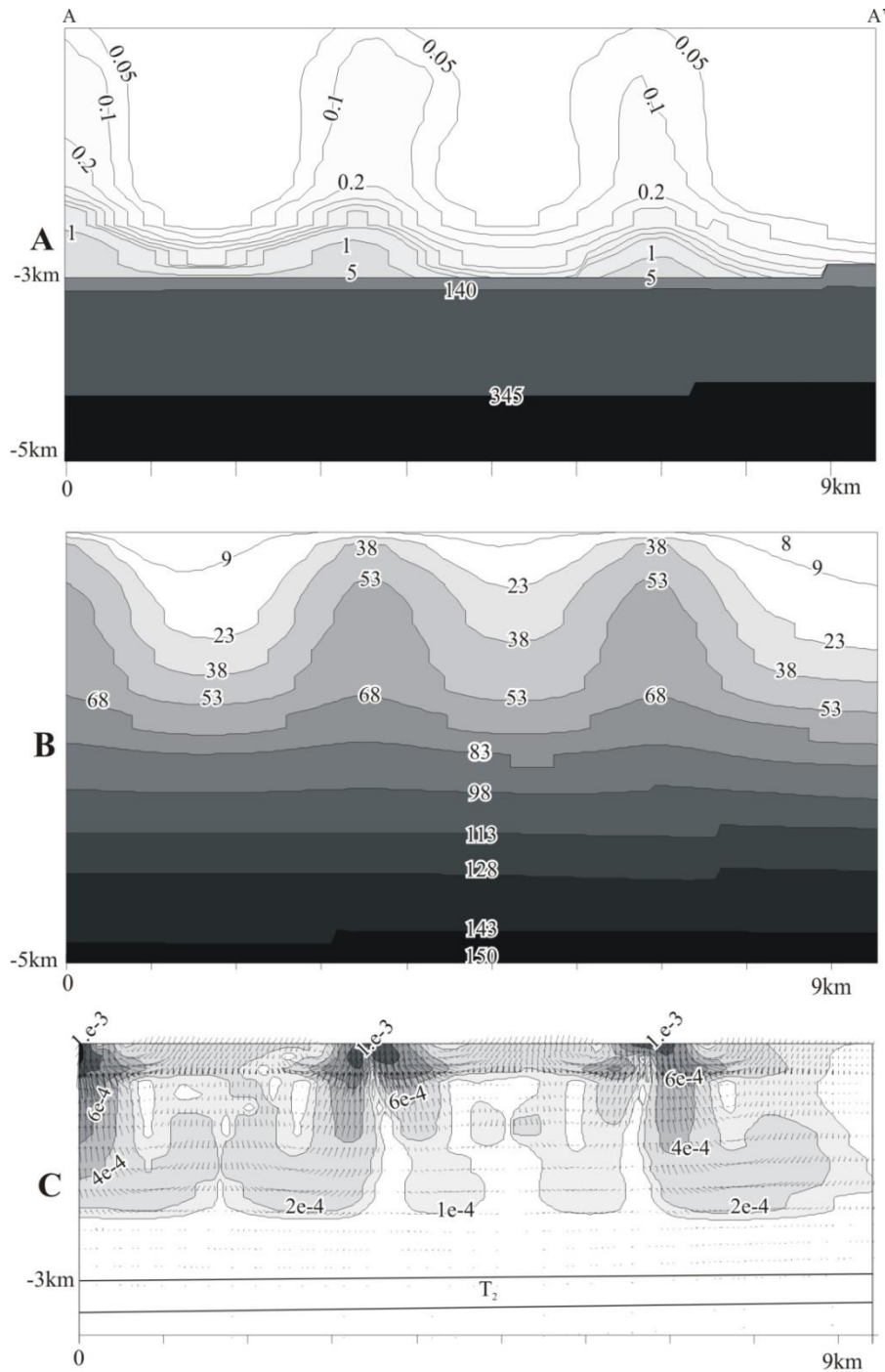


Fig. 9: a) Profile of salt distribution (g/L), b) temperature (°C) and c) velocity field along A-A' resulting from 3D thermohaline simulations at $t = 30$ ka.

2.1 Brine migration: deep salt domes

1: Above the Muschelkalk (located at 3 km of depth), the upward flow is associated with convective transport of dissolved salt which is manifested as salinity plumes protruding throughout the sediments up to the surface. This type of thermohaline convection is often referred to as penetrative. Brine plumes develop as three separated streams forming two well-defined vertically stacked convective cells. The flow field characteristics are in agreement with those derived from theoretical considerations by Rosenberg and Spera (1992). In that study, the authors summarized the various types of dynamics occurring in thermohaline convection in a porous medium heated from below for different sets of initial conditions and buoyancy ratios. Our model scenario corresponds to what they define a “salted from below” boundary condition and “layered box” initial condition at high buoyancy ratio. For this particular configuration, Rosenberg and Spera found that at early computing time the flow field consists of vertically stacked convection cells. In our specific model scenario, the plumes are spaced at about 3 km in the horizontal direction.

2: Below the Muschelkalk the mass transfer is dominated by diffusion. Accordingly, the solute concentration field is not disturbed, showing almost flat isopleths. The interface fresh water/brine is located approximately at 3 km below the surface within the Muschelkalk. This feature can be explained as follows: starting from the initial mass concentration, a transition zone between fresh water and highly concentrated brine develops throughout the Buntsandstein. Due to its very low permeability, the Muschelkalk inhibits the motion and sharply shapes the interface of this transition zone. Accordingly, a very high concentration gradient is formed within this unit.

Fig.9b shows the same system dynamic in terms of temperature distribution: above the Muschelkalk the heat transfer is characterized by protruding plumes reaching the surface locally while at deeper levels heat transfer is dominated by conduction.

By comparing Fig.9a with Fig.9b, an additional feature of the flow dynamic is shown: heat and brine plumes rise together to approximately the same height. In Oldenburg and Pruess (1998; 1999) a detailed explanation of this mechanism is reported which characterizes upward thermohaline convective flows in porous media. Because of thermal retardation due to the heat exchange between the fluid and the solid grains, a density lid is produced which can be seen at the top of the plumes in the concentration profile (Fig.9a).

Fig.9c shows the calculated pore velocities of the convective cells at $t = 30$ ka. Vectors indicate the flow directions. The velocity values range from 37 cm per year in the shallow aquifer to few millimeters per year in the deeper stratigraphic units. The vigour of convective flow decreases by ten orders with increasing depth. This strong velocity contrast is due to the vertical heterogeneity of the layers within the system. Indeed, the shallow aquifer consists of layers which have the highest permeabilities (Table.1). This velocity feature is also confirmed by

2.1 Brine migration: deep salt domes

Rosenberg and Spera (1990), which investigated the role of layered permeability heterogeneities on hydrothermal convection.

A comparison of Fig.9c with Fig.9a and with Fig.9b emphasizes the strong relation between the vigour of upward convective flows and the areas where thermal and solute plumes protrude. Salty water locally reaches the surface where the highest values of temperature and flow velocity are observed.

Fig. 10a, b, c respectively illustrate the calculated mass (g/L), temperature (°C) and velocity (m/d) distribution at the end of the simulation run (200 ka). At this computing time step, the system approaches a steady-state. This feature is once more confirmed by Rosenberg and Spera (1992) which predicted that, the vertical stacked cells observed at early simulation time eventually evolve to a steady-state. However, the closed external boundaries contribute to this effect as mentioned above.

Although the pattern simplifies, the flow regimes persist. The convection pattern is still penetrative but presents only one and a half weak cell. Above the Muschelkalk the concentration and temperature gradients are disturbed by the convective regime while below this stratigraphic unit solute and heat transfer are conductive. The final flow velocities shown in Fig.10c still present higher values in the shallow aquifer, and peak velocity values are observed in those locations of the study area where solute and thermal plumes reach the surface.

Comparison of Fig.10a with Fig.10b shows that the feature of the density lid is still preserved: the highest solute concentrations are at the top of the convection cell at the same height of the heat plumes. It can also be noticed that the density lid promotes lateral flow of the plumes toward A'.

By comparing the isopleths of Fig.10a with those of Fig.9a, it can be inferred that more solute has been advected in the shallow aquifer by upward convective flows. At the end of the simulation run high concentration isopleths come closer to the surface than in earlier phases of the process. Consequently, at the end of the simulation run, the sediments above the Muschelkalk are almost filled with brine and higher concentration values can be observed locally at the basin surface. Therefore the flow velocities will slightly decrease as it can be seen by comparing Fig.10c with Fig.9c. Eventually, some of the weaker convective cells are swallowed up by stronger neighbouring cells. Ranganathan and Hanor (1988) found the same behavior for pore velocities near salt domes.

In summary, the highly refined grid defined for the reduced model scenario allows to account for thermohaline effects. Simulation results prove that temperature effects on fluid density provide buoyancy forces strong enough to generate upward flows driving dissolved halite to the surface.

2.1 Brine migration: deep salt domes

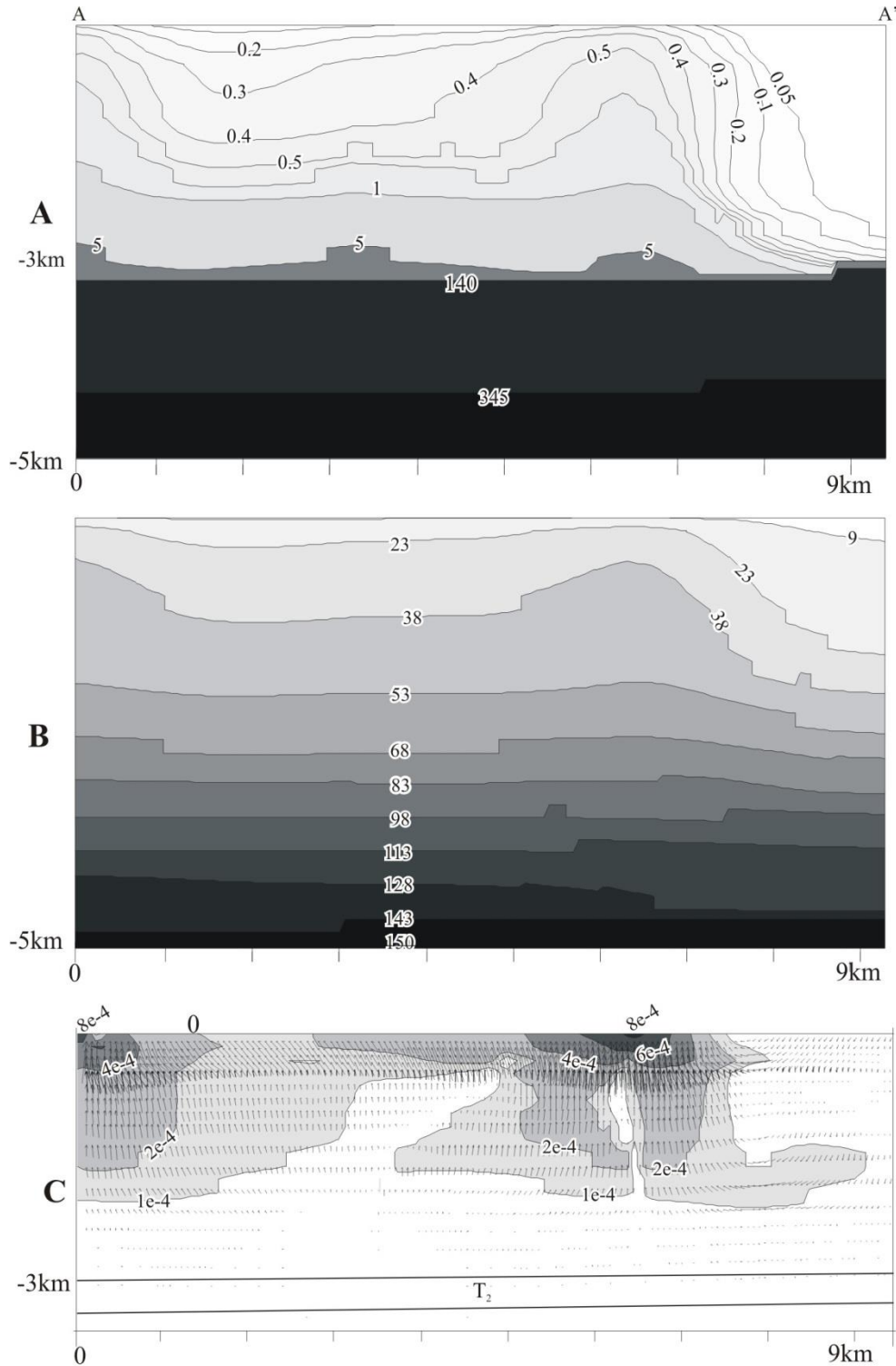


Fig. 10: a) Profile of salt distribution (g/L), b) temperature (°C) and c) velocity field along A-A' resulting from 3D thermohaline simulations at $t = 200$ ka.

Cross-sections of the calculated 3D pattern provide additional insight into the dynamic of the resulting thermally induced flows. Specifically, two major features are found to persist: above the Muschelkalk the vigour of flow is higher and is manifested by convective cells developing

within the sediment fill. On the other hand, below this layer, the system regime is purely conductive. Furthermore, 3D thermohaline simulations emphasize the strong link between concentration and temperature distribution. In both horizontal and vertical direction, thermal and solute plumes always correlate in space and time.

Evolution analysis of the calculated profiles show that dissolved solute continues to fill the shallow aquifer from below as time progresses. Consequently, the increasing concentration weakens the convective cells. Nevertheless, even in the presence of high dissolution rates, the disturbed temperature gradient still generates velocity fields able to drive solute locally up to the surface. Eventually, the system dynamics reaches a steady state favouring lateral directed solute transport.

CONCLUSIONS

The simulation results suggest that two mechanisms play a major role in driving solute within the NEGB. The topographical variations at regional scale can generate hydrostatically driven flow of salty water over large distances. Indeed, no spatial correlation between the location of salt diapirs and the subsurface saline plumes can be inferred from the data. Furthermore, the data show that even at saturation levels the fluid density can decrease with increasing depth due to the effects of higher temperature. Under these conditions, the density stratification is very unstable throughout the basin and the onset of thermally induced convective flows is favoured.

3D numerical simulations of coupled fluid flow, heat and salt transport confirm the observed data. The large model scenario indicates that regional flow is one mechanism driving solute within the basin. Indeed, widely stretched salty plumes spread at the basin surface even without temperature input. The highly refined model scenario additionally accounts for thermohaline effects on the system dynamics. It was found that the patterns are stable even in three dimensions and that the flow regime strongly depends on the basin lithology. Above the Muschelkalk plumes of thermally dissolved salt protrude throughout the sediments fill and reach the surface locally whereas conductive heat and solute transport dominates the deeper part of the basin. The reduced model scenario emphasizes that even without salt diapirs the temperature gradient can be disturbed. Consequently upward solute transport is also possible above flat salt structures due to the resulting thermally induced flow.

Therefore, hydrostatically driven fluid flow and thermohaline convection can be considered among the major mechanisms currently affecting parts of the NEGB, probably even giving rise to the observed saline springs. Like in all hydrothermal systems, the different strata are not homogeneous within the NEGB. The physical parameters are laterally varying due to facies differences and diagenetic differences, and the entire sequence is in many places disturbed by faults.

2.1 Brine migration: deep salt domes

While these additional effects need to be studied in detail, the modeling results already provide strong indication that regional flow and temperature-driven convective flow play an important role in driving solute within the area under consideration.

ACKNOWLEDGEMENTS

This project is supported by the German Science Foundation (DFG) as part of the SPP 1135 “Dynamics of Sedimentary Systems under varying Stress Conditions by Example of the Central European Basin System”. The geological data have been provided by M. Scheck-Wenderoth. We acknowledge Prof. Diersch and Dr. Clausnitzer at WASY Berlin, for providing support in FEFLOW. We also thank the Deep Fluid Flow Working group for discussions and two anonymous reviewers for their help in improving the manuscript.

2.2 Impact of hydraulic and heat conductivity distribution

Int J Earth Sci (Geol Rundsch)
DOI 10.1007/s00531-007-0209-8

ORIGINAL PAPER

Salinization problems in the NEGB: results from thermohaline simulations

Fabien Magri · Ulf Bayer · Maja Tesmer ·
Peter Möller · Asaf Pekdeger

Received: 18 October 2006 / Accepted: 23 May 2007
© Springer-Verlag 2007

ABSTRACTS

The occurrence of salty waters close to the surface is a well-known problem in the North East German Basin. Previous numerical simulations showed that near-surface brine occurrences are due to the interaction of hydrostatic and thermally induced forces (mixed convection). The influence of hydraulic permeabilities and thermal conductivities on the observed patterns remained an open question. Based on a hydro-geochemical dataset, thermohaline simulations are carried out in order to quantify the impact of these physical parameters on brine migration. The results indicate that the salinity and temperature profiles are strongly controlled by hydraulic permeabilities and can locally be influenced by thermal conductivities.

Keywords: numerical simulation, thermohaline flow, brines, hydraulic permeabilities, thermal conductivity, Rupelian clay, North East German Basin

Abbreviations

NEGB: North East German Basin

TDS: Total Dissolved Solids

INTRODUCTION

In the North East German Basin (NEGB), groundwater salinization is a widespread problem. In different areas of the basin, the interface between salty and fresh water is rather shallow. Brines can also reach the surface forming saline springs or pools which are spatially and temporary instable (Fig. 1). This phenomenon is observed since centuries and has been described, among others, by Heck (1932), Johannsen (1980), Hannemann and Schirrmeister (1998), Grube et al. (2000a), Grobe and Machel (2002).

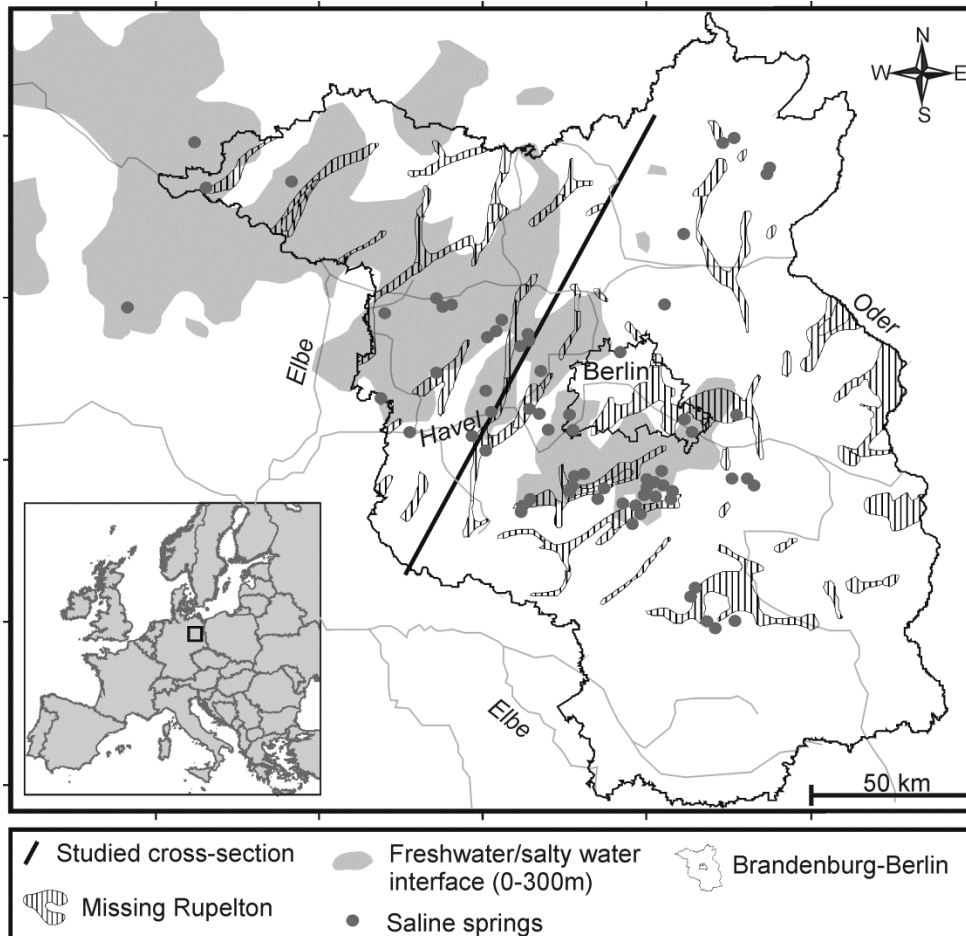


Fig. 1: Salty groundwater distribution (Grube et al. 2000b) and location of the saline springs (Schirrmeister 1996) in the Brandenburg region of the NEGB. The map also illustrates the areas where the Rupelton is missing. Numerical simulations are carried out along the SW-NE cross-section

It has been found that the anomalous salinity of the groundwater is mainly due to upconing of deeper salty waters and dilution of salt diapirs. In addition, numerical simulations of coupled fluid flow, heat and mass transfer (i.e. thermohaline flow) indicated that the upward flow of dissolved halite is induced by the geothermal gradient (Magri et al. 2005a, Magri et al. 2005b). At this state, the question arises to which degree the physical parameters of the stratigraphic units, such as hydraulic and thermal conductivity, can influence the complex brine patterns within the basin.

2.2 Brine migration: impact of hydraulic and heat conductivity distribution

For instance, a feature of the NEGB, not been taken into account in the previous numerical studies, is the presence of a quasi-impervious unit within the Cenozoic, the Rupelian-clay. Due to its low hydraulic permeability, the Rupelian clay acts as a hydraulic barrier separating the Quaternary and Tertiary freshwater complexes from deep saline aquifers. In the areas where this unit is eroded or was not deposited it is supposed that upward flow of salty water may be favored. Nevertheless, by observing Figure 1 it can be seen that the extended areas of salty water and the location of the saline springs are not always spatially related to the zones where the Rupelian is missing. This suggests that the presence of a less permeable unit at shallow depth has an impact on fluid flow but does not prevent brines from reaching the surface. Furthermore, since brine migration is driven by temperature gradients, variations of the thermal conductivity in other layers may also influence salinity distribution.

The goal of this study is to gain insights into the factors and parameters controlling salinity distributions within the NEGB. To address this issue, a set of thermohaline simulations are carried out along a vertical profile (Fig. 1). Among all parameters controlling groundwater flow hydraulic permeability plays a major role. Therefore particular attention will be given to this parameter. The paper is structured as follows: first, a short overview on the hydrogeological setting and on available data is given, and then the numerical results of different model scenarios are presented.

Although these investigations are conducted for the NEGB, the numerical results have generic implications for large-scale transport processes in other geothermal systems. Among the multitude of environmental circumstances where thermohaline convection can arise, transport of pollutants released from waste disposal in salt rock formation (Evans 1989, Van der Lee 2001), saltwater intrusion in exploited costal aquifers (Kohout 1965, Reese 2003) or salt layers embedded in aquifers (Sarkar et al. 1995) can be mentioned. In all these cases, it is proved that density-driven convection can lead to transport of heat and dissolved salt over large spatial scales and significantly shorter migration time scales than compared with diffusion alone (Diersch and Kolditz 2002, Flocks et al. 2001, Hanor 1987, Simmons et al. 2001, Simms and Garven 2004, Straus 1979, Straus and Schubert 1977).

HYDROGEOLOGICAL SETTING AND HYDROCHEMICAL DATA

Hydrogeological setting

The generalised stratigraphic section of the basin fill (Fig. 2a) starts with Permo–Carboniferous volcanics overlaying older Paleozoic sediments. These are overlain by Permian clastics and evaporites, Triassic clastics and carbonates, Jurassic to Lower Cretaceous clastics, Upper Cretaceous chinks and Cenozoic clastics. Briefly, the main part of sediments consists of clastic deposits and represent aeolian, fluvial, and shallow-lake deposits (Scheck and Bayer 1999). The Cenozoic has been further divided in three sub-units by including the Rupelian. The structural

2.2 Brine migration: impact of hydraulic and heat conductivity distribution

data of the Rupelian layer are obtained from drilling and correlate with the available geological maps of this area (Stackebrandt and Manhenke 2002). A sketch of the upper units is shown in Fig. 2b.

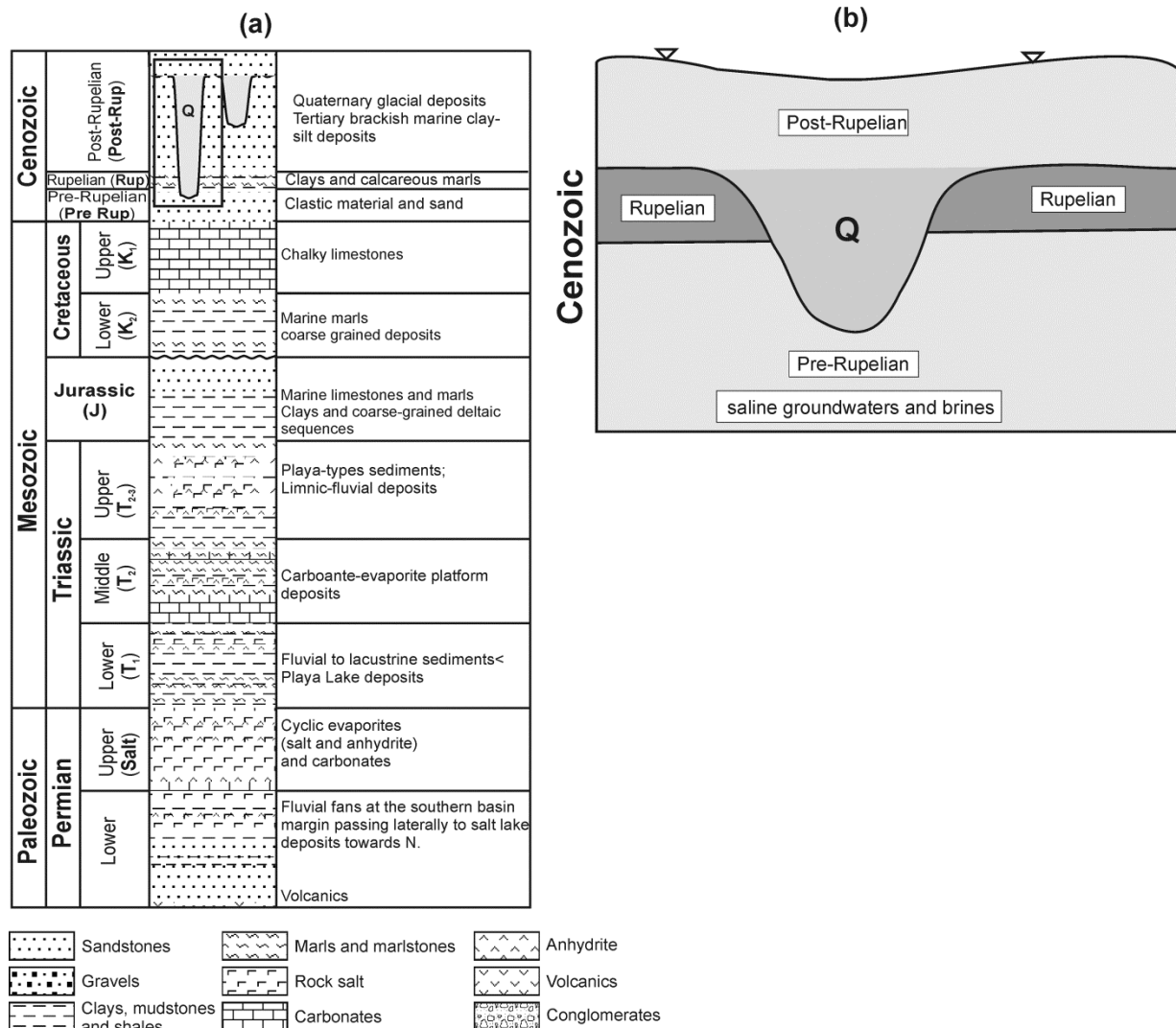


Fig. 2: (a) Litho-stratigraphic column for the NEGB (Scheck 1997) and (b) sketch of a typical incision of Quaternary clastic

Since the dominant lithology of this unit is clay, this quasi-impervious system separates the upper groundwater system from the deep Mesozoic aquifers which are filled with salty waters. However, these two aquifer systems are locally interconnected by channels formed during glacial periods (Fig. 2b). The impact of these channels on fluid flow will also be investigated.

The hydrogeological profile over the studied SW-NE cross section (Fig. 3) is obtained from the existing three-dimensional structural model of the NEGB (Scheck 1997, Scheck and Bayer 1999). The profile extends over 160 km in the horizontal direction. The NEGB is affected by strong salt tectonic. Consequently the depth and thickness of sediments vary throughout the basin. For instance, in the neighborhood of the eastern salt diapir, the Jurassic fill is absent. Nevertheless,

2.2 Brine migration: impact of hydraulic and heat conductivity distribution

the Rupelian unit is rather shallow and its thickness ranges from a few meters to hundred meters. In this model, local faults are not included.

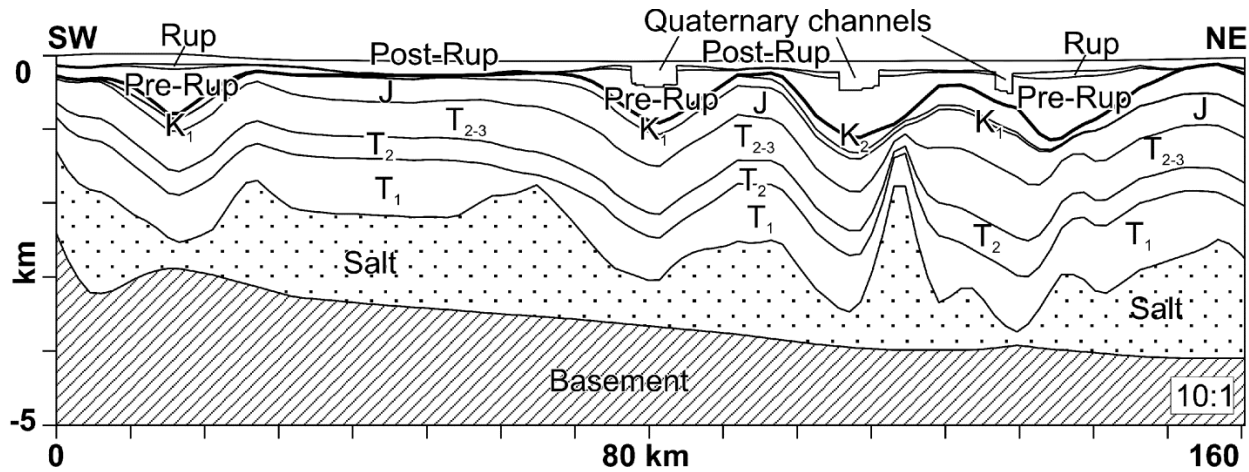


Fig. 3: Hydrogeological profile over the studied SW-NE cross section. For pictorial clarity, a vertical exaggeration of 10:1 is used. The abbreviations of the stratigraphic units are given in Table 1

In summary, the implemented model consists of ten units (from Post-Rupelian down to the Upper Permian), the Quaternary channels and of a basement closing the model at 5 km of depth.

Each stratigraphic unit is considered homogenous and isotropic with regard to its physical properties (e.g. hydraulic conductivity, porosity, etc.). The values of these parameters are given in Table 1. For this study, the spatially available data have been averaged to an appropriate basin scale (i.e. km). Therefore, a certain degree of uncertainty exists due to the spatial variability of hydraulic properties. This first rough hydrogeological model allows differentiating the aquifers at depths, however, without accounting for any heterogeneity in the horizontal direction. The development of a detailed aquifer model with full spatial variations of the physical properties is the aim of further research. By observing Table 1, it turns out that the hydraulic conductivity of the Middle Triassic is five orders less than the average value of the overlying sediments. Therefore, beside the Rupelian unit, the Middle Triassic is also a quasi-impervious complex. Its sedimentary fill is mainly dominated by fine grained carbonates. Particularly, it contains evaporitic units of salt up to some decametres with very low permeabilities. Consequently, these two impervious complexes divide the Post-Permian strata in three major aquifer systems: the Lower Triassic, from the Middle Triassic to the Pre-Rupelian and the Post-Rupelian complex.

2.2 Brine migration: impact of hydraulic and heat conductivity distribution

Table 1: Physical parameters of the model. The values are mainly adopted from Scheck (1997)

Stratigraphic unit (abbreviations)	Hydraulic conductivity (m s^{-1})	Porosity (1)	Volumetric heat capacity ($\text{J m}^3 \text{C}^{-1}$)	Thermal conductivity ($\text{W m}^{-1} \text{C}^{-1}$)	Molecular diffusivity ($\text{m}^2 \text{s}^{-1}$)
Cenozoic					
Post-Rupelian (Post-Rup)	1×10^{-5} 1×10^{-6}	0.23	3.15×10^6	1.5	2×10^{-9} 2×10^{-11}
Quaternary channels	1×10^{-5}	0.26	3.1×10^6	1.5	2×10^{-9}
Rupelian (Rup)	1×10^{-8}	0.2	3.3×10^6	1	2×10^{-12}
Pre-Rupelian (Pre-Rup)	1×10^{-6}	0.1	2.4×10^6	1.9	2×10^{-10}
Upper Cretaceous (K_1)	5×10^{-7}	0.1	2.4×10^6	1.9	1×10^{-10}
Lower Cretaceous (K_2)	5×10^{-7}	0.13	3.19×10^6	2	1×10^{-10}
Jurassic (J)	5×10^{-7}	0.13	3.19×10^6	2	1×10^{-10}
Upper Triassic (T_{2-3})	1×10^{-7}	0.06	3.19×10^6	2.3	2×10^{-11}
Middle Triassic (T_2)	1×10^{-11} 1×10^{-10}	1×10^{-6}	3.16×10^6	1.85	2×10^{-15} 2×10^{-14}
Lower Triassic (T_1)	1×10^{-7}	0.04	2.4×10^6	2	2×10^{-11}
Zechstein Salt	~ 0	~ 0	3.16×10^6	3.5	~ 0
Basement	~ 0	~ 0	2.7×10^6	2.5	~ 0

Hydrochemical data

For a better understanding of salinization processes and groundwater flow a large number of samples has been selected along the studied SW-NE profile in order to cover (i) the diversity of fresh to saline water chemistry, and (ii) the different aquifer systems. These geochemical analyses provided a regional picture of water chemistry and groundwater flow throughout the profile.

Hydrochemical analyses revealed that formation waters have been replaced by geologically younger waters. The samples follow the line of halite dissolution proving that ablation of Permian evaporites is the major cause for groundwater salinization (Fig 4a). Two types of water can be distinguished: diluted waters and highly saline waters. Diluted waters, characterized by mixtures of Pleistocene and recent waters, are found down to 700 m while highly saline waters are present in the deeper aquifers (Fig 4b) suggesting that the salinity distribution within the profile is rather layered. However the depth-salinity trend (Fig 4c) shows anomalies at 700 m depth and in the shallow aquifer, above 200 m. In the shallow aquifer, salinity can range from

2.2 Brine migration: impact of hydraulic and heat conductivity distribution

freshwater conditions to up to 10 g/L of Total Dissolved Solids (TDS). Waters with more than 2 g/L solute reach the surface between 50 and 80 km from the SW-ending of the profile. On the other hand, at 1 km depth salty-waters with low solute concentration (9 g/L of TDS) are locally found, indicating that dilution with freshwater can occur therein.

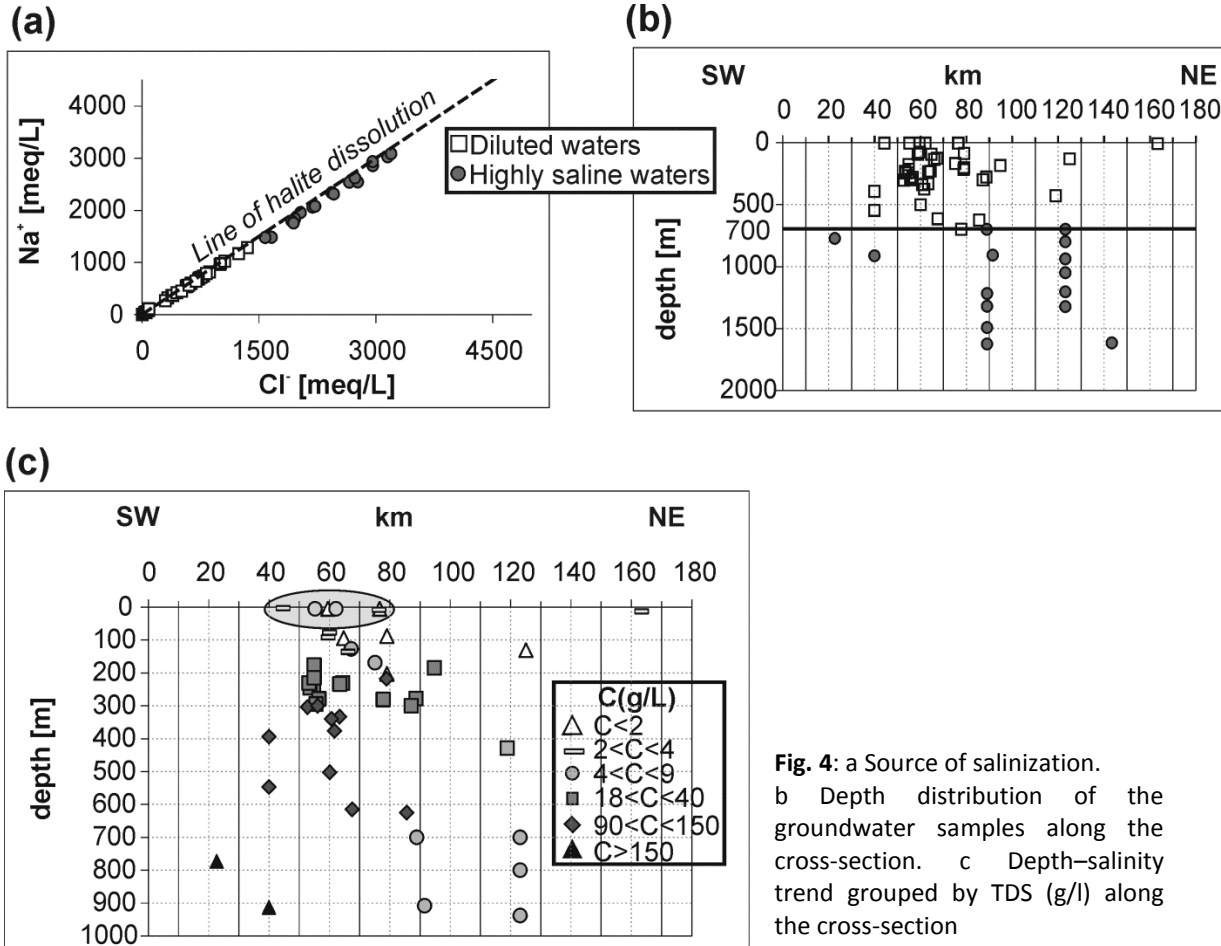


Fig. 4: a Source of salinization. b Depth distribution of the groundwater samples along the cross-section. c Depth-salinity trend grouped by TDS (g/l) along the cross-section

These observations are further supported by the isotope distribution and Rare-Earth elements and Yttrium (REY) analyses which emphasize the existence of different flow regimes within the basin (Tesmer et al. in print). Isotope and REY patterns typical of Pleistocene to Recent replenishment are found in the Pre-Rupelian aquifers. This suggests that head-driven flow (i.e. freshwater regional-flow) plays an important role even below the Rupelian. Specifically, infiltration of surface water in the Pre-Rupelian units can take place in the areas where the Rupelian Clay is few meters thin or absent. REY patterns also show the existence of upward flow even at depth below above 800 m. Furthermore, at this depth, the fluid density data evidence the existence of an unstable density stratification in which dense fluids overlay less dense fluids. This density inversion is caused by an increase of temperature with depth. It occurs even when

2.2 Brine migration: impact of hydraulic and heat conductivity distribution

the fluids are saturated with salt indicating that thermally induced convection of brines is likely a favored flow regime (Magri et al. 2005a).

In summary, the basin is characterized by an inhomogeneous and unstable salinity distribution. Two main large-scale flow regimes control the geochemical conditions of the basin: the hydrostatically-driven regional flow of freshwater which also affects the Pre-Rupelian unit and upward thermohaline flow.

Numerical simulations are performed in order to gain insights into the geological units and the physical parameters involved in these large-scale flow regimes. The geochemical dataset will be used to approach the numerical results in terms of the observed salinity trends.

MODELING APPROACH

For solving the coupled equations governing thermohaline flow, the commercial finite element software FELFOW[®] (WASY-GmbH 2002) has been applied. The mathematical formulation of this strongly coupled system is not recalled here and can be found in Diersch and Kolditz (1998). The finite element mesh used for discretizing the domain consists of 91520 quadrilateral elements defining a horizontal resolution of 180 m. The elements have variable thickness in the vertical direction.

Remarks on dimensionless numbers

Dimensionless numbers such as Rayleigh number, Prandtl number, buoyancy ratio, can be useful to determine the onset of convection for systems having constant physical parameters. Therefore a classification of this real-site problem in terms of such numbers is not practical if not impossible since the aquifers parameters are spatially variable. For the Rayleigh number one can argue that it may be derived for heterogeneous system. However a fundamental condition is that the properties vary within only one order of magnitude (Nield 1994). This is not the case here (Table 1). Furthermore, the geological units have variable thickness and a characteristic length is difficult to determine. A similar conclusion was made by Simmons *et al.* (2001).

Assumptions

Some simplifying assumptions have been made. According to the hydrochemistry results, brines are considered pure NaCl solutions.

In applying the dispersion equations to real problem, it is necessary to determine appropriate values for dispersivity. For this purpose specific data is required. Unfortunately, no field tests were available to evaluate longitudinal and transversal dispersivity for the study case. Therefore, for simplicity these coefficients are set equal to zero. The coefficient of hydrodynamic dispersion is effectively equal to the molecular diffusivity of the solute in the saturated porous medium. By doing so the effect of mechanical dispersion is neglected and fluid

2.2 Brine migration: impact of hydraulic and heat conductivity distribution

spreads the dissolved halite over a smaller volume. However the main features of thermohaline convection are preserved. It should be stressed that hydrodynamic dispersion is very difficult if not impossible to determine for real site problems. Indeed it strongly depends on spatial and temporal scales and on the heterogeneities of the aquifers (Ingebritsen and Sanford 1998; Liu et al. 2004). Furthermore it has been proved that for convective systems the dispersion process is anomalous (Lowe and Frenkel 1996). On the other hand, molecular diffusion, porosity and hydraulic conductivity are correlated as shown in Boving and Grathwohl (2001). For each simulation case presented, the molecular diffusivity is set proportional to the hydraulic conductivity by a factor 2×10^{-4} (Table. 1). Consequently, the assigned molecular diffusions are to some extent averages at basin-scale.

Fluid density data are reproduced by use of polynomial expressions taking into account pressure, temperature and salinity dependencies (Magri et al. 2005a; Magri 2004). On the other hand, viscosity variations are neglected.

Boundary and initial conditions

Boundary conditions

The following boundary conditions are applied:

(1) At the surface, head, temperature and solute boundaries are prescribed. The head is fixed to the local topographical elevation which induces a steady regional flow. Since springs of warmer saline waters are observed in the NEGB (Schirrmeyer 1996; Grube et al. 2000b), heat and dissolved salt are allowed to flow through the surface by use of an open boundary condition (Cauchy). The reference values for the temperature and for the salt concentration at the surface are respectively 8 °C and 0 g/L (i.e. freshwater). Further details on the equations governing these boundary conditions can be found in Magri et al. (2005b) and Magri (2005).

(2) At the bottom, a constant temperature boundary condition of 150 °C is defined. This value corresponds to a linear vertical gradient of 30 °C/km.

(3) At the top of the salt, the brine concentration is fixed at 345.2 g/L, representing an approximate value for halite saturation. By setting a constant concentration value at the Top salt, the basin undergoes a continuous salt replenishment. Nevertheless, the shape of the salt layer remains unchanged. Ranganathan et al. (1988) made a similar boundary assumption for their salt-dome models.

(4) The lateral boundaries are closed to fluid, heat, and mass flow.

Initial conditions

The initial pressure and temperature conditions are respectively derived from steady-fluid flow and steady conductive heat transport models calculated before the thermohaline simulations.

2.2 Brine migration: impact of hydraulic and heat conductivity distribution

The initial temperature distribution is illustrated in Figure 5. The isotherms display the well-known thermal anomalies generated by the strong contrast between the thermal conductivities of the Zechstein Salt and those of the overburden (Table. 1). Within the salt diapirs the isotherms are concave while they are slightly convex above the salt diapirs (Yu et al. 1992).

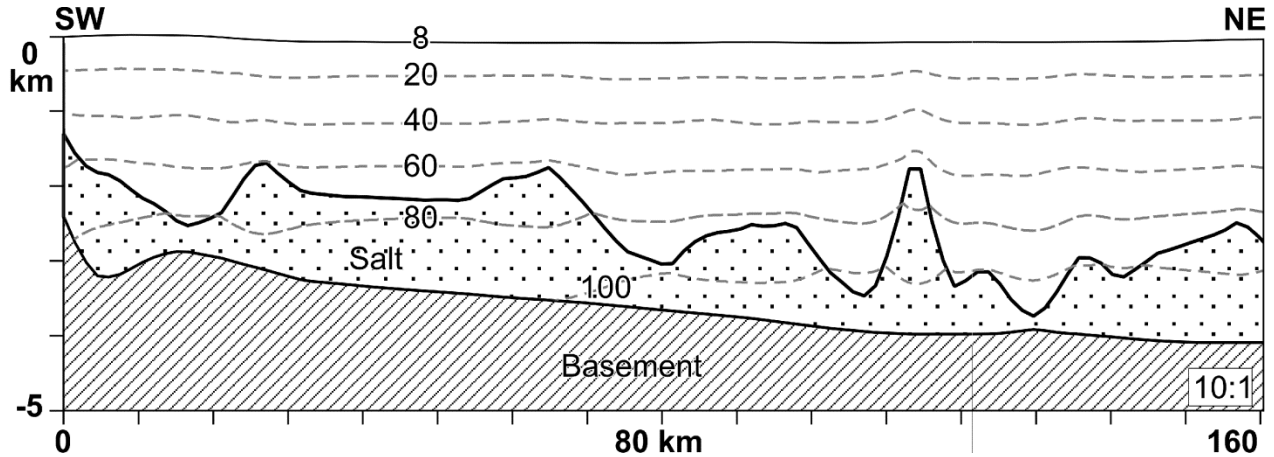


Fig. 5: Initial temperature condition obtained from a stationary conductive heat problem

In the following simulation cases, the initial salt concentration is set to freshwater conditions (i.e. 0 g/L) everywhere above the Zechstein unit. However, the sediments of the NEGB were deposited during marine transgression (Scheck 1997). Therefore different initial salinity profiles accounting for paleo-salinity conditions will also be used (cf. Remark on initial conditions).

NUMERICAL SIMULATIONS

The numerical solutions are obtained from a predictor-corrector forward-Euler/backward-Euler fully implicit time-integration scheme. Streamline upwind dampening is used in the transport equations.

The following transient thermohaline simulations have been carried out over a simulated time period of one million years (1 My). Note that any time period subsequently mentioned refers to a simulated period with no regard to a particular geological period.

Simulation case 1: homogenous Cenozoic

In this model scenario the whole Cenozoic is homogenous, i.e. the Rupelian, Pre-Rupelian sub-units and the channels are not included. The hydraulic conductivity of the whole Cenozoic is equal to $1 \times 10^{-5} \text{ m s}^{-1}$. The values of the other physical properties are those of the Post-Rupelian unit given in Table. 1. The calculated concentration and temperature profile at 100 ky and at the end of the simulation run (1 My) are shown in Figures 6 (a) and (b) respectively.

2.2 Brine migration: impact of hydraulic and heat conductivity distribution

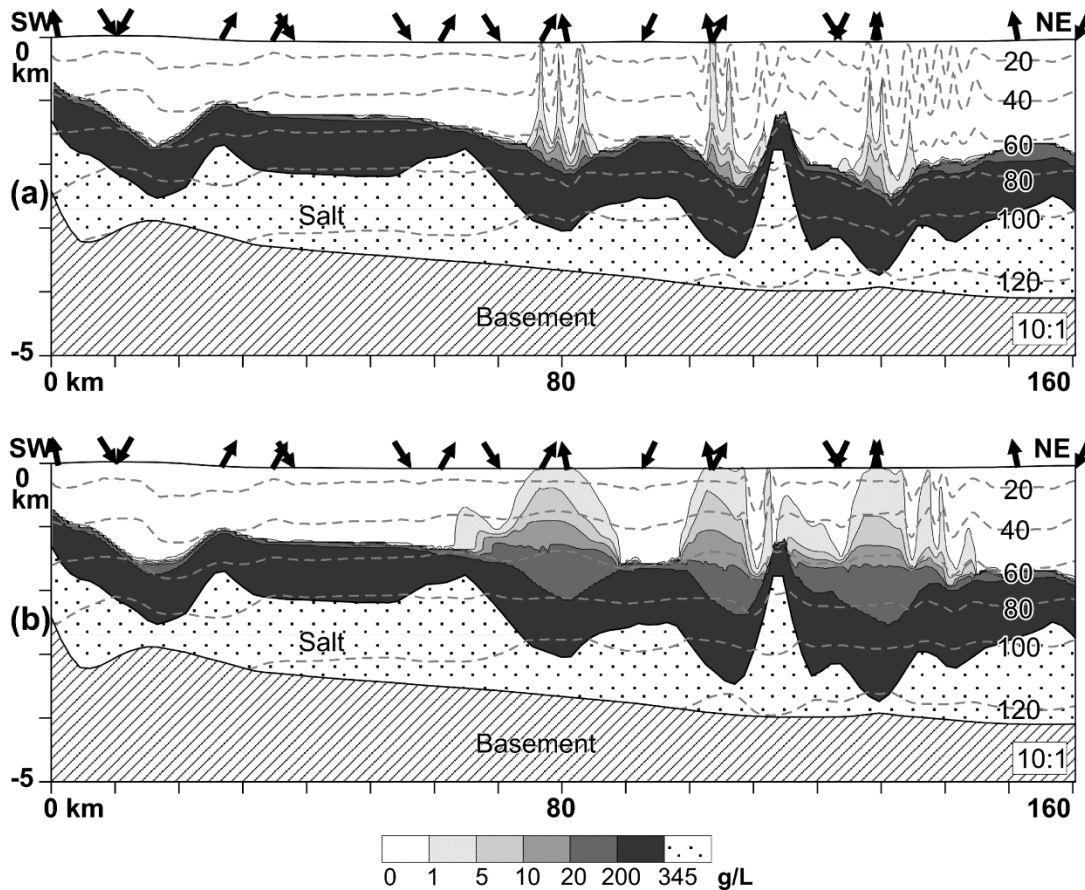


Fig. 6: Simulation case 1: homogenous Cenozoic. Calculated salt concentration (g/l) and temperature ($^{\circ}$ C) profiles at a simulated time period of a 100 ky and b 1 My. Upward and downward-directed arrows locate discharge and recharge areas

At 100 ky (Fig. 6a), a steady mass and temperature distribution is reached within the Lower Triassic. Therein, the salt concentration ranges from 200 g/L up to 345 g/L. Furthermore, the isothermal lines did not vary significantly with regard to the initial temperature profile (compare with Figure 5) indicating that heat transport is conductive within the Middle Triassic. By contrast, above the Middle Triassic thermohaline convection occurs. In the neighborhood of the salt diapirs vertically stretched brine plumes start developing. In those areas, the temperature profile displays oscillatory disturbances which are characteristic of a thermally induced convective regime. Since in thermohaline flow heat and mass transport are strongly coupled (Nield 1968), increased temperature gradients (convex isotherms) induce upward brine migration while downward freshwater flow is related to negative temperature anomalies (concave isotherms).

As time progresses, more dissolved halite continue diffusing through the Middle Triassic (Fig. 6b). As a result, the bottom of the brine fingers is enlarged. Furthermore, brine fingers continue protruding within the sediments driven by thermal buoyant forces. At 1 My, the thermohaline regime still persists which is manifested by oscillations in the temperature profile. Salty waters with more than 1 g/L of dissolved halite stretch over 2 km and reach the surface in relation to

2.2 Brine migration: impact of hydraulic and heat conductivity distribution

discharge areas. On the other hand, regional inflow of freshwater strongly affects the mass distribution within the profile. The brine fingers are rather narrow and separated by wide areas of freshwater inflow. This is in contrast with the observed data that points toward a horizontally layered salinity profile.

In summary, the modeling reveals the role of the major geological units with regard to the fluid-dynamics affecting the basin. Steep salt diapirs provide a continue source of salt replenishment. The dissolved halite is partially bounded by the Middle Triassic and highly saline waters saturate the deeper aquifer. Accordingly, this separation distinguishes two different flow regimes: below the Middle Triassic heat and mass transport are respectively conductive and diffusive while above this unit thermohaline convection persists and lifts deep-seated brines up to the surface.

Although the fluid-dynamic shown by the numerical model is consistent with the hydrochemical data, the calculated mass and temperature patterns are not. Precisely, the observed salinity distributions are horizontally layered rather than vertically stretched (Fig.4). Furthermore, the simulated regional flow is too vigorous leading to wide areas of freshwater. In the next simulation temperature and salinity distributions are therefore investigated in relation to a lower hydraulic conductivity of the whole Cenozoic.

Simulation 2: Impact of the Rupelian-clay

Here the Rupelian clay layer and Pre-Rupelian unit are incorporated in the Cenozoic. In this simulation case, the Quaternary channels are not included. The physical parameters of the units are given in Table 1. The results are illustrated in Figures 7 (a) and (b).

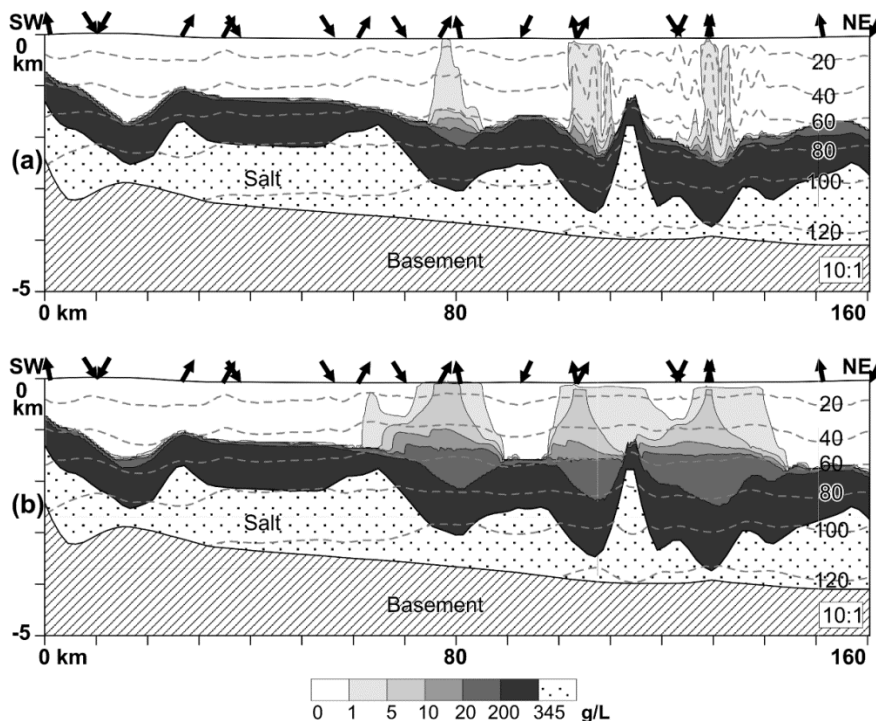


Fig. 7: Simulation case 2: impact of the Rupelton. The hydraulic conductivity of the homogenous Cenozoic is decreased to 10^{-6} m s^{-1} . Calculated salt concentration (g/l) and temperature ($^{\circ}\text{C}$) profiles at a simulated time period of a 100 ky and b 1 My

2.2 Brine migration: impact of hydraulic and heat conductivity distribution

Owing to the presence of the quasi-impervious unit in the Upper Cenozoic, the regional flow does not overwhelm the thermally induced convective cells. Therefore thermohaline convection develops as in a free regime. As a result, narrow brine plumes reach the shallow aquifer at earlier time (approximately 50 ky). At 100 ky, salty fingers have already merged leading to the formation of large plumes (compare Figure 7a and Figure 6a). Accordingly the temperature oscillations are less pronounced. Brine dilution with fresh water is further inhibited by the presence of the Rupelian unit. Consequently, below this unit brine mixing is enhanced: at the end of the simulation run, fluids with 1 g/L of dissolved salt cover wide areas throughout the profile (Fig. 7b). Saltier brines with a concentration of 5 g/L reach the surface in relation to discharge areas. On the other hand heavier fluids with more than 20 g/L of dissolved halite fill deep salt rim synclines. The temperature gradient throughout the profile is close to the initial conductive temperature distribution (cf. Fig. 5).

In the areas of the profile where the Rupelian clay is thin, the regional flow still affects the deep aquifers. For instance, at the 90th km of the profile the Rupelian unit has a thickness of few meters (cf. Fig. 3). At that location, freshwater inflow prevents the vertical brine fronts from merging (Fig. 7b).

Besides affecting the salinities, the Rupelian unit has also an impact on the shape of the mass patterns: below this unit the brine plumes spread in the horizontal direction and the upconings of saltier water have a truncated tip (Fig. 7b).

The numerical simulations revealed that salty water can leach through the Rupelian clay up to the surface covering larger areas. Below the Rupelian unit, the finger regime evolves in a rather layered mass stratification. With respect to the previous cases (i.e. homogenous Cenozoic), the salt content in the pore water increased except in the areas where the Rupelian unit is few meters thin. In those locations, deep inflow of freshwater occurs and dilution is favoured. To some extent, this is in agreement with the hydrochemical investigations which point toward the presence of Pleistocene waters, though only within the Pre-Rupelian aquifers.

Although the spatial distribution of the mass patterns correlates with the data, the calculated concentrations are still too low everywhere. For instance, the data show that in some areas fluids with more than 10 g/L of TDS spread underneath the Rupelian unit and can also be observed locally at the surface. Therefore, before investigating the role of Quaternary channels cutting the Rupelton, an attempt to approach the observed depth-salinity trend is done. For this purpose, an additional simulation based on this hydrogeological setting has been performed.

Simulation 3: Increased hydraulic conductivity in the Middle Triassic

In this model scenario, the Rupelian unit is still considered closed (i.e. no Quaternary channels are included). Here the hydraulic conductivity of the Middle Triassic is increased to 10-10 m s⁻¹ while the values of the others parameters remain unchanged. The calculated salt concentration and temperature at 1 My are shown in Figure 8. By increasing the hydraulic conductivity of the

2.2 Brine migration: impact of hydraulic and heat conductivity distribution

Middle Triassic by one order of magnitude, more dissolved halite fills the sediments. The differences in the concentration values can be directly inferred by comparing Figures 8 and Figure 7b. Highly saline waters with 20 g/L of salt content are not anymore seated in deep salt rim synclines but stretch horizontally at 1 km depth. At the discharge areas, the concentration ranges from 1 g/L up to 10 g/L of dissolved halite as it is the case in the central part of the profile. An additional brine plume forms at the western end of the section in relation to the salt diapir. In the areas where the Rupelian unit is thin, fluids are still diluted and this time only within the Pre-Rupelian, in good agreement with the hydrochemical data. Furthermore, in those areas the salinity is about 250 mg/L which is not displayed in the concentration range. As heavier fluids migrate within the basin, the convective cells decay at earlier times and heat transport approaches a steady state solution at the end of the simulation run.

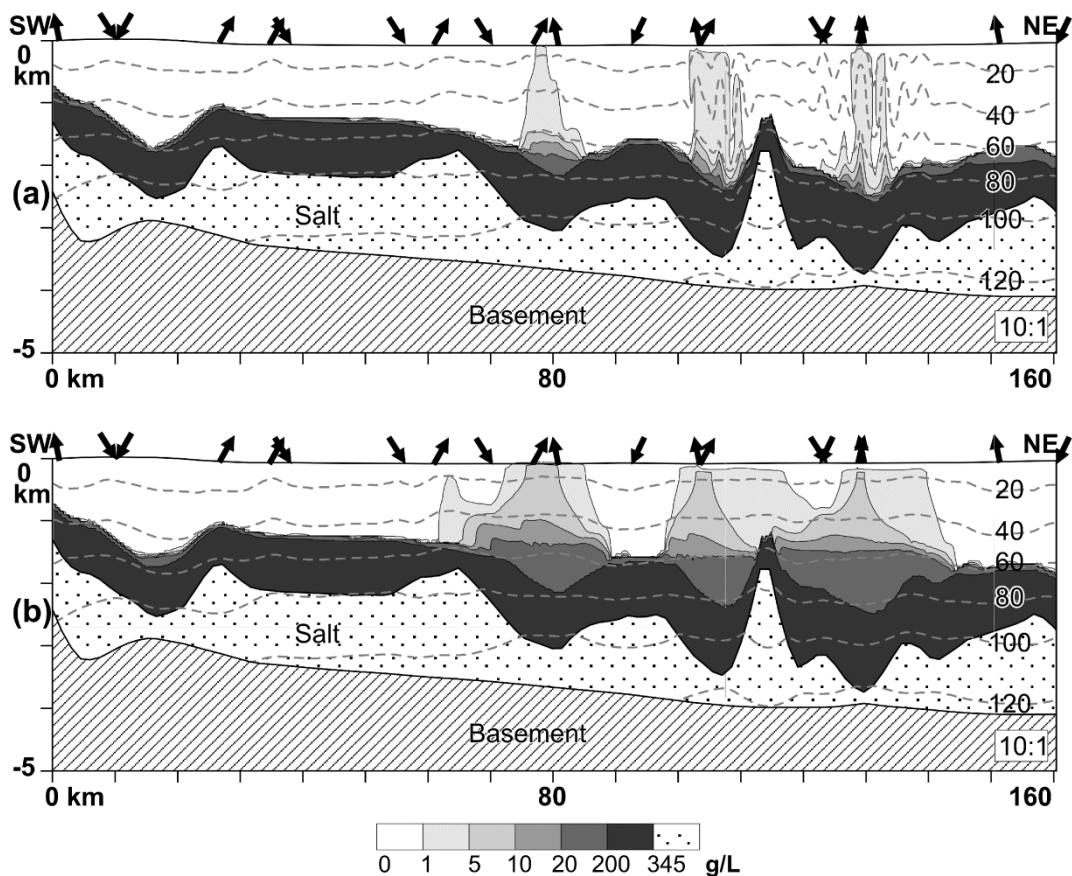


Fig. 8: Simulation case 3: the Rupelton is incorporated and the hydraulic conductivity of the Middle Triassic is increased to $10\text{--}10\text{ m s}^{-1}$. Calculated salt concentration (g/l) and temperature ($^{\circ}\text{C}$) profiles at a simulated time period of 1 My

This model scenario indicates that the hydraulic conductivity of the Middle Triassic strongly controls the salt concentrations throughout the entire profile. The results suggest that increased vertical permeability within this unit or deep cutting faults can further induce upward migration of saltier basinal water. These structural features are not investigated in this context and should be the subject of future studies.

2.2 Brine migration: impact of hydraulic and heat conductivity distribution

Overall, the calculated concentrations correlate better with hydrochemical data. In the following modeling, the hydraulic conductivity of the Middle Triassic is therefore set equal to $10^{-10} \text{ m s}^{-1}$.

Simulation 4: Impact of permeable channels within the Rupelian clay

The Quaternary channels are situated in the vicinity of the major discharge areas as illustrated in Figure 9, together with the calculated mass and temperature profiles at 1 My. The physical parameters of these structures are listed in Table. 1. Here it is worth recalling that the hydraulic conductivity of the Post-Rupelton sediments is 10^{-6} m s^{-1} . The channels are more permeable ($k=10^{-5} \text{ m s}^{-1}$).

In the Upper Cenozoic, both temperature and concentration isolines are shaped by the channels (Fig. 9). Salt water with 5 to 10 g/L spread just underneath the flanks of the channels. Within these more permeable structures, the imposed steady-state regional flow dilutes the discharging brines. Consequently, upconing have a thinner tip and brine concentrations at the surface are slightly lower (compare Figure 9 and Figure 8. On the other hand, deep salt water stratification is not affected.

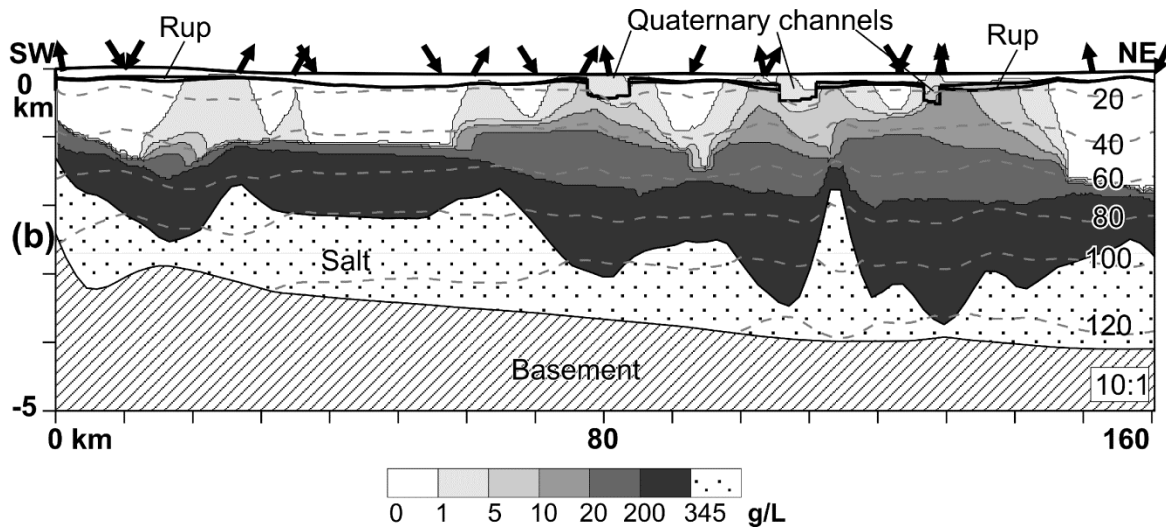


Fig. 9: Simulation case 4: impact of permeable channels within the Rupelian unit. The hydraulic conductivity of the Middle Triassic is kept to $10^{-10} \text{ m s}^{-1}$. Calculated salt concentration (g/l) and temperature ($^{\circ}\text{C}$) profiles at a simulated time period of 1 My

The results indicate that the presence of more permeable sediments within the Rupelian clay favors inflow of freshwater rather than carrying discharge fluids up to the surface. This is further supported by an additional simulation in which larger channels cut the Rupelian unit. As the channels are wider, areas with more diluted brines form within the Pre-Rupelian units.

Until now, the numerical investigations focused on the impact of the hydraulic conductivity on temperature and salinity gradients. However, other parameters can influence the flow regime. For instance, a variation in the ratio between the thermal conductivity of the stratigraphic units

can lead to a different geothermal field. Since brine migration in the NEGB is thermally driven, the salinity distribution may vary as well.

Simulation 5: Impact of thermal conductivities

For simplicity, the simulation case 3 (Fig. 8) is used to investigate the effect of thermal conductivities on the studied patterns: no channels cut the Rupelian unit and the hydraulic conductivity of the Middle Triassic is $10^{-10} \text{ m s}^{-1}$.

Several stationary conductive heat problems have been run in order to generate a different geothermal field. For each simulation, the thermal conductivities of the stratigraphic units have been varied gradually. The thermal conductivities of the Salt is increased to $4 \text{ W m}^{-1} \text{ }^\circ\text{C}^{-1}$ while those of the other units range between $1 \text{ W m}^{-1} \text{ }^\circ\text{C}^{-1}$ within the Cenozoic up to $2.5 \text{ W m}^{-1} \text{ }^\circ\text{C}^{-1}$ at higher depth. The calculated temperature field is shown in Figure 10 and is also used for initializing the set of thermohaline simulation presented here. By comparing Figure 5 and Figure 10, it can be seen that increased temperatures are found at the western side of the steepest salt diapir.

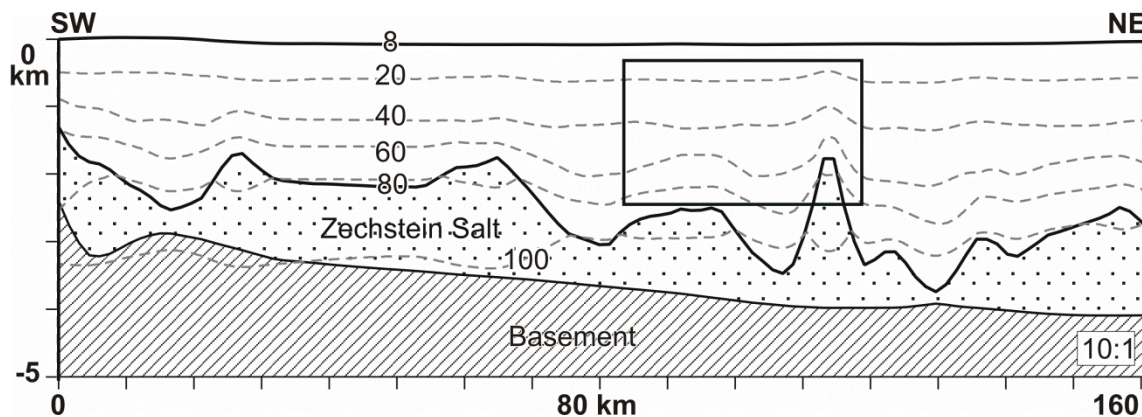


Fig. 10: Geothermal field obtained from a stationary conductive heat problem in which the Salt thermal conductivity is $4 \text{ W m}^{-1} \text{ }^\circ\text{C}^{-1}$

Consequently, in this location thermal buoyant forces are stronger. As a result, upward brine migration is enhanced and an upconing of deep saline waters develops (Fig. 11): 20 g/L of dissolved halite reaches the Rupelton Clay. At the surface the calculated concentrations are higher. Furthermore, concentration isopleths are concave in direct relation to the increased temperature gradient (compare Figure 8 and Figure 11). The temperature profile is still disturbed indicating that the convective regime persists. The oscillation wavelength is about 20 km. By contrast, far from the salt diapir the isotherms remained rather flat. Accordingly, in the western ending of the profile the mass patterns did not vary.

2.2 Brine migration: impact of hydraulic and heat conductivity distribution

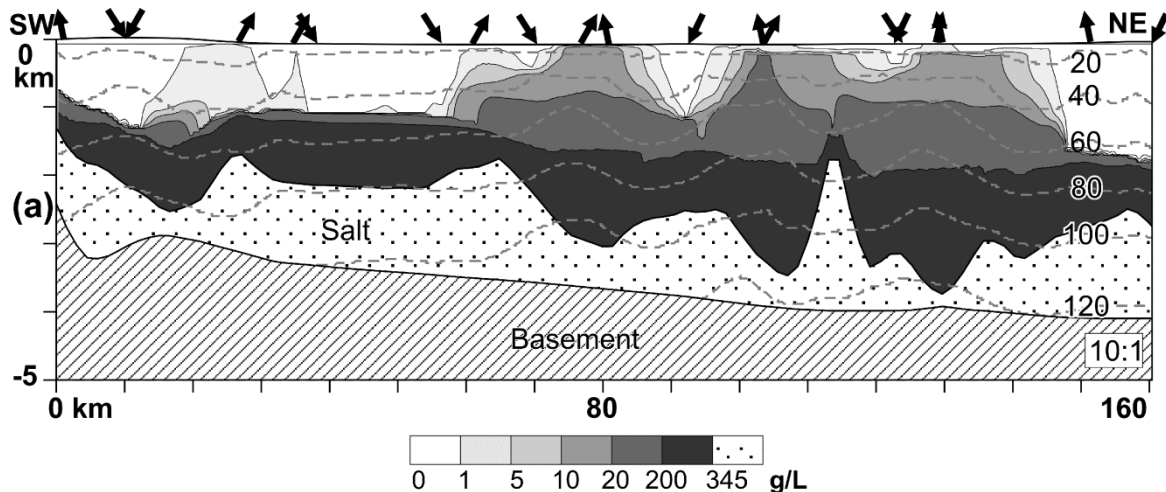


Fig. 11: Simulation case 5: impact of thermal conductivities. The salt thermal conductivity is $4 \text{ W m}^{-1} \text{ C}^{-1}$. Calculated salt concentration (g/l) and temperature ($^{\circ}\text{C}$) profiles at a simulated time period of 1 Ma

This simulation case allowed assessing the impact of thermal conductivity. This parameter does not strongly change the concentration patterns as it is the case for the hydraulic permeability. Nevertheless, a higher contrast between the thermal conductivity of the sediments induces a more vigorous convective regime which does not decay in time. As a result, upward brine movement increases.

Remarks on the initial conditions

Two different initial salinity conditions have been tested in order to reproduce paleo-salinity conditions. In the first, the salt concentration of the pore water is set equal to 40 g/L everywhere above the Salt unit. In the second, fluid concentration increases linearly from few mg/L within the Post-Rupelton up to saturation values at the Upper Permian.

It turned out that each model scenario lead to similar concentration patterns independent from the initial salinity condition. As time progresses, the saline water which initially saturates the shallow aquifer is diluted and flows through discharge areas. Throughout the profile, the uniform salt water distribution gradually evolves to the final solution.

To some extent, the results are in agreement with hydrochemical data which show that formation waters have been replaced by geologically younger waters. The present hydrochemical condition of the NEGB might result from the hydrogeothermal setting of the basin itself rather than being caused by paleo-salinity distributions.

SUMMARY AND DISCUSSIONS

The NEGB is characterized by an inhomogeneous and unstable salinity distribution. The available geochemical dataset indicate that above the Rupelian clay, dilution with freshwater is the dominant process. Furthermore, isotope and REY patterns point toward the presence of Pleistocene to Recent replenishment even in the Pre-Rupelian aquifer system. These inflows of freshwater occur in relation to areas where the Rupelian clay is thin or eroded. Even at depth of 1500 m, data provided evidence for an inversion of the fluid density due to increased temperature gradients leading to upward brine migration. In the deeper aquifers, the mass stratification is rather layered with salt concentration ranging from 200 g/L up to saturation value. Geochemical investigations also showed that older formation waters have been replaced by geologically younger waters. In summary, the present hydrochemical condition of the basin might be controlled by upward thermohaline flow and mixing with the regional flow.

The observations are further supported by the numerical investigations. Thermohaline simulations along a vertical profile of the NEGB have been performed in order to investigate the factors and the physical parameters involved in the formation of brine patterns within the basin. The numerical studies mainly focused on the hydraulic conductivity within the Cenozoic unit. Therein, the Rupelian-clay has been incorporated. The numerical results revealed that temperature and salt concentration gradients are very sensitive to the hydraulic permeability of the stratigraphic units. With a homogeneous Cenozoic, thermally induced brine plumes develop in a finger regime. Lower value of the hydraulic conductivity within the Cenozoic led to the formation of large areas of salty water, but still not in good agreement with observed data. The simulations showed that the Rupelian unit plays a major role in controlling both spatial distribution of salt content and inflow of freshwater. Precisely, this less pervious unit does not prevent brackish water from reaching the surface. Above the Rupelian clay, the brine mixes with freshwater and spread over larger distances. Below this unit, the salinity content of the pore water increases. However, in areas where the Rupelian clay is thin, inflow of freshwater reaches the Pre-Rupelian aquifer, which is showed by the geochemical investigations as well. The role of Quaternary channels cutting the Rupelian clay has also been investigated. Even if located in relation to discharge areas, these permeable conduits allow dilution of salty waters with freshwater rather than enhancing an outflow of brines. On the other hand, the Quaternary channels do not affect deep fluid regimes. The Middle Triassic is a key unit controlling the salinity distribution throughout the profile. Below this unit, the aquifer is saturated with more than 200 g/L of dissolved halite and heat transport is conductive. By increasing the hydraulic permeability of this unit by only one order of magnitude, salt water concentration varied drastically. More dissolved halite fills the sediment and the mass stratification is layered. With a slightly more pervious Middle Triassic, the numerical results fit better the general salinity trends. Contrast in thermal conductivity has also an impact on the calculated gradients. Higher thermal conductivity contrasts can enhance thermohaline convection. Accordingly, the

2.2 Brine migration: impact of hydraulic and heat conductivity distribution

convective cells persist and temperature oscillations affect the whole profile. The numerical results are independent from the initial salinity distribution suggesting that the present hydrochemical condition of the basin might not result from paleo-salinity.

To some extent the numerical results correlate well with the hydrochemical data. However, it should be pointed out that transport processes in geothermal basin are three dimensional. Therefore the numerical models presented here cannot reproduce observation data in details. Furthermore, the hydrogeological model used here is rather rough accounting only for vertical heterogeneities. The parameters were uniformly varied within the units. The simulations suggested that local heterogeneities in the hydraulic and thermal conductivity may play a major role in controlling transport processes. Specifically, faults provide preferential pathways for migration of brines and strongly affect heat transport. In their studies, Lampe and Person (2002) showed that fault-related factors such as size and depth penetration have a major role in determining fluid flow patterns and the geothermal regime. Other aspects that should also be taken into account are anthropogenic activities which can influence transport processes in the shallow aquifer. Therefore further research should be devoted to build a more detailed conceptual model with regard to the geological structures (e.g. faults), the spatial distribution of the physical parameters and pumping rates.

While these effects need to be studied in detail, the numerical investigations already show that two major factors have a significant impact on the formation of near-surface brine occurrences: (i) the interaction between density-driven flow induced by temperature gradients and regional flow, (ii) the hydraulic and thermal conductivity of the different stratigraphic units within the basin.

ACKNOWLEDGEMENTS

This project is supported by the German Science Foundation (DFG) as part of the SPP 1135 “Dynamics of Sedimentary Systems under varying Stress Conditions by Example of the Central European Basin System”. The geological data of the NEGB have been provided by Dr. M. Scheck-Wenderoth. The structural data of the Rupelton have been provided by Christoph Jahnke and Prof. Hans-Jürgen Voigt. We acknowledge Prof. Diersch and Dr. Clausnitzer at WASY Berlin, for providing support in FEFLOW. We thank Prof. E. Holzbecher and Prof. M. Koch for their suggestions and corrections.

2.3 Brine migration: shallow salt structures

Tectonophysics 470 (2009) 183–194



Contents lists available at ScienceDirect

Tectonophysics

journal homepage: www.elsevier.com/locate/tecto



Salty groundwater flow in the shallow and deep aquifer systems of the Schleswig–Holstein area (North German Basin)

Fabien Magri^{a,*}, Ulf Bayer^a, Asaf Pekdeger^b, Roland Otto^c, Claudia Thomsen^c, Ulrike Maiwald^b

^a GeoForschungsZentrum Potsdam 4.3, Telegrafenberg, 14473 Potsdam, Germany

^b Freie Universität Berlin Department of Earth Science Malteserstr. 74-100, 12249 Berlin, Germany

^c Landesamt für Natur und Umwelt des Landes Schleswig–Holstein, Hamburger Chaussee 25, 24220 Flintbek, Germany

ABSTRACT

In the Schleswig-Holstein area, salty groundwaters are not always spatially related to the presence of shallow salt structures. Furthermore, hydrochemical data point to instable salinity profiles and to the occurrences of deep brines close to the surface. Therefore, complex interaction between shallow and deep solute migration must occur. Numerical simulation of fluid flow, mass and heat transport have been carried out in order to understand the role of shallow salt dissolution and young geological features on groundwater flow as well as to investigate the interrelationships between shallow and deep aquifer-systems. For these purposes, a shallow (-500 m) and a deep profile model (- 5 km) have been constructed.

The results indicate that different flow regimes coexist within the study area. Shallow brine migration is strongly controlled by the geological features of the basin such as faults, glacial channels and sand layers. Furthermore, shallow salt dissolution is the major cause for gravitational convection in the deeper aquifers. This source of salinization from above leads to the formation of instable salinity profiles at 2 km depth. Further interactions between shallow and deep fluid flow exist in the eastern part of the basin where brine upconing is due to both topography-driven flow and thermohaline convection. The simulations also showed that the hydraulic conductivity of the stratigraphic units influences the brine regime on a regional-scale. Gravitational convection is likely to occur in permeable units located near shallow salt structures, while thermohaline convection persists within thick permeable areas in which salt dissolution is not the dominant process.

The presented study provides new insights into fluid basin processes. The described flows could develop in any geothermal basin hosting salt diapirs which pierce shallow aquifer systems.

Keywords: Shallow salt diapir; brines; thermohaline convection; density-driven flow; numerical modeling; Schleswig-Holstein

INTRODUCTION

In different regions of the NE German Basin (NEGB), salty water reaches the shallow aquifer system. This long-term phenomenon is manifested by the occurrences of salty springs and by the growth of seashore salt grass in the inner part of the basin. Recent maps locating the observed salty springs and the brine patterns throughout the NEGB have been compiled by Müller (1993), Schirrmeister (1996) and Grube (2000b). Around 25% of North Germany is affected by inland salinity (i.e. originating from upconing of deep-seated salt waters and dilution of salt diapirs) and about 5% sea water intrusion. The chemistry of these brines indicates that most of the waters originate in the deeper part of the aquifers (Lehmann, 1974b, 1974a Voigt, 1972). In their studies, Hannemann and Schirrmeister (1998) concluded that the waters of the springs originated mainly in the deeper Pre-Tertiary sub-ground. Numerical models of coupled fluid flow, mass and heat transport (i.e. thermohaline flow) supported this thesis. The results have shown that upward solute migration takes place within the NEGB. At 4 km depth, salty waters forming near deep-seated salt structures ascend up to the surface driven by thermal buoyant forces (Magri et al., 2005a, 2005b, in print).

On the other hand, it is still not clear how salt structures piercing the surface aquifers influence the complex dynamics of salty groundwater flow. Steep salt diapirs close to the basin surface provide a source of high salinity for shallow groundwater. Consequently, denser brines can sink into deeper aquifers. The resulting density-driven flow is often referred to as gravitational convection (Garven, 1995). In the NEGB, gravitational convection of brines has not been investigated yet and its effects on groundwater flow are unknown. Furthermore, the interaction between shallow and deep aquifers in relation to salty groundwater flow remains poorly understood. Not at least, other issues that need to be addressed are the role of young basin features such as faults, sand units and glacial channels.

For investigating these aspects, the Eastern part of Schleswig-Holstein region (S-H) is the most suitable study area. This region (Fig. 1) is delimited by natural boundary conditions. An elongated salt wall reaching the basin surface stretches over more than 40 km along the Western part, while deeper salt pillows affect the Southern and Eastern area. The Trave River and the Baltic Sea bound the region in the North-East. Furthermore, wide areas of the basin are affected by faults and Pleistocene dorrs cutting into deeper strata (Fig. 1). Hydrogeologically the aquifer consists of two Mesozoic-Tertiary basins, the Oldesloe Trough and the Hemmelsdorf basin.

2.3 Brine migration: shallow salt structures and Pleistocene channels

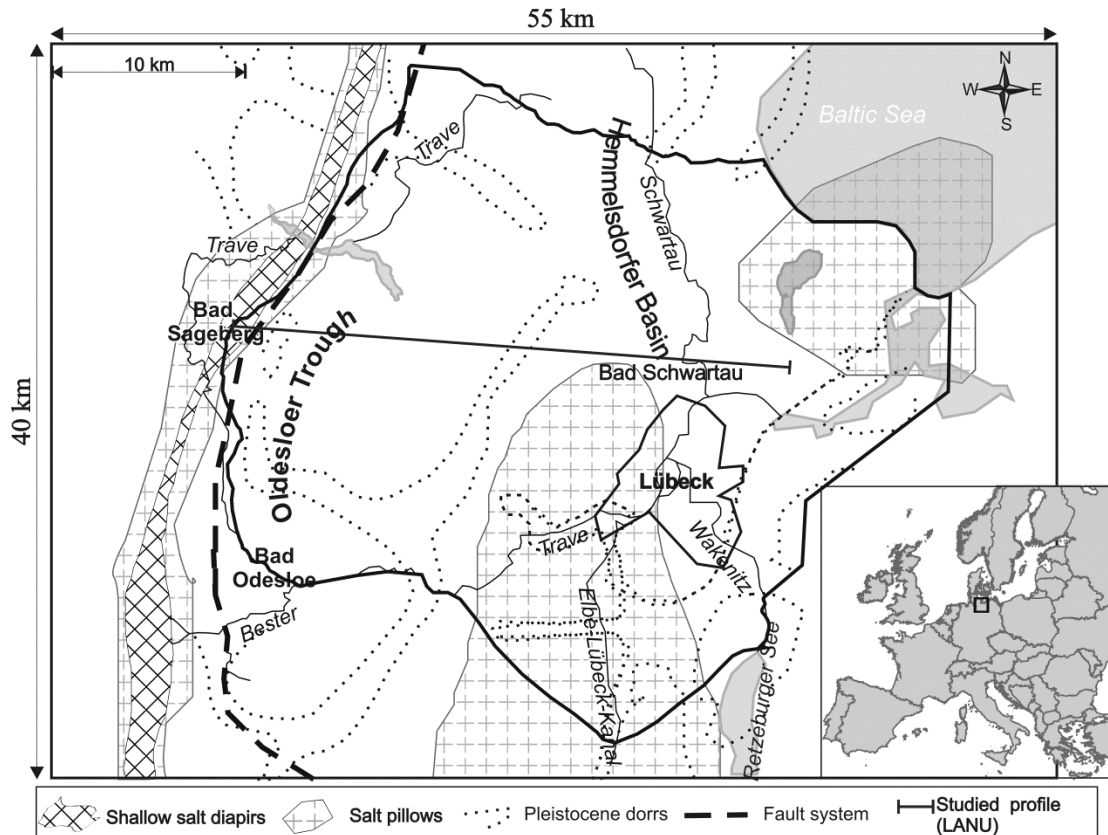


Fig. 1: Study area and location of: the salt structures (salt pillows from Weber, 1977 — salt diapirs from Baldschuhn et al., 2001), Pleistocene dorrs (Hinsch, 1974) and the shallow geological profiles investigated by the “Geological Survey” LANU (Agster, 2005)

Owing to the natural features of the S-H area, it will be possible to study the impact of shallow salt structures on salty groundwater flow, the interrelationships between shallow brine migration and young geological structures as well as the interaction between shallow and deep groundwater flow.

For these purposes, transient numerical simulations of groundwater flow are carried out along a selected profile of the basin (located in Fig.1) for two scenarios: a shallow and a deep aquifer-system.

The paper is structured as follows. First an overview about the hydrochemical data and the two hydrogeological settings is given. Afterwards, the modeling approach is briefly recalled and the numerical results will be presented for both model scenarios. Summary and conclusions of the major outcomes of these investigations are given at the end of the paper.

Understanding the mentioned shallow-deep interactions and their interrelationships with inherited geological features will provide new insights into the origins and formation of shallow and deep brine patterns within sedimentary basins.

HYDROCHEMICAL DATA AND HYDROGEOLOGICAL SETTINGS

Hydrochemical data

Friedrich (1902, 1917) investigated groundwater salinization in Schleswig-Holstein first. Further research was performed by Heck (1931, 1932, 1944, 1948a, 1948b, 1949). Johannsen (1954) and Vinck (1955) contributed additional aspects of groundwater salinization. Small scale maps by Johannsen (1979, 1980) and Grube et al. (1996) localize groundwater salinization in Schleswig-Holstein. Local investigations concentrated on the area of Bad Oldesloe and Lübeck (Johannsen, 1960; Löhnert, 1968, 1969; Bach et al., 1974; Schenck, 1978; Agster 2000a, 2000b, 2001; Köhler et al., 2005). Saltwater intrusion in coastal aquifer systems was widely investigated e.g. by Dittmer (1953, 1956), Petersen (1956), Schneider (1979) and Johannsen (1980). A summarizing review is given by Grube et al. (1996) and Pekdeger et al. (2006). Groundwaters are generally characterized by Ca and HCO₃ (Fig. 2). Alkaline waters have a medium mineralization of few g/l of Total Dissolved Solids (TDS). The salinization is mainly due to Cl and Na ions. Other widespread ions are Mg and SO₄.

Groundwater salinization is related to structural elements such as shallow salt diapirs, fault zones or interglacial channels. Widespread higher groundwater mineralization (up to several g/TDS) exists in aquifer systems located close to salinar structures, e.g. within the Oldesloe Trough (Fig.2). Nevertheless, most of the saline water occurrences in the Eastern part of the basin cannot be directly related to the presence of any shallow salt structures or faults neither to seawater intrusions. These waters are deep formation brines which reach the surface (Heck, 1932; Johannsen, 1980). In different areas of the Hemmelsdorf basin, the temperature field indicate anomalies which are characteristic of a convective regime (Pekdeger et al., 2006). Therein, thermally induced upward flows may play an important role. However, this hypothesis needs to be verified.

2.3 Brine migration: shallow salt structures and Pleistocene channels

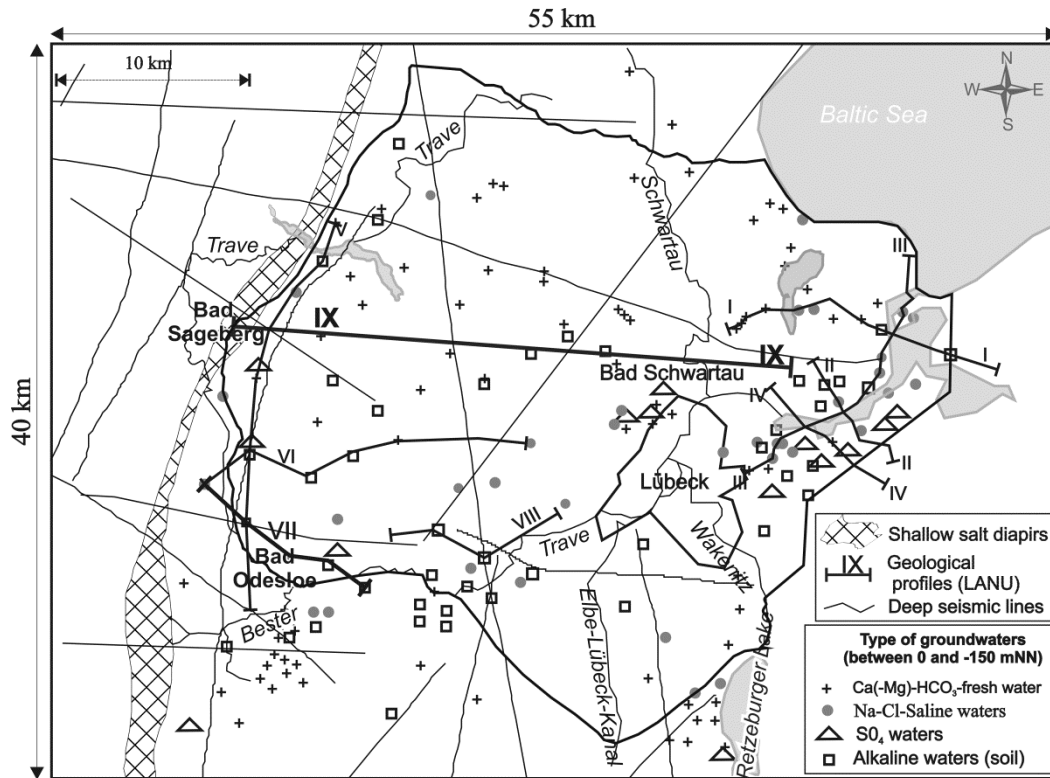


Fig. 2: Provides a map of the different types of groundwater in the Schleswig–Holstein aquifer at depth between 0 and –150 m. (Pekdeger et al., 2006) together with the location of: the salt structure (Baldschuhn et al., 2001), and the shallow geological profiles provided by the “Geological Survey” LANU (Agster, 2001)

With regard to anthropogenic impact, highly saline groundwater mainly occurs in the neighbouring of the towns as well as along the coastline and the rivers system where the aquifer is most exploited. In these areas, upconing of saltwater reaches the surface and forms saline springs. Examples are the saline springs in the discharge area of the river Trave (Löhnert, 1968; Cimiotti, 1983). Seawater intrusion is restricted to highly exploited costal aquifers.

Hydrochemical data also consist of shallow profiles provided by the Geological Survey LANU, as located in Fig. 2. These profiles were derived from wells drilled in the areas in which groundwaters are saline. They include the different lithologies and the types of groundwaters within the upper aquifers down to a depth of -500 m. More details concerning the stratigraphy will be given below. Hydrogeochemical data have been collected and compiled at the Freie Universität Berlin (Pekdeger et al., 2006). By example, in Fig. 3, the types of groundwaters and brine concentrations are shown for one of these profiles. Higher brine concentration is found in the Western part of the profile which is close to the Bad Segeberg salt diapir. Within the rest of the profile the TDS of the waters is rather low. Instable fluid density profiles form locally. These brine lenses are characterized by an inverted salinity gradient in which salinity decrease with increasing depths (Fig. 3). This feature is reflected throughout the whole S-H and its origin is unclear.

2.3 Brine migration: shallow salt structures and Pleistocene channels

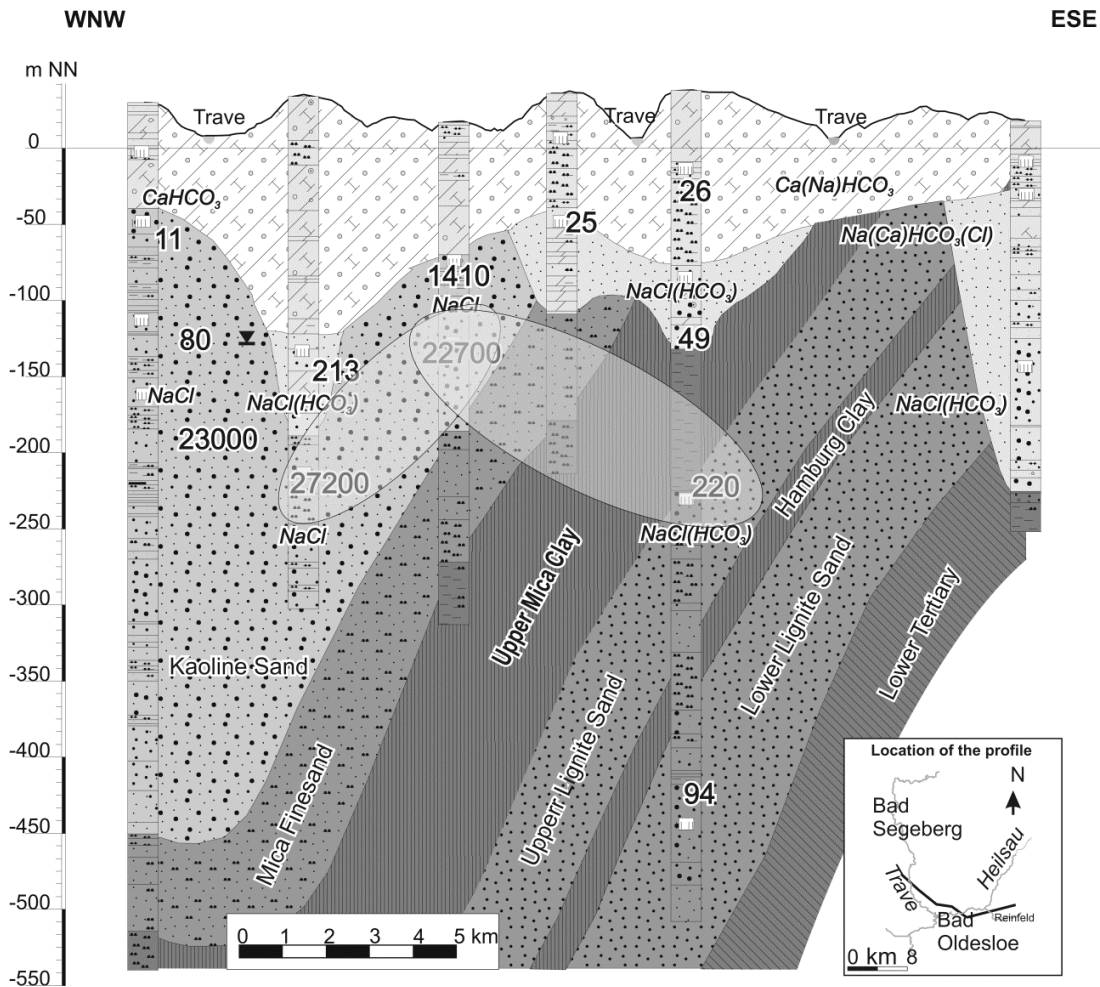


Fig. 3: Example of hydrogeochemical profile modified after Pekdeger et al., 2006 (Number VII, in Fig. 2). The chemistry of different brines is shown together with TDS concentration in mg/L. The shaded circles highlight instable stratification of brines (i.e. high salinity above more diluted brines). For clarity a 35:1 vertical exaggeration is used

Hydrogeological settings

Two structural settings are used for carrying out the numerical investigations. The first hydrological scenario is the shallow profile IX (Fig. 2). The second structural model is based on the Profile IX and also includes deep units (down to -5 km).

- The structural data of the shallow aquifer are based on geological profiles provided by the LANU (Agster, 2000a; 2001, 2005). The Profile IX is 30 km long and in the West-East and 500 m deep. The cross-section clearly shows different geological features which can influence transport processes (Fig. 4). All along the profile, the surface elevation varies. These topographical variations induce a regional flow from the highlands (recharge areas) to the lowlands (discharge areas). Regional flow enhances fluid circulation due to the viscous drag, promotes salt dissolution and drives salty plumes away from the salt domes (Evans et al., 1991).

2.3 Brine migration: shallow salt structures and Pleistocene channels

At the western ending of the profile the Zechstein-Salt is strongly uplifted. Besides being a source of salinity for groundwater, this salt structure provides a natural impervious boundary condition to fluid flow owing to its very low hydraulic conductivity. In that location, the vertical dipping fault points towards active salt-tectonics. Steep folds can be seen in the central part of the profiles together with two differently filled channels. The western channel is mainly composed of Quaternary sediments (till) while the central Pleistocene channel is filled with lacustrine sands. These units can act as preferential conduits for inflows of freshwaters as well as for uprising flow of deep-seated waters.

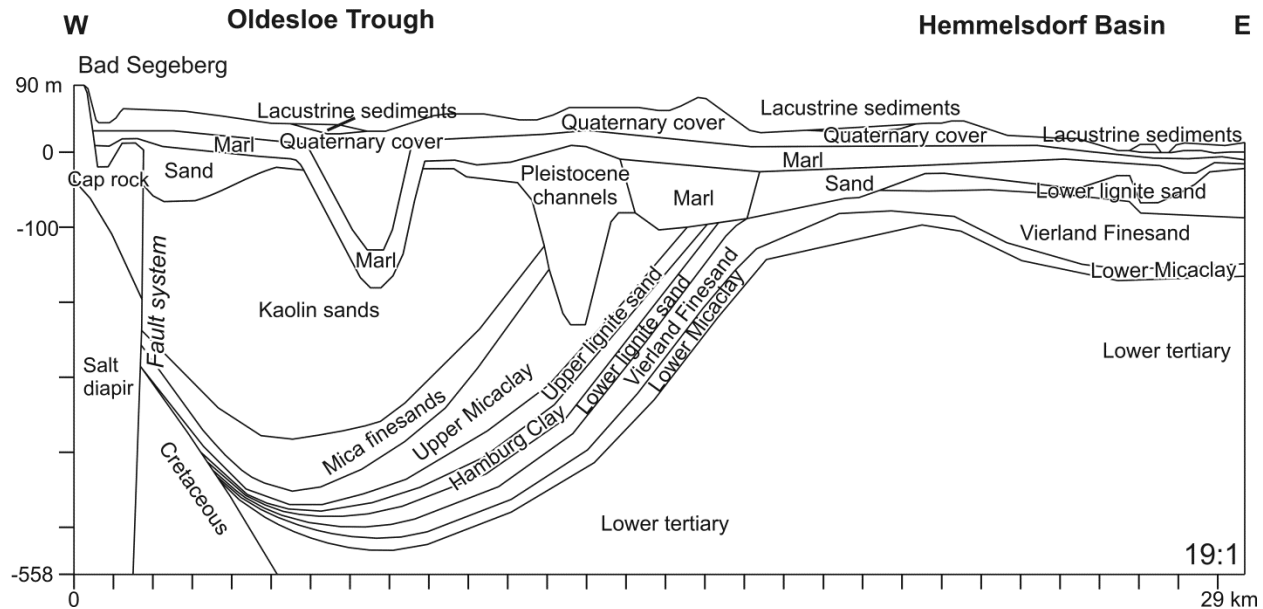


Fig. 4: Interpreted geological profile (profile IX in Fig. 2). This profile is used as structural setting for the numerical investigations of shallow fluid flow and brine migration. For clarity a 19:1 vertical exaggeration is used

The Oldesloe Through is built up of lower Mica Clay. This syncline is mainly composed of sand strata down to a depth of 450 m below the sea level. The Hemmelsdorf basin displays a sequence of Tertiary sands uplifted at a depth of -150 m. The upper aquifer of the entire system is bounded at the bottom by a unit of marl which can be considered quasi-impervious (aquitard). A similar groundwater system for this area is thoroughly described by Grube (2004).

This profile will serve as structural model for numerically investigating shallow fluid flow and brine migration with regard to the described geological features of the basin.

- Concerning the deep structural data, this area has been the subject of many studies and industrial exploitations. In addition to wells and seismic data, structural maps were provided by the Federal Department of Geosciences and Mineral Resources (BGR; Baldschuhn et al., 1996) which cover the area under consideration. The digital version of depth maps from the Geotectonic Atlas of NW Germany (Baldschuhn et al., 2001) was integrated into a three-dimensional structural model by Maystrenko et al. (2005, 2006). This 3D model was finally adjusted by using the results from seismic interpretation. The reflection seismic profiles (located

2.3 Brine migration: shallow salt structures and Pleistocene channels

in Fig.2) were interpreted down to the Zechstein (Maystrenko et al., 2005, 2006). Therefore, the geologic identification of the different stratigraphic units along the studied profile is also well established (Fig. 5). Furthermore, the major geological features of the shallow aquifer systems described in Fig. 4 have been incorporated within the Post-Paleogene unit (Fig.5). They include interbedded sand and clay strata as well as the glacial channels. These units and the rims of the diapirs provide the contact zones between the deep and shallow aquifers.

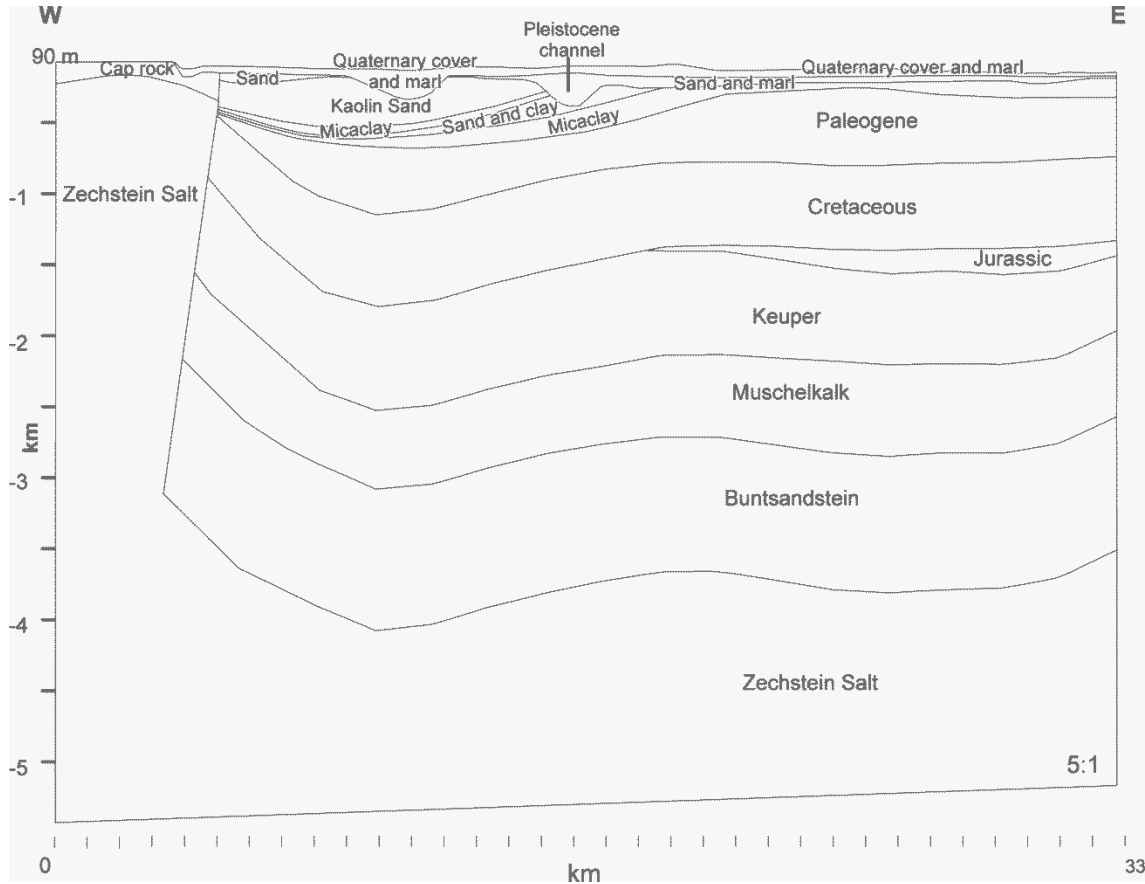


Fig. 5: Deep profile structure along the studied profile (according to the data from Maystrenko et al., 2005). The Post-Paleogene unit includes the major features of the shallow profile illustrated in Fig. 4. For clarity a 5:1 vertical exaggeration is used

In summary, the implemented deep model consists of eight units: from Post-Paleogene down to the Zechstein Salt which closes the model at 5.5 km of depth. The deep model has been extended to 33 km by incorporating a 4 km thick salt diapir. This will allow to take into account thermal effects resulting from the physical properties of the salt. At these scales, thick salt structures strongly disturb the temperature field owing to their high thermal conductivity. The resulting thermal anomalies can induce upward migration of dissolved halite which will interact with the shallow aquifer.

This profile will be used for investigating deep-fluid circulation. Owing to the mentioned structural characteristics, it will allow studying the interaction between deep brine plumes and the upper aquifer as well as the impact of the geothermal gradient on transport processes.

MODELING APPROACH

For solving the equations governing fluid flow, mass and heat transport, the commercial finite element software FEFLOW® (WASY-GmbH, 2002) has been applied. The mathematical formulation of these equations is not recalled here and can be found in Diersch and Kolditz (1998). The finite element mesh used for discretizing the shallow profile of Fig. 4 consists of approximately 101,000 triangular elements. The elements define a horizontal resolution of 20 m and have variable thickness in the vertical direction.

With regard to the deep profile of Fig. 5, a coarser mesh resolution of 120 m was used to discretize the units from the Paleogene to the Zechstein Salt. The grid of the Post-Paleogene unit, instead, is finer in order to accurately preserve the geometry of the smaller structures. Therein the resolution varies between 20 m and 40 m; the grid of the deep profile is made of 110,000 triangular elements.

The grids satisfy the regularity conditions and the resolution allows to model variations in fluid density.

Some simplifying assumptions have been made. According to hydrochemistry, major ions are Na and Cl. Therefore, brines are considered pure NaCl solutions. Fluid density data are numerically reproduced by use of polynomial expressions taking into account pressure, temperature and salinity dependencies (Magri, 2004; Magri, 2005). On the other hand, viscosity variations are neglected.

Model parameters

Each stratigraphic unit is considered homogenous and isotropic with regard to its physical properties (e.g. hydraulic conductivity, porosity, etc.). The values of these parameters for the shallow and the deep profile are given in Table 1 and Table 2, respectively. Although physical heterogeneities in the horizontal direction are not accounted, this first rough hydrogeological model allows differentiating the major aquifers at depths.

For this study, the available data have been averaged to an appropriate spatial basin-scale (i.e. km). Therefore, a certain degree of uncertainty exists due to the spatial variability of hydraulic properties. By observing Table. 2, it can be noticed that the whole Post-Paleogene unit has been considered homogeneous with respect to its thermal properties, while the structures within it are hydraulically different.

2.3 Brine migration: shallow salt structures and Pleistocene channels

Table 1: Parameters for the shallow profile of Fig. 4 (values are adapted from Agster, 1996 Grube and Lotz, 2004 and Martens, 2006)

Units	Hydraulic conductivity (10^{-4} m s^{-1})	Porosity (1)	Molecular diffusivity ($10^{-9} \text{ m}^2 \text{ s}^{-1}$)
Quaternary cover aquifer (Till)	4	0.3	80
Aquitard (Marl)	$7 \cdot 10^{-3}$	0.1	0.14
Lower Lignite Sand	2.8	0.1	56
Lacustrine sands Pleistocene channel	} 10	0.6	200
Kaolin Sand	3.2	0.3	64
Mica Finesands	$5 \cdot 10^{-2}$	0.2	1
Upper Micaclay	$5 \cdot 10^{-5}$	0.5	$1 \cdot 10^{-3}$
Upper Lignite Sand	1	0.6	20
Hamburg Clay	$5 \cdot 10^{-5}$	$5 \cdot 10^{-2}$	$1 \cdot 10^{-3}$
Lower Lignite Sand	2.8	0.1	56
Vierland Finesand	0.3	$2 \cdot 10^{-2}$	6
Lower Micaclay	$1 \cdot 10^{-5}$	0.5	$2 \cdot 10^{-4}$
Lower Tertiary	$1 \cdot 10^{-2}$	0.1	0.2
Salt diapir – Cap rock	$1 \cdot 10^{-16}$	$1 \cdot 10^{-6}$	$2 \cdot 10^{-15}$

Table 2: Parameters for the deep profile of Fig. 5. The values for the Post-Paleogene units (in the brace) are averages at basin-scale. The parameters for the deep units are adapted from Scheck (1997)

Units	Hydraulic conductivity (10^{-4} ms^{-1})	Porosity (1)	Volumetric heat capacity ($10^6 \text{ J m}^3 \text{ C}^{-1}$)	Thermal conductivity ($\text{W m}^{-1} \text{ C}^{-1}$)	Molecular diffusivity ($10^{-9} \text{ m}^2 \text{ s}^{-1}$)
Quaternary cover and marl	$1 \cdot 10^{-2}$	0.3	3	1.3	0.2
Sand and marl	0.1	0.5	3	1.3	2
Sand	5	0.6	3	1.3	100
Kaolin Sand	3.20	0.3	3	1.3	64
Mica Finesand	$5 \cdot 10^{-2}$	0.2	3	1.3	1
Micaclay	$1 \cdot 10^{-5}$	0.32	3	1.3	$2 \cdot 10^{-4}$
Sand and clay	$1 \cdot 10^{-3}$	0.3	3	1.3	$2 \cdot 10^{-2}$
Paelogene	0.5	0.23	3.15	1.5	10
Cretaceous	0.2	0.11	2.5	1.9	4
Jurassic	$1 \cdot 10^{-4}$	0.13	3.19	2	$2 \cdot 10^{-3}$
Keuper	$1 \cdot 10^{-6}$	$1 \cdot 10^{-4}$	2	2.5	$2 \cdot 10^{-5}$
Muschelkalk	$1 \cdot 10^{-7}$	$1 \cdot 10^{-6}$	2.4	1.85	$2 \cdot 10^{-6}$
Buntsandstein	$1 \cdot 10^{-4}$	$4 \cdot 10^{-2}$	3.15	2	$2 \cdot 10^{-3}$
Cap Rock	$1 \cdot 10^{-16}$	$1 \cdot 10^{-6}$	1.9	3	$2 \cdot 10^{-15}$

2.3 Brine migration: shallow salt structures and Pleistocene channels

Zechstein Salt	$1 \cdot 10^{-16}$	$1 \cdot 10^{-6}$	1.81	3.5	$2 \cdot 10^{-15}$
----------------	--------------------	-------------------	------	-----	--------------------

Boundary conditions

The following boundary conditions are applied:

- At the surface, head, temperature and solute boundaries are prescribed. The head is fixed to the local topographical elevation which induces a steady regional flow. Since springs of warmer saline waters are observed in the study area (Schirrmeister, 1996; Grube et al., 2000), heat and dissolved salt are allowed to flow through the surface by use of an open boundary condition (Cauchy). The reference values for the temperature and for the salt concentration at the surface are respectively 8 °C and 0 g/L (i.e. freshwater). Further details on the equations governing these boundary conditions can be found in Magri et al., (2005b) and Magri (2005).
- At the bottom, a constant temperature boundary condition of 160 °C was defined. This value corresponds to a linear vertical gradient of approximately 30 °C/km.
- At the top of the salt, the brine concentration was fixed at 345 g/L, representing an approximate value for halite saturation. By setting a constant concentration value at the Top salt, the basin undergoes a continuous salt replenishment. Nevertheless, the shape of the salt layer remained unchanged.
- The lateral boundaries are closed to fluid, heat, and mass flow.

Initial conditions

The initial pressure and temperature conditions are respectively derived from steady-fluid flow and steady conductive heat transport models

The initial salt concentration is set to saturation concentration (i.e. 345 g/l) within the salt while freshwater conditions (i.e. 0 g/L) are defined everywhere above the Salt unit. However, the sediments of the NEGB were deposited during marine transgression (Scheck, 1997). Therefore, an initial salinity profile in which brine concentration increases linearly with depth has also been tested in order to account for paleo-salinity conditions.

NUMERICAL SIMULATIONS: RESULTS

Different types of numerical simulations have been carried out.

- Coupled fluid flow and mass transport simulations are run in the shallow and in the deep model scenarios (Par. 4.1 and 4.2 respectively).
- The impact of the geothermal gradient is then investigated in the deep model scenario (Par. 4.3).

Shallow profile scenario

Large-scale topography-driven flow (i.e. regional flow) and density-driven flow develop within the profile (Fig. 6a). Generally, in areas of variable topographic relief, the groundwater flows from recharge to discharge areas parallel to the land-surface topography. Here, the numerical simulations also indicate that the stratigraphic framework of the units strongly control brine migration within the shallow aquifer. Three units play a major role: the fault along the salt flank, the glacial channels and the interbedded sand units. Vigorous recharge inflow occurs from the uplifted cap rock along the fault system (Fig. 6a). In that area, close to the surface, flow rates can reach values up to 1 m/d. Brine plumes form in the upper part of the salt flank, just below the cap rock (Fig. 6b). These saline plumes protrude within the Kaolin Sand unit at few centimetres per day. Therein, streamlines are parallel to the Upper Micaclay unit, which bounds the flow due to its low hydraulic conductivity (Table 1). Within the Quaternary channel, brine with several g/l of dissolved salt discharges through the surface advected by the intense regional flow (Fig. 6b). Within this glacial channel, the vertical stretched plumes define a narrow lens in which the salinity distribution is inverted. This is in good agreement with the hydrochemical observations (Fig.3). By contrast, the eastern neighbouring Pleistocene channel enhances inflow of freshwater as it is located in a recharge area. Within the Pleistocene channel the inflow is less intense (few centimetres per day) since the upper part of this unit is bounded by a marl cover which reduces the velocity field (Fig 6a). As a result, this unit favours freshwater and brine mixing. Therein, the TDS concentration is close to freshwater conditions (Fig. 6b: few mg/l, not displayed in the legend) and no brine lenses form.

2.3 Brine migration: shallow salt structures and Pleistocene channels

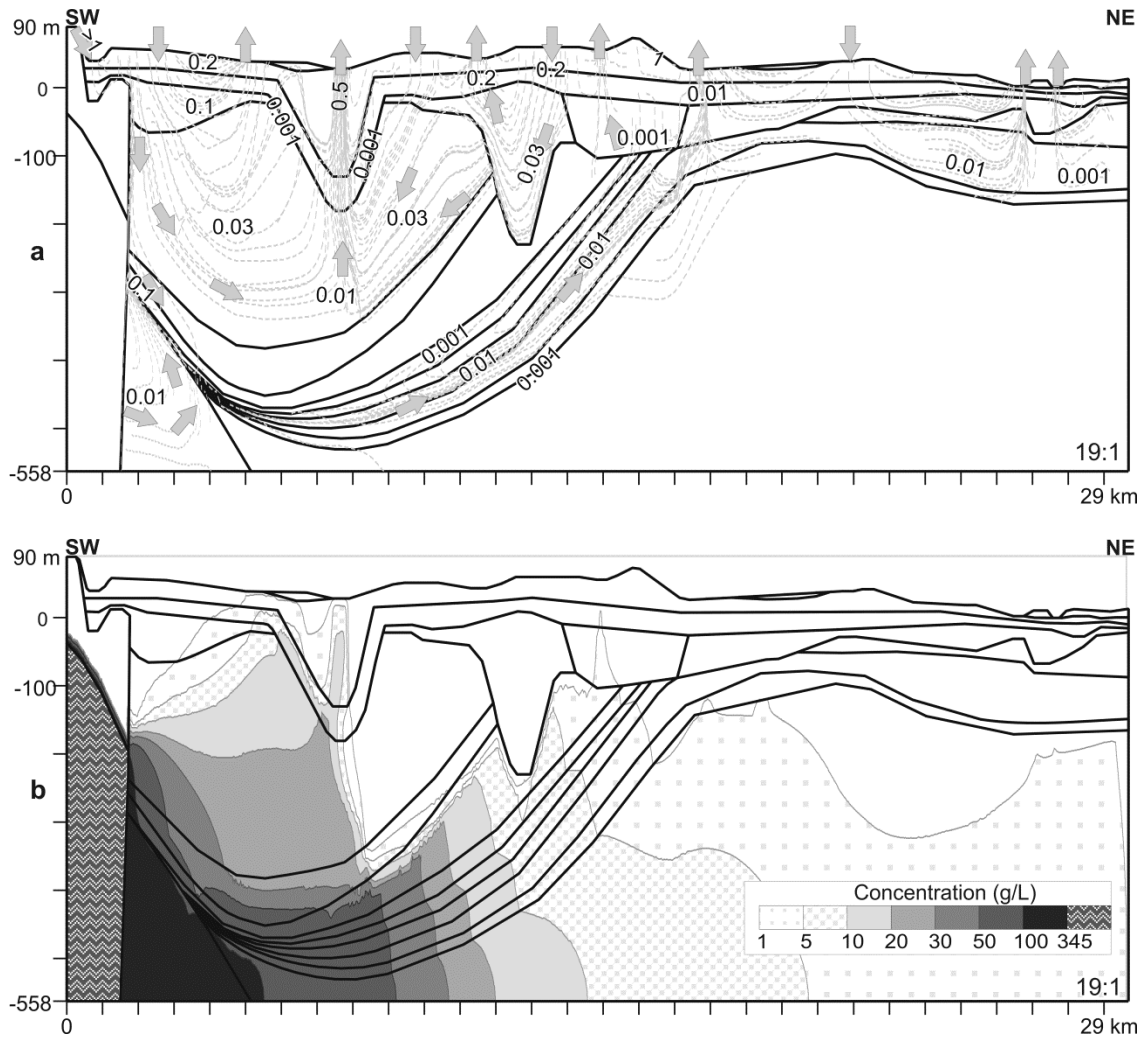


Fig. 6: (a) Pore velocity field (meters per day) calculated from a coupled fluid flow and mass transport problem. Dashed lines depict the groundwater flow pathways, arrows indicate the flow direction. (b) and (c) Calculated brine concentration (g/l) at (b) 50 y and (c) 52 ky. For clarity a 19:1 vertical exaggeration is used

Within the Cenozoic, downward groundwater flow along the salt flank is further enhanced by strong salt dissolution. Highly concentrated brines sink from the salt flank into the Cenozoic unit driven by density (Fig. 6b), generating a gravitational convective cell (Fig. 6 a).

As time progresses, the brine patterns within the Kaolin unit and the Quaternary channel do not vary (compare figures 6c and 6b) suggesting that therein a steady concentration gradient is reached. On the other hand, the dissolved halite saturating the Cenozoic migrates toward the steep sand units in the central part of the profile (Fig 6c). In this scenario, interbedded sand units provide a preferential channel for rising brine flow. Therein, salty waters ascend at few centimetres per day over more than 15 km below the upper part of the aquifer-system. This channelled groundwater flow exfiltrates in the lacustrine sediments of the Hemmeldorf Basin at 18 km from the Bad Segeberg salt diapir. Within the Lower Tertiary salt diffusion is dominant. This process is very slow and saturates the whole unit with brackish waters.

2.3 Brine migration: shallow salt structures and Pleistocene channels

It turned out that the simulated flow and brine patterns were not drastically affected by changing the hydraulic conductivity of the different units, while the velocity field strongly depends on this parameter. In the presented scenarios, the flow velocity is rather heterogeneous ranging from half meter per day in the upper part of the aquifer-system to few millimetres per day in the more impervious units. However, the velocity field allows a rough evaluation of brine residence times within the profile. By example, the brine plumes forming within the Kaolin unit need approximately 50 years to spread over the surface. On the other hand, the brine flow forming at the Bad Segeberg diapir takes more than 5,000 years to ascend over the central sand unit. This time-scale is in good agreement with the results obtained by Grube and Lotz (2004). However, in their simulations, salt dissolution was not taken into account.

In summary, the results of these simulations indicate that the groundwater flow is affected by the presence of the fault, the glacial channels and the sand units. The fault along the salt flank provides the major inflow conduit of groundwater. Descending waters dissolve the salt and form density-driven brine flow. These salty waters are then released through the Quaternary channel of the Oldesloe Trough, advected toward the surface by vigorous topographic-driven flow. As a result, bifurcated plumes rising to the surface provide the primary cause for the observed instable brine lenses within the shallow aquifer.

Ascending brine migration also takes place through the sand units which discharge the saline waters farther East within the Hemmelsdorf Basin. On the other hand, the Pleistocene channel recharges the sediments with freshwater which prevents brines from reaching the surface. Heavy saline waters sink into the bottom aquifer and saturate the Cenozoic. A salty front slowly diffuses throughout the Lower Tertiary. With regard to these deeper brine flows, the bottom boundary conditions are dominant. The prescribed no flow condition impedes saline waters to sink into the deeper units, forcing salt to diffuse eastward.

The deep profile scenario will allow investigating the interaction between shallow and deep transport processes.

Deep profile

The results of coupled fluid flow and mass transport simulations are illustrated for two time steps in Figures 7. At the beginning of the simulation process, brine patterns develop within the upper aquifer (Fig 7a). The dissolved salt stretches horizontally over 5 km from the salt diapir. A brine lens forms within the Quaternary channel and reaches the surface at its middle, advected by the regional flow. The process is analogous to the brine migration described in the previous shallow model scenario (compare Fig 7a and Fig. 6b). However, different fluid-dynamic processes are involved. Below the horizontal brine plume several brine fingers form and sink in the Paleogene unit (Fig. 7b). This source of salinity from above leads to an instable density stratification which in turn generates gravitational convective cells. In this scenario, the flow

2.3 Brine migration: shallow salt structures and Pleistocene channels

rate of the cells is few millimetres per day. By increasing the hydraulic conductivity of the Palaeogene, the cells developed at higher flow rates (up to several centimetres per day). At the same time, highly saline patterns form along the steep salt flank and start sinking into the deeper units.

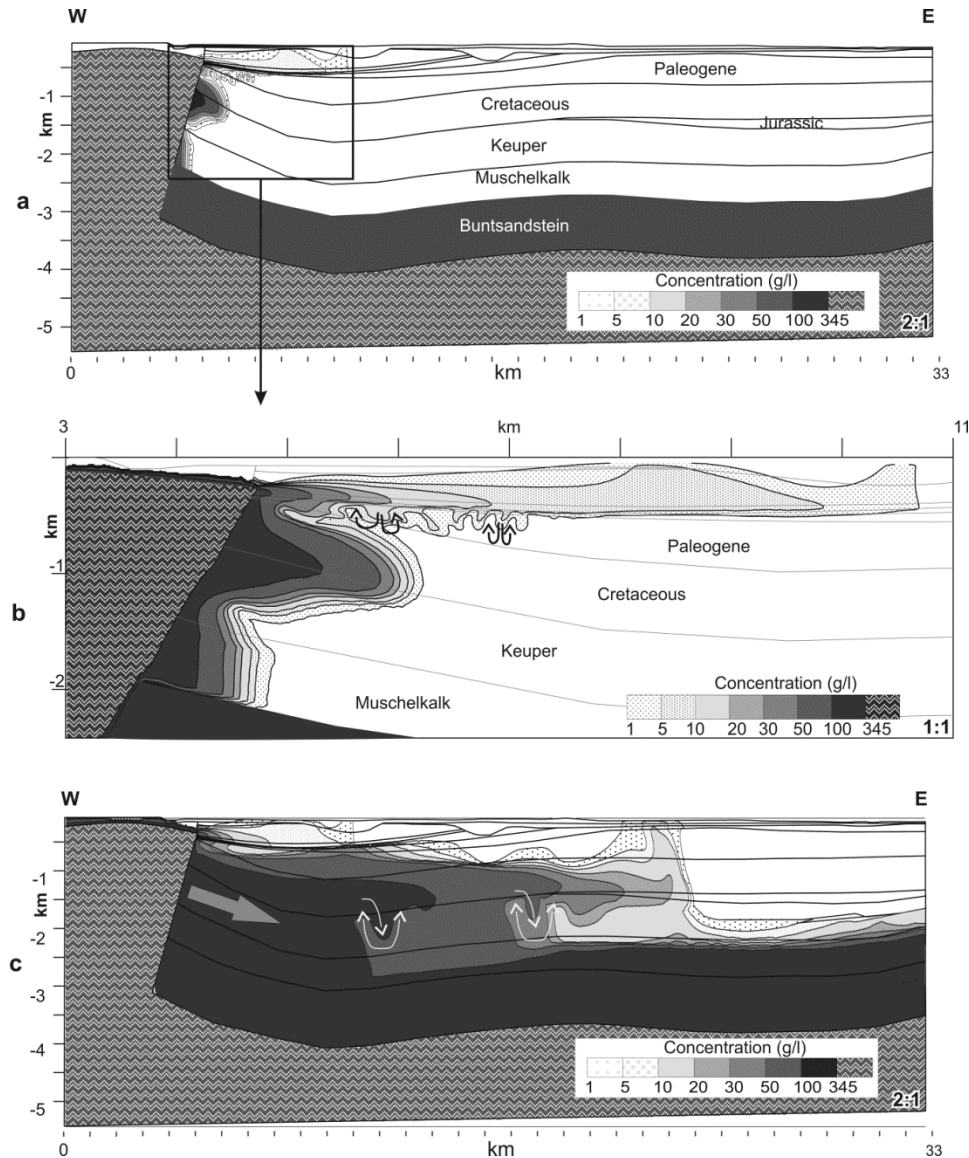


Fig. 7: Deep profile: coupled fluid flow and mass transport simulation. (a) and (b): Calculated salinity profiles in g/l at 290 y and (c) at 10 ky. The vectors depict the direction of the gravitational convective flow. For clarity a 2:1 vertical exaggeration is used

As time progresses, the sinking brine fingers merge within the Palaeogene (Fig. 7c). Consequently, the convective regime evolves to a linear salinity gradient. On the other hand, within the Cretaceous and the Keuper, the dense brine plumes continue protruding eastward affected by gravitational convection. Density-driven cells of 1 km radius develop at the brine fronts. This can be explained as follows. Since the Cretaceous is more permeable than the Keuper (Table. 2), a brine front descends faster within the Cretaceous than it migrates within

2.3 Brine migration: shallow salt structures and Pleistocene channels

the Keuper. As a result, a finger-tip forms and sinks under gravitation into the underlying slower migrating brines. The downward movement of the brine lid pushes the deeper brines upwards generating the convective cells.

At the final stage of the simulation, an extended brine plume stretches horizontally over 18 km. Since the plume forms at the salt diapir, the concentration gradient decreases in the eastward direction. Eventually, brines flowing at 2 km depth within the Cretaceous are advected toward the surface of the Hemmelsdorf basin, in relation to the discharge area. In the presented case, the brines reached the shallow aquifer 10,000 years after their formation at the Bad Segeberg salt diapir. At the Hemmelsdorf basin, an initially linear salinity profile (paleo-salinity conditions) also evolved to a brine upconing. This suggests that, at that location, surficial salty waters can be a mixture of formation waters (paleo-brines) and brines forming at the salt diapir.

Sensitivity analyses were used to study the effects of varying hydraulic conductivity of the Cretaceous and Keuper. By increasing this parameter by one order of magnitude, the general flow patterns did not change significantly. However, brines formed and migrated much faster. At a given time steps, the calculated concentrations throughout the whole profile were also higher. The deep gravitational convection cells disappeared when the hydraulic conductivity of the Keuper was drastically decreased (set to almost impervious). In this case, a single brine tip developed migrating within the Cretaceous toward the Hemmelsdorf basin.

These simulations allowed studying the interrelationships between shallow salty water and deep brine flow. Dissolution of halite from above provides an instable source of salinization for the deep aquifer systems. Small convection cells driven by gravity form and brine lenses sink vertically toward the Paelogene unit. At the same time, highly saline plumes developing within the Mesozoic units are affected by gravitational convection but at larger scale. This fluid-dynamic does not affect brine distribution within the shallow aquifer. However, gravitational convection within deep aquifers strongly perturbs the concentration field. The simulations indicate that, on a local scale (i.e. in a range of few km), these cells can be responsible for salinity inversion. Furthermore, the described deep fluid-dynamics are controlled by the hydraulic conductivity of the Mesozoic units. By decreasing the value of this parameter, the gravitational convection did not develop, suggesting that this phenomenon is likely to occur in permeable units close to shallow salt structures.

The simulations also showed that in the Hemmelsdorf Basin the regional flow can form upconing of deep formation waters and brine plumes. This is in good agreement with the hydrochemical data.

Deep profile: impact of the geothermal gradient.

At this state, the effect of the geothermal gradient on fluid transport processes has to be investigated. For this purpose, two different simulations have been carried out. In the first case, a coupled fluid flow and heat transport model is run (thermally induced flow). Subsequently, the effects of dissolved salt are also accounted (thermohaline flow).

Thermally induced flow

The temperature field calculated from a coupled fluid flow and heat transport simulation is illustrated in Fig. 8. Different regimes developed within the profile.

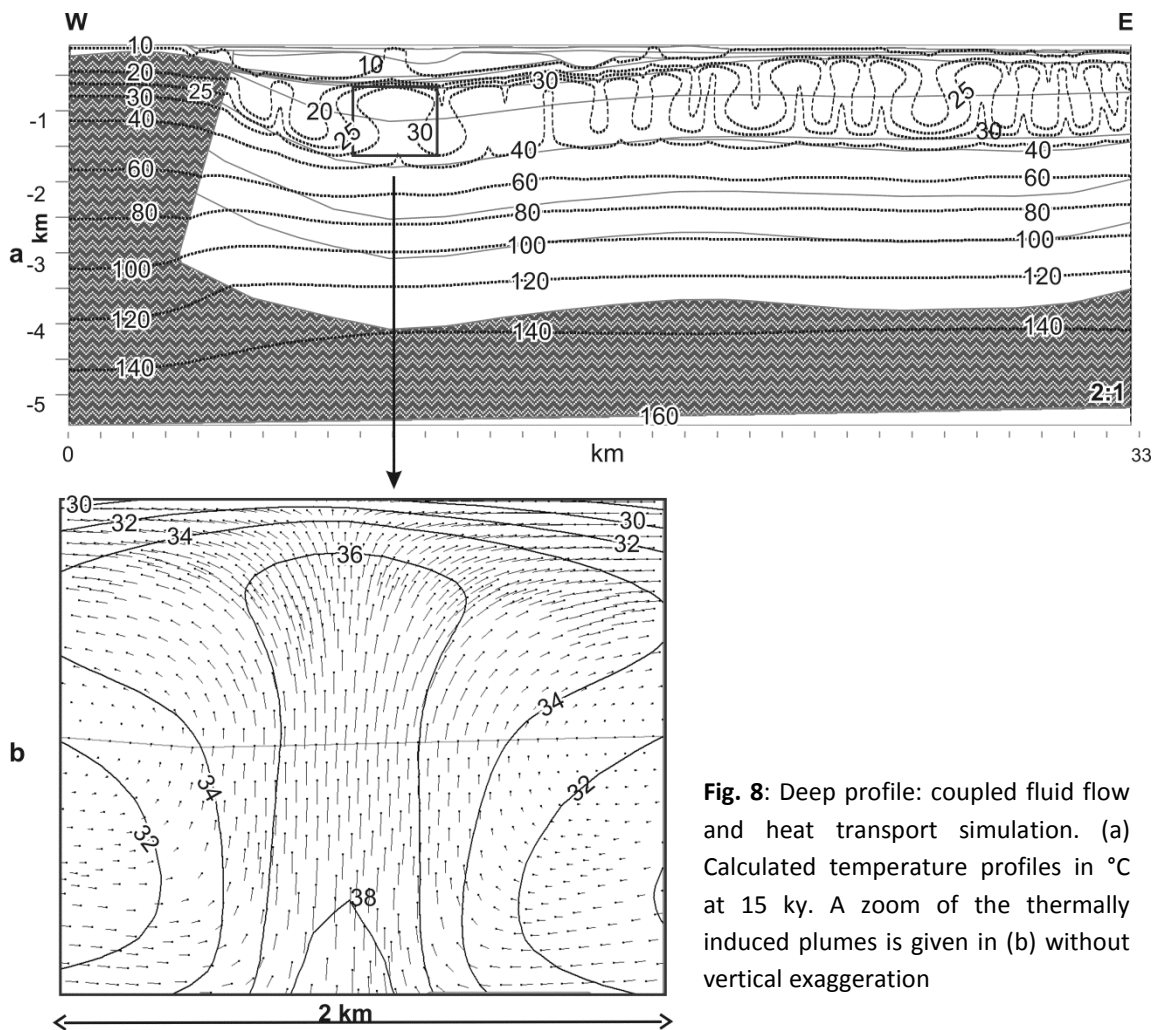


Fig. 8: Deep profile: coupled fluid flow and heat transport simulation. (a) Calculated temperature profiles in °C at 15 ky. A zoom of the thermally induced plumes is given in (b) without vertical exaggeration

Within the salt unit, the thermal regime is conductive. Owing to the strong contrast between the thermal conductivity of the salt and the neighbouring sediments (Table. 2), concave isotherms are found within the salt diapir while convex isotherms are adjacent to the salt flank.

2.3 Brine migration: shallow salt structures and Pleistocene channels

These anomalies are well known and found in geothermal basins hosting salt structures (e.g. O' Brien and Lerche, 1984).

Above the salt, advective, convective and conductive heat flow affect the whole profile. Within the Post-Paleogene units, the regional flow is dominant. Increased temperature gradients are found in direct association with discharge areas. For instance, the fluid temperature within the Quaternary channel increases by about 2 °C. A similar temperature increase can be observed at the discharge area of the Hemmelsdorf Basin. On the other hand, inflow of colder water decreases the temperature in the recharge areas.

According to the Rayleigh theory in a porous media, the onset of multi-cellular convection is favoured in thick and permeable units (Nield, 1968). This is the case for the Paleogene and the Cretaceous units where a thermally induced convective regime controls the flow. Thermal plumes of 1.5 km height rise vertically from the Cretaceous basis up to the surface, bounded by the regional flow. A zoom of an ascending thermal plume is shown in Fig 8b. The cell radius is 1 km and the flow rate in the central part of the plume is few millimetres per day.

In the deeper units the isotherms are not perturbed and the regime is conductive.

Thermohaline flow

Here the salinity effects are also accounted in the simulations, providing a complete picture of the major transport processes within the profile. Temperature and salinity profiles are shown in Fig.9.

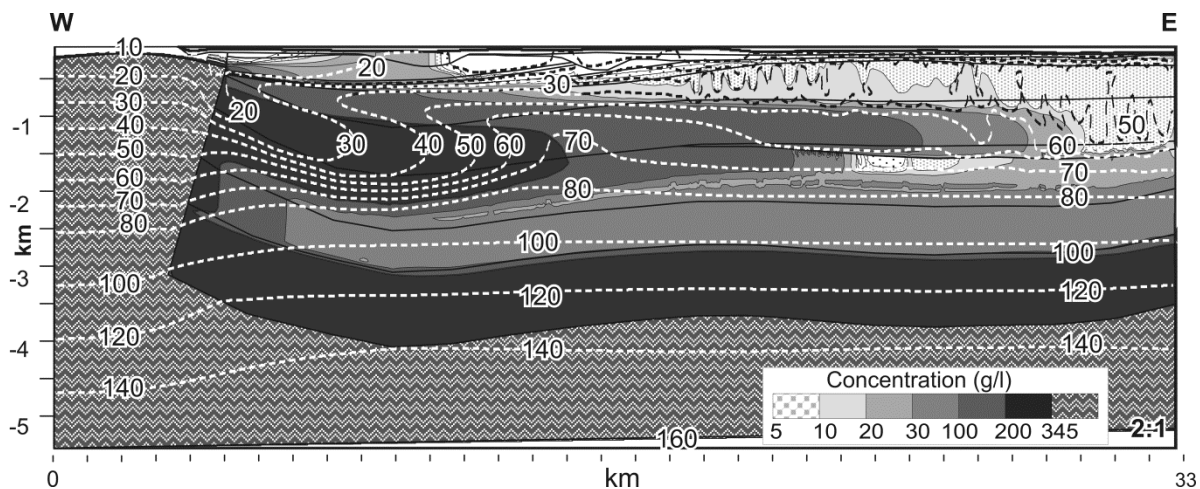


Fig. 9: Deep profile: thermohaline simulation. Calculated mass (filled patterns, g/l) and temperature profiles (dashed lines, °C) at 15 ky

Highly saline brines protruding from the salt diapir into the Cretaceous overwhelm the less intense thermal convective regime. Heat plumes do not stretch vertically but develop almost horizontally in the brine flow direction (compare figures 9 and 8). Therefore, the temperature

gradient increases horizontally from the salt flank toward the center of the profile. As a result, the temperature field can undergo several inversions with increasing depth in the western part of the profile.

In the Paleogene unit of the Hemmeldorf basin, thermohaline convection persists. Above the horizontally stretched plume, the temperature oscillations generate small convective brine cells (half kilometre radius). As a result, thermally driven saline waters ascend up to the shallow aquifer and spread locally at several points of the surface.

On the other hand, in the other units of the profile, the geothermal gradient do not significantly influence brine patterns. Within the Post-Paelogene, the regional flow drives heat and dissolved salt. Within the Bunstandstein and the Muschelkalk, the regimes are mass diffusion and heat conduction.

SUMMARY AND CONCLUSIONS

Hydrochemical data indicate that in S-H salty groundwater occurrences are partly related to structural features of the basin such as shallow salt structures, faults and glacial channels. The salinity profiles highlighted the presence of brine lenses and inverted salinity profiles throughout the basin. Furthermore, deep formation brines observed at the surface of the Hemmeldorf basin point toward strong interaction between deep fluid flow and shallower aquifer systems.

Numerical simulations of fluid transport processes have been carried out on a shallow and deep profile scenario in order to study: (1) the role of shallow salt dissolution and young geological units on groundwater flow, (2) the interrelationships between shallow brine migration and deep fluid flow and (3) the impact of the geothermal gradient on the whole groundwater system.

These investigations provided possible explanations for the unsolved issues and allowed to gain insights on transport processes within geothermal basin.

Brine flow within the upper shallow aquifer is strongly controlled by the different geological units. The fault system along the salt diapir is the major conduit for freshwater inflow. This groundwater recharge favours salt dissolution along the salt flank. The resulting brines flow easily within highly permeable aquifers. Quaternary channels located in discharge areas provide preferential conduits for brine outflow. Therein vertically stretched brine plumes define narrow brine lenses and inverted salinity profile. By contrast, this feature does not concern highly permeable channels located in recharge areas. The Oldesloer Trough sand units underlying the whole aquifer system promote ascending flow of brines. Brines can migrate within interbedded sand units over several km and discharge far from the salt diapirs where they formed.

The deep profile scenario allowed studying shallow and deep flow interactions and inferring the fluid-dynamics affecting brine flow within S-H.

2.3 Brine migration: shallow salt structures and Pleistocene channels

Shallow salt dissolution provides an instable source of salinization for the deeper aquifers. Brine plumes sinking into permeable units can generate gravitational convection. This flow perturbs the salinity gradient leading to instable fluid-density stratification in which heavier fluids overlay lighter brines.

Deep formation waters can be advected toward the surface of the Hemmelsdorf basin by the regional flow. However, in this area, the geothermal gradient is also responsible for upward migration of deep brines. Therein thermohaline convection developed and salty waters reached the surface in different areas. By contrast, thermally induced flow is overwhelmed by vigorous downward flow of highly saline brines.

Beside topography-driven flow, the different convective regimes are a mechanism for extensive solute exchange between shallow and deep aquifers. The described flows could develop in any basin hosting salt diapirs piercing shallow aquifer-systems.

ACKNOWLEDGMENTS

This project is supported by the German Science Foundation (DFG) as part of the SPP 1135 “Dynamics of Sedimentary Systems under varying Stress Conditions by Example of the Central European Basin System”. The geological data of the NEGB have been provided by Dr. M. Scheck-Wenderoth and Dr. Y. Maystrenko. We acknowledge LANU (Landesamt für Natur und Umwelt) for the support and providing additional data.

2.4 Transition zones and variable viscosity

GEOFLUIDS

Geofluids (2009) 9, 182–194

doi: 10.1111/j.1468-8123.2009.00242.x

Impact of transition zones, variable fluid viscosity and anthropogenic activities on coupled fluid-transport processes in a shallow salt-dome environment

F. MAGRI^{1,2}, U. BAYER², U. MAIWALD¹, R. OTTO³ AND C. THOMSEN³

¹Fachrichtung Geochemie, Hydrogeologie, Mineralogie, Freie Universität Berlin – Institut für Geologische Wissenschaften, Berlin, Germany; ²Helmholtz Centre Potsdam GFZ German Research Centre for Geosciences Deutsches GeoForschungsZentrum, Telegrafenberg, Potsdam, Germany; ³Landesamt für Natur und Umwelt des Landes Schleswig-Holstein, Flintbek, Germany

ABSTRACT

In the Schleswig-Holstein region (S-H) of Germany, most observed near-surface saline ground waters originate from dissolution of shallow salt domes. Previous numerical simulations of thermohaline flow clarified the major mechanisms controlling large-scale density-driven flow. It has been found that, in addition to topographically driven flow, gravitational and thermohaline convection are the primary mechanisms for extensive solute exchange between shallow and deep aquifers. Geological features such as glacial channels control recharge/discharge processes at the surface. Here we address several previously unresolved issues: (1) the impact of a permeable unit (transition zone) between the salt and adjacent units; (2) the role of variable brine viscosity in affecting regional- (i.e., km-) scale heat and mass patterns; and (3) the influence of anthropogenic activities such as pumping stations on density-driven flow. We found that geophysical factors play a major role in determining the dynamics of fluid processes. The transition zone significantly influences the flow field and the distribution of heat, slowing the formation of highly concentrated salty plumes. The impact of variable fluid viscosity on the coupled heat and brine flow is twofold. In a colder and highly concentrated environment, such as a shallow salt-dome crest, it retards brine flow. In a less saline environment, variable fluid viscosity enhances thermally induced upward fluid flow. Groundwater extraction from production wells only affects brine and heat flow locally within the upper aquifers.

Keywords: shallow salt dome, variable brine viscosity, brine density, numerical modeling, thermohaline flow, pumping well, German Basin

INTRODUCTION

Shallow salt domes are common geological features in many sedimentary basins (Jackson and Talbot 1991). Salt domes strongly influence groundwater transport processes as they create permeability discontinuities and generate hydraulic, thermally and density-driven forces that lead to thermohaline flow. Thermohaline flow is extensively documented in studies of the Gulf Coast region of the United States (e.g., Evans and Nunn 1989, Evans et al. 1991, Hanor 1987, Ranganathan and Hanor 1988, Sharp et al. 2001, Wilson and Ruppel 2007). Thermohaline convection in the vicinity of salt domes can explain field-based observations of salinity and thermal anomalies around salt structures (Williams and Ranganathan 1994, Sharp et al. 2001). In salt-dome environments groundwater can be driven by density gradients induced by thermal and salinity effects of the salt itself (Evans et al., 1991). Thermally driven convection near salt domes is a possible transport mechanism for upward flow provided that thermal effects are not overwhelmed by salinity effects (Evans & Nunn 1989).

In these studies, complex allochthonous salt structures have been idealized as cylindrical or rectangular-shaped bodies. Furthermore, the surrounding porous medium has usually been considered a structurally simplified homogeneous flow domain.

The Northeast German Basin (NEGB) has recently served as a study area for simulating thermohaline flow within a real basin hosting different salt structures. These simulations have provided interesting examples of diapir-related thermohaline convective flow in a basin whose stratigraphy is constrained by seismic lines and deep boreholes and is therefore geologically well defined. It has been found that upward solute migration takes place within the NEGB. At 4 km depth, salty waters forming near deep-seated salt structures ascend to the surface, driven by thermal buoyant forces (e.g., Magri et al. 2007).

Additional investigations based on the Schleswig-Holstein (S-H) region, Germany (Fig.1) have highlighted how shallow salt structures piercing the surface aquifers influence the complex dynamics of saline groundwater flow. In this area, salt domes are among the sources of observed groundwater salinity near the surface of the basin. Other causes of salinity are upconing of deep-seated brines, seawater intrusion in coastal aquifers, and groundwater pumping stations (e.g., Agster 2001, Grube and Lotz 2004, Tesmer et al. 2007, Möller et al. 2008). Previous numerical models of thermohaline flow carried out along a vertical profile through the S-H region (Magri et al. 2008) have shown that brines forming near salt structures can ascend to the surface, driven by topographically induced flow and thermal buoyant forces (mixed convection). Furthermore, the numerical results indicate that, in addition to mixed convection, downward gravitational convection generated by unstable salinity profiles occurs near salt structures within the deeper units. These convective phenomena are likely the major

mechanisms for solute migration and heat transfer between shallow and deep aquifer systems of the S-H region.

Although previous simulations were based on a real geological setting in the S-H area, three important simplifying assumptions were made. First, it has always been assumed that the salt defines a sharp boundary, in direct contact with the surrounding units. This is probably not the case in actuality because salt tectonics involve complex salt flow dynamics and irregular deformation of surrounding sedimentary rocks (e.g., Jackson and Talbot 1991). Along the studied profile (Fig. 1), the salt diapir developed as buried low-density salt deposits coalesced and flowed upward, driven by higher-density surrounding sedimentary rocks (Agster 2000, Maystrenko et al 2006). As the diapir ascended, a shear zone likely developed between the salt and the surrounding sedimentary rocks. This shear zone is presumably characterized by very high strain and intermixing of salt and fragments of sedimentary rock. This zone is here referred to as the transition zone. Although the exact structure and relative proportions of salt and sedimentary rock within this transition zone remain unknown, it is reasonable to assume that its permeability lies between that of the salt and that of the sedimentary rock. Thus in the simulations described here, a transition zone between the salt flank and the sediments is included to investigate its influence on groundwater transport processes. A second important simplification concerned fluid viscosity, which was assumed constant. However, when salinities and temperatures vary over a wide range, fluid viscosity cannot be regarded as a constant property. Patil and Vaidyanathan (1982) found that variable fluid viscosity decreases the critical Rayleigh number and therefore enhances the onset of thermohaline convection. In simplified models, Ophori (1998) proved that variation of fluid viscosity affects groundwater dynamics significantly. Nevertheless, the influence of variable fluid viscosity on rising/sinking heat and brine plumes in real basins remains poorly understood. Here, viscosity variations due to temperature and salinity dependences are included in order to assess which of the dependencies has a major impact on the thermohaline regime of a basin system. Finally, the impact of pumping stations on solute and heat transport has previously been ignored despite the fact that the aquifers of the S-H are widely exploited. It has not been clear to what extent groundwater withdrawal affects thermohaline flow and increases brine-plume advection towards the surface. All three of these open issues are addressed by the numerical simulations of transient thermohaline flow presented here .

The paper is structured as follows. Following a short overview of the hydrogeological setting, numerical results are compared to previous studies. The major outcomes are summarized in the conclusions. In the appendix, a short description of the equations is given, together with the equation of state (EOS) for variable brine density and viscosity as employed in the simulations.

Although our simulations focus on the S-H region, a similar flow field could develop in any geothermal basin hosting shallow salt structures. The results give new insights into the

interrelationships between brine migration and inherited geological features, as well as the role of variable fluid viscosity in controlling heat and mass patterns in a real basin.

HYDROGEOLOGIC SETTING

The S-H region (Fig. 1) is located in northern Germany and is delimited by natural boundary conditions. An elongated salt wall reaching the basin surface stretches over more than 40 km along the western part while deeper salt pillows affect the southern and eastern area (Fig 1A). The Trave River and the Baltic Sea bound the region in the northeast (Fig 1B). The aquifer basin consists of two Mesozoic-Tertiary basins, the Oldesloe Trough and the Hemmelsdorf Basin. Wide areas of both basins are affected by faults and Pleistocene channels. The aquifers are most strongly exploited in the eastern part of the region, near Lübeck and the coastal area of the Baltic Sea. Groundwater withdrawal also occurs in the Oldesloe Trough, not far from the Bad Segeberg salt diapir.

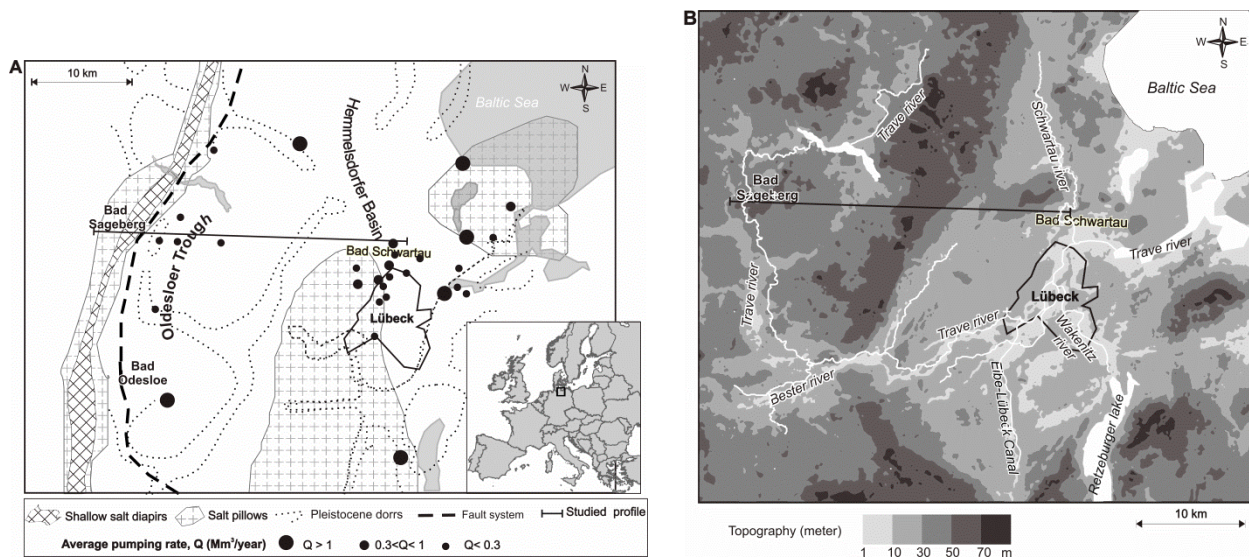


Fig. 1: (A) Study area and location of the studied profile, salt structures (salt pillows from Weber 1977 and salt diapirs from Baldschuhn et al. 2001), Pleistocene dorr (Hinsch 1974), and average pumping rates in Mm³ per day from LANU (Otto 2002). (B) Topography of the study area, river systems, and profile location

Stratigraphy along the studied profile is shown in Figure 2. The geologic identification of the different stratigraphic units along the studied profile is well established (Baldschuhn et al. 2001, Maystrenko et al. 2005, Maystrenko et al. 2006). Stratigraphical investigations carried out by the Geological Survey of the State Agency for Nature and Environment of S-H (LANU) provide further details on the hydrogeological structure of the uppermost units (LANU 2002).

The profile consists of seven post-Permian units comprising a 5-km-thick sequence of sedimentary deposits in which the western salt diapir reaches the near-surface. Hydrogeologically, the groundwater system can be divided into the upper fresh water / brackish

2.4 Brine migration: transition zones and variable viscosity

water system and the Mesozoic deep salt water system, as shown in the stratigraphic chart (Fig. 3A). These two systems are separated by the Lower Tertiary Clay, which acts as a regional aquitard. In the Mesozoic strata (mainly carbonates, marls and sandstones), groundwater salinity increases with depth, but density inversions are also observed (Tesmer et al., 2007; Möller et al., 2008). Total dissolved solids (TDS) reach concentrations of 270 g/l at depth of around 2 km. Groundwater from Permian aquifer complexes (intrasaliniferous carbonates and fluvial sandstones) are close to halite saturation with mean values of 350 g/l.

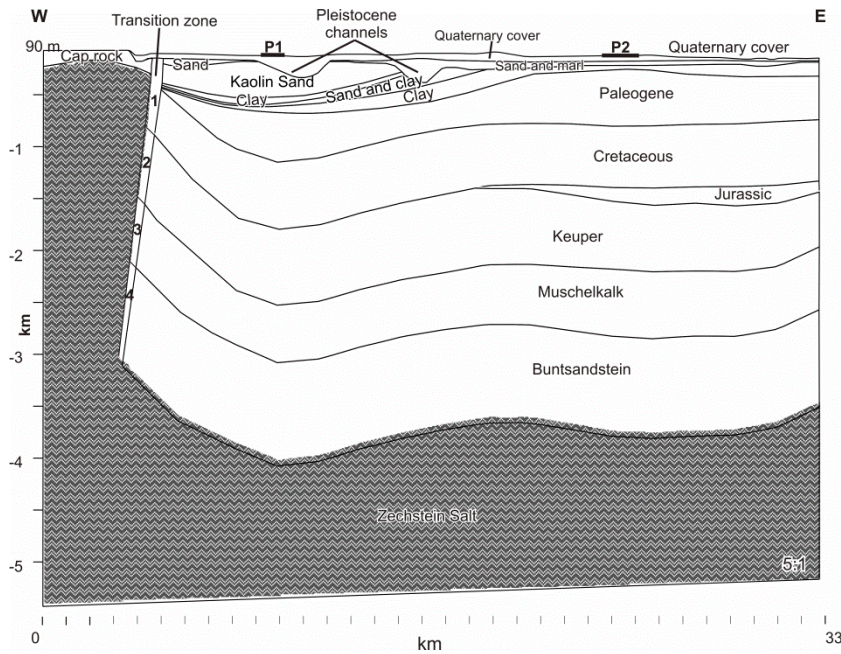


Fig. 2: Geological structure of the studied profile (derived from the 3D model of Maystrenko et al. 2005) and location of pumping stations (1 and 2). The post-Paleogene unit includes the major features of the shallow profile (according to data from LANU). The physical properties assigned to each unit are given in Table 1. For clarity, a 5:1 vertical exaggeration is used

The fresh-water/brackish-water complex consists of heterogeneous Pleistocene sequences of gravel, sand, silt, and clays, which are highly variable in thickness and lateral extent (Fig. 3B). Buried subglacial channels are significant features. These channels have different hydrogeological characteristics depending on fill deposits that consist of sand and/or till (Gabriel et al., 2003). The Quaternary deposits are locally more than 500 m thick and provide local connections between shallow and deep aquifers. In the North German Basin, the glacial channels are extensively developed as groundwater reservoirs and can be vulnerable to contamination by dissolved halites (Wiederhold et al., 2002; Gabriel et al., 2003). In general, salinity within the Quaternary cover remains rather low (from zero to few mg/l) but can locally reach concentrations of several g/l TDS.

2.4 Brine migration: transition zones and variable viscosity

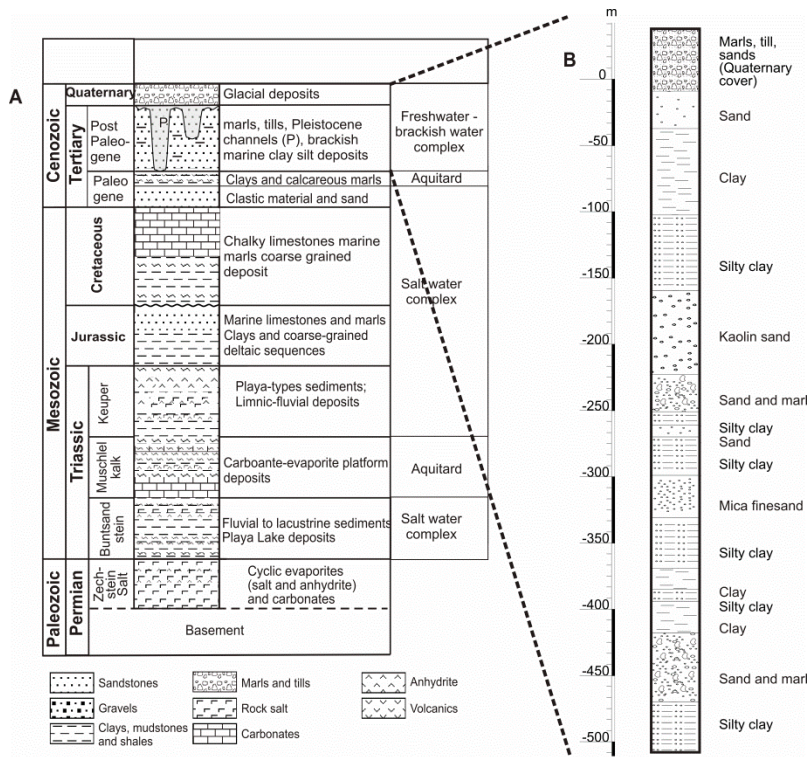


Fig. 3: (A) Stratigraphic chart and hydrogeological complexes of the North German Basin (modified after Scheck & Bayer 1999; and Möller et al. 2008). (B) Lithostratigraphic column of the uppermost units (to 500 m depth) from Agster (2005)

Water analyses in S-H date back more than a century. The groundwater is generally characterized by Ca^+ , HCO_3^- , Na^+ and Cl^- ions. A comprehensive description of the groundwater chemistry for the shallow and deep aquifers is given by , amongst many others, Friedrich (1902, 1917), Heck (1949), Grube et al. (1996), Tesmer et al. (2007), and Möller et al. (2008).

Groundwater salinity is related to structural elements such as shallow salt diapirs, fault zones or interglacial channels. Although several low-permeability units are present, upward flowing saline waters do enter the shallow post-Rupelian aquifer, mixing with meteoric waters (Möller et al. 2008).

NUMERICAL APPROACH

The transient equations governing fluid flow and mass and heat transport, were solved using the FEFLOW® commercial finite-element software (WASY GmbH, 2002). Mathematical formulation of these equations is briefly recalled in the appendix. Further details can be found in Diersch and Kolditz (1998).

The mesh resolution for discretizing the units from the Paleogene to the Zechstein Salt (Fig. 2) is 120 m. A finer resolution of 20 m to 40 m was applied to the Post-Paleogene unit to accurately preserve the geometry of the smaller structures. In the vicinity of the pumping wells, an even finer resolution of 3 m was used. In total, the grids contain 110,000 to 135,000 triangular elements. The resolution allows us to model variations in fluid density and viscosity on a

2.4 Brine migration: transition zones and variable viscosity

regional scale while retaining acceptable computer execution time. Further mesh refinements did not change the calculated patterns.

The brines are considered pure NaCl solutions. Fluid density and viscosity variations are calculated using polynomial expressions that take into account pressure, temperature and salinity dependencies (see appendix).

Model parameters

Each stratigraphic unit is considered homogeneous and isotropic with regard to the physical properties (e.g., hydraulic conductivity, porosity) listed in Table 1. A transition zone between the salt diapir and the adjacent units occurs along the salt flank. Whereas the modeled transition zone does not reproduce complex internal structures, it does allow us to consider vertical heterogeneity in hydraulic properties. Because the transition zone formed while the salt was rising, it consists of a mixture of salt, cap rocks, and mixed sediments from the neighbouring units (Dr. R. Otto, LANU, oral). Therefore, it is reasonable to assume that its hydraulic permeability is lower than that of the overburden (Frisch, 1993; Geluk, 2005; Dr. R. Otto, LANU, oral), but higher than that of the salt. There is substantial uncertainty regarding the spatial variability of hydraulic properties.

Table 1: Physical parameters assigned to the units. The values for the Post-Paleogene units (above the dashed line) and the transition zone are averages at basin-scale. The parameters for the deeper units are adapted from Scheck (1997)

Units	Hydraulic conductivity (10^{-4} ms^{-1})	Porosity (1)	Volumetric heat capacity ($10^6 \text{ J m}^3 \text{ C}^{-1}$)	Thermal conductivity ($\text{W m}^{-1} \text{ C}^{-1}$)	Molecular diffusivity ($10^{-9} \text{ m}^2 \text{ s}^{-1}$)
Cap Rock	~ 0	$1 \cdot 10^{-6}$	1.9	3	$2 \cdot 10^{-15}$
Quaternary cover and marl	$1 \cdot 10^{-2}$	0.3	3	1.3	0.2
Sand	5	0.6	3	1.3	100
Kaolin Sand	3.2	0.55	3	1.3	64
Clay	$1 \cdot 10^{-5}$	0.32	3	2.1	$2 \cdot 10^{-4}$
Sand and Clay	0.1	0.5	3	1.3	2
Sand and marl	0.1	0.6	3	1.3	2
Paleogene	0.5	0.23	3.15	1.5	10
Cretaceous	0.2	0.11	2.5	1.9	4
Jurassic	$1 \cdot 10^{-4}$	0.13	3.19	2	$2 \cdot 10^{-3}$
Keuper	$1 \cdot 10^{-7}$	$1 \cdot 10^{-4}$	2	2.5	$2 \cdot 10^{-6}$
Muschelkalk	$1 \cdot 10^{-6}$	$1 \cdot 10^{-6}$	2.4	1.85	$2 \cdot 10^{-5}$
Buntsandstein	$1 \cdot 10^{-4}$	$4 \cdot 10^{-2}$	3.15	2	$2 \cdot 10^{-3}$
Zechstein Salt	~ 0	$1 \cdot 10^{-6}$	1.81	3.5	$2 \cdot 10^{-15}$
Transition zone					
1	0.01	.15	3.15	1.5	10
2	$5 \cdot 10^{-8}$	$1 \cdot 10^{-4}$	2	2.5	$1 \cdot 10^{-7}$
3	$5 \cdot 10^{-7}$	$1 \cdot 10^{-6}$	2.4	1.85	$1 \cdot 10^{-6}$
4	$5 \cdot 10^{-5}$	$4 \cdot 10^{-2}$	3.15	2	$1 \cdot 10^{-4}$

Boundary and initial conditions

Boundary and initial conditions were identical to those used in previous simulations described by Magri et al. (2008). Briefly, at the surface, head, temperature and solute boundaries were prescribed. A Dirichlet boundary condition was used for the head, whereas heat and dissolved salt were allowed to flow through the surface via Cauchy boundary conditions using a reference temperature of 8 °C and a reference solute concentration of 0 g/l. At the bottom of the model, a constant-temperature boundary condition of 160 °C was defined. This value corresponds to a linear vertical gradient of approximately 30°C/km as observed in the Northeast German Basin (Bayer et al., 1997). Along the salt borders, brine concentration was fixed at 345 g/L, representing an approximate value for halite saturation. In simulations including the transition zone, nodes on the salt-dome/transition-zone interface were also assigned that constant concentration. Lateral boundaries were closed to fluid, heat, and mass flow.

Pumping stations were modeled as local sinks. A series of hydraulic wells were assigned to the nodes representing the pumping stations (as located in Fig. 2). Total groundwater withdrawal was set to approximately 5 Mm³/year. Based on several long-term hydrographs provided by LANU, the proposed withdrawal was constrained such that the simulated groundwater head of the shallow aquifer falls a few meters below the initial water-table level.

The initial pressure and temperature conditions were derived from steady fluid-flow and conductive-heat-transport models. A salinity gradient increasing linearly with depth up to brine saturation is used to represent paleo-salinity conditions.

The transient thermohaline simulations were carried out over a simulated time period of 100 ky. This time period does not refer to a particular geological period and in fact a transient solution will never correspond to a precise geological period as there are too many unknowns. For instance, the initial conditions from which these processes started are unknown, and the geological configuration of the system probably changed through time due to active salt tectonics.

NUMERICAL RESULTS

Impact of the transition zone

In a set of models to assess the impact of the transition zone, fluid viscosity is treated as constant. The results of thermohaline flow simulations are illustrated for two model scenarios. In the first scenario (Fig. 4), the transition zone is absent, and the Zechstein salt is in direct contact with the other units.

Highly saline brines ($C > 100$ g/l) sink directly from the salt diapir into the Cretaceous sediments (Fig. 4). Saline plumes migrate eastward and reach the surface through the Quaternary channel.

2.4 Brine migration: transition zones and variable viscosity

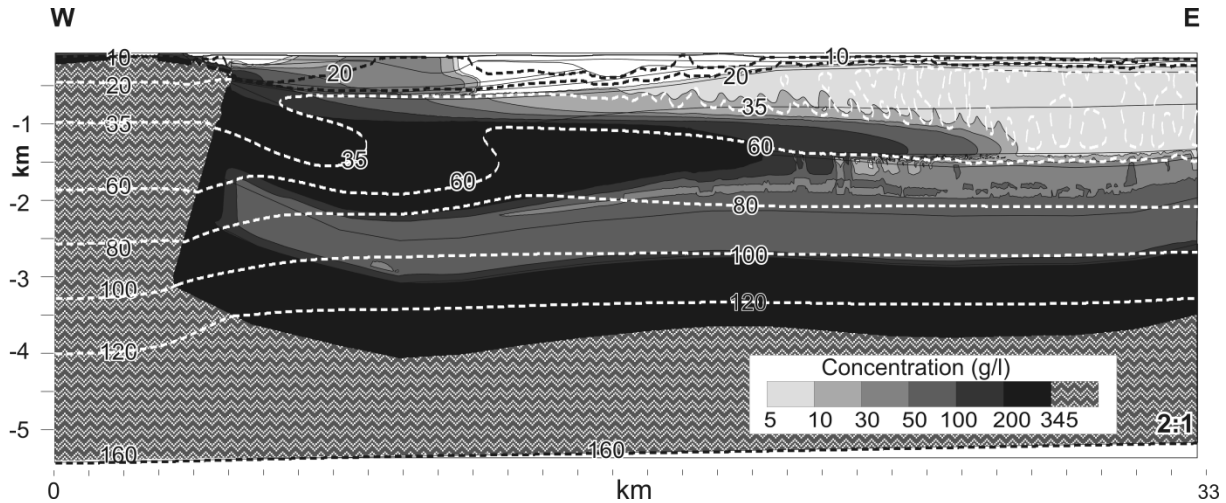


Fig. 4: Simulated profile without transition zone and constant fluid viscosity, showing calculated mass (g l^{-1}) and temperature (dashed lines, in $^{\circ}\text{C}$)

The saline waters originating at the salt-dome crest have an average temperature of 20°C , and downward brine flow carries cool waters to the deeper units (Fig. 4). As a result, within the extended brine plume the simulated temperature field undergoes multiple inversions with increasing depth.

In the eastern part of the profile, thermohaline convection affects the uppermost units, which are more permeable (Table 1). Above the horizontally extensive plume, temperature oscillations generate small convective brine cells (of half-kilometer radius). Thermally driven saline waters ascend into the shallow aquifer and spread locally at several points. In contrast, within the deeper Buntsandstein and the Muschelkalk, the transport regimes are dominated by mass diffusion and heat conduction.

These features of thermohaline and gravitational flow are preserved in the presence of a transition zone between the salt diapir and the adjacent units (Fig. 5A). However, the system dynamics are different. As halite dissolves along the salt flank, the transition zone becomes gradually saturated with heavy saline water. As a result, the eastward extension of the brine plumes is delayed. In the absence of the transition zone, a brine plume with 200 g/l of dissolved halite extends over more than 12 km (Fig. 4). In contrast, with the transition zone present, the brine plume has just begun to develop within the transition zone at a simulation time of 100 ky (Fig. 5A). Further, in the upper part of the transition zone, regional recharge is enhanced (Figs. 5B and C). Mixing of saline and fresh waters decreases both concentration and temperature. The velocity of the mixing process is on the order of centimeters per day (Fig. 5C). Eventually, the salty waters discharging at the surface of the Quaternary channel are more diluted (Fig. 5A).

Thus in this model scenario the presence of a transition zone along the salt diapir down the formation of highly concentrated brine plumes. At the same time, mixing between topography-

2.4 Brine migration: transition zones and variable viscosity

related recharge and saline groundwater is enhanced. The eastward brine migration is delayed and the calculated groundwater-discharge concentration is lower.

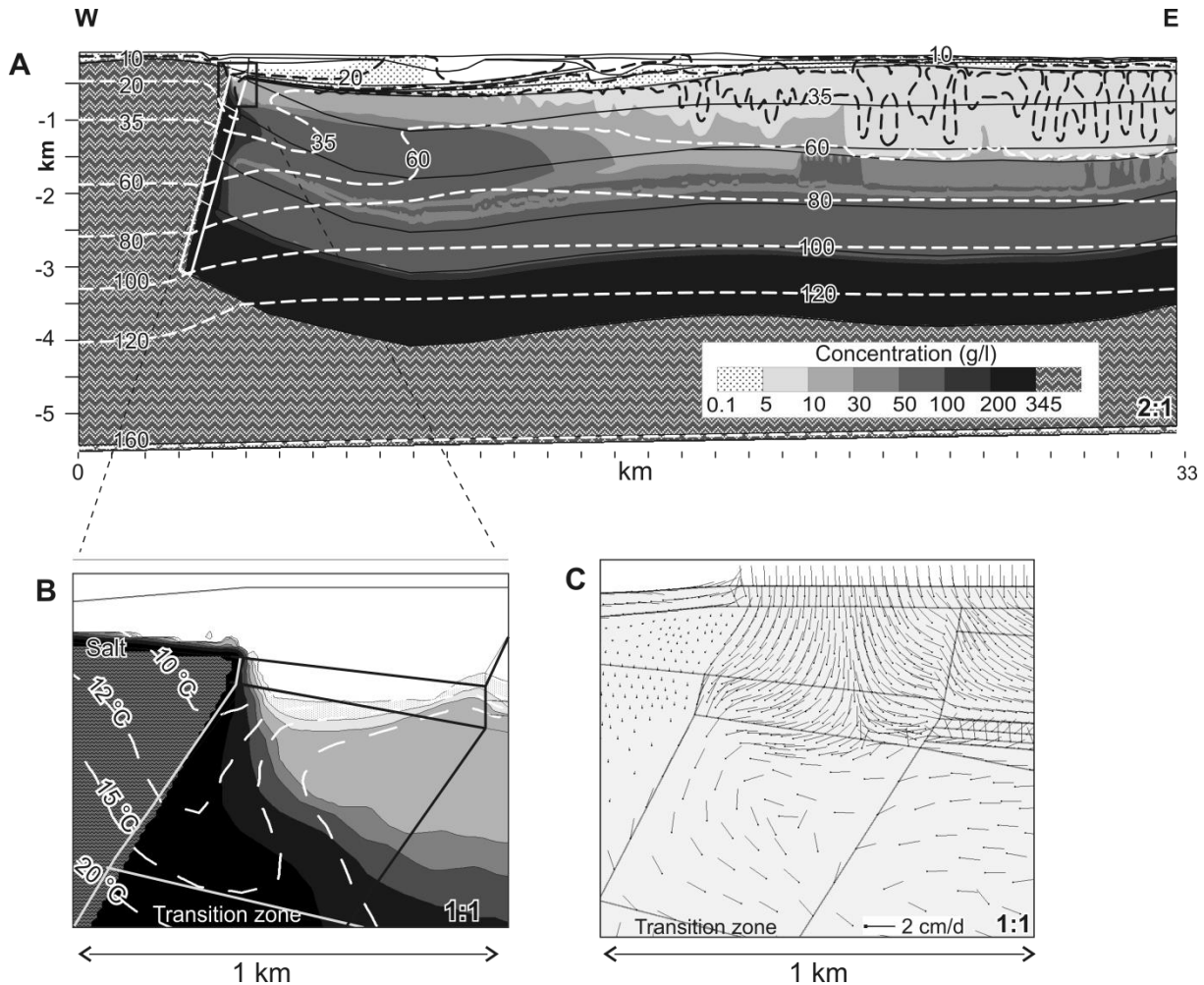


Fig. 5: (A) Simulated profile with a transition zone along the salt flank and constant fluid viscosity, showing calculated mass (g l)⁻¹ and temperature (°C) profiles. (B) Enlargement of the calculated mass (g l)⁻¹ and temperature (°C) profiles in the upper part of the transition zone. (C) Velocity field (cm day)⁻¹ with vectors are linearly scaled to the largest flow arrow

Impact of variable fluid viscosity

The previous set of simulations was repeated, taking into account variable fluid viscosity. Brine-viscosity dependence on temperature and concentration is computed via the equation of state given in the appendix (Eq. 10) and is illustrated in Figure 6. At a given temperature, fluid viscosity increases with concentration. For example, at the relatively low temperature of 10 °C, the viscosity of brines with 200 g/l of dissolved salt is twice the viscosity of freshwater. On the other hand, at a given concentration, viscosity decreases rapidly with increasing temperature. The hydraulic conductivity of the units (K) is inversely proportional to the fluid viscosity (see appendix, Eq. 5). Therefore, units saturated with colder and highly concentrated brines (with

2.4 Brine migration: transition zones and variable viscosity

high viscosity) are less permeable to groundwater flow. The effective hydraulic conductivity of the units saturated with warmer and more dilute fluids (low viscosity) is increased.

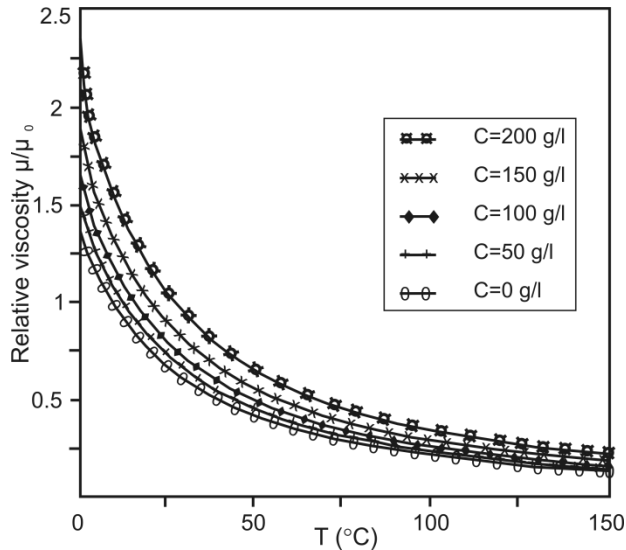


Fig. 6: Relative brine viscosity (μ / μ_0) as function of temperature (T , in °C) at selected concentrations (C , in g/l). The equation of variable fluid viscosity as function of temperature and concentration (WASY-GmbH 2002) is given in the appendix (Eq. 10)

The simulation results are presented in Figure 7A and can be directly compared with Figure 5 in which the fluid viscosity is constant (at). In the shallow salt-dome area, variable fluid viscosity inhibits the protrusion of brine plumes. Heavy brines form in a relatively cold near-surface environment (i.e., $T \sim 10$ °C). This setting is therefore characterized by higher fluid viscosity (Fig. 6) which in turn decreases the effective hydraulic conductivity of the transition zone and the neighboring units. As a result, brine migration is retarded; the Cretaceous is saturated with less concentrated brine. Whereas in the previous case (constant viscosity) the calculated concentration of the elongated finger is more than 50 g/l (Fig. 5), here a brine plume with concentrations less than 30 g/l extends over 10 km in the horizontal direction at 1 km depth (Fig. 7A). The calculated concentration at this depth is in good agreement with the available data (Möller et al. 2008). Variable fluid viscosity also affects the temperature field because the less-dense brine flow does not overwhelm the thermal convective regime (Fig. 7A). Temperature oscillations persist below the Pleistocene channel. Within the Cretaceous, thermohaline convection drives the tip of the brine plume upward along the increased temperature gradient. In contrast, constant fluid viscosity resulted in the formation of sinking heavy brines which cut off thermally induced convection cells (Fig. 5).

2.4 Brine migration: transition zones and variable viscosity

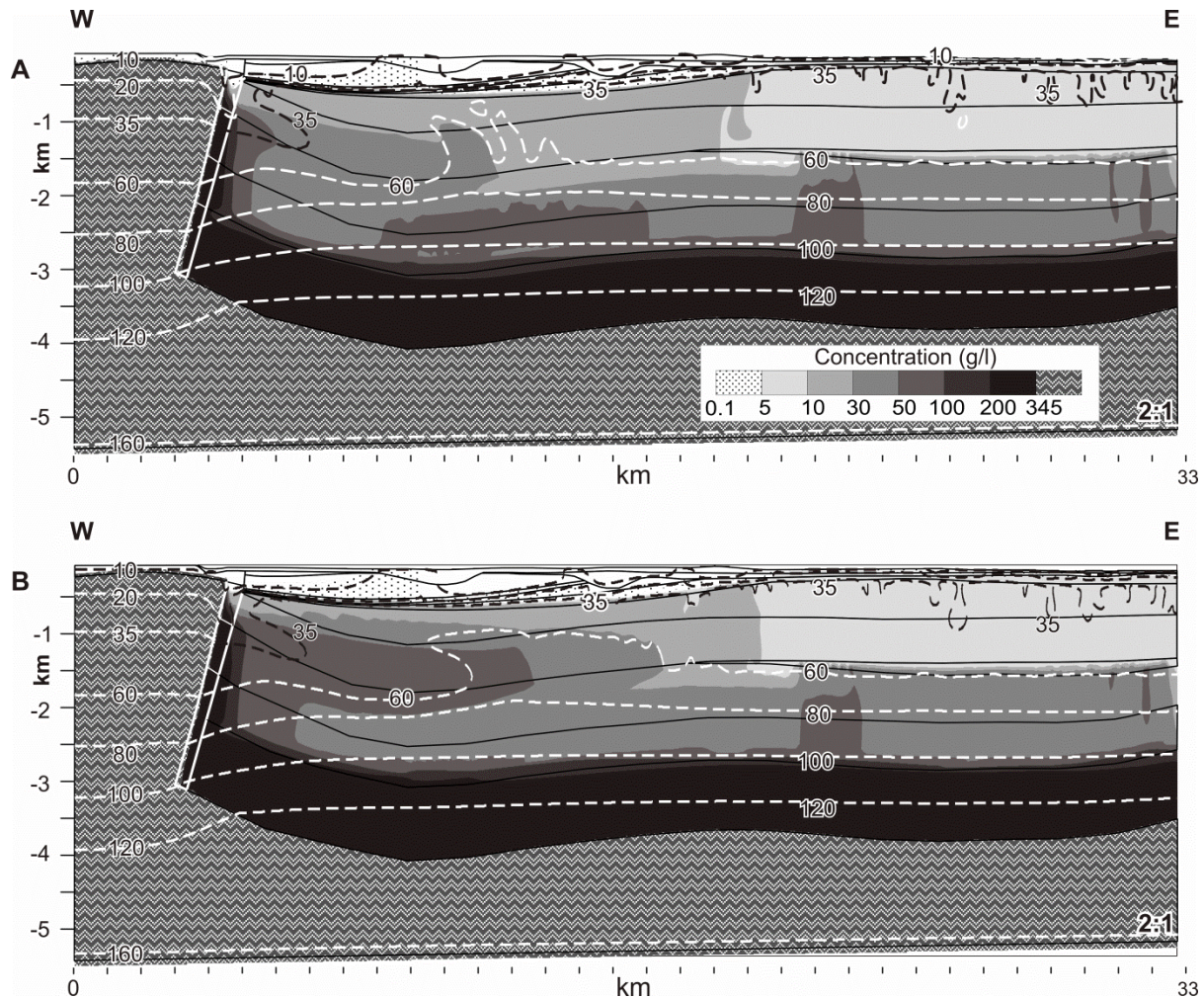


Fig. 7: Simulated profile with a transition zone along the salt flank and variable fluid viscosity, showing calculated mass (g/l) and temperature (dashed lines, in °C). A) Viscosity is temperature- and salinity-dependent. B) Viscosity is temperature-dependent only

Furthermore, owing to the fluid-viscosity dependence on temperature, brine flow is locally enhanced by increased temperature. This phenomenon can be seen in two parts of the profile (Fig. 7A). In the central part, brines with 10 g/l TDS at 35 °C are closer to the surface, spreading below the clay unit. At the eastern end of the profile, the thermal convective cells have merged, indicating a more vigorous thermally induced flow.

For comparison, a simulation was performed in which viscosity variations due to salinity were ignored. The results are given in Fig.7B. They show that viscosity variations due to salinity have a major impact on calculated solute-concentration patterns. By neglecting the concentration-dependence of viscosity, more salt is likely to be dissolved. A brine finger with a salinity of 50 g/L stretches eastward over 10 km, whereas in the previous scenario (Fig. 7A) the same brine plume had just begun to form along the salt flank. By neglecting viscosity variations due to salinity, the effective hydraulic conductivity is artificially increased. As a consequence, more concentrated brines form near the salt diapir. Because heavier brine extends eastward, the

2.4 Brine migration: transition zones and variable viscosity

gravitational regime overwhelms the convective cells: the thermal plumes observed below the Pleistocene channels are flattened (compare Fig. 7A and B).

The impact of temperature- and concentration-dependent brine viscosity is twofold. In a colder and highly concentrated environment, such as a shallow salt-dome crest, it retards brine flow. In a less saline environment, variable fluid viscosity further enhances thermally induced upward due to increased temperature gradients. The simulation results also indicate that viscosity variations due to salinity alone have a major effect on the flow field. If this dependence is neglected, saltier brine plumes migrate within the basin.

Impact of pumping stations

Groundwater withdrawal has been simulated for a period 100 years in order to investigate the potential impact of anthropogenic activities on large-scale brine migration within the Quaternary aquifers. Based on the previous model scenario, series of pumping wells have been added in two locations (Fig. 2): near the Pleistocene channel (P1) and further east, representing the exploited area of Lübeck (P2).

The effects of groundwater extraction near the Pleistocene channel are illustrated in Figure 8. Before groundwater withdrawal, brackish waters are found at a depth of a few hundred meters below the surface (Fig 8A). By the end of the simulation run, brine upconing has occurred (Fig. 8B). The calculated salt concentration at the surface is 200 mg/L. It took approximately 20 simulated years for this concentration increment to occur. Owing to a sequence of thick clay units at a depth of 1 km, deep fluid processes are not affected by upconing; temperature oscillations continue in a free-convection regime at depth, generating small brine fingers (Fig. 8B).

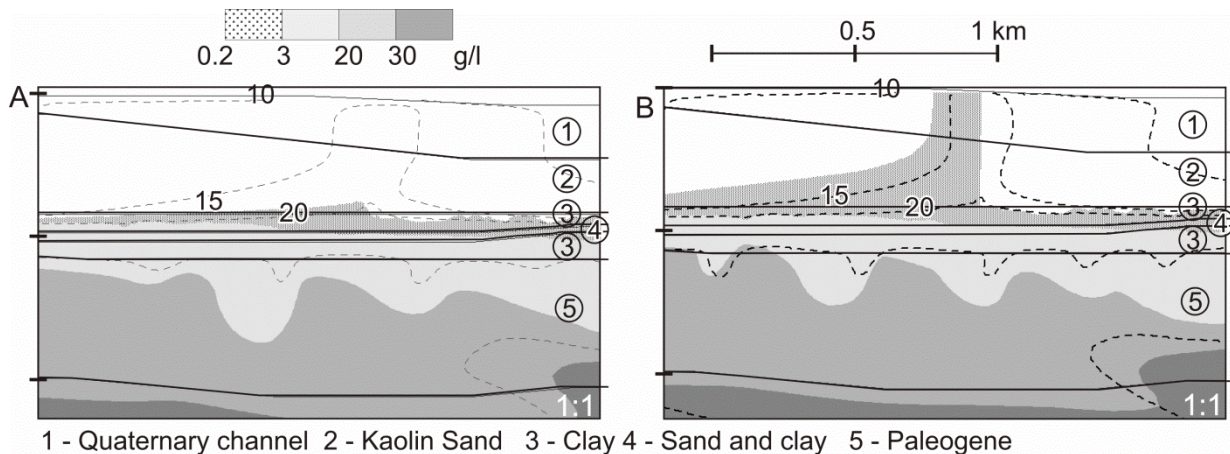


Fig. 8: Calculated mass (g/l) and temperature (dashed lines, in °C) distribution within pumping area P1 (as located in Fig. 2): A) Before groundwater withdrawal and B) after groundwater withdrawal

2.4 Brine migration: transition zones and variable viscosity

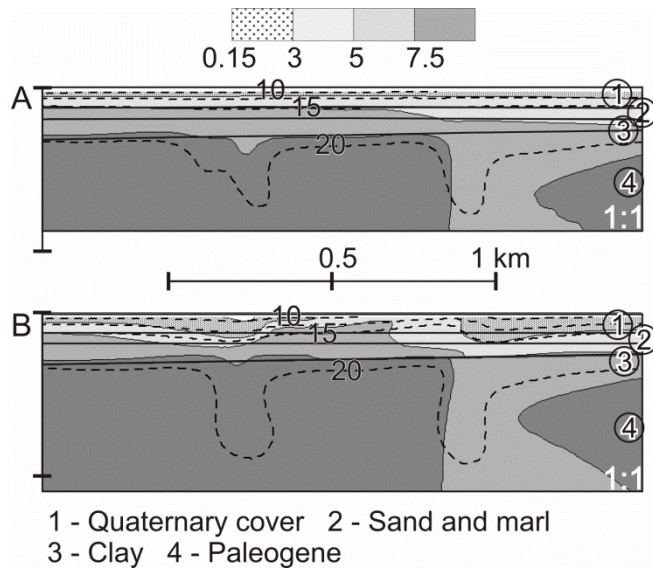


Fig. 9: Calculated mass (g/l) and temperature (dashed lines, in °C) distribution within pumping area P2 (as located in Fig. 2) A) Before groundwater withdrawal and B) after groundwater withdrawal

A qualitatively similar response to groundwater withdrawal is observed in the eastern part of the profile (Fig. 9). However, in detail it can be seen that saltier and warmer groundwater spreads at the surface following upconing (Fig. 9B). Locally, the calculated concentration and temperature reach as much as 5 g/l and 12 °C, respectively. In this location, the thin clay unit does not provide a sufficient barrier to intrusion of geogenic saline groundwater into the shallow aquifer.

SUMMARY AND CONCLUSIONS

Numerical simulations were performed to address the following points: (1) the impact of a permeable unit (transition zone) between the salt flank and adjacent units, (2) the role of variable brine viscosity in affecting heat and mass patterns, and (3) the influence of anthropogenic activities on large-scale density-driven flow. A deep vertical profile through the S-H region served as geological setting for carrying out the numerical simulations.

Brines at near-saturation concentration form where the units are in direct contact with the diapir. Downward density-driven brine flow is dominant and has the potential to overwhelm upward, thermally induced flow. The presence of a transition zone between the salt flank and the adjacent units delays gravitational convection. By adding a transition zone, the hydraulic conductivity of the sediments in direct contact with the salt is lowered. This reduces the flow velocity of groundwater near the salt flank. As less dissolved halite enters the flow system, groundwater recharge within the sedimentary rock remains more dilute.

Variable viscosity strongly controls mass and temperature patterns as it effectively changes the hydraulic conductivity of the units. By keeping viscosity constant in a variable-density flow system, salinity gradients are likely to be overestimated. Variable brine viscosity hinders the sinking of cold heavy brine plumes at the regional- (i.e., km-) scale. When both transition-zone

2.4 Brine migration: transition zones and variable viscosity

and viscosity effects are included in the simulations, calculated concentrations are in better agreement with available mass trends. Furthermore, with a variable viscosity the temperature oscillations in the convective regime persist.

To some extent the numerical models also allowed us to investigate the potential impact of anthropogenic activities such as pumping stations on brine flow. The sequence of clay units below the Pleistocene channels provide a good barrier between the upper (exploited) freshwater system and the deeper saline groundwaters; deep transport processes do not seem to be directly affected by pumping stations. However, groundwater withdrawal accelerated brine upconing within the Quaternary channel. Particularly where the clay unit thins towards the East, groundwater withdrawal has the potential to locally advect saltier and warmer brines to the surface.

Although these models are a rough approximation of deep and shallow transport processes at the basin scale, they provide new insights into the geophysical factors controlling brine and heat flow within sedimentary basins hosting shallow piercing salt domes. Based on the results presented here, it is apparent that the geological characteristics of salt diapirs and surrounding sediments, as well as the physical properties of brines (such as variable density and viscosity), strongly control the regional-scale behaviour of thermohaline flow. Extensive groundwater withdrawal in the upper aquifers is not likely to affect the deep fluid dynamics, provided that shallow and deep aquifer systems are separated by impervious units.

ACKNOWLEDGMENTS

This project is supported by the German Science Foundation (DFG) as part of the SPP 1135 “Dynamics of Sedimentary Systems under varying Stress Conditions by Example of the Central European Basin System”. The geological data of the NEGB have been provided by Dr. M. Scheck-Wenderoth and Dr. Y. Maystrenko while LANU (Landesamt für Natur und Umwelt) provided additional unpublished data. Brine density data used for computing the EOS have been made available by Dr. T. Driesner from ETH, Zürich. The authors thank Prof. Steve Ingebristen and two anonymous Geofluids reviewers for their comments that significantly improved the paper. Dr. Volker Clausnitzer at WASY is greatly acknowledged for the support in FEFLOW.

CHAPTER 3

3. GEOTHERMAL ENERGY MIGRATION IN FAULTED AREAS: THE SEFERIHISAR-BALCOVA GEOTHERMAL BASIN (SBG)

EXAMPLE

Contents

3.1	Impact of faults.....	114
3.2	Thermally induced seawater intrusions.....	140

This chapter is dedicated to the primordial role of faults in controlling fluid transport processes within basin systems. As explained in chapter 1.2 (figure below or figure 1.4), faults can be preferential pathways for fluid flow and at the same time enhance heat convection also in the surrounding sediments.

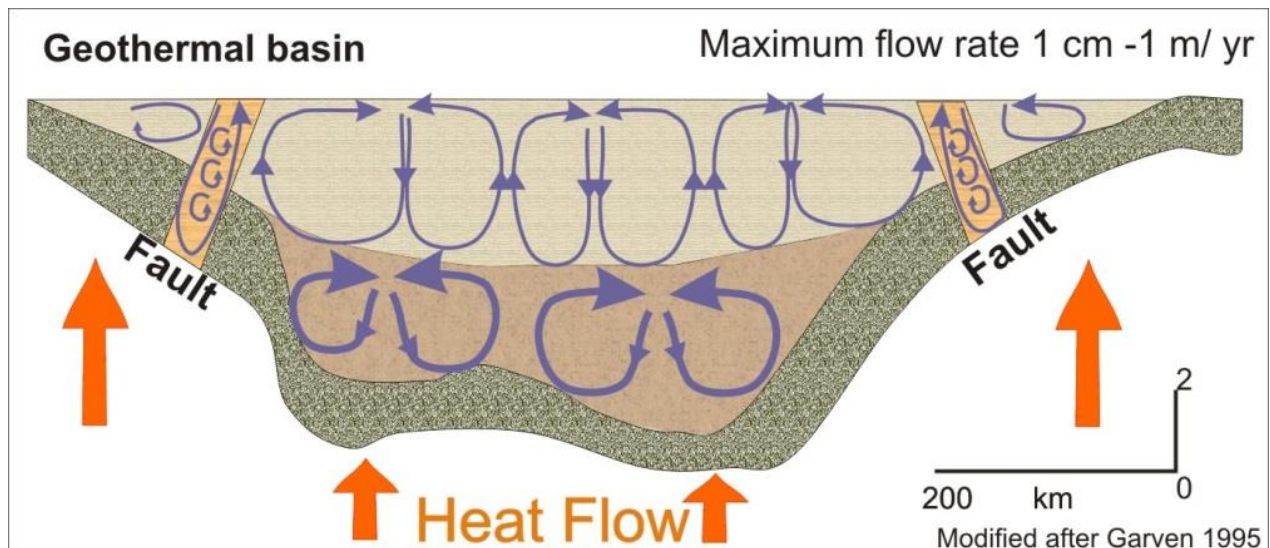


Fig. 3.1: Thermally driven flow (free convection) in a geothermal basin (see Fig. 1.4 in the Introduction)

To some extent, the previous chapter already gave some indications as to how cutting channels and transition zones can modify heat and mass flow. Here, transport processes are numerically investigated in the faults of the Seferihisar-Balcova Geothermal system (SBG), Western Anatolia. In this hydrothermal system, natural springs at temperatures ranging between 30 and 78 °C form along the major faults. An interesting feature of this system is the regional variable salinity of springs: in the north, thermal waters have low chloride (Cl) contents, whereas in the south, thermal waters are salty with a strong seawater contribution.

CHAPTER 3

The picture below, shot during a field trip in the southern SBG, illustrates a sea Arrowgrass near a hot thermal spring (left) and dolomitization processes along the wall of a natural geothermal pool (right).



Fig. 3.2: Sea Arrowgrass near a hot thermal spring (left) and dolomitization processes along the wall of a natural geothermal pool (right), Southern SBG.

Furthermore, it is not clear what forces drive salty water inland; highly-salty groundwater extends 10 km inland along the major southwest-northeast-trending faults. The simulation results in **chapter 3.1** indicate that large-scale free convection induced by buoyancy-driven flow develops in all faults driving hot basinal fluids from the basement to the surface. The vigorous upward flow in the faults can induce km-scale convective cells in the surrounding Mélange. These fault-induced convection cells develop in areas where the regional flow is weak, such as below horizontal alluvium deposits and seafloors. In the latter case, the convection cells that extend to the freshwater/seawater interface can drive salty waters toward the faults and inland units. This hypothesis is verified in **chapter 3.2** by running a simulation that couples solute transport to fluid flow and heat transport. The results show that at the fault intersections, seawater mixes with ascending thermal waters. The salinity of the resulting springs is likely controlled by different flow rates of the regional flow and structural features of the basin: In the northern area, extended areas of low TDS are due to both the strong topographic gradients and thick deposits of alluvial and Mélange sediments. By contrast, in the south, the flat topography, thin alluvium, and the uplifted basement reduce the depth of seawater penetration and favour the merging of plumes into wide saline areas.

Though this chapter illustrates the SBG example, the described processes concern faults which can be encountered in many geothermal systems in the world. The described fault-induced convection cells could by example explain outflow of relict brine through the faults of the

CHAPTER 3

Tiberias Lake, the presence of dissolved halite within the faults of the Rhine Graben, Germany or the mineral deposits in the Polish Basin.

3.1 Impact of faults

GEOFLUIDS

Geofluids (2010) 10, 388–405

doi: 10.1111/j.1468-8123.2009.00267.x

Deep geothermal groundwater flow in the Seferihisar–Balçova area, Turkey: results from transient numerical simulations of coupled fluid flow and heat transport processes

F. MAGRI¹, T. AKAR², U. GEMICI² AND A. PEKDEGER¹

¹*Freie Universität Berlin – Institut für Geologische Wissenschaften, Fachrichtung Geochemie, Hydrogeologie, Mineralogie, Berlin, Germany;* ²*Department of Geological Engineering, Dokuz Eylül University, Buca-Izmir, Turkey*

ABSTRACT

The Seferihisar-Balçova Geothermal system (SBG) is characterized by complex temperature and hydrochemical anomalies. Previous geophysical and hydrochemical investigations suggest that hydrothermal convection in the faulted areas of the SBG and recharge flow from the Horst may be responsible for the observed patterns. A numerical model of coupled fluid flow and heat transport processes has been built in order to study the possible fluid-dynamics of deep geothermal groundwater flow in the SBG. The results support the hypothesis derived from interpreted data. The simulated scenarios provide a better understanding of the geophysical conditions under which the different fluid-dynamics develop. When recharge processes are weak, the convective patterns in the faults can expand to surrounding reservoir units or below the seafloor. These fault-induced drag forces can cause natural seawater intrusion. In the Melange of the Seferihisar Horst, the regional flow is modified by buoyant-driven flow focused in the series of vertical faults. As a result, the main groundwater divide can shift. Sealing caprocks prevent fault-induced cells from being overwhelmed by vigorous regional flow. In this case, over-pressured blind geothermal reservoirs form below the caprocks. Transient results showed that the front of rising hot waters in faults is unstable: the tip of the hydrothermal plumes can split and lead to periodical temperature oscillations. This phenomenon known as Taylor-Saffman fingering has been described in mid-ocean ridge hydrothermal systems. Our findings suggest that this type of thermal pulsing can also develop in active faulted geothermal systems. To some extent the role of an impervious fault-core on the flow patterns has been investigated. Although it is not possible to reproduce basin-scale transport processes, this first attempt to model deep groundwater geothermal flow in the SBG qualitatively supported the interpreted data and described the different fluid-dynamics of the basin.

Keywords: numerical modeling, hydrothermal system, Turkey, convection, fault

INTRODUCTION

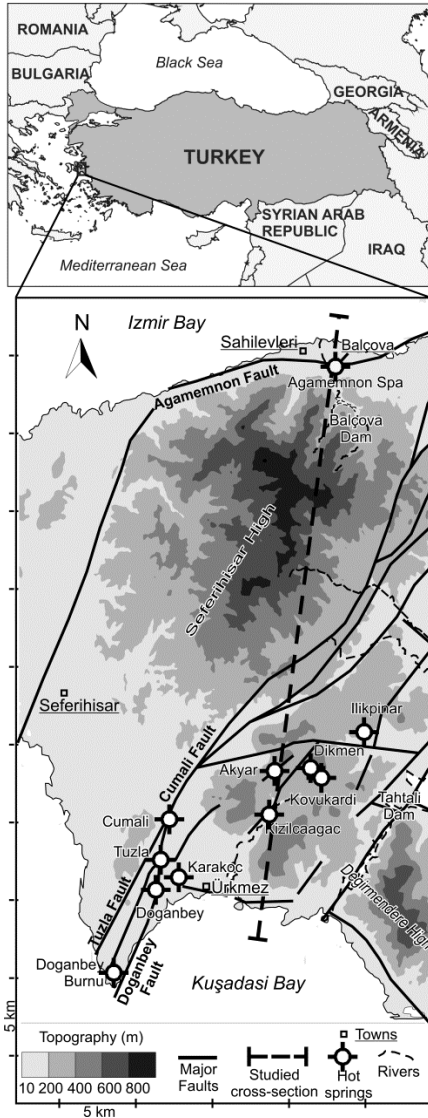
The Seferihisar-Balçova Geothermal system (SBG) is located in the Aegean region, western Turkey (Fig. 1). This amagmatic system is characterized by an average heat flow of 110 mW/m² (Ilkisik 1995; Sari and Salk 2003) and abundant geothermal activity controlled by fault tectonics. The main faults are the Agamemnon, Cumalı, Tuzla and Doğanbey. These strike-slip and normal faults break into several splays along which natural hot springs form (Fig. 1). Venting temperatures range between 30 and 78 °C (Tarcan and Gemici 2003). Temperature maps compiled by Eşder and Şimşek (1975) in the area between Seferihisar and Değirmendere highs show that in the mid 1970's the temperature of the Akyar, Ilikpınar, Kovukardı, Dikmen and Kizilcaagac springs ranged between 33 and 38 °C. At the date this paper is written, Ilikpınar spring is cold (i.e. 21 °C) while the others could not be located anymore, indicating that in this area of the SBG geothermal processes are still transient. In the aquifers surrounding the major faults, temperature gradients are anomalously high (3.5 - 5°K/10 m, Eşder and Şimşek 1977) and spring temperatures can reach 78 °C (e.g. Doganbey spring).

Geothermal exploration in the SBG started in the early 1960's. Approximately 50 wells have been drilled by the General Directorate of Mineral Research and Exploration of Turkey (MTA) both for developing and monitoring geothermal energy production. Based on the well log data, geophysical and hydrochemical investigations have been carried out over the SBG in order to define its major tectonic features (e.g. Dominco 1969; Eşder and Şimşek 1977; Ercan et al. 1986; Drahor and Berge 2006; Uzel and Sözbilir 2008) and to delineate the possible groundwater flow paths (e.g. Genç et al. 2001; Serpen 2004; Erdogmus et al. 2006; Aksoy et al. 2008).

These studies suggest that deep circulation of groundwater affects the SBG. Meteoric waters from the Seferihisar Horst (Fig. 1) infiltrate down to 2 km depth or more. After being heated by an unidentified heat source, the hot and less dense deep waters ascend to the surface along the major faults and fractures. The geothermal waters discharge then through the Quaternary sediments of the alluvium. The observed temperature anomalies and hot springs could therefore be due to mixing of ascending deep groundwater and shallow recharge waters (Serpen 2004; Aksoy et al. 2009).

At present however, this hypothesis is not supported by any large-scale numerical model of the SBG. Furthermore, the interrelationships between the hypothesized fluid flow patterns and the geophysical characteristics of the basin are still not clear.

3.1 Geothermal energy migration: the impact of faults



In the last decade, numerical models of coupled fluid and heat flow are increasingly used to improve the understanding of hydrothermal systems and their natural evolution, especially in fractured environments.

Amongst hundreds of numerical investigations, recently modeled faulted-areas include the Rhine Graben Germany (Bächler et al. 2003; Bense et al. 2008; Graf and Therrien 2009), the Basin and Range USA (Wisian and Blackwell 2004; McKenna and Blackwell 2004), the Ashanti belt Ghana (Harcouet-Menou et al. 2009), the Mc Arthur and Mount Isa basins Australia (Garven et al. 2001; Yang et al. 2004; Kühn et al. 2006; Yang et al. 2009). A comprehensive review of geothermal system simulations is given by O'Sullivan et al. (2001).

The major outcome of all these studies is that convection induced by thermal buoyant forces is a major mechanism driving hot basinal fluids. Faults play a dominant role in density-driven flow as they control recharge and discharge. Depending on their hydraulic properties, faults can also allow deep fluid-circulation within impervious basement and act as fast flow pathways for both solute and energy transport.

Fig. 1: Study area, the Seferihisar Balçova Geothermal system (SBG). Fault and spring locations as shown in Esder and Simsek (1975), Genç et al. (2001), Drahor and Berge (2006) and Uzel and Sözbilir (2008). Topography derived from SRTM data (Reuter et al. 2007).

In their pioneering investigations on groundwater flow in fault zones, Lopez and Smith (1995, 1996) found that the different regimes of heat transfer (i.e. conductive, advective, stable or unstable convective) fall within discrete ranges of permeability contrasts between the fault zone and the surrounding country rock. Furthermore, fault-zones can induce convection in neighbouring units where geophysical conditions are, in principle, not favourable for convective flow (Simms and Garven 2004). Therefore, in a hydrothermal system, multiple heat transport processes are likely to co-exist.

The main goal of this paper is to present a first transient numerical model of deep geothermal groundwater flow in the SBG in order to elucidate its possible fluid-dynamics. First, the existing data, including the hydrogeologic setting, temperature profiles and hydrochemistry, are briefly presented. Then the modeling approach of coupled fluid flow and heat transport in the faulted SBG system is described. The results illustrate the calculated flow paths as well as fluid temperature and pressure patterns.

3.1 Geothermal energy migration: the impact of faults

The numerical simulations will allow better understanding of the nature and evolution of the observed thermal anomalies in the SBG in relation to thermally- and topography-driven flow. Although based on the SBG, the presented models could describe deep flow patterns of any geothermal systems with similar geological features.

DATA

Owing to extensive drilling-campaigns mostly carried out by the MTA, the geological and hydrological settings of the study area are well-defined. The wells are located throughout the Northern and Southern coastal aquifers of the SBG, respectively around the Balçova and Ürkmez areas. Their depths vary from 100 m (shallow wells) to more than 2 km (deep wells). Furthermore, borehole temperature and hydrochemical data from the geothermal waters have been collected during the surveys by different Turkish research groups. A comprehensive dataset is given in the report of Satman et al. (2002). The interpreted data are mostly published and the major outcomes are briefly recalled here.

Hydrogeologic setting

The SBG is a complex horst-graben system. Several rock groups and formations can be distinguished, as defined, amongst many others, by Genç et al. (2001), Aksoy (2001), Drahor and Berge (2006) and Uzel and Sözbilir (2008). In summary, the study area is made up of Paleozoic metamorphic rocks of the Menderes Massif, Mesozoic Bornova Flysch or Mélange, Cenozoic volcano-sedimentary rocks, and Quaternary alluvium deposits.

The metamorphic rocks and the Bornova Mélange crop out respectively in the south-eastern and western part of the SBG while the Cenozoic successions are mainly exposed between the Seferihisar and Değirmendere highs (Fig. 2A). Quaternary deposits are found along the coasts and river systems.

3.1 Geothermal energy migration: the impact of faults

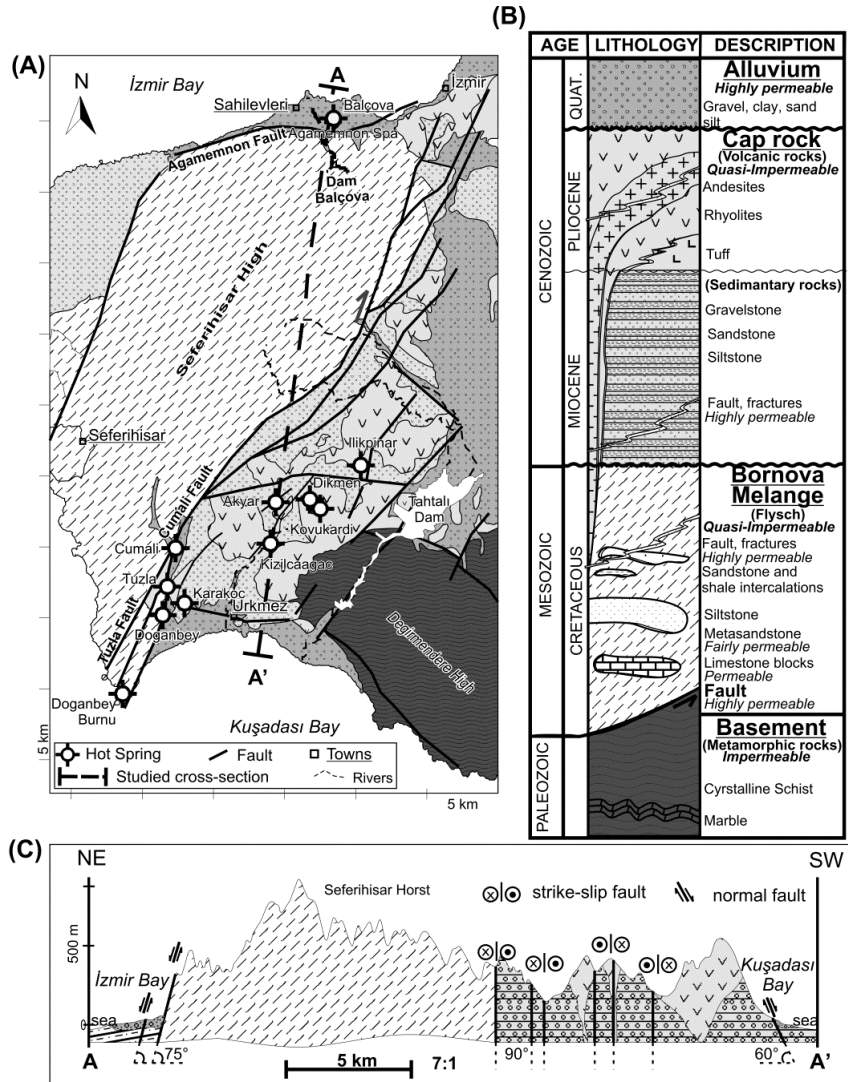


Fig. 2: (A) Simplified geological map of the SBG, modified after Genç et al. (2001). (B) Generalized stratigraphic chart of the SBG, modified after Serpen (2004) and Aksoy et al. (2009). (C) Interpreted geological cross-section of the studied profile as located in plates A and B, modified after Genç et al. (2001) and Uzel and Sözbilir (2008)

A representative stratigraphic chart of the study area is given in Figure 2B. Hydrogeologically, the metamorphic basement is an impervious unit made up of crystalline schist, marble and phyllites intercalations. Detailed description of the basement rocks can be found in Akartuna (1962), Eşder and Şimşek (1975) and Kaya (1981). The overlying Bornova Mélange is mostly composed of deformed and locally metamorphosed blocks of limestones, metasandstones, serpentinites and spilitic lavas (e.g. Erdoğan and Güngör 1992). This quasi-impervious unit is considered to be the main geothermal reservoir (Eşder and Şimşek 1975; Aksoy et al. 2008) and will therefore also be referred to as “the reservoir unit”. The permeability of the Bornova Mélange is largely secondary and is provided by faults, fractures, metasandstone intercalations and volcanic intrusions. Within the SBG, the reservoir unit thickness can vary between a few hundred meters in the Ürkmez area to more than 2 km in the Balçova area as shown by several well core observations (e.g. Eşder and Şimşek 1977; Öngür 2001). The volcano-sedimentary unit acts as an impervious cap rock partly overlying the Bornova Mélange. It is made up of impervious clayey Flysch units in which volcanic tuffs, rhyolites and andesites have intruded

3.1 Geothermal energy migration: the impact of faults

locally to form domes. The youngest rocks are Quaternary, unconsolidated alluvial sediments that consist mostly of clayey-sands, silt and gravels. These sediments comprise an extremely permeable shallow aquifer whose thickness ranges between 50 and 150 m. Major recharge sources are precipitation and infiltration from the horsts. Groundwater from this shallow aquifer is used for drinking and irrigation.

As a result of intense graben tectonics, the whole SBG is affected by steeply dipping strike-slip and active normal faults that cut from the basement to the Quaternary deposits. An interpreted regional NE-SW profile displaying the major structural features of the upper part of the SBG is illustrated in Figure 2C. The dip angles of the normal faults near the NE and SW ends of the profile are 75° and 60° respectively (Tezcan 1966; Yilmazer 1989). The strike-slip faults cut the volcanic rocks vertically.

It is believed that in Western Anatolia the graben tectonics reduce the thickness of the crust to less than 25 km (Tesauro et al. 2008; Aksoy et al. 2009). The conductive heat flux around these grabens is therefore higher than the normal terrestrial heat flow (Sari and Salk 2003). Since free convection in highly permeable fractured zones can occur even at relatively low heat flow (e.g. Hochstein et al. 1990; Gvirtzman et al. 1997), the geothermal waters of the SBG could likely be driven by thermal convection (Serpen 2004), as also revealed in the temperature logs and hydrochemistry studies discussed below

Temperature logs

Examples of temperature-depth profiles of shallow and deep wells located in the Balçova area are shown in Figure 3. The maximum well temperature is 140 °C. Similar trends are observed in the southern part of the SBG, where bottom well temperatures reached 153 °C (not displayed in Fig. 3). As pointed out by Serpen (2004), two major flow structures can be distinguished within the sedimentary fill: a shallow one between 40 and 100 m and a deeper flow pattern below 300 m (wells BD- 1 4 and 7). High temperature gradients of 5°K/10m have been measured in the shallow aquifer in which waters reach near-boiling conditions. These anomalously increased temperatures indicate outflows of deep hot fluid from neighbouring fractured areas into the alluvium. Positive anomalies are not only confined to the alluvium but also affect deeper parts of the basin, as shown by well BD-5 in which a peak temperature of 120 °C is recorded at 700 m depth. Below this depth, the temperature-depth trend is inverted. In geothermal systems, temperature reversals of this nature are related to the presence of convective flows (e.g. Ziagos and Blackwell 1986). By contrast, the measured temperatures in the well BD-3 increase almost linearly, indicating conductive cap-rock properties down to a depth of 400 m.

3.1 Geothermal energy migration: the impact of faults

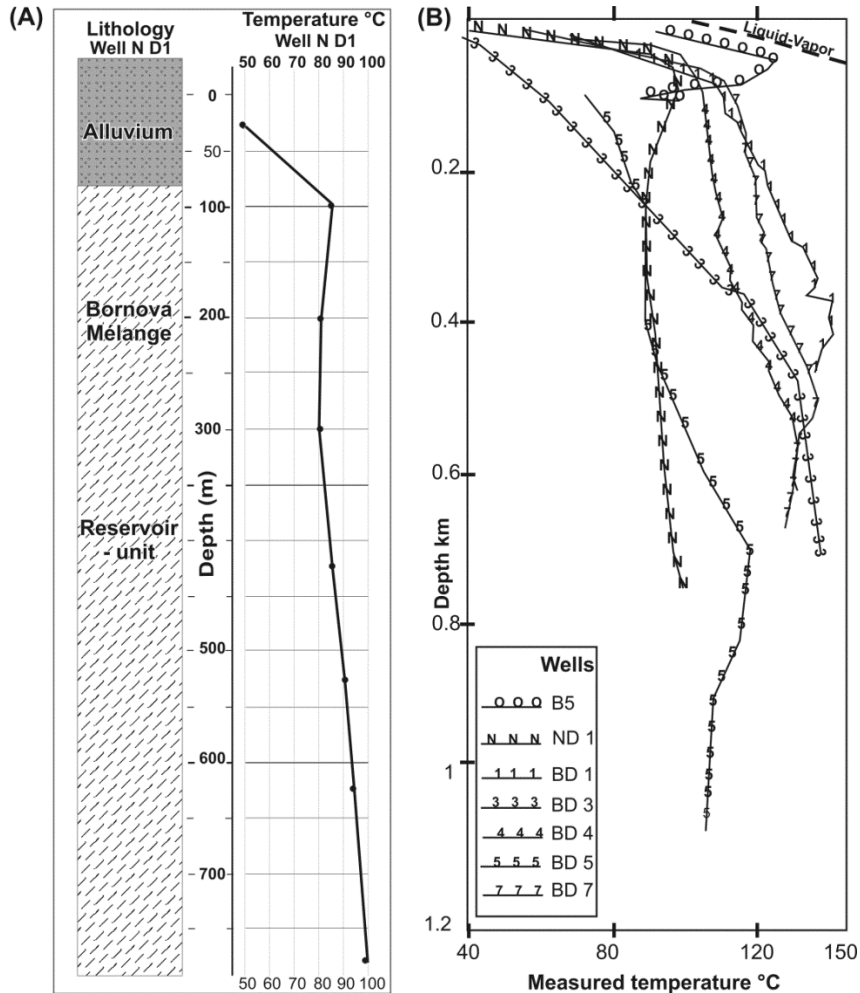


Fig. 3: (A) Example of temperature-depth profile of geothermal waters and lithology derived from the monitoring well ND 1. Dots indicate the measured temperatures in the well (B) Temperature-depth profile of geothermal waters from several wells prior to exploitation (modified after Serpen 2004). The well locations are given in Aksoy et al. (2008)

These temperature profiles indicate that ascending deep geothermal waters flow into both the shallow alluvium and the reservoir unit at depth between 400-700 m. Hydraulic connection between these two units is further supported by linear pressure-depth trends down to 1 km depth (Serpen 2004). Owing to the existence of a naturally high conductive heat flow, deep hot geothermal waters are driven upward by buoyant forces generated by a decrease in fluid density. Preferential conduits for these large-scale density-driven flows are highly permeable units, such as faults and fractures. Fault-controlled upward flow is also indicated by hydrochemistry studies.

Hydrochemistry

Isotopic analyses are used in order to infer the origin and evolution of the geothermal fluids. Deeply circulating groundwater acquires an isotopic composition that reflects water-rock and fluid mixing processes undergone during the fluid migration. Different isotopic analyses have been carried out in Western Anatolia.

Oxygen, hydrogen, boron and strontium isotopes studies show that the geothermal waters have two main origins: (1) meteoric waters (heated groundwater) and (2) seawater. Heated

3.1 Geothermal energy migration: the impact of faults

groundwater types with low total dissolved solids (TDS) content are found in the Balçova geothermal field (Tarcan and Gemici 2005; Tarcan et al. 2005) whereas the thermal waters in the Ürkmez area, southern SBG, originated from a mixture of seawater and local meteoric groundwater (Conrad et al. 1995; Vengosh et al. 2002; Tarcan and Gemici 2003).

It has been hypothesized that the Balçova geothermal fields are fed by meteoric groundwater seeping into the reservoir unit from terrains at elevations of about 500 m above sea level (Yilmazer 1989; Aksoy 2001). Oxygen isotope compositions show that meteoric water has been heated at great depths before rising to the surface (Filiz et al. 1993). Therefore topography-induced flow (i.e. regional flow) from the horsts toward the coastal aquifers also determines the geothermal behaviour of the SBG. Hydrochemical analyses performed by Tarcan and Gemici (2003) show that seawater intrusion affects the aquifers of the Ürkmez area. Seawater and freshwater mixing occurs both in the shallow aquifer and in the deeper part of the Bornova Mélange. However it is not yet clear whether those salty thermal waters mixed with cold seawater before and/or after convective heating at depth. Circulation of ascending thermal waters at different depths could explain the variation in salinity of the southern springs (Tarcan and Gemici 2003). In a recent hydrochemical study, Mutlu et al. (2008) found helium and other crustal volatiles in surface waters. The authors proposed deep groundwater circulation along faults as a plausible transport mechanism.

In summary, all data strongly suggest that both density-driven convective flow within permeable fractured areas and forced convection imposed by the horst are likely to be responsible for the observed anomalies and hot springs in the SBG. Since the Bornova Mélange thickness is 2 km and might even reach 4 km or more (Öngür, 2001), ground water circulation is assumed to reach a depth of at least 2 km (Serpen 2004; Aksoy 2008). This hypothesis was tested through coupled fluid flow and heat transport modeling discussed below. The plausibility of deep convective flows extending through basement rocks of the SBG has not yet been investigated.

NUMERICAL MODELING OF THE SBG

A transient fluid flow and heat transport numerical model was built in order to investigate thermally induced density-driven flow along a selected profile of the SBG (located in Figure 1 and Figure 2A). As this paper is a first attempt to simulate regional-scale geothermal groundwater flow in the SBG, the two dimensional approach is preferred. The flow is therefore constrained in the vertical x-z plane. A small 3D model has been built by Gök et al. (2005) with the aim of matching well temperatures in a 12 km² wide x 1.5 km deep site in Balçova. At the present state of the research, the structural data of the whole SBG needs to be refined further in order to satisfy the numerical requirements of a full 3D regional-scale model.

3.1 Geothermal energy migration: the impact of faults

The commercial finite-element software FEFLOW® (WASY-GmbH 2002) was applied to solve the strongly coupled conservation laws of momentum and energy. FEFLOW® fully implements variable-density and viscosity form of the Darcy law as, for example, described in the theory of Garven (1989). Details on the numerical solver can be found in Diersch and Kolditz (1998).

The profile

The simplified structural and stratigraphic components of the modeled region are illustrated in Figure 4. The study profile extends over 59 km north to south across the SBG and includes the seafloors of İzmir and Kuşadası Bays. This cross-section has been chosen because: (1) the sea provides suitable natural boundary conditions for the model, (2) it includes the highest topographic variation, (3) it crosses the major river-fault-systems, and (4) most of the boreholes are drilled in the Balçova-Ürkmez areas. Furthermore, the geological structure of the cross-section is known as it is derived from available lithological borehole logs published in the MTA reports (Eşder 1975; Yilmazer 1984; Demirel and Şentürk 1996; Çetiner 2004). The upper part of the studied profile integrates the interpreted 2D cross-section described in the “Hydrogeologic setting” (Fig. 2C).

The conceptual stratigraphy comprises the alluvium, the Quaternary seafloor, the Bornova Mélange (i.e reservoir unit) and the metamorphic basement which closes the model at 6.9 km of depth (Fig. 4). The lateral boundaries of the area are located 10 km beyond the pinchouts of the alluvium.

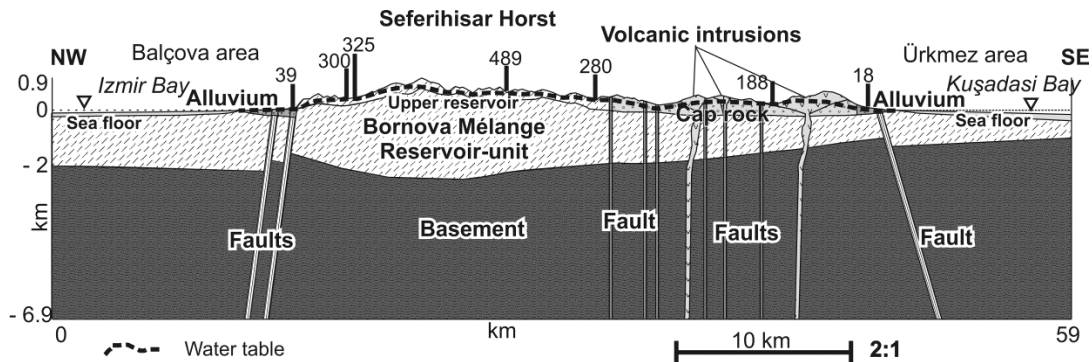


Fig. 4: Geologic setting of the studied profile as located in figures 1 and 2 and upper water table level Bold vertical lines locate head constraints defined by artesian wells and river (given in meters)

According to the borehole logs, the average alluvium thicknesses are 150 m and 50 m in the Balçova and Ürkmez areas, respectively. The alluvium deposits gradually decrease in thickness toward the sea.

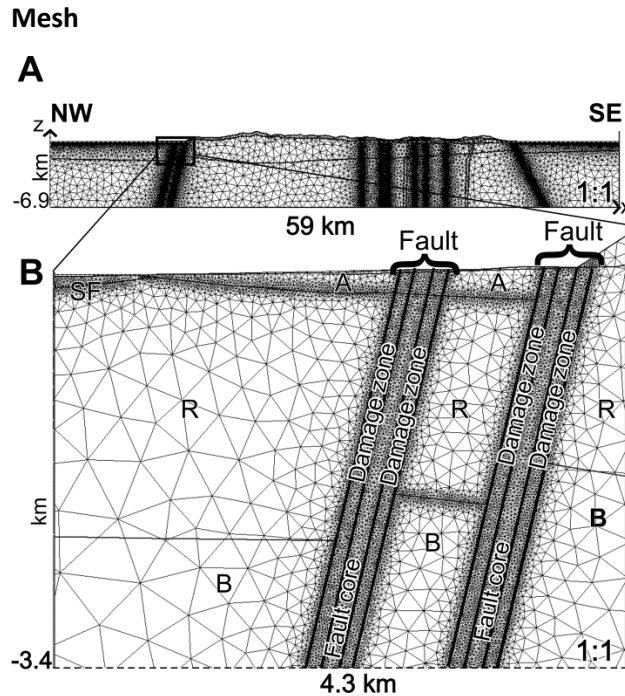
The seafloor is made up of Quaternary sediments. Depth and thickness of the seabed are based on the bathymetric studies of Ocakoğlu et al. (2005). In the cross-section, the seabed is modeled as a 100 m thick unit distinct from the reservoir unit.

3.1 Geothermal energy migration: the impact of faults

The Bornova Mélange thickness is assumed to be 2 km in the Balçova area, diminishing to approximately 1 km in the Ürkmez area. The reservoir/basement interface below the Seferihisar Horst is constrained by gravity studies carried out by Drahor et al. (1999). The reservoir unit in the southern part of the profile is partly overlain by a 300 m thick cap rock unit and locally by volcanic domes. The upper reservoir in the Seferihisar High serves as an additional unit in order to numerically vary topography-driven recharge.

Two parallel-dipping faults cut the Balçova areas whereas the other faults and magmatic intrusions occur individually. In this study, faults are modeled as equivalent porous media (EPM): they are represented as highly permeable areas of finite width extending from the basement to the top of the model. The EPM approach is a well-established technique for representing faults and fractured zones (Weatherill et al. 2008). It requires less computational effort than discrete-fracture models. EPM has been used for modeling free and forced convection in fractured porous media by Yang et al. (2004), Simms and Garven (2004), Bataillé et al. (2006) and Graf and Therrien (2009). It is known that faults can have twofold hydraulic behaviours (e.g. Haneberg 1995; Fairley and Hinds 2004a; Rowland and Sibson 2004; Bense and Person 2006). On the one hand, damage or deformation zones increase the fault permeability so that the fault can function as a flow conduit. On the other hand, core zones, fault gouges or mineralization processes can locally seal the fault causing it to become a barrier to groundwater flow. In some specific cases, faults can act as a combination of conduits and barriers to subsurface fluid flow (Heffner and Fairley 2006). In this study, faults are made up of two permeable damage zones surrounding an impervious core, as explained in the next paragraph. The faults of the study profile have different widths representing the estimated thickness of the combined fault-core and damage zones based on well-tests carried out by Onur et al. (2002): the two parallel-dipping faults in the Balçova area are 300 m wide while the fault near Ürkmez is 250 m wide. The width of the minor vertical strike-slip faults of the Seferihisar Horst, near the central-southern end of the profile, is 170 m. The dip angles of the faults are 75°, 60° and 90° respectively.

3.1 Geothermal energy migration: the impact of faults



Triangular elements with variable width have been used in order to preserve the different unit structures (Fig. 5A). All faults are made up of a central core flanked by a damage zone, as proposed in the conceptual models of Caine et al. (1996).

Fig. 5: (A) Finite element mesh used to discretize the study profile as illustrated in figure 4. (B) Zoom showing the numerical hydrostratigraphy (SF: sea floor; A: alluvium; R: reservoir unit, Bornova Mélange; B: basement) and the fault architecture: Faults consist of a core bounded by damage zones

Accordingly, the faults are subdivided into three numerically independent areas (Fig. 5B) which allows investigation of the role of an impervious core and more permeable flank zones. For simplicity, fault core and neighbouring damaged flanks have the same width. The spatial discretization is a crucial aspect. In their analytical investigations, Weatherill et al. (2008) proved that a fine grid spacing is required at the matrix interface to correctly simulate diffusive-dispersive processes in fractured porous media. Within the faults and highly permeable alluvium the mesh resolution is approximately 15 meters. Element spacing grows gradually from a few meters at the fault interface to hundreds of meters in the central part of the reservoir unit and in the basement. The whole profile has been discretized with 155,000 triangular elements satisfying the Delaunay criterion. Finer meshes did not affect the calculated patterns.

Unit and fluid properties

Each stratigraphic unit is considered homogeneous with respect to its physical properties (hydraulic conductivity, porosity, heat capacity and thermal conductivity). The model values of these properties are basin-scale averages based on previous statistical and numerical modeling studies (Göktürkler et al. 2003; Gök et al. 2005; Arkan and Parlaktuna 2005), general lithological considerations and field investigations (Tezcan 1966; Yılmaz 1989; Karakullukcu 1991; Tarakci 1999; Öngür 2001; Satman et al. 2002; Sarı and Şalk 2003; Serpen 2004), and tracer- and well-tests (Aksoy 2001; Onur et al. 2005; Aksoy and Serpen 2005). An anisotropy factor of the type $k_x:k_z = 10:1$ is used to represent the interbedding of permeable and less permeable aquifers within the units. Faults and their core are considered isotropic. The seabed was considered to be permeable, as in the work of Simms and Garven (2004). Although homogeneous units are a simplification of the real geological conditions, the model adequately represents the

3.1 Geothermal energy migration: the impact of faults

hydrogeology at the considered regional-scale. Values of model parameters are summarized in Table 1.

Table 1: Values of physical parameters assigned to the hydrogeologic units. The values represent basin-scale averages

Units	Hydraulic conductivity (m year ⁻¹)		Porosity (1)	Volumetric heat capacity (10 ⁶ J m ³ C ⁻¹)	Thermal conductivity (W m ⁻¹ C ⁻¹)
	k _x	k _z			
Alluvium	320	32	0.5	1.7	1.5
Upper Reservoir	0.032	3.2 · 10 ⁻³	5 · 10 ⁻³	2	2.3
Cap rock	3.2 · 10 ⁻³	3.2 · 10 ⁻⁴	5 · 10 ⁻³	2.1	3
Sea floor	0.032	3.2 · 10 ⁻³	2 · 10 ⁻²	2	2.3
Reservoir	0.32	0.032	5 · 10 ⁻²	2.4	2.8
Basement	~ 0	~ 0	10 ⁻³	2.1	3.5
Fault - damage zone	32	32	0.3	1.8	2
Fault - core	~ 0	~ 0	10 ⁻³	2.1	3.5
Volcanic intrusions	0.32	0.032	5 · 10 ⁻³	2.1	3

With regard to fluid properties, the SBG can be classified as a single-phase liquid-dominated system bearing groundwater close to freshwater conditions (Onur et al. 2005). Local exceptions are the Doğanbey, Cumalı and Tuzla salty springs in the southern part of the SBG (Fig. 2) where the coastal aquifers are affected by seawater intrusion (Tarcın and Gemici 2003). Salinity effects on the thermal regime are not taken into account but will be investigated in a forthcoming paper. Following the approach of Alkan et al. (1995), temperature and pressure dependences on both fluid density and fluid viscosity are reproduced by use of polynomial fittings (Magri 2004; Magri et al. 2009). The fittings have been calibrated in order to match the Equation of States (EOS) given in the International Association for the Properties of Water and Steam (Wagner and Pruss 2002) in the liquid phase in a range of temperature 0 < T < 350 °C and pressure p_{sat} < p < 100 MPa where p_{sat} is the saturation pressure. By doing so, rates of variable-density and viscosity groundwater flow are computed in the modified form of Darcy's law.

Boundary and initial conditions

Lateral boundaries are closed to fluid and heat flow. At the top of the profile, hydraulic head and temperature values are prescribed. The groundwater table is locally set equal to the surface elevation in direct relation to rivers and artesian wells, as shown in Figure 4. Elsewhere within the upper reservoir of the Seferihisar Horst the head is thought to vary between 70 and 100 m below the elevation of the ground surface (Prof. Gemici, oral commun. 2009). Additional constraints are provided by piezometric levels in the Balçova and Ürkmez area where the groundwater table lies only few meters below the alluvium surface, mimicking the topography (Serpen 2004). Along the seafloor, an equivalent freshwater head boundary condition is specified. Heat is allowed to flow through the ground surface of the inland basin via a third type boundary condition (i.e. Cauchy). By doing so, the surface temperature can vary as a result of heat transport processes in the subsurface. The reference temperature applied to the subaerial portions of the upper boundary is set equal to 18 °C which is the annual mean temperature of the SBG (Serpen 2004). The transfer heat coefficient is assumed to be 2.3 W m⁻² °K⁻¹ (Gök et al. 2005). The seabed has a constant temperature of 10 °C (Sayın et al. 2006).

At the bottom of the model, heat flow and temperature boundary conditions have been tested in a range from 80 to 100 mWm⁻² and 200 to 270 °C, respectively. Both the specified heat flux and temperature boundary condition types gave qualitatively similar results, differing in calculated temperature peaks and buoyant flow rates. The models presented here used a constant bottom temperature of 250 °C. This value is derived from a previous crustal-scale conductive heat model of Western Anatolia (Göktürkler et al. 2003) which takes into account the effects of temperature dependent thermal conductivity and crustal heat production down to a depth of 35 km. According to the models of Göktürkler et al. (2003), the calculated average temperature at 7 km depth is likely to be 250 °C ± 20 °C, depending on the presence or absence of less thermally conductive grabens.

Lin et al. (2000) demonstrated that neglecting thermal feedbacks from deeper basement rocks can lead to numerical artefacts. Therefore an 11 km deep model with a constant bottom temperature of 400 °C has also been run. In this specific case, a thicker basement did not significantly modify the calculated temperatures of the upper units, suggesting that a 7 km deep model is suitable for modeling thermally-driven flow in the Mesozoic and Cenozoic units of the SBG.

Initial pressure and temperature conditions were derived from steady-state fluid flow and conductive heat transport models which were run before the fully coupled models. Coupled fluid flow and heat transport simulations were carried out over a time period of 100 ky. Long-term simulations over 4 My proved that 100 ky is a sufficiently large time interval for the specific model to converge to a solution. It is important to note that any time period mentioned

3.1 Geothermal energy migration: the impact of faults

in this paper does not refer to a particular geological period but only to a simulated time interval.

RESULTS

The first set of simulations examined the effects of fully permeable faults by setting the properties of the fault core equal to those of the damage zones (Table 1). The impacts of impervious fault cores on the calculated patterns are described separately, at the end of this section. The numerical models presented here are not intended to reproduce measured data, but rather to gain insights into the transport processes developing in the SBG and their interrelationships with the observed thermal and hydrochemical anomalies.

Topography driven flow: no geothermal gradient

The topography-driven flow (i.e. regional flow) patterns calculated in the absence of the geothermal gradient are illustrated in figure 6A. In the Bornova Mélange of the Seferihisar Horst, a groundwater divide located about 24 km from the western boundary separates westward and eastward groundwater flow. In both cases, much of this flow is captured by the bounding faults, which channel flow downward. Some of the groundwater continues to flow toward the Balçova and Ürkmez areas. Within the reservoir and basement units, there is no direct hydraulic connectivity between the different faults; faults act as independent recharge conduits of the basin units. In the larger faults of the Balçova and Ürkmez areas, Darcy velocities range from a few centimetres per year to 0.2 m year⁻¹, whereas in the vertical, thinner faults of the Seferihisar Horst inflow rates span between 0.7 and 2 m year⁻¹. The regional flow reaches a maximum depth of 4 km where the velocity field is close to zero (stagnation zones).

3.1 Geothermal energy migration: the impact of faults

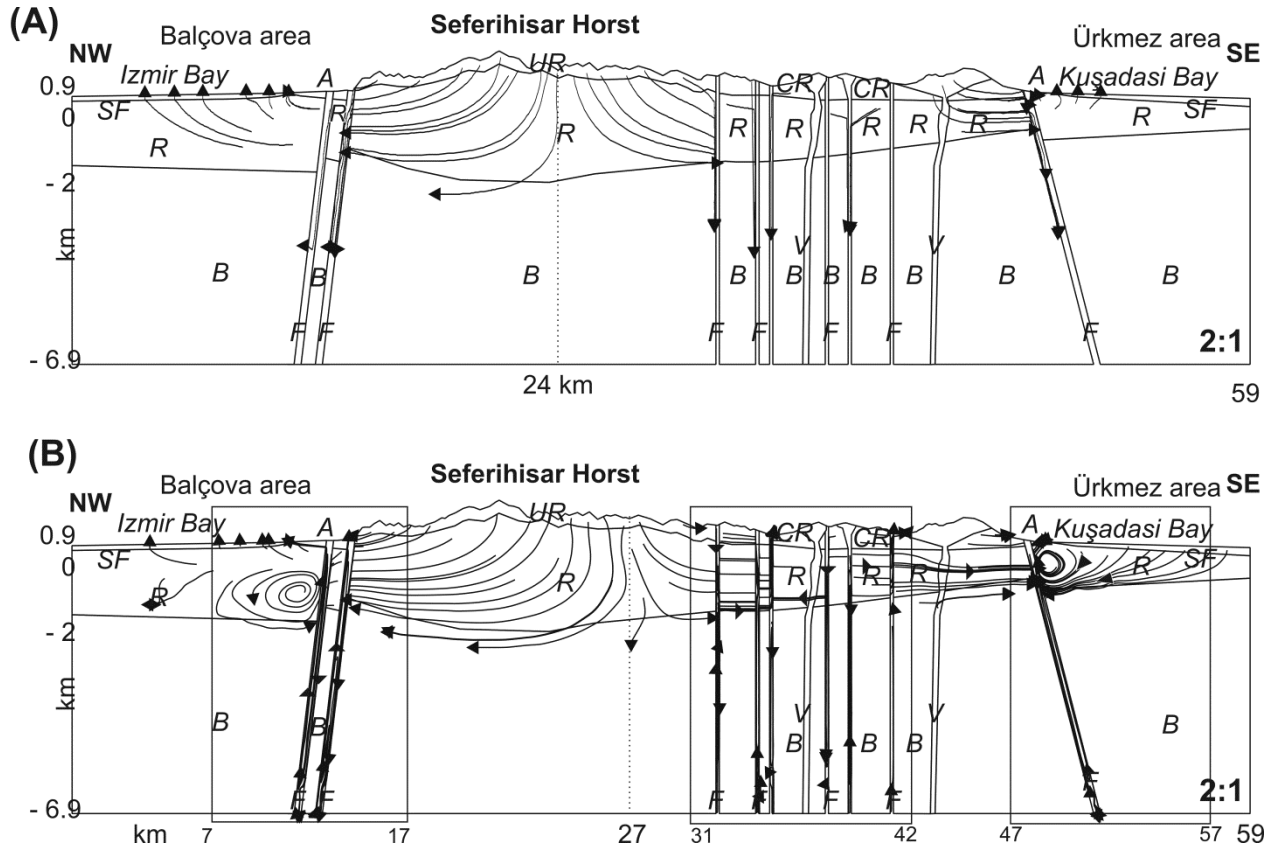


Fig. 6: Calculated topography-driven flow patterns: (A) in the absence of geothermal gradient. (B) resulting from coupled heat and flow transport simulations accounting for density- and viscosity- dependent fluid properties. Lines show the tracks (paths, no streamlines) of selected groundwater particles. Vectors indicate the flow direction. The dashed line locates the natural groundwater divide. The rectangles locate selected areas in which calculated temperature, pressure and flow patterns are illustrated in other figures. (SF: sea floor; A: alluvium; R: reservoir unit Bornova Mélange; UR: Upper Reservoir; CR: Cap Rock; V: Volcanic intrusions; B: basement). A 2:1 vertical exaggeration is used

Coupled heat and flow transport processes: density-driven flow

The results presented next illustrate how flow is affected by changes in fluid density and viscosity as a result of changes in temperature and pressure. The onset of thermal convection can be determined by using Rayleigh theory, as defined by Nield (1968). However, an accurate stability analysis of transient large-scale models is challenging, if not impossible, because the physical properties of fluid and basin units are not constant (Simmons et al. 2001). A coupled fluid flow and heat transport simulation in which the faults are not included was run in order to verify whether the natural geothermal gradient of the SBG could induce convection in the basin. The results do not display any convection, implying that the geophysical properties of the SBG are below the critical Rayleigh number. The onset of thermal convection in the reservoir units is triggered at a hydraulic conductivity of 32 m year⁻¹ which is two orders of magnitude higher than the estimated value of the Bornova Mélange (Serpen, 2004).

3.1 Geothermal energy migration: the impact of faults

Flow paths

The calculated flow paths (Fig. 6B) show that thermally-induced convective flow affects the fault zones through their whole length down to the basement. The convective circulation of hot geothermal waters within the faulted zones has three major consequences on the whole flow regime of the SBG (compare figures 6 A and B): (1) Convective cells develop locally in the Balçova and Ürkmez reservoir units, adjacent to the faults. It is worth recalling that these cells can not be generated by the geothermal gradient of the basin itself since without faults the geophysical properties of the SBG fall in subcritical Rayleigh conditions. They are therefore induced by the buoyant flow in the faults. These patterns are henceforth referred to as fault-induced cells. Similar cells have been described by McKibbin (1986) and Simms and Garven (2004) who found that convective flow in the faults can expand to the surrounding units. (2) The vertical faults of the Seferihisar Horst are now hydraulically interconnected in that the groundwater circulation in the surrounding reservoir units is induced by the convective regime of the fault themselves. (3) As a consequence, the groundwater divide in the Mélange of the Seferihisar Horst shifts. In this specific scenario, it has moved 3 km eastward along the profile, causing deep waters that previously flowed eastward to circulate in the opposite direction, toward the Balçova fault. The calculated flow paths, temperature and pressure patterns are shown in more detail in Figure 7 for three selected faulted-areas of the profile noted in Figure 6B.

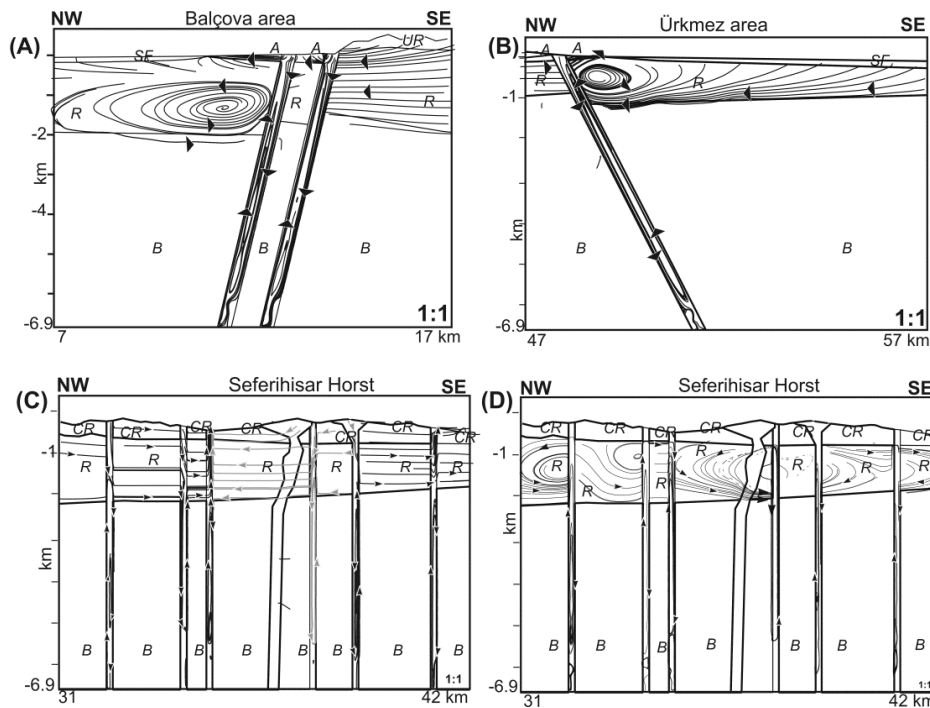


Fig. 7: Calculated flow patterns (A), Balçova area, (B) Ürkmez area, (C) Seferihisar Horst, (D) Seferihisar Horst with impervious caprocks. The faults are homogeneous (no cores). Vectors indicate the flow direction. (SF: sea floor; A: alluvium; UR: Upper Reservoir; CR: Caprock; R: reservoir unit, Bornova Mélange; B: basement). No vertical exaggeration is used

3.1 Geothermal energy migration: the impact of faults

In the Balçova area, the westward regional flow from the adjacent Seferihisar Horst infiltrates along the eastern flank of the fault (Fig. 7A). Owing to the natural geothermal gradient, groundwater is heated at the fault bottom and rises along the western flank of the same fault, driven by buoyancy forces. The upwelling flow is then advected by the regional flow into the adjacent parallel fault where groundwater undergoes a second convective overturn before discharging into the alluvium of the coastal aquifer. Within the Balçova faults the calculated velocities of the downward and upward convective flow are respectively 1.8 m year⁻¹ and 3.7 m year⁻¹. Velocities gradually decrease to 0.4 m year⁻¹ in the central part of the fault. The vigorous ascending flow of deep waters along the fault generates a 5 km wide by 1 km thick convection cell within the reservoir unit at about 1 km depth below the surface. In the Balçova reservoir unit, the cell is right-bounded by the fault; consequently, its vorticity is counter-clockwise. Sensitivity analysis showed that, for reservoir conductivity of 16 m year⁻¹, the fault-induced cell allows circulation of groundwater up to several dm per year⁻¹. Due to the impervious nature of the basement, the fault-induced convective pattern does not extend below the basement/reservoir interface. Furthermore, the strong topography-driven flow in the Seferihisar High prevents convection from developing in the reservoir unit there.

Similar flow dynamics and velocities develop in the Ürkmez faulted area (Fig. 7B). However, because of the uplifted basement, the fault-induced cell in the reservoir unit is closer to the alluvium and seafloor. As a result, the flow pathlines around the cell can stretch vertically over several km from the seafloor to the fault. Additional simulations have revealed that this flow pattern remains even when the seafloor is quasi-impermeable. These results indicate that outflows of hot geothermal water in coastal aquifers have the potential to generate drag forces that are directed vertically from the seafloor toward the fault. Under specific tectonic settings, such as an uplifted basement/Mélange interface, these forces can be close enough to the seabed to induce seawater intrusions within basin rocks and faults. This hypothesis needs however to be further assessed by including salinity effects on the thermally driven flow (i.e. thermohaline flow). Such convective cells could explain why the springs of the Ürkmez area are a mixture of sea and geothermal waters whereas those near Balçova are relatively fresh.

Vigorous topography-driven flow can hinder the formation of fault-induced cells in the reservoir units as, for example, in the Seferihisar Horst (Fig. 7C). Nevertheless, the series of vertical faults there strongly disturbs the natural regional flow within the reservoir unit. While recharge/discharge zones are determined by the imposed hydraulic head gradients, groundwater circulation is modified by the convective regime that develops in the faults. The location of faults strongly affects groundwater flow patterns at the regional scale. For instance, the flow pathlines illustrated in Figure 7C show that a groundwater particle initially flowing from the western end of the profile toward the east can undergo several convective overturns in three different faults before discharging through the fractured caprock. As at the basin scale, a certain degree of uncertainty about the caprock permeability exists. A sensitivity analysis was

3.1 Geothermal energy migration: the impact of faults

conducted in which the hydraulic conductivity of the upper reservoir and caprock units were systematically decreased. The results prove that in the Melange of Seferihisar, the interaction between hydrostatic and buoyant forces depends strongly on permeability. For less vigorous regional flow caused by lower permeability in the upper units, convective cells can persist adjacent to the faults. (Fig. 7D). In other words, impervious caprocks decouple the regional flow from the underlying hydrothermal system (e.g. Hayba and Ingebritsen 1997). In this particular setting, groundwater flow in the Melange is driven by convection in the faults.

Temperature patterns

The density- and topography-driven flows have a major impact on the geothermal gradient and temperature patterns (Fig. 8). In the Balçova area (Fig. 8A), decreased temperature gradients correspond to downward flow along the eastern flank of the faults, whereas upwelling groundwater flow generates elevated temperature gradients along the western flank of the faults. As a result, the isotherms within the faults are deflected parallel to the fault flanks.

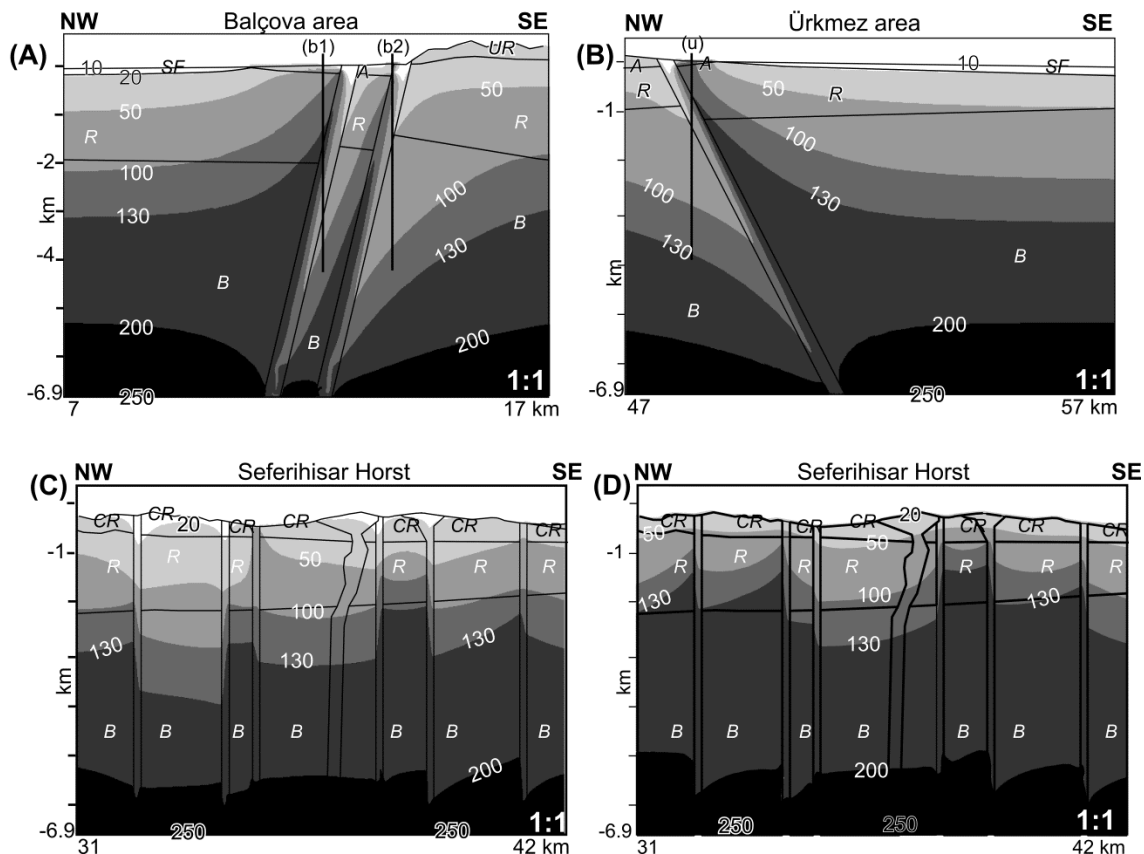
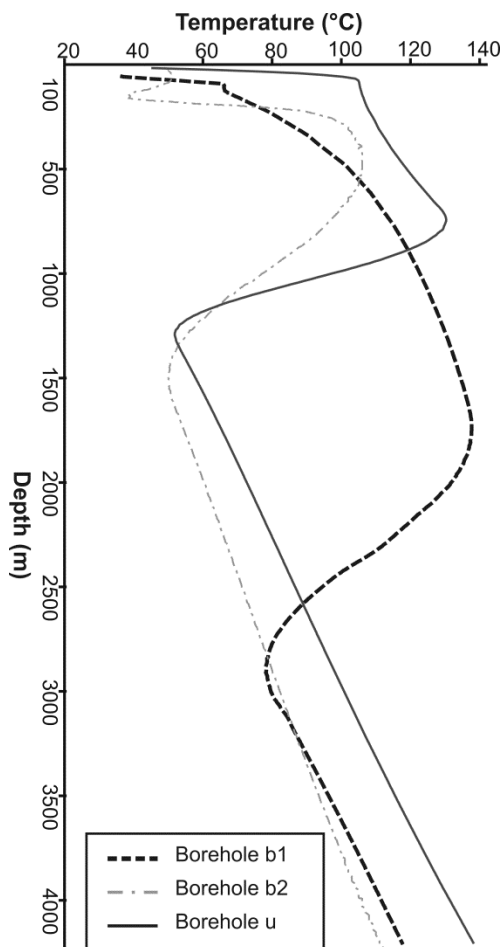


Fig. 8: Calculated temperature field in °C. (A), Balçova area, (B) Ürkmez area, (C) Seferihisar Horst (D) Seferihisar Horst with impervious caprocks. The faults are homogeneous (no cores). The bold lines locate putative boreholes whose temperature-depth trends are illustrated in Fig. 9 (SF: sea floor; A: alluvium; UR: Upper Reservoir; CR: Caprock; R: reservoir unit, Bornova Mélange; B: basement). No vertical exaggeration is used

3.1 Geothermal energy migration: the impact of faults

Although the two faults in Balçova are modeled as symmetrical and physically identical, the temperature patterns are slightly different. In the eastern fault, a hot plume of 130 °C reaches approximately 2 km depth, whereas in the western fault a plume of the same temperature ascends to just 700 m below the alluvium. The reason for this difference is that the cold recharge from the Seferihisar High infiltrates directly along the eastern fault, whereas warmer, deeper water ascends along the western fault. The circulation of cold/hot waters within the faults generates positive and negative temperature anomalies. These anomalies are defined as the difference between the temperatures observed at a point and the initial temperature distribution at that depth and can reach magnitudes as high as $\pm 90^\circ$ C. Similar temperature patterns are observed in the Ürkmez area and in the faulted parts of the Seferihisar High (Fig. 8C). In simulations with an impervious caprock sealing the upper part of the faults, the hydrothermal plumes rise through the fault up to the caprock/reservoir boundary (Fig. 8D). Channelled hot waters accumulate below the caprock, forming local “blind” geothermal systems (i.e. with no spring manifestations at the surface). Furthermore, the dense spacing of vertical faults in the Seferihisar Horst prevents temperature in the basement units from returning to its initial conductive state (Figures 11C and 12).



In Figure 9, the calculated temperatures are displayed along 3 putative boreholes, as located in Figures 8A and B. The temperature-depth profiles “b1” and “u” (Fig. 9) clearly show that in the shallow aquifers (down to 100 m depth) high temperature gradients up to 5 °C /10 m are generated by the upflow of hot geothermal waters. In borehole b2, the water temperature decreases abruptly at 150 m depth due to the recharge from the flanking Horst. At the surface, temperatures range between 40°C and 60 °C, in good agreement with the measurements of spring temperatures from Tarcan and Gemici (2003).

Fig. 9: Calculated temperature-depth trend along three putative boreholes as located in Fig. 8. The boreholes b1 and b2 cut respectively the western and eastern faults of the Balçova area. The borehole u1 is located in Ürkmez area

3.1 Geothermal energy migration: the impact of faults

All plots also exhibit sections in which temperatures increase and decrease almost linearly. Sharp temperature decreases in the profiles correspond to locations where the boreholes intersect faults, thus leaving zones of groundwater upwelling and entering zones of groundwater downwelling.

Pressure distribution

Channeled groundwater flow in highly permeable conduits and thermal anomalies strongly influences the pressure distribution within the aquifers (Cathles 1977; Haneberg 1995; Bense and Person 2006; Bense et al. 2008). An example is illustrated in Figure 10A for the faulted Balçova-area. Pressure drops occur in the faults throughout the basement. At the fault/reservoir intersections, the corresponding head level decrease is as much as 120 m. In the upper part of the profile, the pressure gradient is linear, close to hydrostatic conditions. Throughout the profile, these fault-related pressure drops develop within the basement, in direct relation to the convective flow.

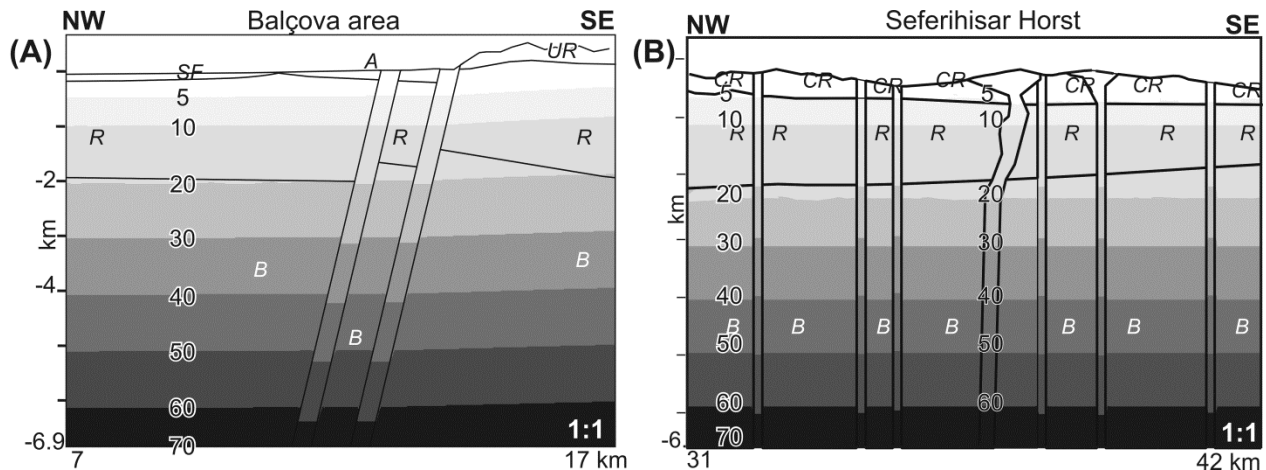


Fig. 10: Calculated pressure profile in MPa. The faults are homogeneous (no cores). (A), Balçova area, (B) Seferihisar Horst (SF: sea floor; A: alluvium; UR: Upper Reservoir; CR: Caprock; R: reservoir unit, Bornova Mélange; B: basement). No vertical exaggeration is used

If the simulations include an impervious caprock sealing the upper faults, pressure drops are constrained to the deeper parts of the faults and overpressured zones form below the reservoir unit (Fig. 10B). In these locations, the pressure rise is caused by the underlying convective flow which is prevented from discharging at the surface because of the sealing caprocks. In his investigations on groundwater flow across faults, Haneberg (1995) calculated that the head (i.e. pressure) offsets due to groundwater flow in faulted aquifers occur at the edge of the faults and are directly proportional in magnitude to the transmissivity contrast between faults and the surrounding aquifers. Accordingly, the more permeable Bornova Mélange allows head perturbations to be dissipated, creating a flat isobar pattern.

3.1 Geothermal energy migration: the impact of faults

Evolution of the thermal plumes

The results described thus far are snapshots at the ends of simulation runs. In the discussion that follows, the temperature patterns are illustrated at different time-steps in order to gain insights into the evolution of the hydrothermal plumes. The reported time-steps do not correspond to any specific geological history, but represent elapsed time. Figures 11A shows the thermal plumes developing at an early time of 589 years in the Balçova faults at depths between 2 and 6 km. Several convection cells are present within the thermal plumes (Fig. 11A).

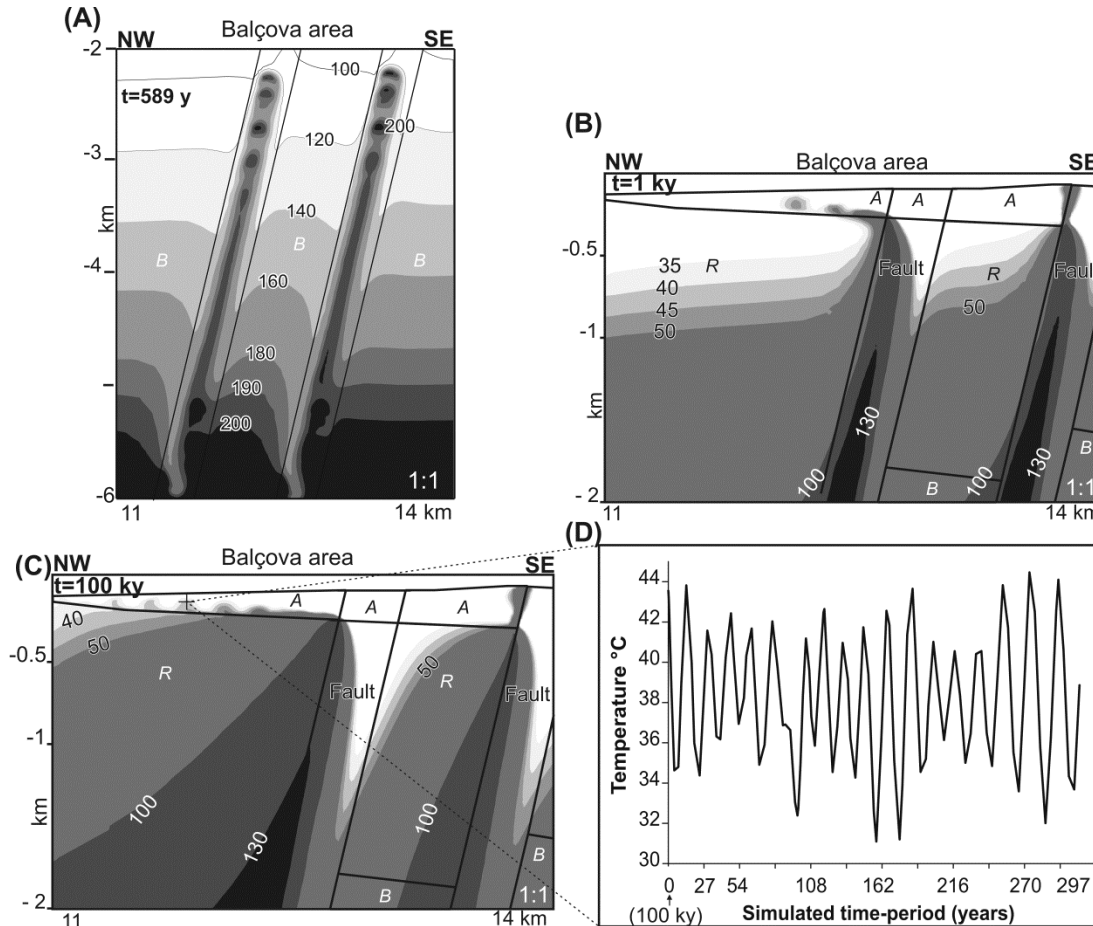


Fig. 11: Calculated temperature field in °C in the faults of the Balçova area at different time-steps and depths. The faults are homogeneous (no cores). (A) At simulated time $t= 589$ y at depths below 2 km (B) At simulated time $t= 1$ ky at depths above 2 km (C) At the end of the simulation run, 100 ky at depths above 2 km (D) temperature-time history of a grid point in the alluvium unit as located in plates B and C

These convection currents partition the plume into discrete segments. A plume of $\sim 200^{\circ}$ C water forms at a depth of about 5.2 km and rises vertically along the fault over 2 km. By the time the plume has ascended to a depth of about 3.5 km, the cooler, denser and more viscous environment has caused the plume to break up into several highly unstable “droplets”. By a simulated time period of 1 ky (Fig. 11B), the hydrothermal plume has nearly reached the surface. The plume-tip breaks down at the alluvium/fault interface at a rate of 20 m yr⁻¹. The

3.1 Geothermal energy migration: the impact of faults

thermal droplets migrate westward in the alluvium at an average flow velocity of 14 m yr⁻¹. As the underlying convective regime in the fault reaches a steady-state, the break up of the plume-tip is sustained over large temporal scale. As a result, after 100 ky, a series of regularly spaced thermal fingers with temperatures of 45 – 50 °C align within the alluvium (Fig. 11C). On average, plumes break with a periodicity of approximately 20-25 years (Fig. 11D). This process generates local temperature variations at the surface of 15 °C (Fig. 11D). Although the temperature oscillations displayed in the alluvium are similar to those of a multi-cellular convective regime, these fluctuating patterns are exclusively caused by the periodical splitting of the plume-tip, as also shown by the velocity field which is parallel to the alluvium bottom (Fig. 7A). Where regional flow rates are low, the broken plumes vent at the surface vertically, as in the eastern fault, where the split tip spreads through the discharge area. Hydrothermal plumes also break down at the Ürkmez fault/alluvium boundary. By contrast, in the minor vertical faults of the Seferihisar Horst the splitting of the plumes occurs only in the deeper part of the model, at early time periods.

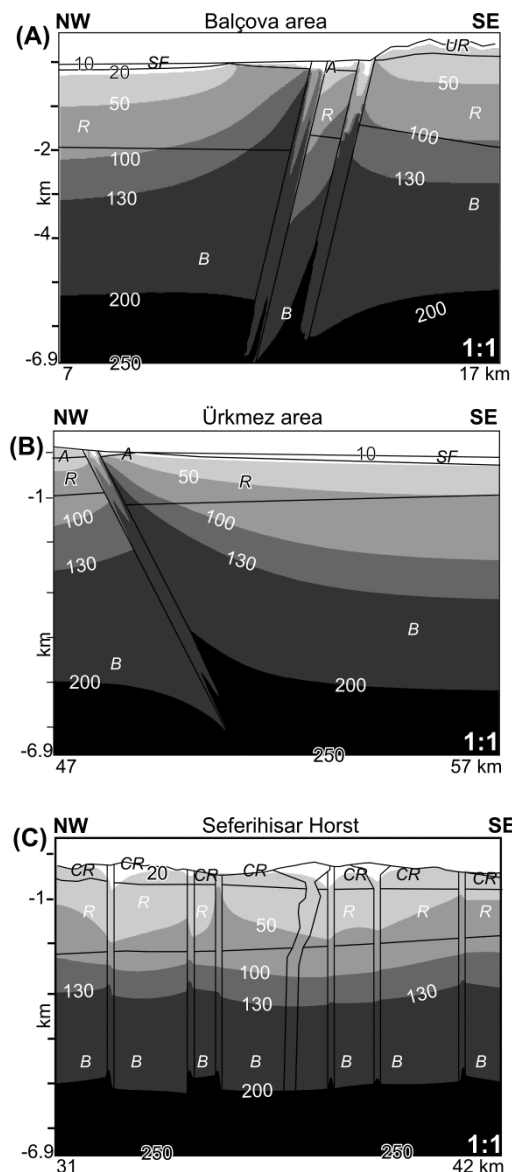
Splitting of plumes in porous media is a known process for the case of two immiscible fluids (Chouke et al. 1959; Kessler and Levine 1986). This phenomenon, also called Taylor-Saffman instability, is triggered when a less viscous fluid displaces a more viscous one (Saffman and Taylor 1958). In a hydrothermal system, the ascent of hot groundwater (low-density, low-viscosity fluid) into a colder fluid with high density and viscosity can induce the splitting of the plume interface. Schoofs and Hansen (2000), and Coumou et al. (2006) studied the Taylor-Saffman instability in mid-ocean ridge hydrothermal systems. The latter demonstrated that if convection is vigorous enough, an upward flowing fluid of 40 °C into a 10°C overlying fluid can generate viscosity-density contrasts strong enough to destabilize the rising front. In the SBG, these conditions are satisfied within the faults. The authors also found that the splitting of the plumes has a period of decades and persists over thousand of years, in agreement with our findings. Unfortunately, in the SBG, no monitoring surveys have ever been conducted that could confirm such temperature variation in the geothermal waters. The only observations are those of the springs venting between the Seferihisar and Degirmendere High (Esder and Simsek 1975).

Effect of impervious fault-core and volcanic intrusions

The hydraulic architecture of faults can change groundwater flow patterns (e.g. Fairley and Hinds 2004b). In this section, the interrelationships between fluid flow and fault heterogeneity are addressed by including an impervious core within the damage zone, as explained in the “Mesh” section above. The physical properties of the core zone are given in Table 1. Although extremely simplified, this is a more realistic representation of faults, as clogging and mineral precipitation are common processes associated with hydrothermal flow. The results showed that if the damage zones have a hydraulic conductivity of 32 m year⁻¹ or less and the cores are impervious, thermal convection does not develop in the faults. The calculated isotherms are flat

3.1 Geothermal energy migration: the impact of faults

and the temperature gradient throughout the profile is close to the initial conductive state. The impervious core effectively reduces the conductivity of the whole fault zone and therefore its ability to conduct fluid and heat. Lopez and Smith (1995) determined that the boundary between a conductive and convective regime in a faulted system depends linearly upon both width and permeability of the fault. Additional simulations revealed that for a damage zone conductivity of at least 95 m year⁻¹, thermal plumes start rising in the faults with convective dynamics similar to those in the homogeneous case. Here convection is confined to the damage zones, with upflow along both fault-flanks and downflow at the core sides, while the core itself is a no-flow zone. As a result, major differences can be observed in the temperature patterns, where temperatures in the basement closely resemble the initial conductive state and temperatures in the overlying sediments are strongly affected by groundwater advection (Fig. 12).



In the Balçova and Ürkmez areas (Fig. 12 A and B) the plumes have bifurcated tips along the core sides and temperature-depth inversions can also occur within the fault cores. On the other hand, in the upper Seferihisar Horst the plumes are similar to those of the homogeneous fault case, because there the regional flow is the main control of the temperature distribution (compare Figures 12C and 8C). Qualitatively the pressure patterns are similar to those of the homogeneous case, in that head drops and increases are observed in relation to upflow of hot waters and presence of sealing impervious caprocks, respectively. The magnitude of these anomalies is however higher, because the convective flow is constrained in the thinner damage zones.

Fig. 12: Calculated temperature field in °C. The faults include an impervious core. (A), Balçova area, (B) Ürkmez area, (C) Seferihisar Horst (SF: sea floor; A: alluvium; UR: Upper Reservoir; CR: Caprock; R: reservoir unit, Bornova Mélange; B: basement). No vertical exaggeration is used

3.1 Geothermal energy migration: the impact of faults

In the current study area, volcanic intrusions have thermal properties very similar to those of the reservoir (Esder and Simsek 1975). It is known that contrasts in thermal conductivity can lead to temperature variations. A series of simulations in which the thermal conductivity of the magmatic intrusions is varied indicates that, in the SBG, these geological features are too thin to affect conductive and convective heat flow regimes at a regional scale.

SUMMARY AND CONCLUSIONS

In recent years, geothermal explorations performed by the MTA demonstrated the existence of anomalous heat distribution in the SBG. In the faulted aquifers, temperature logs display steeply increasing gradients at shallow depths as well as inverted temperature-depth trends whose causes are not fully understood. Additional hydrochemical and geophysical investigations carried out by different Turkish research groups suggest that the hydrothermal phenomena of the SBG result from deep groundwater circulation in highly permeable faults. Isotopic analyses also indicate strong interactions – from near the surface to depths of two km or more – between inflows of colder recharge water from the horsts and upwelling hot fluids from depth. This mechanism could explain the observed temperature anomalies as well as the presence of crustal volatiles in surficial waters. An observation that remains unexplained is the different chemical compositions of the thermal springs in the northern and southern coastal aquifers: prior to geothermal exploration, springs in the Balçova area had dilute meteoric compositions, whereas springs venting in the Urkmez area contained a component of seawater.

A numerical model of coupled fluid flow and heat transport was built along a well-constrained north-south trending geological profile across the SBG in order to gain insights into the possible transport mechanisms of this geothermal system. The simulation results support the hypothesis that hot basinal fluids flow in the faults from the basement to the surface. The simulations provide significant insights into the fluid-dynamics underlying this process. Specifically, large-scale free convection induced by buoyancy-driven flow develops in all faults. Within the faults, the direction of flow in the convective cells is determined by the prevailing topography-driven flow: while downward flow of water occurs along the flank closer to the Horst, heated fluids rise along the more distal flank before discharging at the surface. The vigorous upward flow in the faults can induce km-scale convective cells in the surrounding Bornova Mélange, despite the fact that these units have sub-critical Rayleigh conditions. These fault-induced convection cells develop in areas where the regional flow is weak, such as below horizontal alluvium deposits and seafloors. In the latter case, if the convection cells extend to the freshwater/seawater interface they could likely drive salty waters toward the faults and inland units. This hypothesis, however, needs to be verified by running a simulation that couples solute transport to fluid flow and heat transport. In the Mélange of the Seferihisar Horst, fault-induced cells are overwhelmed by the prevailing regional flow. Nevertheless, the regional patterns are modified by the buoyancy-driven flow focused in the series of vertical faults. Groundwater undergoes several

3.1 Geothermal energy migration: the impact of faults

convective overturns in the different faults before discharging through fractured caprocks. As a result, the main groundwater divides in the basin shift relative to their positions in the absence of convective circulation. Simulations that included sealing caprocks had the effect of decoupling the regional flow from the underlying geothermal system and allow fault-induced cells to persist in regions of strong topographic variation.

The models provided reasonable representations of the temperature patterns of the SBG. The calculated temperature-depth trends that intersect faults are qualitatively similar to those measured from logs. The observed temperature patterns result from the interaction of convective flow and meteoric recharge from the horst into the faults (i.e. mixed convection). The calculated temperature patterns in the faulted Seferihisar area further highlight the role of the regional flow in advecting hot water through fractured caprocks. If caprocks are sealed, the underlying thermal plumes reach the upper reservoir boundary, forming over-pressured blind geothermal systems (with no thermal manifestations at the surface).

Heated water reaches the surface in a relatively short time period (a thousand years). Residence-times of geothermal water can be much longer, since groundwater undergoes several convective overturns within the faults before discharging to the surface. A transient phenomenon characterising the ascent of hot fluids is the splitting of the thermal plumes within the faults. This process, called Taylor-Saffman fingering, can generate periodical temperature variation in the more permeable alluvial units. To date, field evidence from long-term temperature monitoring is not available to confirm this process.

Impervious cores change flow temperature and pressure patterns. Convection is confined to the damage zones while the cores act as no-flow zones. As a result, thermal plumes have bifurcated tips and temperature inversions can also be observed within the faults. Higher head offsets occur than in the homogeneous fault case, within the thinner permeable damage zones of the faults.

This study is the first attempt to build a comprehensive regional model of coupled ground-water and heat flow of the SBG. Large-scale models like the one presented here are based on many assumptions on fluid and basin unit properties and boundary and initial conditions. Further major simplifications concern the structural characteristics of the basin and the complex architecture of the faults. Therefore, absolute flow magnitudes and temperature profiles cannot be calibrated by such models (Gvirtzman et al. 1997; Fairley 2009). Furthermore, convective flow patterns in faulted areas have 3D features (e.g. Lopez and Smith 1995; Zhao et al. 2003) which are not treated by the models. Though these aspects need additional research, the results obtained thus far support the flow and temperature patterns hypothesized by field observations. The simulation scenarios illustrate the fluid-dynamics that affect the SBG and the geophysical conditions under which they most likely form. Additional hydrochemical

3.1 Geothermal energy migration: the impact of faults

investigations are currently being carried out in order to provide further constraints on the described coupled heat transport processes.

ACKNOWLEDGMENTS

This research was funded by the German Science Foundation (DFG) and The Scientific and Technological Research Council of Turkey (Tübitak) through grants DFG Ma 4450/1 and Tübitak (107Y345). We thank C. Sarı, G. Göktürkler from the Dokuz Eylül University, İzmir for their insightful remarks on heat flow in Western Anatolia. We would like to acknowledge Prof. Şakir Şimşek from the Hacettepe University, Ankara for providing additional temperature data and for discussing the simulation results. We are grateful to Dr. Volker Clausnitzer, Prof. Diersch and DHI-WASY support staff in Berlin for their assistance in FEFLOW. The authors thank Prof. Martin Appold from the University of Missouri-Columbia and an anonymous reviewer whose contributions significantly improved the paper.

3.2 Thermally induced seawater intrusions



ABSTRACT

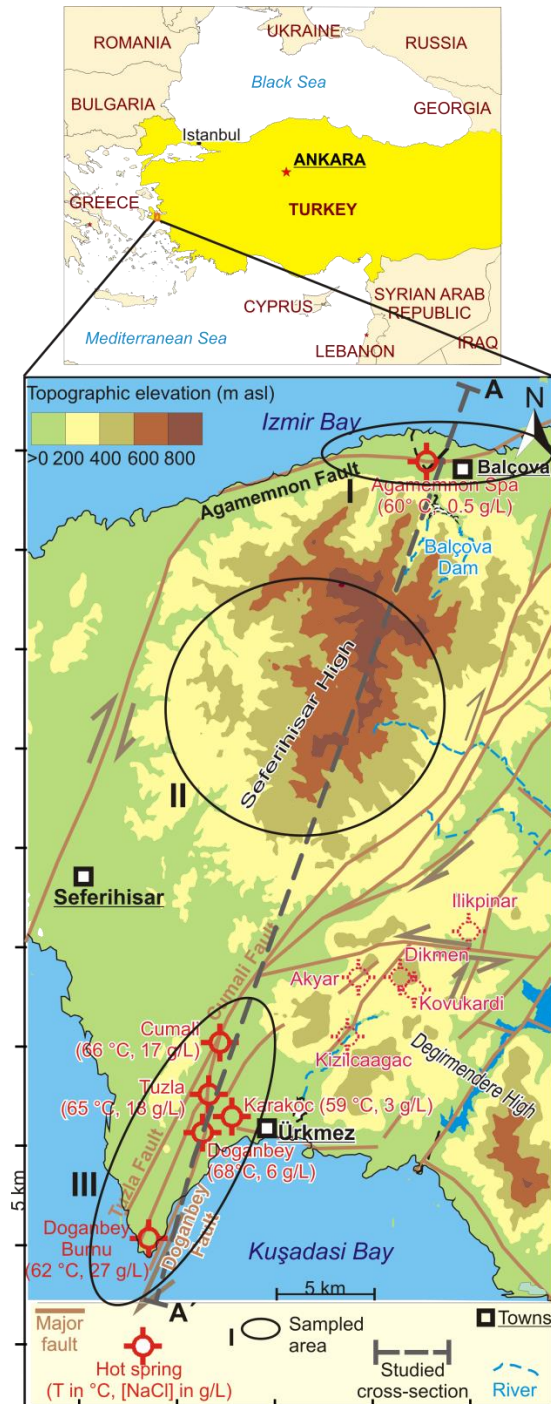
The Seferihisar-Balçova Geothermal system (SBG), Turkey, is characterized by temperature and hydrochemical anomalies along the faults: thermal waters in northern Balçova are heated meteoric freshwater, whereas the hot springs of the southern Seferihisar region have a strong seawater contribution. Previous numerical simulations of fluid flow and heat transport indicated that focused upsurge of hot water in faults induces a convective-like flow motion in surrounding units. Salt transport is fully coupled to thermally-driven flow to study whether fault-induced convection cells could be responsible for seawater encroachment in the SBG. Isotope data are presented to support the numerical findings. The results show that fault-induced convection cells generate seawater plumes that extend from the seafloor toward the faults. At fault intersections, seawater mixes with rising hot thermal waters. The resulting saline fluids ascend to the surface along the fault, driven by buoyant forces. In Balçova, thick alluvium, minor faults and regional flow prevent ascending salty water from spreading at the surface, whereas the weak recharge flow in the thin alluvium of the southern SBG is not sufficient to flush the ascending hot salty waters. These mechanisms could develop in any faulted geothermal system, with implications for minerals and energy migration in sedimentary basins.

Keywords: numerical modeling, Turkey, thermal conditions, fault, seawater intrusion

3.2 Geothermal energy migration: induced seawater intrusions

INTRODUCTION

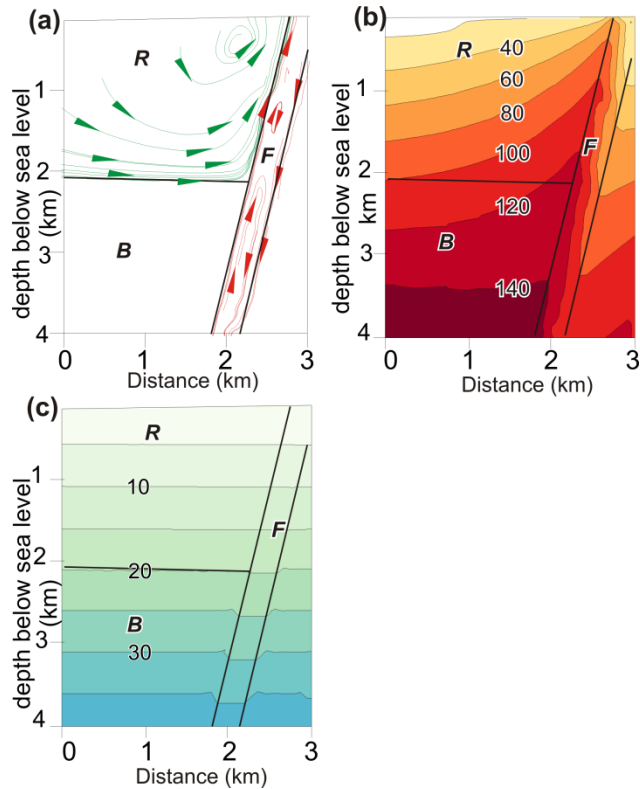
The Seferihisar-Balçova geothermal system (SBG) is located in the Aegean region, western Turkey (Fig. 1). The SBG is characterized by an average heat flow of 110 mWm^{-2} which is associated with the metamorphic massifs, granitic intrusions and young volcanism. The SBG thermal activity is manifested by hot springs that form mainly along the major fault systems (Eşder and Şimşek 1975).



Previous numerical simulations of coupled fluid flow and heat transport (Magri et al. 2010) were built in order to understand the physical mechanisms underlying the observed phenomena. The results indicated that large-scale free convection induced by buoyancy-driven flow develops in all faults (Fig 2a, red lines) in agreement with the hypothesis made by Serpen (2004). Hot and therefore less dense basinal fluids flow in the faults from the basement to the surface (Fig 2b). The simulations also revealed that, owing to the outflow of hot water through the faults, the pressure in the faults is lower than in the surrounding units (Fig. 2c). As a result, the flow is directed toward the faults and generates km-scale groundwater motion (Fig. 2a, green lines). The described flow patterns resemble convective cells, though they form under sub-critical Rayleigh conditions and are henceforth referred to as fault-induced cells. Similar cells have been described in theoretical studies by McKibbin (1986) and Simms and Garven (2004).

Fig. 1 Study area, the Seferihisar Balçova Geothermal system (SBG) and sampled areas. Fault and spring locations as shown in Eşder and Şimşek (1975), Genç et al. (2001), Drahor and Berge (2006) and Uzel and Sözbilir (2008). Hot springs: measured temperature in °C and NaCl concentration in g/L-1 (Vengosh et al. 2002, Tarcan and Gemici 2003). Topography derived from SRTM data (Reuter et al. 2007)

3.2 Geothermal energy migration: induced seawater intrusions



An observation that remains unexplained to date is the different salinity of the thermal springs in the northern and southern coastal aquifers of the SBG (Fig. 1). In the Balçova geothermal field in the north, thermal waters have low chloride (Cl) contents, whereas in the Doğanbey - Ürkmez area, in the south, thermal waters are salty with a strong seawater contribution (Tarcan and Gemici 2003; Tarcan et al. 2005). Furthermore, it is not clear what forces drive salty water inland; highly-salty groundwater extends 10 km inland along the major southwest-northeast-trending faults.

Fig. 2: Close-up of the upper 4 km of the calculated (a) flow pathlines (no streamlines), (b) temperature (°C) and (c) pressure (kPa) patterns derived from an 11-km deep model of coupled fluid flow and heat transport (no mass-transport equation). Faults are equivalent porous media, 7 km deep and 300 m wide. This model uses a basal heat flow of 100 mW m⁻². Red flow patterns are thermally-driven convective cells developing in the faults at velocities between 2 and 7 m year⁻¹. Flow lines induced by the convective regime in the faults (i.e. fault-induced convection cells) are illustrated in green. Fault-induced convection cell velocities are in the order of a centimeter per year (R: Reservoir; F: Fault; B: Basement). No vertical exaggeration is used. Modified after Magri et al. (2010)

NaCl content ranges from 3 gL⁻¹ at Karakoç spring to 17-18 gL⁻¹ at the Tuzla and Cumalı springs located at fault intersections. The 62 °C Doğanbey Burnu spring on the coast is slightly more dilute than seawater with a total dissolved solids (TDS) content of 27 gL⁻¹. Hydrochemical investigations indicated that the hot salty springs of the SBG result from a mixture occurring at different depths between seawater and ascending thermal waters (Conrad et al. 1995; Vengosh et al. 2002; Tarcan and Gemici 2003). The previous simulations (Magri et al. 2010) suggested that fault-induced cells could cause seawater circulation. However, in those simulations, the salinity effects on fluid density and viscosity were not computed and it was not possible to verify whether fault-induced cells could drive seawater to flow inland and mix with ascending thermal waters.

This study investigated the feasibility of fault-induced seawater circulation by running fully-coupled fluid-flow, heat and salt-transport models (i.e. thermohaline flow). The study also investigated why the springs of the Ürkmez area are salty whereas those near Balçova are relatively fresh. The numerical results illustrate the calculated flow paths, as well as fluid

3.2 Geothermal energy migration: induced seawater intrusions

temperature and salinity patterns supported by new isotopic analyses. The results give insights into the dynamic underlying mixing of salty water, ascending geothermal water and regional flow, as well as the impact of minor faults and more permeable units.

As a result of parameter uncertainty, it is not possible to precisely calibrate thermohaline patterns at basin-scale and to predict salinity. The intention of this study is not to present a calibrated model of thermohaline patterns to be used to predict salinity in the basin, but rather, to provide possible explanations for seawater intrusion in the SBG.

Although this study focuses on the coastal aquifers of the SBG, the geological conditions described here occur in many sedimentary basins of the world. Therefore, the illustrated patterns could develop not only in coastal environments, but in any faulted geothermal system. Accordingly, fault-induced cells could influence the transport and fate of minerals, dissolved salt bodies or relict brines.

DATA

Geothermal explorations in the SBG started in the early 1960s. Approximately 50 wells have been drilled by the General Directorate of Mineral Research and Exploration of Turkey (MTA) both for developing and monitoring geothermal energy production. The depths of the wells vary from 100 m (shallow) to more than 2 km (deep). In the north, the wells are located around the Agamemnon Spa (Fig. 1). In the south, most of the drilling has been performed along the Doğanbey fault near the Doğanbey, Tuzla and Cumalı hot springs (Fig. 1). This extensive drilling campaign has allowed various Turkish research groups to collect geophysical, temperature and hydrochemical data that define the major tectonic features (e.g. Dominco, 1969; Eşder and Şimşek, 1977; Ercan et al.1986; Aksoy, 2001; Drahor and Berge, 2006; Uzel and Sözbilir 2008) and possible groundwater flow paths of the SBG (e.g. Genç et al. 2001; Serpen 2004; Erdogmus et al. 2006; Aksoy et al. 2008). Comprehensive datasets are given in Satman et al.(2001) and in the reports of the MTA (Eşder 1975; Yilmazer 1984; Demirel and Sentürk 1996; Çetiner 2004 Satman et al. 2002).

Hydrogeologic setting – studied profile

The studied profile (Fig.1) extends over 62 km from Izmir Bay to Kuşadası Bay. This transect was chosen in preference to the one in Magri et al. (2010) because it incorporates new structural data that were not available before. Specifically, the Balçova alluvium interface is now better defined and minor faults cutting the Balçova alluvium and the Kuşadası seafloor are included. The seafloor topography of the Kuşadası Bay is very well defined by bathymetric and seismic studies (Ocakoğlu et al. 2004, 2005). Thus the new transect provides good structural constraints for the reservoir-basement interface. Furthermore, the southern part of the selected profile

3.2 Geothermal energy migration: induced seawater intrusions

crosses the Cumali, Tuzla and Doğanbey faults, where most of the new hydrochemical samples have been taken.

The geologic cross-section for the transect is schematically illustrated in Fig. 3. Major stratigraphic units include Quaternary alluvium and seafloor sediments, the Cretaceous Bornova Mélange, and the Paleozoic metamorphic basement, which closes the model domain at 6.9 km depth bsl (below sea level). The lateral boundaries of the area are located 10 km beyond the pinchouts of the alluvium which prevents any numerical artifacts of the boundary conditions affecting the flow patterns.

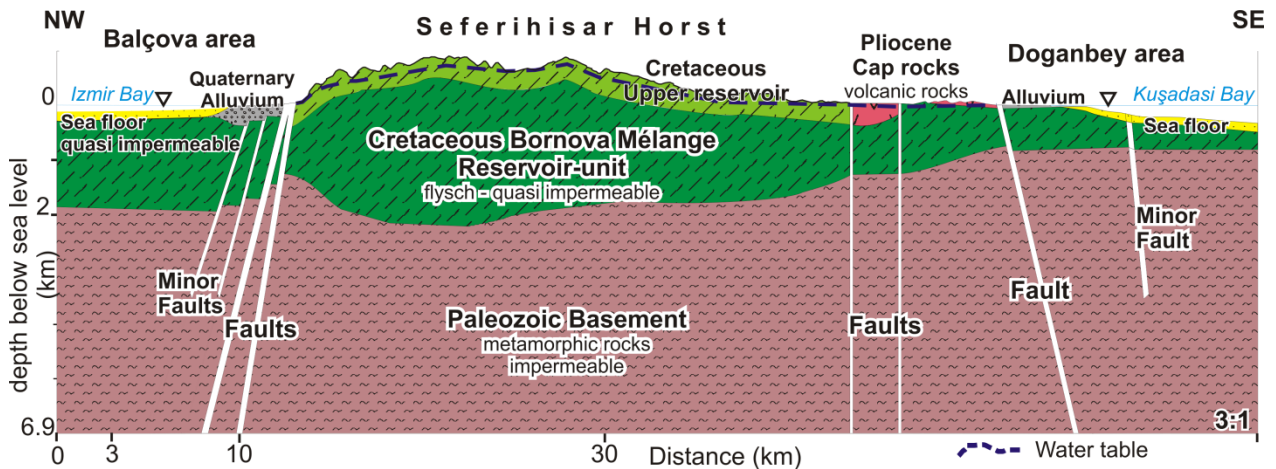


Fig. 3: Hydrostratigraphy of the northwest (NW)-southeast (SE) studied profile. Several rock groups and formations can be distinguished, as defined, amongst many others, by Genç et al. (2001), Uzel and Sözbilir(2008). A 3:1 vertical exaggeration is used.

Hydrogeologically, the metamorphic basement is a very low-permeability unit made up of crystalline schist, marble and phyllite intercalations (Akartuna 1962, Eşder and Şimşek 1975 and Kaya 1981). The topology of the upper basement has been defined by gravity studies (Drahor et al. 1999). On average it is located at least at 2.5-km depth below land surface in the Seferihisar Horst. By contrast, in the Doğanbey area, seismic profiling clearly shows that the metamorphic rocks have been uplifted to depths of less than 500 m (Ocaköğlu et al. 2004).

The overlying Bornova Mélange is composed mostly of deformed and locally-metamorphosed blocks of limestones, metasandstones, serpentinites and spilitic lavas (e.g. Erdoğan and Güngör 1992). This unit is considered to be the main geothermal reservoir (Eşder and Şimşek 1975; Aksoy et al. 2008) and will therefore also be referred to as “the reservoir unit”. The permeability of the Bornova Mélange is largely secondary and is produced by faults and fractures. Within the SBG, the reservoir-unit thickness can vary between a few hundred meters in the Doğanbey area to more than 2 km in the Balçova area, as shown by several well-core observations (e.g. Eşder and Şimşek 1977; Öngür 2001).

3.2 Geothermal energy migration: induced seawater intrusions

The reservoir unit in the southern part of the profile is partly overlain by a 300-m thick volcanic-sedimentary unit that acts as an impervious cap rock. The upper reservoir in the Seferihisar High consists mainly of a clayey Flysch unit.

The youngest rocks in the study area are Quaternary, unconsolidated alluvial sediments that consist mostly of clayey-sands, silt and gravels. These sediments comprise an extremely-permeable shallow aquifer, whose thickness ranges between 150 m and only 50 m in the Balçova and Doğanbey areas, respectively. The alluvium deposits gradually decrease in thickness toward the sea.

As a result of intense graben tectonics, the whole SBG has been dissected by steeply-dipping strike-slip and active normal faults that extend from the basement to the Quaternary deposits. The dip angles of the normal faults near the northeast and southwest ends of the profile are 54° and 60° respectively (Tezcan 1966; Yilmazer 1989). The strike-slip faults cut the volcanic rocks vertically.

In this study, faults are made up of two permeable damage zones surrounding an impervious core, as proposed in the conceptual models of Caine et al.(1996). The Caine et al. model is the best-known of the fault-hydrology conceptual models. Other conceptual models for faults in alluvium and poorly-lithified sediments (Rawling et al., 2001) and clastic sedimentary rocks such as sandstones (Antonellini and Aydin, 1995) generally predict lowered permeabilities in the damage zones of faults that cross-cut these lithologies (as opposed to the Caine et al. model). As pointed out by Heffner and Fairley (2006), there are many situations where these models would be expected to apply but do not. As a result, none of these three conceptual models are universally applicable. Careful field investigation on a case-by-case basis is necessary to assign an appropriate conceptual model to a particular fault zone. Based on well-tests carried out by Onur et al. (2002) and Uzel and Sözbilir (2008) in structural studies, the estimated thickness of the combined fault-core and damage zones is 300 m.

Bathymetric and seismic-reflection surveys revealed that the seafloor and underlying Mélange units are faulted, and that the basement-Bornova Mélange interface is highly fractured (Ocakoğlu et al. 2004, 2005; Prof. Dr. M. Yılmaz Savaşçın Dokuz Eylül Üniversitesi, personal communication, 2010) suggesting that the basement interface is not a sharp but rather gradational boundary with less-consolidated sediments comprising the lower Bornova Mélange.

That groundwater flow, hydrochemical and hydrothermal patterns of the SBG are strongly controlled by fault tectonics is also shown by temperature logs and hydrochemistry data.

Temperature logs

Temperature-depth trends of several deep wells can be found in Eşder and Şimşek (1975; 1979), Serpen (2004) and the reports from Balçova geothermal company (İzmir Jeotermal AŞ) (e.g. Satman et al. 2001).

As described in Serpen (2004), the temperature profiles indicate that deep geothermal waters ascend into both the shallow alluvium and the reservoir unit at depths between 400 and 700 m (bsl), leading to temperature gradients of $0.5\text{ }^{\circ}\text{C m}^{-1}$ in the shallow aquifers. Hydrological studies carried out by different Turkish research groups suggest that SBG thermal waters are fed by meteoric groundwater that infiltrated from the Seferihisar Horst (Fig. 1) into the reservoir units down to a depth of at least 2 km bsl (Serpen 2004). Owing to the existence of a naturally-high conductive heat flow, deep, hot geothermal waters are driven upward by buoyant forces generated by a decrease in fluid density. Preferential conduits for these large-scale density-driven flows are highly-permeable units, such as faults and fractures (i.e. hydrothermal convection). The observed temperature anomalies and hot springs are therefore due to mixing of ascending deep groundwater and shallow recharge waters (Aksoy et al. 2008) as also supported by previous numerical results (Fig. 2).

Hydrochemical data

The present study has also generated new chemical-composition data for fluids circulating through the SBG. A more detailed manuscript about the chemical and isotopic composition of all sampled SBG waters is currently under preparation by the present authors. Here, only the isotope findings are briefly noted.

Apart from the existing hydrochemical database published by different Turkish researchers in the MTA reports (e.g. Satman et al. 2001), during the last two years, additional field campaigns have been carried out by the present authors. The sampled areas are (Fig. 1):

- in the north: the thermal sites around the Agamemnon Spa and the existing boreholes throughout the Balçova alluvium.
- in the central part, the recharge areas and natural springs of the Seferihisar Horst
- in the south, the hot springs along the major faults as well as several shallow wells in the Doğanbey-Ürkmez alluvium ;

In total, more than 50 new samples have been collected during different periods from 2008 to 2010. The standard procedure applied in situ consisted of measuring temperature, pH and electrical conductivities with a multi-parameter device, filtering and storing samples in polyethylene bottles. Henno Meyer from the Alfred Wegener Institute (AWI) in Potsdam measured the content of stable isotopes.

3.2 Geothermal energy migration: induced seawater intrusions

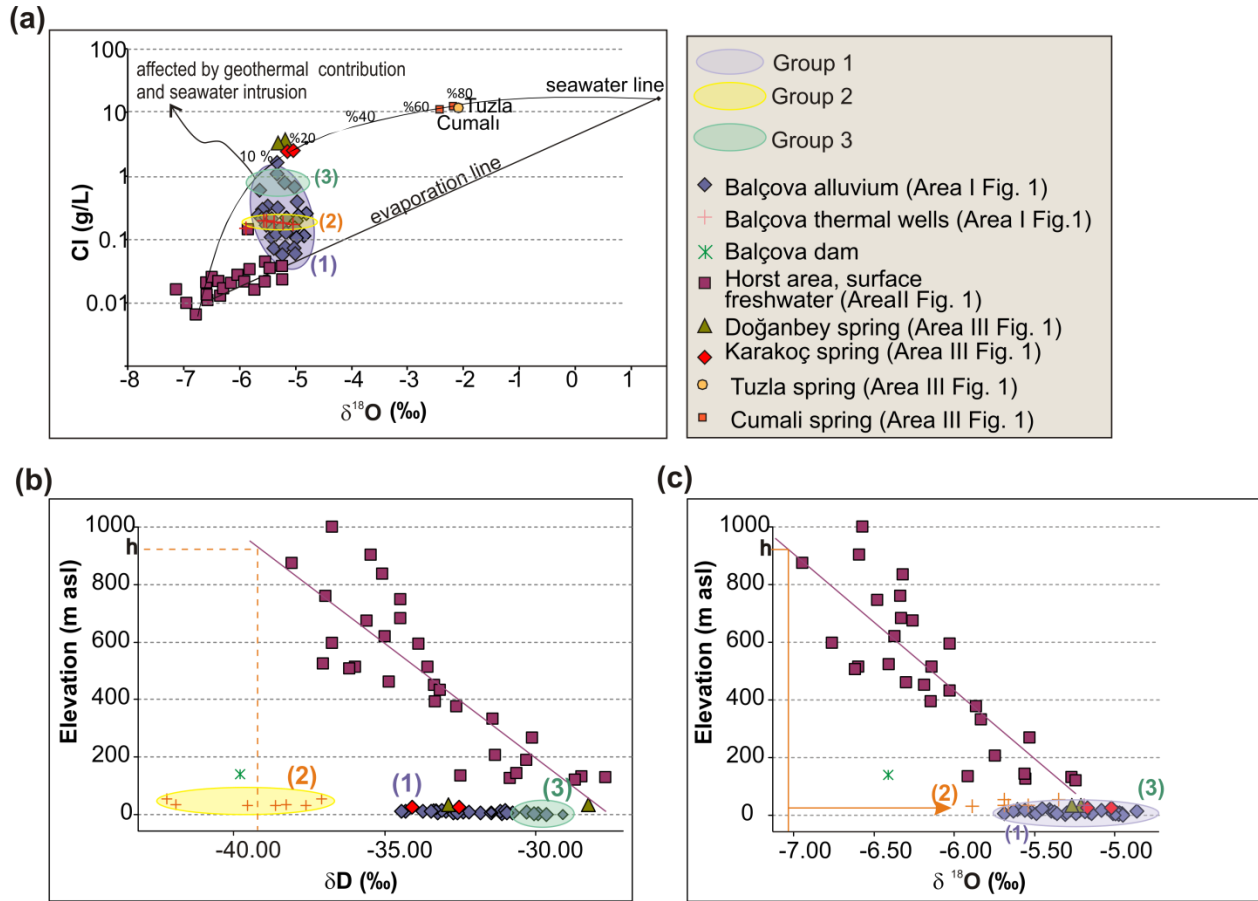


Fig. 4: (a) Chloride content of the sampled waters during the 2009 field campaign (no deep wells) as function of $\delta^{18}\text{O}$. Seawater amounts are in percentages on the mixing line. The Balçova alluvium waters (group 1) have both thermal water (group 2) and seawater (group 3) fingerprints. (b) δD and (c) $\delta^{18}\text{O}$ values (‰) of the waters sampled as a function of altitude. For pictorial clarity, δD and $\delta^{18}\text{O}$ values of Cumali, Tuzla and seawaters are not displayed. The dashed orange line in panel (b) represents the inferred recharge altitude h (m) of the thermal waters. $\delta^{18}\text{O}$ ‰ shifting of thermal waters (group 2) is indicated by the bold orange arrow in panel (c). The purple line is the regression line of the horst samples

The new analyses confirmed the previous conclusions from Conrad et al. (1995), Vengosh et al. (2002) and Tarcan and Gemici (2003), that the geothermal waters have two main origins: meteoric waters (heated groundwater) and seawater, as shown by δD and $\delta^{18}\text{O}$ compositions of the sampled waters as a function of chloride content (Fig. 4a) and altitude (Fig. 4b, c).

- *Northern SBG:* Balçova alluvium waters (group 1, Fig 4a) are a mixture of meteoric and thermal waters (group 2). These alluvial waters may also have been slightly affected by influx of marine water (group 3), as shown by the shifting of Balçova samples from the dilute meteoric fluids (evaporation line) toward the seawater mixing line. Chloride content is low and reaches a maximum of 1 gL^{-1} near the seashore. It is well known that $\delta^{18}\text{O}$ measurements can be strongly affected by geothermal processes (Clark and Fritz 1997) Therefore δD data are preferred for elevation estimates (Fig 4b). It was found that Balçova alluvium waters are fed by recharge from terrains at elevations between 100 and 500 m above sea level (asl), whereas Balçova thermal

3.2 Geothermal energy migration: induced seawater intrusions

waters from the deep wells originated in the Seferihisar Horst at about 900 m above sea level (h, in figure 4b). This suggests that surface waters have been deeply entrained in the subsurface before rising again. The proposed mechanism is that surface waters from the bounding horst have descended to great depths where they were heated before rising back to the surface (Serpen, 2004). Ascending flow of meteoric water is further supported by the shift of $\delta^{18}\text{O}$ ‰ toward less negative values (Fig. 4c), indicating water-rock interaction. Therefore, the regional flow from the horst toward the coastal aquifers also determines the geothermal behaviour of the SBG, especially in the alluvial sediments. These findings are in good agreement with previous studies from Yilmazer (1989), Filiz et al.(1993) and Aksoy (2001).

- *Southern SBG*: The thermal waters in the Doğanbey-Ürkmez area, southern SBG, originated from a mixture of seawater and local meteoric groundwater. The seawater amount can be as high as 80% at the Tuzla and Cumalı springs (Fig. 4a) which are located several kilometers inland at the fault intersections. The recharge altitude of the southern hot springs does not exceed 400 m above sea level. Owing to the rather flat topography, the regional flow in the southern part is weak. Well logs show that seawater and freshwater mixing occurs both in the shallow aquifers and in the deeper parts of the basin (Conrad et al. 1995; Vengosh et al. 2002; Tarcan and Gemici 2003). To date, the geothermal resources in the Ürkmez area have been poorly exploited. Therefore, seawater intrusion in the southern springs is unlikely to be due to anthropogenic activities, but rather, mixing between ascending thermal waters along the faults and seawater at different depths (Tarcan and Gemici 2003). Similar conclusions have been drawn for the eastern Black Sea area (Çağatay 1993).

It is known that during the Neogene Period, repeated inland marine transgressions occurred in the Eastern Mediterranean area that reached inland several tens of kilometers (Uluğ et al. 2005). As pointed out by Vengosh et al. (2002), the Na–Cl geothermal waters of the Çanakkale area, situated about 100 km north of İzmir on the Aegean coast, originated from deep fossil brines trapped in the Miocene sediments. These events could also have left residual seawater in the SBG, particularly along the SE-NW faults crossing the Doğanbey region, though not yet demonstrated by the available data.

In summary, the SBG hydrothermal waters are deeply-circulating meteoric waters. The preferential discharge conduits are the major faults. The regional flow from the highs also determines the geothermal behaviour of the SBG, especially in the alluvium of the northern Balçova system. Seawater contribution to groundwater salinity is very low in the northern SBG. By contrast, in the southern SBG, the major component of the hydrothermal waters is seawater, which can be observed as far as 10 km inland along the major faults.

MODELING OF THERMOHALINE FLOW OF THE SBG

Although the data suggest that faults are the main control on temperature and hydrochemical patterns, the underlying mechanisms driving saltwater inland are not known. Previous numerical models of thermally-driven flow suggested that fault-induced convection could be a possible mechanism (Magri et al. 2010). However, these earlier models did not assess directly the impact of variable salinity on thermally-driven flow because they did not incorporate mass transport. This proposed mechanism has not yet been investigated and could provide a possible explanation for the hydrochemical anomalies of the SBG.

Following the approach described in Magri et al. (2010), the commercial finite-element software FEFLOW® (WASY-GmbH 2002) was applied to solve the strongly-coupled equations governing fluid flow and heat and mass transport. FEFLOW® fully implements the variable-density and viscosity form of Darcy's law as, for example, described in the theory of Diersch and Kolditz (1998). Temperature, pressure and salinity dependences of both fluid density and viscosity are implemented in the groundwater flow equation as formulated for example in Garven (1989) and Appold and Monteiro (2009). The equations of state for brine density are given in Magri (2010). The dynamic viscosity of brine implemented in the model is the empirical fit derived by Herbert et al. (1988). By doing so, rates of variable-density and viscosity groundwater flow are computed in the generalized form of Darcy's law.

Key assumptions

The models presented here attempt to investigate the feasibility of fault-induced seawater intrusion and are not intended to predict measured data. Several assumptions and simplifications were made in order to reduce computational time.

The two-dimensional (2D) approach was preferred to a three-dimensional (3D) study. This simplification implies that convection parallel to the fault plane, which is the most likely convective mode in fractured media (e.g. Murphy, 1979; Simmons et al. 2008), is not computed. It is worth recalling that groundwater circulation in the units surrounding the faults is driven by the pressure gradients induced by the buoyant flow in the faults (e.g. Fig 2c). Flow is directed toward the faults because of the outflow of hot water through the faults, independently from the convective mode of the cells. In 3D studies, the number of springs in the fault plane will determine focused inflow and outflow points along the surface trace of the fault (Lopez and Smith 1996). Therefore, the 2D models presented here cannot account for more complex 3D flow patterns crossing the study transect, but can still provide significant insights into the driving mechanisms of the fault-induced cells, and can allow their impact on seawater transport to be assessed.

Each stratigraphic unit is considered homogeneous with respect to its physical properties (hydraulic conductivity, porosity, heat capacity and thermal conductivity). The model values of these properties are basin-scale averages based on previous statistical and numerical modeling

3.2 Geothermal energy migration: induced seawater intrusions

studies (Göktürkler et al. 2003; Gök et al. 2005; Arkan and Parlaktuna 2005), general lithological considerations and field investigations (Karakullukçu 1991, Öngür 2001, Satman et al. 2002, Tarakçı 1999, Tezcan 1966, Yilmazer 1989; Sarı and Şalk 2003; Serpen 2004), and tracer- and well-tests (Aksoy 2001; Onur et al. 2005; Aksoy and Serpen 2005). An anisotropy factor of the type $k_x:k_z = 10:1$ (i.e. ratio of horizontal to vertical hydraulic conductivities) is used to represent the interbedding of permeable and less-permeable aquifers within the units. Longitudinal and transverse dispersivity are respectively 10 m and 1 m throughout the whole profile, in order to compute transport mechanisms due to hydrodynamic dispersion. Though these coefficients are strongly scale-dependent and cannot be measured at the regional scales simulated here, the given values fall in the range given by Gelhar (1986).

Table 1 Physical parameters assigned to the units in the numerical model. The parameters are averages at basin-scale. Longitudinal and transverse dispersivity are respectively 10 m and 1 m throughout the whole profile

Units	Hydraulic conductivity (m year ⁻¹)		Porosity	Volumetric heat capacity (10 ⁶ J m ³ °C ⁻¹)	Thermal conductivity (W m ⁻¹ °C ⁻¹)
	$k_{x \text{ horizontal}}$	$k_{z \text{ vertical}}$			
Alluvium	320	32	0.5	1.7	1.5
Upper reservoir	0.032	$3.2 \cdot 10^{-3}$	$5 \cdot 10^{-3}$	2	2.3
Cap rock	$3.2 \cdot 10^{-3}$	$3.2 \cdot 10^{-4}$	$5 \cdot 10^{-3}$	2.1	3
Sea floor	0.032	$3.2 \cdot 10^{-3}$	$2 \cdot 10^{-2}$	2	2.3
Reservoir	0.32	0.032	$5 \cdot 10^{-2}$	2.4	2.8
Basement	~ 0	~ 0	10^{-3}	2.1	3.5
Fault - damage zone	32	32	0.3	1.8	2
Fault - core	~ 0	~ 0	10^{-3}	2.1	3.5
Volcanic intrusions	0.32	0.032	$5 \cdot 10^{-3}$	2.1	3

Faults and their cores are considered to be isotropic. Faults are modeled as equivalent porous media (EPM); in other words, they are represented as permeable areas of finite width extending from the basement to the top of the model. The EPM approach is a well-established technique for representing faults and fractured zones (Weatherill et al. 2008, Graf and Therrien , 2009) which requires less computational effort than discrete-fracture models. It is known that faults can have twofold hydraulic behaviours (e.g. Fairley and Hinds 2004; Bense and Person 2006). On the one hand, damage or deformation zones increase the fault permeability so that the fault can function as a flow conduit; on the other hand, core zones, fault gouges or mineralization processes can locally seal the fault, causing it to become a barrier to groundwater flow. In some specific cases, faults can act as a combination of conduits and barriers to subsurface fluid flow (Heffner and Fairley 2006).

For simplicity, the two surrounding damage zones and the central fault-core have the same width (i.e. three dipping slots, each of approximately 100-m width).

The seabed was considered to be quasi-permeable, as in the work of Simms and Garven(2004). Although homogeneous units are a simplification of the real geological conditions, it is believed

3.2 Geothermal energy migration: induced seawater intrusions

that the model adequately represents the hydrogeology at the considered regional scale. Values of model parameters are identical to those of the previous model (Magri et al. 2010), and are summarized in Table 1.

Mesh

The studied profile (Fig.3) was discretized with triangular elements of variable width in order to preserve the different unit structures. Within the faults and highly-permeable alluvium, the mesh resolution is approximately 15 m. Element spacing grows gradually from a few meters at the fault interface to hundreds of meters in the central part of the reservoir unit and in the basement. The whole profile was discretized with 155,000 triangular elements, satisfying the Delaunay criterion (i.e. ensuring that no vertex lies within the interior of any of the circumcircles of the triangles). A double refinement of the meshes did not affect the calculated patterns.

Boundary and initial conditions

Boundary conditions are defined at the bottom, top and lateral sides of the model

Lateral boundaries are closed to fluid and heat flow.

At the top of the profile, hydraulic head, temperature and concentration values are prescribed:

Head: Within the upper reservoir of the Seferihisar Horst, the potentiometric surface is thought to vary between 70 and 100 m below the elevation of the ground surface (Prof. Gemici, Dokuz Eylül Üniversitesi, personal communication, 2009). Additional constraints are provided by: (1) measured piezometric levels in the Balçova and Ürkmez area, where the groundwater table lies only a few meters below the alluvium surface, mimicking the topography (Serpen 2004); and (2) rivers and wells. Along the seafloor, an equivalent freshwater-head boundary condition is specified.

Temperature and concentration: Heat and dissolved salt are allowed to flow through the ground surface of the inland basin via a third type of boundary condition, given by:

$$q_{\tau}(t) = -\phi_{\tau}(T^* - T) \quad (1)$$

$$q_c(t) = -\phi_c(C^* - C) \quad (2)$$

where q_{τ} and q_c are the prescribed boundary heat and mass flux per surface unit in Wm^{-2} and $\text{kg m}^{-2} \text{s}^{-1}$ respectively. Accordingly, both surface temperature (T) and salinity (C) can vary as a result of coupled heat and mass transport processes in the subsurface. The reference temperature (T^*) and concentration (C^*) applied to the sub-aerial portions of the upper boundary are set equal to $18\text{ }^{\circ}\text{C}$, the annual mean temperature of the SBG (Serpen 2004) and 0 gL^{-1} , respectively. The heat and mass transfer coefficients (ϕ_{τ} and ϕ_c) are assumed to be $2.3\text{ W m}^{-2}\text{ }^{\circ}\text{C}^{-1}$ (Gök et al. 2005) and $3.15\text{e}^{-2}\text{ m yr}^{-1}$. The seabed has a constant temperature of $10\text{ }^{\circ}\text{C}$ and constant salt concentration of 33 g L^{-1} (Sayın et al. 2006).

3.2 Geothermal energy migration: induced seawater intrusions

The models presented here used a constant bottom temperature of 250 °C (Dirichlet type). According to the crustal-scale heat model of Western Anatolia (Göktürkler et al. 2003), the calculated average temperature at 6-km depth bsl is likely to be 250 °C ± 20 °C, depending on the presence or absence of less thermally-conductive grabens. It is well known that neglecting thermal feedback from deeper basement rocks can lead to numerical artifacts (Lin et al. 2000). Imposing a Dirichlet boundary condition at the fault base implies that an infinite amount of heat is pumped into the system. In the SBG, this is unlikely, because no magma chambers are known at 7-km depth. Models that used a constant heat flux of 110 mW m⁻² along an 11-km deep basement have also been run. With a constant temperature at the base of the fault, the temperature gradient is steeper than in the case of a deep basement and the calculated temperatures are slightly higher. However, the thicker basement did not significantly modify the flow patterns of the upper units (e.g. compare the patterns in Fig. 2a and those illustrated hereafter), suggesting that a 7-km deep model is suitable for describing the driving mechanisms of groundwater flow in the Mesozoic and Cenozoic units of the SBG.

Initial pressure and temperature distributions were derived from steady-state fluid flow and conductive-heat transport models which were run before the fully-coupled models. The salinity profile within the seafloor decreases linearly with depth, from 33 g L⁻¹ at the top to freshwater conditions at the bottom. Elsewhere, the units are saturated with freshwater. This initial mass distribution allows the evolution of salt plumes to be inferred.

RESULTS

The calculated flow, heat, and mass patterns are illustrated at the end of the simulation run for the Balçova and Doğanbey coastal areas (Fig.3). In the section entitled “Controlling factors” below, particular attention will be given to the impact of units’ permeability on salinity distribution. Test cases including a permeable basement interface as well as the minor fault systems cutting the alluvium and the seafloor are presented

Flow paths

Simulated flow paths and velocity fields in the Balçova and Doğanbey areas are illustrated in Figure 5. Three flow patterns can be distinguished: (1) In the Balçova area, the steep topography gradients drive groundwater from the horst to the coastal alluvium (i.e. regional flow, blue lines). The main discharge zone is the seafloor / alluvium interface. The steep topography gradients lead to very vigorous flow in the alluvium, with peak velocities of 15 m year⁻¹ (Fig. 5a). Recharge water also infiltrates through the upper reservoir units into the adjacent fault at velocities of a few centimeters per year. In Doğanbey, the regional flow is extremely weak because of the rather flat topography and the presence of very thin alluvium. (2) In the faults, convective cells (red lines) develop as a result of thermal-buoyant forces; groundwater percolates from the horst to great depths where it is heated by the geothermal gradient. The

3.2 Geothermal energy migration: induced seawater intrusions

warm and less-dense water ascends along the faults and vents through alluvium. The velocities of these fault-bounded convective cells range between 2 and 7 m year⁻¹ (Fig. 5). As a result of the focused outflow of thermal water, the fluid pressure in the faults from the basement to the lower reservoir interface is less, compared to what it would be if cooler waters were in the fault, as thoroughly explained in Magri et al. (2010). These pressure offsets are also referred to as pressure drops. (3) As a consequence, in the reservoir unit kilometer-scale flow patterns similar to convective cells (green lines) stretch from the seafloor and alluvium units toward the fault.

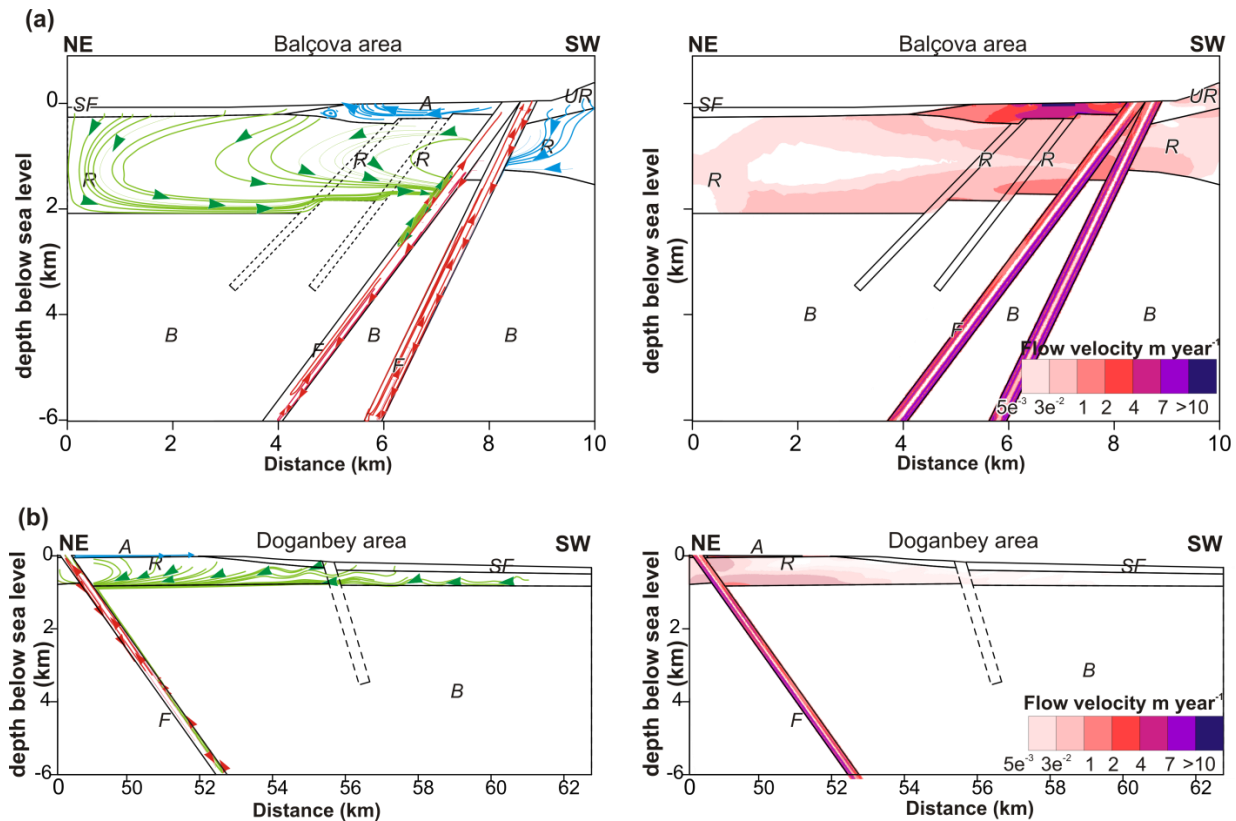


Fig. 5: Flow pathlines (no streamlines) and velocity field (m/year) calculated from transient thermohaline simulations at 300 kyrs for: (a) Balçova, Northern SBG; and (b) Doğanbey, Southern SBG. The arrows indicate the flow direction. Red flow patterns are free-thermally induced cells in the faults. The resulting fault-induced cells are illustrated in green. Recharge flow from the horst is in blue. Minor faults (dashed lines) are not included in the simulations. (SF: sea floor; A: alluvium; UR: Upper Reservoir; R: reservoir unit, Bornova Mélange; B: basement; F: fault; NE: northeast; SW: southwest). No vertical exaggeration is used

Groundwater motion in the reservoir units is driven by the pressure-gradient forces resulting from the constant head at the seafloor and the thermally-induced pressure drop in the faults. In other words, the free convective regime in the faults induces convective-like recirculation in the surrounding units. Simulations without faults do not show convective circulation, but only topography-driven flow originating from the horst. Because of the impervious nature of the basement, the flowlines run parallel to the upper-basement boundary before they are captured by the NE convective flow in the fault. As a consequence, fault-induced convection cells are well-

3.2 Geothermal energy migration: induced seawater intrusions

developed in the 2-km thick Balçova reservoir, but are poorly defined in the thin aquifer above the uplifted basement in the Doğanbey area. The fault-induced flow velocities range from a centimeter per year near the seafloor to half a meter per year at the edge of the fault (Fig. 5).

Studies by Lopez and Smith (1995) show that a topography-driven flow (i.e. forced convection) can hinder or even suppress convection formation. As explained in Magri et al. (2010), due to the presence of strong topography-driven flow in the horst, the normal faults cutting the Seferihisar High display a different transport regime than those cutting the flat alluvial areas described here. In the Seferihisar High, the regional flow overwhelms the free-convective regime in the upper part of the horst faults, in agreement with Lopez and Smith's findings.

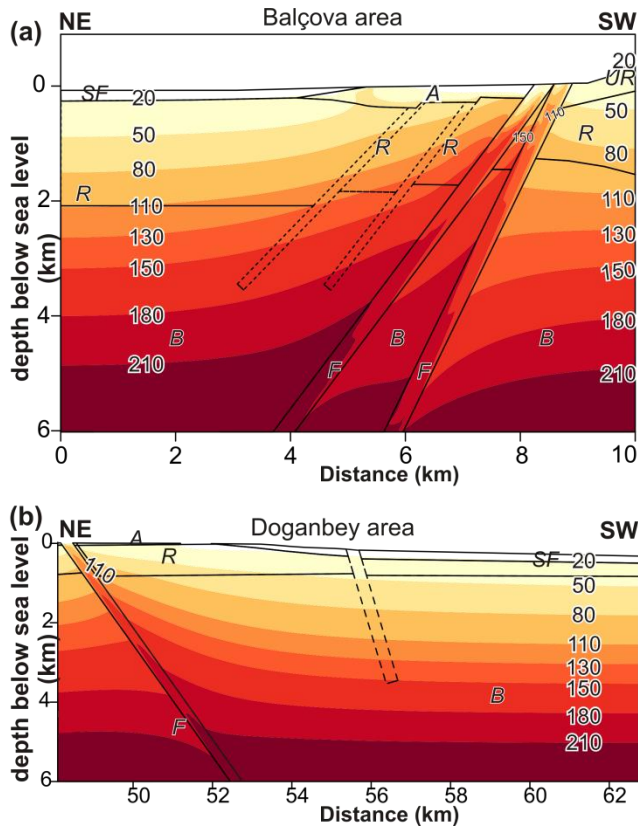
An important result of the full thermohaline simulations is that the flow patterns and velocities are qualitatively similar to those calculated by numerically excluding the salinity effects on the fluid properties from the conservation laws. This finding indicates that in the SBG, the salinity contribution to density-driven flow is negligible compared to that of the heat contribution.

The described flow patterns have major impacts on both the temperature (Fig. 6) and mass distribution (Fig. 7) in the profile.

Temperature and concentration patterns

The ascending buoyant plumes generate elevated temperature within the faults (Fig. 6). As a result, the isotherms within the faults are deflected parallel to the fault leading to several temperature inversions. Temperatures higher than 80 °C occur locally within the alluvium at fault intersections where thermal waters vent. In the Balçova area, the vigorous regional flow generates a thermal plume that reaches 50 °C upon discharging at the ground surface. Advected thermal plumes of this nature are unlikely to develop in the Doğanbey area, where the regional flow is less vigorous. Far from the faults, the geothermal gradient is purely conductive, suggesting that the fault-induced cells are not generated by the geothermal gradient of the basin (i.e. there is no free convection). The onset of thermohaline convection can be determined by calculating thermal and solutal Rayleigh numbers, as defined by Nield (1968). However, an accurate stability analysis of transient large-scale models is challenging, if not impossible, because the physical properties of fluid and hydrogeologic units are not constant (Jones et al. 2004). Several simulations in which the reservoir permeability has been gradually increased showed that the onset of thermal convection is triggered in the Balçova and Doğanbey reservoir units at hydraulic conductivities of 17 m year⁻¹ and 32 m year⁻¹ respectively.

3.2 Geothermal energy migration: induced seawater intrusions

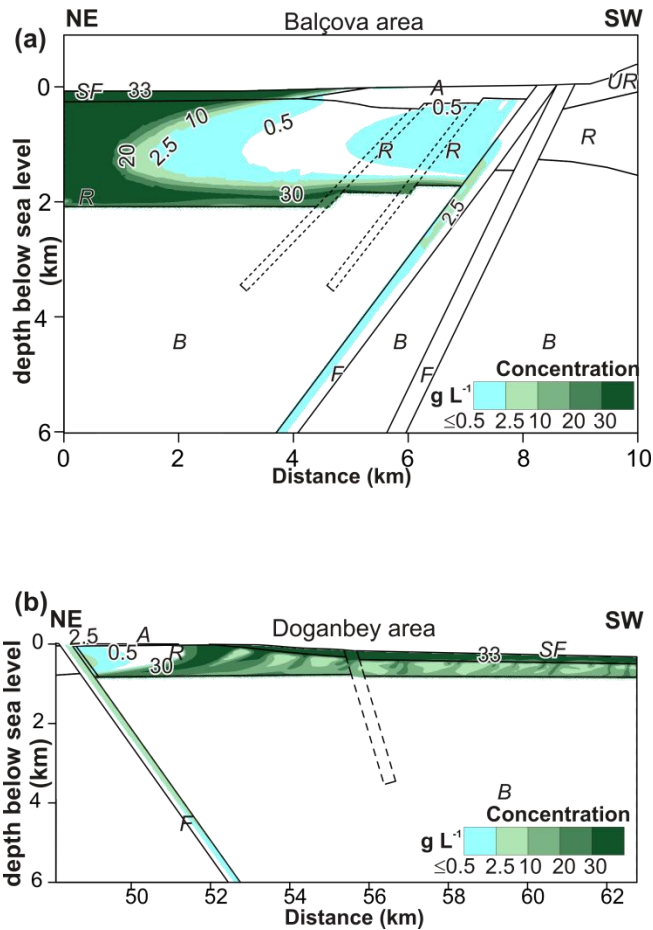


These values are one to two orders of magnitude higher than the estimated value of the Bornova Mélange (Serpen, 2004) suggesting that thermally-induced free convection in the reservoir units is unlikely.

Fig. 6: Temperature (°C) calculated from transient thermohaline simulations at 300 kyr for: (a) Balçova, Northern SBG; and (b) Doğanbey, Southern SBG. Minor faults (dashed lines) are not included in the simulations. (SF: sea floor; A: alluvium; UR: Upper Reservoir; R: reservoir unit, Bornova Mélange; B: basement; F: fault; NE: northeast; SW: southwest)

By comparing the calculated concentrations (Fig. 7) with the corresponding flowlines (Fig. 5), it can be inferred that the fault-induced cells determine the salinity distribution within the reservoir unit. In the Balçova area, a 30 g L⁻¹ seawater finger stretches from the seafloor toward the fault (Fig. 7a). In the Doğanbey area, several heavy plumes sink within the longer and thinner reservoir unit (Fig. 7b). A coupled fluid-flow and mass-transport simulation showed that without a geothermal gradient the initial linear salinity distribution within both seafloors remains unchanged. Therefore, the seawater plumes in the reservoir units do not result from density-driven convection, in which a denser fluid sinks into an underlying lighter fluid, but from the forced convection induced by the hydraulic head patterns. The fault-induced cells in both the Balçova and Doğanbey areas generate a second plume that spreads 0.5 g L⁻¹ of TDS away from the fault flank. In the Balçova area, the top of the plume is shaped by the topography-driven flow in the alluvium, which further dilutes salty water, preventing it from reaching the surface (Fig. 7a). This numerical finding is in good agreement with the isotopic data (Fig. 4) which show both seawater and thermal-water fingerprints in the Balçova alluvial water samples. By contrast, because of the weak regional flow in the Doğanbey area, the heated seawater emanating from the fault reaches the surface, forming hot salty springs (Fig. 7b). During its migration in the reservoir, the plume tip mixes with freshwater leaching from the upper alluvium, forming areas

3.2 Geothermal energy migration: induced seawater intrusions



bearing few mg L^{-1} of dissolved salt in both the Balçova and Doğanbey areas (white areas in the Figure 7). A temporal evolution of the salty-plume protrusion toward the fault is illustrated for the Doğanbey system in Figure 8. In the faults, the highest concentrations occur near their intersection with the basement, along the bottom of the convection cells (e.g. Fig 8d). Thereafter, the seawater is heated further and driven upward by the vigorous upward flow in the fault (Fig. 8e).

Fig. 7: Concentration (g L^{-1}) calculated from transient thermohaline simulations at 300 kyr for: (a) Balçova, Northern SBG; and (b) Doğanbey, Southern SBG. Minor faults (dashed lines) are not included in the simulations. (SF: sea floor; A: alluvium; UR: Upper Reservoir; R: reservoir unit, Bornova Mélange; B: basement; F: fault; NE: northeast; SW: southwest)

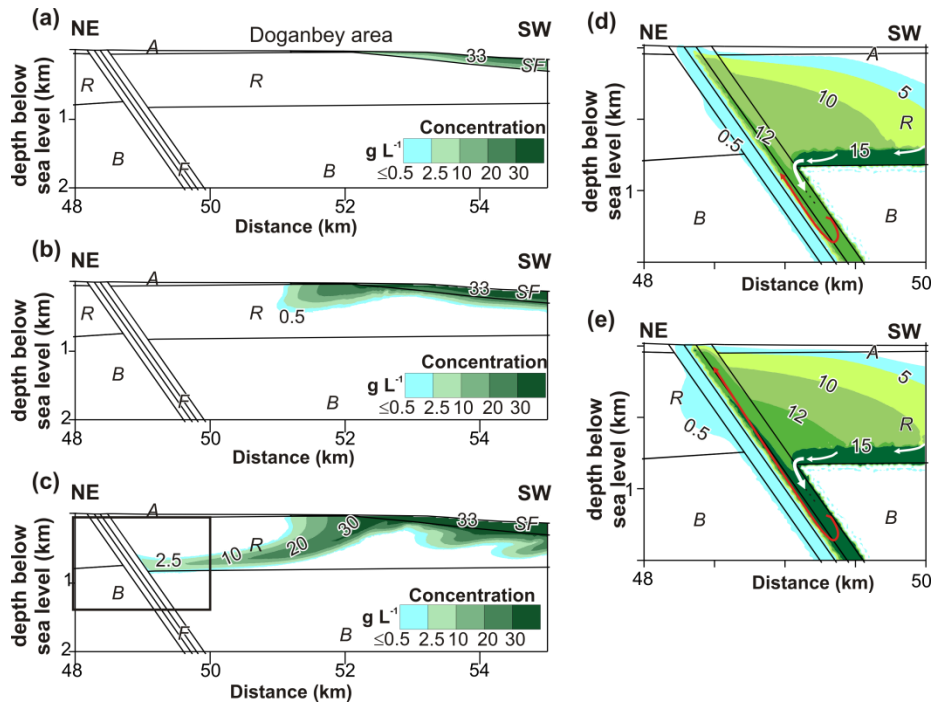


Fig. 8: Time-series of the calculated concentration (g L^{-1}) derived from transient thermohaline simulations of the Doğanbey area at: (a) 0 kyrs – initial condition; (b) 37 kyrs; (c) 75 kyrs; (d) and (e) panels are enlargement of the rectangular area indicated in (c) at 151 kyrs; and 300 kyrs, respectively. Orange arrows indicate flow direction

3.2 Geothermal energy migration: induced seawater intrusions

An additional simulation was run in which the physical properties of the alluvium were set equal to those of the reservoir unit (i.e. the alluvium is absent), in order to highlight the impact of the regional flow.

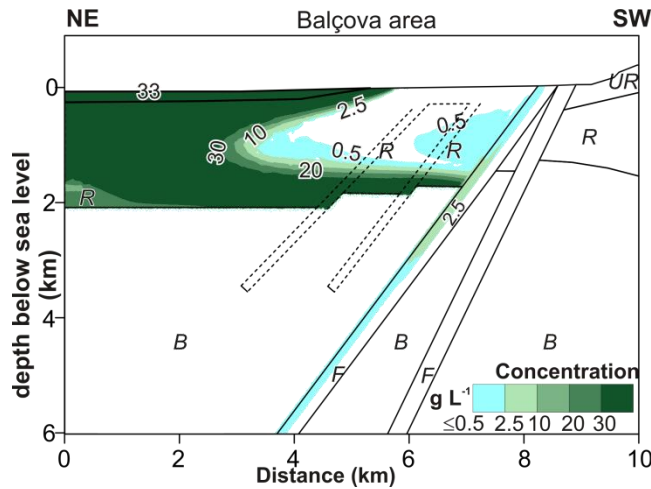


Fig. 9: Alluvium impact. Concentration (g L^{-1}) calculated from thermohaline simulations in which the properties of the alluvium in the Balçova area are equal to those of the surrounding reservoir (i.e. no alluvium). Minor faults (dashed lines) are not included in the simulations. (SF: sea floor; A: alluvium; UR: Upper Reservoir; R: reservoir unit, Bornova Mélange; B: basement; F: fault; NE: northeast; SW: southwest)

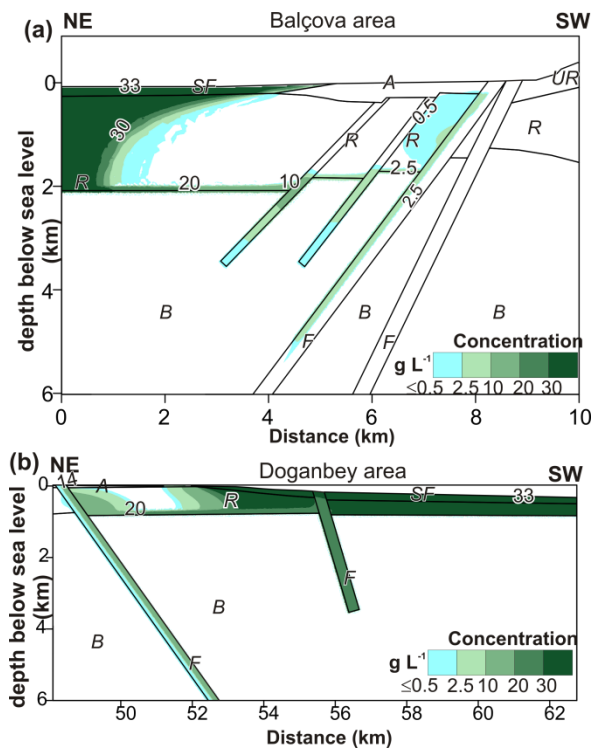
The calculated flow patterns for the Doğanbey area are similar to those from before, but in the Balçova area, the salty water ascending within the fault can also spread through the surface (Fig. 9). Once the salty finger is entrained into the fault, it reaches the surface in the Balçova and Doğanbey areas after approximately 17'000 years (i.e. 17 kyrs) and 8 kyrs, respectively. The different residence times of the salty water in the faults are due to the dissimilar tectonic features of the basin. In the Balçova area, the basement intersects the fault at a depth of 2 km, whereas in the Doğanbey area, the basement intersects the fault at a depth of less than 1 km, so that the distances travelled are different. However, it is not possible to calculate migration times directly by considering only velocity fields and fault lengths, as groundwater undergoes several convective overturns before venting at the surface.

Controlling factors

Seawater circulation has been thoroughly investigated in carbonate platforms of continental margins (e.g. Sanford et al. 1998; Jones et al. 2000, 2004; Wilson 2003, 2005). In those studies, several sensitivity analyses were carried out in order to understand which factors control both flux and patterns of fluid circulation, given the expected ranges of those factors in nature. The parameters examined included fluid and rock properties as well as platform geometries. Based on these previous findings, and given both the physical properties of the study area and the calculated flow velocities, it can be inferred that in the SBG, kilometer-scale groundwater and chemical patterns are likely to be controlled mainly by hydraulic conductivity distribution. Therefore, a sensitivity analysis in which the hydraulic conductivity is varied has been carried out, to test its effect on fluid flow and transport patterns.

3.2 Geothermal energy migration: induced seawater intrusions

values that were used fall in the range given by Gök et al. (2005). As seawater motion is driven by the fault-induced convection cells, a more vigorous buoyant-flow in the faults increases seawater flux in the reservoir units. Simulations in which both fault flanks are an order of magnitude more permeable than the standard case induced higher recirculation velocities in the reservoir, preserving the flow and seawater patterns. Figure 10 illustrates the calculated salinity for the case in which the hydraulic conductivity of the inner fault flank is 150 m year^{-1} and the basement interface is incorporated. It can be seen that whereas in the Balçova area the regional flow is the predominant process preventing salty water to spread through the surface, in the Doğanbey area the interplay between fault-induced convection and free-convective flow in the faults has the potential to lift 14 g L^{-1} of TDS up to the surface, in good agreement with the concentrations observed in southern SBG (Fig. 1).



Minor faults can also alter the flow field because they can cut through the alluvium or seafloor units. Here, their physical properties are equal to those of the major faults of the standard case. In Balçova, the minor faults enhance freshwater recharge, impeding the second salty plume that emanates from the major fault to flow further along the alluvium (Fig 11a).

Fig. 11: Minor-faults impact. Concentration (g L^{-1}) calculated from thermohaline simulations including the minor fault systems cutting the Balçova alluvium and the Doğanbey seafloor, for: (a) Balçova, Northern SBG; and (b) Doğanbey, Southern SBG. (SF: sea floor; A: alluvium; UR: Upper Reservoir; R: reservoir unit, Bornova Mélange; B: basement; F: fault; NE: northeast; SW: southwest)

For a hydraulic conductivity of 150 m year^{-1} , recharge entering the horst is mostly captured in the fault systems intersecting the alluvium, which in turn prevents seawater from reaching the major fracture systems, which would provide an additional cause of the lower salinities of the springs in that area. By contrast, in the Doğanbey area, the faulted seafloor does not dramatically change mass concentration patterns, as convective cells in the shorter faults keep recirculating trapped seawater (Fig. 11b).

SUMMARY AND CONCLUSIONS

Geophysical data clearly indicate that the thermal waters of the SBG are deeply-circulating meteoric waters that ascend to the surface, driven by thermally-induced buoyant forces. The preferential discharge conduits are faults in which hydrothermal convection generates temperature inversions. Hydrochemical and isotope data point toward extensive seawater intrusion along the faults of the southern SBG. In contrast, the thermal waters of the northern SBG originate in the Seferihisar Horst and have salinities near those of freshwater. However, seawater fingerprints can be seen locally in the alluvium deposits, though seawater makes a small contribution to overall groundwater salinity. Although these anomalies in the SBG have been recognized for decades, the mechanisms underlying seawater encroachment and the mixing processes had not been well understood. Furthermore, it was also not clear why the northern groundwater is relatively fresh compared to the highly-saline southern springs.

Transient numerical simulations of thermohaline flow reveal that both temperature and salinity anomalies are controlled by the interaction between convective and topography-driven flow. Thermally-induced convection develops within the permeable faults, allowing the colder regional flow to reach basement depths before venting at the surface at high temperature. In turn, convection in the faults generates cellular patterns in the surrounding reservoir units (i.e. fault-induced convection cells) that drive seawater along the basement-reservoir interface. At the fault intersections, seawater mixes with ascending thermal waters. The resulting salty water is channelled toward the upper aquifers through several convective overturns. In the Balçova area, the ascending hot salty waters are flushed away by the dominant regional flow from the horst, whereas in the Doğanbey area the topography-driven flow is too weak to prevent salty water from spreading along the ground surface. These findings suggest that the observed springs are the result of two types of mixing processes that occur: (1) at the basement-fault intersections and involve seawater that has travelled several kilometers along the basement interface and deep circulating thermal waters in the faults; and (2) at alluvium depths between the resulting thermal salty waters and the regional flow. The salinity of springs is likely controlled by topography-driven flow from the horst.

The different tectonic features of the SBG also have a critical control on the salinity distribution within the deeper part of the reservoir, as they determine permeability distributions and therefore the balance between recharge of freshwater and fault-induced recirculation of seawater. In the Balçova area, extended areas of low TDS are due to both the strong topographic gradients and the thick deposits of alluvial and Mélange sediments. In the Doğanbey area, the flat topography, thin alluvium, and the uplifted basement reduce the depth of seawater penetration and favour the merging of plumes into wide saline areas. These contrasting salinity distributions also persist in the presence of a more-permeable basement interface that is intended to represent unconsolidated sediments above the metamorphic rocks.

3.2 Geothermal energy migration: induced seawater intrusions

To some extent the simulations demonstrate that salinity distribution in the basin is also dependent upon the spatial variations in permeability within the faults. For more permeable flanks, the magnitude of fault-induced seawater circulation is higher, and salty plumes reach the fault flanks faster while flow and mass patterns are similar. The minor fault systems cutting the alluvium could also be responsible for the low TDS observed in the Balçova area, as they favour inflow of freshwater from the horst. By contrast, a faulted seabed does not alter the patterns of fault-induced seawater flux. Hydrothermal convection in the faults develops at high flow rates, suggesting that if any relict brines were trapped in the upper Pliocene, these would be rapidly flushed away.

Owing to the two-dimensional limitations of the models, it has not been possible to investigate the impact of transverse faults that cross-cut or are parallel to the profile. Intersecting faults can further focus refluxing seawater and mixing processes and could therefore impact the salinity distribution at a regional-scale. Though these features can only be tackled by building a full three-dimensional model, the presented results demonstrate that fault-induced seawater circulation is a possible mass-transport mechanism underlying the observed anomalies. Given the general tectonic features of the SBG, the described process could likely develop in many faulted geothermal systems in the world. The kilometer-scale nature of the described cells suggests that fault-induced convection can significantly impact the transport and fate of dissolved solutes over regional distances. For example, fault-induced convection could explain outflow of relict brine through the faults of the Tiberias Lake _Israel (Bergelson et al. 1999), the presence of dissolved halite within the faults of the Rhine Graben, Germany (Bächler et al. 2003) or the mineral deposits in the Polish Basin (Schmidt Mumm and Wolfgramm 2004). In a broader context, fault-induced convection has the potential to jeopardize freshwater resources located several kilometers away from deep aquifers used for waste waters or CO₂ storage.

ACKNOWLEDGMENTS

This research was funded by the German Science Foundation (DFG) through grant DFG Ma 4450/1-2, and The Scientific and Technological Research Council of Turkey (TÜBİTAK) through grant 107Y345. All hydrochemical analyses were performed at the laboratories of the Freie Universität Berlin (FUB), Germany, by Heide Helke. Henno Meyer from the Alfred Wegener Institute (AWI) in Potsdam, Germany, measured the isotope content. Martin S. Appold (University of Missouri), Steve Ingebritsen (United States Geological Survey, Menlo Park, California), and Mark Person (New Mexico Tech), and Richard Boak, are greatly acknowledged for their comments and corrections which significantly improved the paper.

4. DISCUSSIONS AND CHALLENGES

The studied cases illustrate two examples of how the conjoint use of numerical modeling and hydrochemical investigations is useful to advance our understanding of environmental issues in sedimentary basins. The processes studied here are related to groundwater salinization in the NEGB due to dissolution of salt domes (chapter 2) and pollution of shallow aquifers in the SBG caused by the upsurge of hot thermal waters and seawater intrusion (chapter 3).

In general, the main focus of these research papers is the study of the dynamical effects arising from the interaction between the existing hydrologic regimes, i.e. the coupling of existing driving forces. Hydrochemical investigations are used as fundamental dataset to calibrate the numerical results in terms of observed temperature/salinity patterns and to restrain the possible process couplings. In the NEGB, hydrochemical data show that fluid density inversions could be due to both temperature gradients and dissolution of salt diapirs at different depths. In the SBG, isotopes data indicate that the springs are a mixture of meteoric, sea and deep geothermal waters at different ratios. To some extent, the numerical simulations allowed illustrating the possible coupled processes responsible for the observed environmental issues. The studied couplings can mainly be summarized as follows:

- (i) *Coupling between density-driven forces* induced by variable temperature and salt content (thermohaline convection, chapter 2). On one hand, depending on the physical properties of the sedimentary fill, increasing temperature can induce buoyant forces which can destabilize the initial hydrostatic equilibrium. On the other hand, salt can be either stabilizing (concentration increasing with depths) or destabilizing (concentration decreasing with depths). In the first case, as by example the dissolution of deep salt structures, the resulting dynamic effects are vertically stretching brine plumes (chapters 2.1 and 2.2). In the second case, shallow salt dissolution generates sinking brines which have the potential to invert density profiles (chapters 2.3 and 2.4).
- (ii) *Coupling between topography-driven flow and density-driven flow* (mixed convection, all chapters). Mixed convection is the dominant hydrologic regime controlling fluid transport processes in sedimentary basins. In the NEGB, where topographic variations are not so strong, the resulting regional flow interacts with thermally-induced brine plumes by driving the dissolved salt towards the main discharge areas (chapter 2). This process determines the shapes of the observed surficial brine patterns. In the northern SBG instead (chapter 3), where the topography imposes strong pressure gradients, the induced regional flow dominates over thermohaline convection preventing thermal waters to reach the surface (chapters 3.1 and 3.2). By contrast, in the southern part of the SBG, where the topography is rather flat, upsurging of thermal water and seawater intrusions are not hindered by the weak forced convection.

The numerical results also highlight the major controlling factors of solute and heat migration at basin scale. These are mainly (i) the heterogeneity of hydraulic conductivity and unit thicknesses, as well as (ii) the variable fluid properties.

4. Discussions and ongoing challenges

- (i) The onset of convective flow is related to the type of heterogeneity of the hydraulic permeability. In all simulations, the units are modeled as homogenous. Therefore permeability variations are only accounted in the vertical direction. This kind of layered permeability distribution favours thermally-induced brine flow if the most permeable units are thick enough to allow the growth of convective instabilities. In the NEGB, the presence of thin clay units in the shallow aquifers (Rupelton, Chapter 2.2) prevents the formation of multicellular convective regime in the upper basin but does not hinder the onset of thermal convection in the deeper units where the temperatures are high. By contrast, in the SBG, convective flow develops only within long and almost vertical permeable fault zones. As a consequence, the hydrothermal features of the SBG are strongly controlled by the major faults wherein buoyant thermal waters discharge through the alluvial sediments.
- (ii) The presence of heat and salt mainly affect fluid density and viscosity. As these parameters appear in the Darcy law (Equation 2 and 6, Appendix), they have a large impact on the system behavior. The author of this work developed a polynomial EOS into FEFLOW in order to simulate fluid density and viscosity variations in a wide range of temperature and concentration (Appendix). In the NEGB, variable viscosity is primordial in controlling flow rates because the effective hydraulic conductivity decreases in the areas where the migration of highly viscous brine plumes occur (Eq. 6, appendix). This case is nicely illustrated for shallow salt dissolution in chapter 2.4. By contrast, in the SBG the effective hydraulic permeability of the fault zones is increased by the hot and less viscous thermal waters flowing through these conduits.

To some extent this work also gives a methodology for building large-scale numerical models that can be reapplied to any software package or existing open source code. Numerically, the critical aspects to tackle are the spatial discretization of the units for the correct representation of the properties distributions and the implementation of proper equations of state to reproduce fluid properties dependencies (Appendix). Nevertheless, several simplifications are made in order to simulate basin-scale transport processes in a reasonable computational time.

Simplifications

2D vs 3D

The numerical studies of real site applications are based on simplifying assumptions of both structural setting and lithological properties of the system. The major simplification is the reduction of the study area to 2-dimensional vertical profiles, although in nature fluid transport processes mainly occur in three dimensions. Because 2D models are computationally less demanding and easier to handle, there has been a limited effort in tackling numerical models of coupled transport processes in three dimensions. Furthermore, despite the significant increase of computer power, some codes still do not allow parallel processing to speed up 3D calculations. Nevertheless, recent three-dimensional benchmark studies suggest that the third dimension is essential to correctly describe the flow field, particularly in fractured areas. As highlighted by Simmons et al. (2008), in the majority of the scenarios, 2D models oversimplify the system, and the conclusions derived from such investigations might not be fully correct, particularly when no calibration with observed data can be obtained. Currently, 3D simulations

4. Discussions and ongoing challenges

of heat flow in the NEGB are carried out in the NEGB by [Cherubini et al. \(2013\)](#) and [Kaiser et al. \(2013\)](#). In their scenarios, it is shown that 3D convection persists locally where the pressure forces are weak and are controlled by the thickness and permeability of the respective layers

Preliminary 3D numerical simulations of the southern SBG ([Magri et al. 2011](#)) show that in the case of planar high permeability regions such as faults, 2D and 3D patterns vary significantly, the latter being allowed to develop perpendicular and/or parallel to the fault planes (figure 4.1).

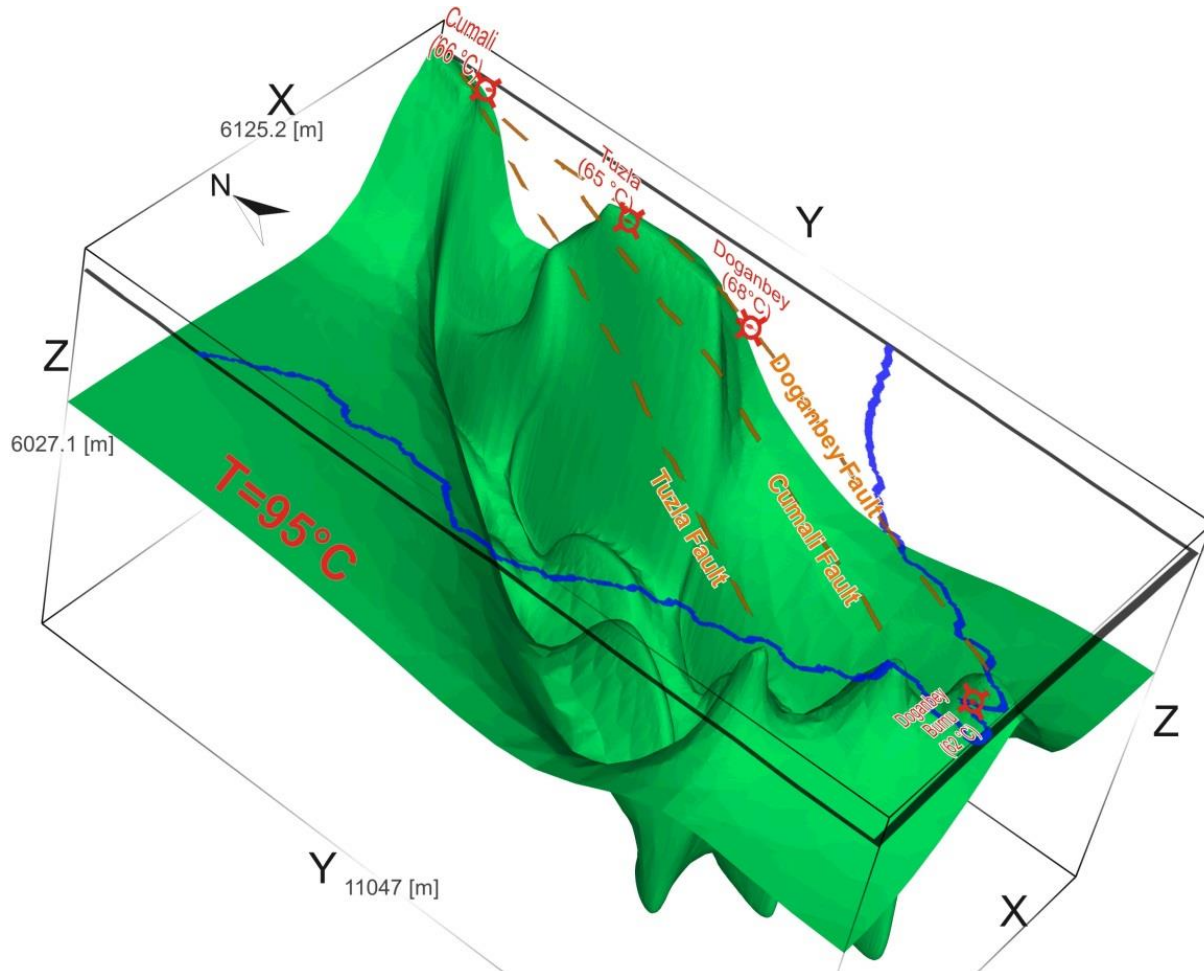


Fig. 4.1: 3D numerical results of coupled heat and flow transport processes in the SBG ([Magri et al. 2011](#)). Isosurface $T=95\text{ }^{\circ}\text{C}$. The resulting thermally-induced flow is characterized by 3D finger patterns controlled by highly permeable faults.

This is an important finding which so far has not been studied explicitly in applied field settings, except for the Rhine Graben in Germany ([Bächler et al. 2003](#)), Mount Isa in Australia ([Kühn et al. 2006](#)), the Ashanti belt in Ghana ([Harcouet-Menou et al. 2009](#)). These studies indicate that several convective modes can form and that the patterns are definitely not constrained to a 2D plane. The 3D numerical simulations of the SBG ([Magri et al. 2011](#)) further show that the convective cells in the fault plane can generate springs, manifested as locally focused outflow points along the surface trace of the fault (Figure 4.2).

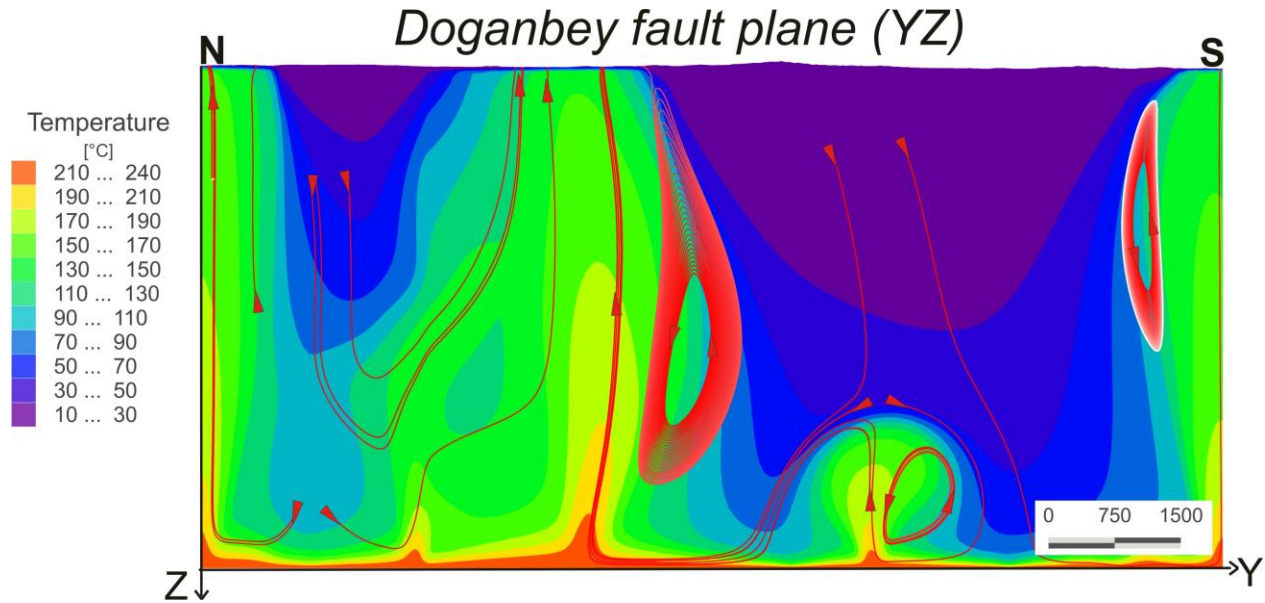


Fig. 4.2: 3D numerical results of coupled heat and flow transport processes in the SBG (Magri et al. 2011): Calculated T (°C) along the Tuzla fault (located in figure 4.1). Several convective cells (red vectors) drive hot water toward the surface. As a result, springs along the fault trace may form.

Therefore, the 2D models presented in this work cannot account for more complex 3D flow patterns that cross the study transects. 3D modeling is the key to gain insights into coupled transport processes in fractured areas. Such models need actual field studies which provide data allowing to better define the possible modes of convection and fluid flow interactions. This will be the topic of a forthcoming DFG project entitled “*Hydrogeological and hydrochemical modeling of density-driven flow in the Tiberias Basin*” (Magri Ma 4450/2).

While 3D studies need further research, the 2D results presented here still provide significant insights into the driving mechanisms of the coupled processes.

Spatial and temporal distributions of physical properties

Depending on the structural features of the study basin, the sedimentary deposits are represented by a series of hydrogeologic units with homogenous and constant physical properties. In the NEGB, hydraulic permeability, thermal properties and diffusivity are averaged values based on available literature whereas in the SBG also tracing tests and log data obtained from the drilling campaign of the sixties are used.

However, these properties can undergo strong variations over the geologic time periods of basin-scale fluid processes (10^3 - 10^6 years). The causes can have (i) chemical origins as precipitation/dissolution reactions, or (ii) mechanical as consolidation/fracturing processes. Both mechanisms can reduce/increase pore space. In the models of this work, the distribution of transient properties is not simulated and therefore the calculated flow fields cannot fully capture the highly transient nature of fluid coupled processes. In the NEGB, diagenetic processes triggered by the long residence time of saturated brines are likely a mechanism that determined the evolution of the flow field.

Fluid composition and phases

In all presented papers, the fluids are modeled as aqueous NaCl solutions (liquid phase). However, the hydrochemical analyses of both NEGB and SBG systems show that the brine compositions are more complex, involving different dissolved components. Commonly brines are modeled as NaCl solutions because of the lack of laboratory data and constitutive equations describing multi-component fluids. Furthermore, in many geothermal systems, depending on the Pressure-Temperature-Concentration conditions, coexisting vapour and brine phases can be very similar or strongly differ in density (Figure 4.3) and viscosity, making the modeling of multi-phase flow in geological systems a very complex problem (Driesner and Heinrich 2007).

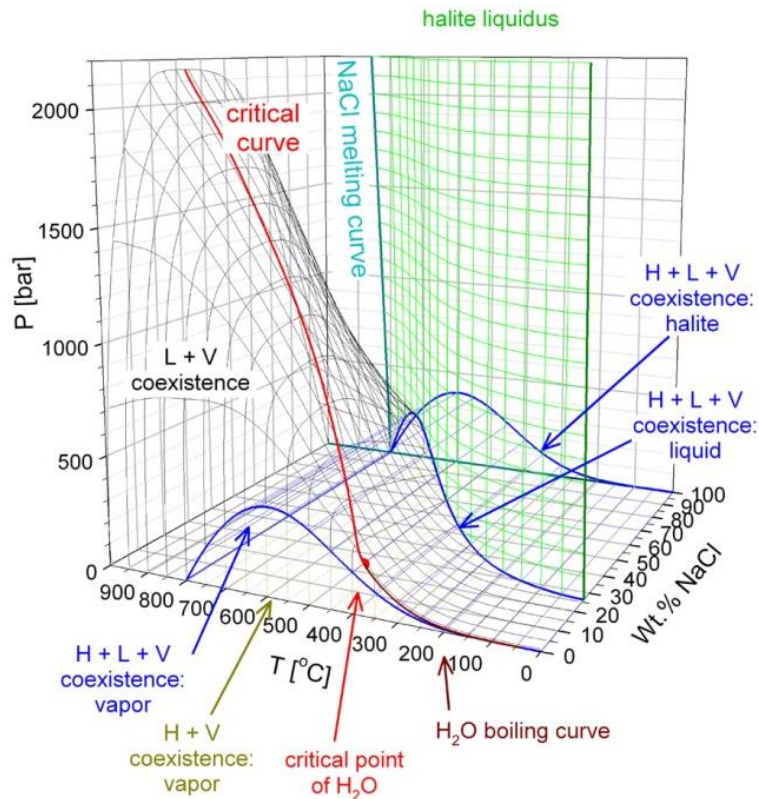


Fig. 4.3: Phase diagrams for Temperature-Pressure-Composition of H₂O-NaCl (Driesner and Heinrich 2007). Beside the liquid single phase, depending on the T-P-C coordinates, hydrothermal systems may encounter the Halite + Vapor (H+V) and the Liquid + Halite (L+H) two-phase regions as well as the three-phase Halite + Liquid + Vapor (H+L+V) region.

For instance, in the: NEGB (Chapter 2) mineral precipitation most likely occurs along the salt flanks or in the nearly-saturated deep units (e.g. Buntsandstein) leading to the formation of a solid/liquid phase region. In the SBG, dolomitization and degassing processes are visible in most of the springs of the SBG (Chapter 3) indicating that beside the solid phase also the vapour phase is involved in the transport processes.

To date, there are still few numerical simulators that include multi-phase and supercritical flow (i.e. >350 °C approximately). A review of these studies can be found in Ingebristsen et al. (2010).

Ongoing challenges

As mentioned previously, mechanical and reactive transport processes have strong feedbacks on the fluid flow field as they dynamically alter both fluid and rock properties, particularly porosity and hydraulic conductivity. To date, coupling chemical reactions and deformation with

4. Discussions and ongoing challenges

the classical formulation of fluid transport processes as modelled here (Appendix) is the major challenge.

Figure 4.4 summarizes the couplings of fluid transport processes and their feedbacks to hydraulic conductivity, which is the primary control of basin-scale regional flow (see Introduction).

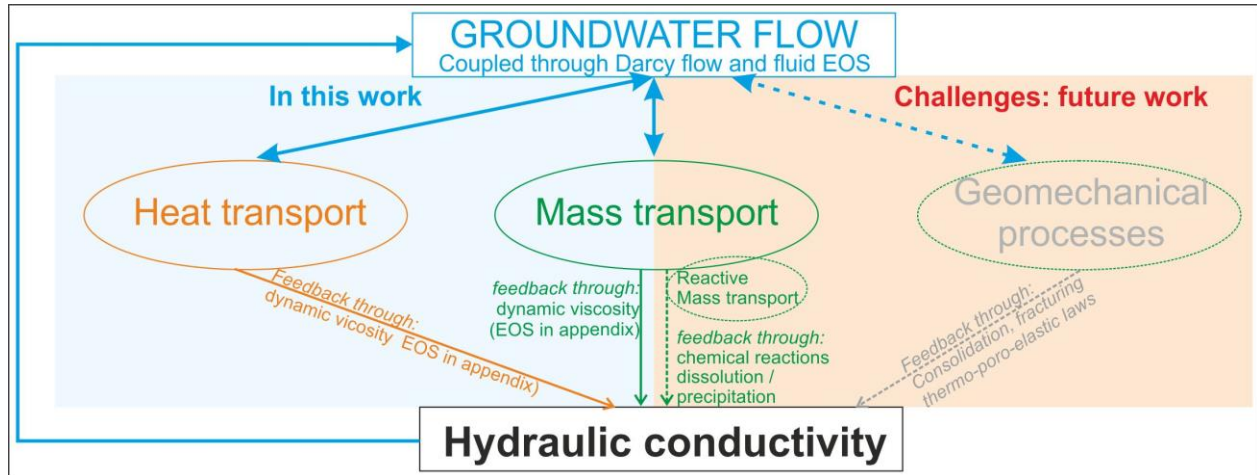


Fig. 4.4: Coupling between fluid transport processes at basin-scale and their feedbacks to hydraulic conductivity. In this work (left panel, light blue), coupled groundwater flow, heat and mass transport are modeled. The dynamic viscosity appearing in the hydraulic conductivity equation (EOS Eq. 6, appendix) is temperature and concentration dependent. The challenges not addressed in these simulations (right panel, light orange) are: reactive mass transport and geomechanical processes as well as their impact on hydraulic conductivity.

The figure is split in two parts. In the cyan panel, the couplings addressed in this work are highlighted: as explained previously, the papers in chapters 2 and 3 provide excellent example of heat and mass transport coupling. The feedbacks to hydraulic conductivity are also included through the fluid viscosity EOS which is temperature and concentration dependent. An example of their impacts on the effective hydraulic conductivity distribution is given in chapter 2.4. The processes and coupling not addressed in this work are illustrated in the orange panel. These are reactive mass transport and geomechanical processes. Dissolution of solids into the local formation water can initiate a variety of geochemical reactions depending on the temperature and the composition of both pore-water and surrounding formations. Some of these reactions could decrease the hydraulic permeability, for instance by forming new carbonate minerals. By contrast, other types of reaction may increase permeability, and aid the migration of fluids (Rochelle et al. 1999). A key challenge is modeling the dynamical changes in permeability resulting from the geochemical processes and their impact on the flow field. Furthermore, geomechanical processes can activate existing fractures and faults, or create new pathways which could result in new flow pathways. Therefore numerical simulations must also include the coupling between poro-thermo-elastic processes and the regional flow.

Although both chemical and mechanical processes impact permeability and porosity, they are till date modeled separately because solving the fully coupled formulation of Thermal-Hydrological-Mechanical-Chemical (THMC) requires an enormous amount of computational power due to the high number of variables and degree of freedom involved.

4. Discussions and ongoing challenges

In summary, since the first studies of large-scale groundwater flow (Introduction), great progresses have been made to model coupled fluid transport processes at basin-scale. Today even 3D analyses on fine meshes are possible thanks to the increase in processing power.

This work also suggests that further research needs to be carried out by addressing the coupling between mechanical/chemical processes and the density-driven flow at basin-scale presented in this work (Figure 4.4). While this major challenge will require the developments of new benchmark studies and improvement of software capabilities, the numerical simulations illustrated here allowed increasing our understanding of the basic processes of coupled heat, mass and fluid flow in sedimentary basin.

REFERENCES

REFERENCES

- Agster, G., 2000a. Untersuchungsprogramm zur Ermittlung des Grundwasserdargebotes im Raum Lübeck - Hydrogeologischer Bericht zu den Ergebnissen der Bohrmassnahmen 1999. LANU 511 (unveröffentlicht).
- Agster, G., 2000b. Untersuchungsprogramm zur Ermittlung des Grundwasserdargebotes im Raum Lübeck - Teilprojekt Untertraverinne. LANU 532, LANU, Flintbeck.
- Agster, G., 2001. Untersuchungsprogramm zur Ermittlung des Grundwasserdargebotes im Raum Lübeck - Hydrogeologischer Bericht zu den Ergebnissen der Bohrmassnahmen 2000. LANU 512, LANU, Flintbek.
- Agster, G., 2005. Hydrogeologie im Großraum Lübeck. In: L.f.N.u.U.d.L. Schleswig-Holstein (Editor), 72. Tagung der Arbeitsgemeinschaft Norddeutscher Geologen. Geologischer Dienst Schleswig-Holstein, Lübeck, pp. 13-14.
- Agster, G., 2005. Geologischer Profilschnitt durch das Arbeitsgebiet. F&E-Vorhaben: Untersuchung zur Genes und Dynamik der Grundwasserversalzung im Raum Lübeck, LANU 512.
- Akartuna, M., 1962. İzmir-Torbalı-Seferihisar-Urla bölgesi jeolojisi hakkında [Geology of İzmir-Torbalı-Seferihisar-Urla region. Mineral Research and Exploration Institute (MTA) of Turkey, 59, 1-18.
- Aksoy, N., 2001. Monitoring the Balçova-Narlıdere geothermal system using tracers. In: Izmir, Turkey, Dokuz Eylül University Graduate School, PhD, 150.
- Aksoy, N., Serpen, U., 2005. Reinjection Management in Balçova Geothermal Field. In: Proceedings World Geothermal Congress 2005 Antalya, Turkey, 24-29 April 2005.
- Aksoy, N., Serpen, U., Filiz, S. 2008. Management of the Balçova-Narlıdere geothermal reservoir, Turkey. *Geothermics*, 37, 444-466.
- Aksoy, N., Simsek, C., Gunduz, O., 2009. Groundwater contamination mechanism in a geothermal field: A case study of Balçova, Turkey. *Journal of Contaminant Hydrology*, 103, 13-28.
- Alkan, H., Babadagli, T., Satman, A., 1995. The prediction of the PVT/phase behavior of the geothermal fluid mixtures. *Proceedings World Geothermal Congress 1995, Florence*, 3, 1659-1665.
- Anders, E., Grevesse, N., 1989. Abundance of elements: meteoric and solar. *Geochim Cosmochim Acta* 53, 197-214.
- Anderson, M.P., Woessner, W.W., 1992. *Applied Groundwater Modelling*. Academic Press, San Diego, 381 pp.
- Antonellini, M., Aydin, A., 1995. Effect of faulting on fluid flow in porous sandstones: geometry and spatial distribution. *American Association of Petroleum Geologists Bulletin*, 79(5), 642-671.
- Appold, M.S., Monteiro L.V.S., 2009. Numerical modeling of hydrothermal zinc silicate and sulfide mineralization in the Vazante deposit, Brazil. *Geofluids* 9, 96-115.
- Arkan, S., Parlaktuna, M., 2005. Resource Assessment of Balçova Geothermal Field. In: Proceedings World Geothermal Congress 2005 Antalya, Turkey, 24-29 April 2005.
- Bach, H., Hinsch, W., Johannsen, A., 1974. Hydrogeologische und geologische Ergebnisse einer neuen Solebohrung in Bad Schwartau (Schleswig-Holstein). *Meyniana*, 25, 1-10.

REFERENCES

- Bachu, S., Gunter, W.D., and Perkins, E.H., 1994. Aquifer disposal of CO₂: hydrodynamic and mineral trapping, *Energy Convers Manage* 35:269–279.
- Baldschuhn, R., Binot, F., Fleig, S., Kockel, F., 2001. Geotektonischer Atlas von Nordwest-Deutschland und dem deutschen Nordsee-Sektor. *Geologisches Jahrbuch, Reihe A, Heft 153*.
- Baldschuhn, R., Frisch, U., Kockel, F., (eds.) 1996. Geotektonischer Atlas von NW-Deutschland 1:300000. 4 pp., 65 maps, Bundesanstalt für geowissenschaften und Rohstoffe, Hannover.
- Bächler, D., Kohl, T., Rybach, L., 2003. Impact of graben-parallel faults on hydrothermal convection—Rhine Graben case study. *Physics and Chemistry of the Earth*, 28, 431-441.
- Bataillé, A., Genthon, P., Rabinowicz, M., Fritz, B., 2006. Modeling the coupling between free and forced convection in a vertical permeable slot: Implications for the heat production of an Enhanced Geothermal System. *Geothermics*, 35, 654-682.
- Bau, M. 1999. Scavenging of dissolved yttrium and rare earths by precipitating iron oxyhydroxide: experimental evidence for Ce oxidation, Y–Ho fractionation, and lanthanide tetrad effect. *Geochim Cosmochim Acta* 63, 67–77.
- Bau, M., Dulski, P. 1996. Anthropogenic origin of positive gadolinium anomalies in river waters. *Earth Planet Sci Lett* 143, 245–255.
- Bausch, W.M., 1968. Outlines of distribution of strontium in marine limestones. In: Müller G, Friedman GM (eds) *Carbonate sedimentology in Central Europe*. Springer, Berlin, pp 106–115.
- Bayer, U., Scheck-Wenderoth, M., Koehler, M. 1997. Modeling of the 3D thermal field in the Northeast German Basin. *Geologische Rundschau*, 86, 241-251.
- Bayer, U., Clausnitzer, V., Fuhrmann, J., 2002. Unsteady thermal convection in the North-east German Basin. Technical Report, WIAS Berlin.
- Bear, J., Verruyt, A., 1987. *Modelling Groundwater Flow and Pollution*. Reidel Publishing Co., Dordrecht, Holland, 414 pp.
- Bear, J. 1991 *Modelling transport phenomena in porous media. Convective Heat and Mass Transfer in Porous Media* 7-69.
- Bein A., Dutton A.R., 1993. Origin, distribution, and movement of brine in the Permian Basin (USA): a model for displacement of connate water. *Geol Soc Am Bull* 105, 695–707.
- Bennett, S.S., Hanor, J.S., 1987. Dynamics of subsurface salt dissolution at the Welsh Dome, Louisiana Gulf Coast. In: Lerch I, O’Brien JJ (eds) *Dynamical geology of salt and related structures*. Academic, Orlando, pp 653–677.
- Bense, V.F., Person, M.A., 2006. Faults as conduit-barrier systems to fluid flow in siliciclastic sedimentary aquifers. *Water Resour. Res.*, 42, W05421, doi:10.1029/2005WR004480.
- Bense, V.F., Person, M.A., Chaudhary, K., You, Y., Cremer, N., Simon, S., 2008. Thermal anomalies indicate preferential flow along faults in unconsolidated sedimentary aquifers. *Geophysical Research Letters*, 35, L24406, doi:10.1029/2008GL036017.
- Bergelson, G., Nativ, R., Bein, A., 1999. Salinization and dilution history of ground water discharging into the Sea of Galilee, the Dead Sea Transform, Israel. *Applied Geochemistry* 14.

REFERENCES

- Berner, Z.A., Stüben, D., Leosson, M.A., Kling, H., 2002. S- and O isotopic character of dissolved sulphate in the cover rock aquifer of a Zechstein salt dome. *Appl Geochem* 17, 1515–1528.
- Bitzer, K., Trave, A., and Carmona, J.M., 2001, Fluid flow processes at basin scale: *Acta Geologica Hispanica*, v. 36 p. 1-20.
- Bjørlykke, K., Mo, A., Palm, E., 1988. Modelling of thermal convection in sedimentary basins and its relevance to diagenetic reactions. *Marine and Petroleum Geology* 5, 338 - 351.
- Blum, J.D., Erel, Y., 1995. A silicate weathering mechanism linking increase in marine $^{87}\text{Sr}/^{86}\text{Sr}$ with global glaciation. *Nature* 373, 415–418.
- Boussinesq, J., 1903. *Théorie analytique de la chaleur, mise en harmonie avec la thermodynamique et avec la théorie mécanique de la lumière*, p. 172, Gauthiers-Villars, Paris.
- Boving, T.B., Grathwohl, P., 2001. Tracer diffusion coefficients in sedimentary rocks: correlation to porosity and hydraulic conductivity. *Journal Contaminant Hydrology* 53, 85-100.
- Bredehoeft J.D., Norton D.L., 1990. Mass and energy transport in a deforming Earth's crust. *The Role of Fluids in Crustal Processes*: 27-41.
- Bruland, K.W., Lohan, M.C., 2004. Controls of trace metals in seawater. In: Holland HD, Turekian KK (eds) *Treatise on geochemistry*, vol 6, pp 23–47. Elsevier, Amsterdam.
- Buckau, G., Artinger, R., Geyer, S., Wolf, M., Fritz, P., Kim, J.I., 2000. ^{14}C dating of Gorleben groundwater. *Appl Geochem* 15, 583–597.
- Bullen, T.D., Kendall, C., 1998. Tracing of weathering reactions and water flowpaths: a multi-isotopic approach. In: Kendall C, McDonnell JJ (eds) *Isotope tracers in catchment hydrology*. Elsevier Amsterdam, pp 611–646.
- Çağatay, M.N., 1993. Hydrothermal alteration associated with volcanogenic massive sulfide deposits; examples from Turkey. *Economic Geology* 88: 606-621 DOI 10.2113/gsecongeo.88.3.606.
- Caine, J.S., Evans, J.P., Forster, C. B., 1996. Fault zone architecture and permeability structure. *Geology*, 24, 1025-1028.
- Carpenter, A.B., 1978. Origin and chemical evolution of brines in sedimentary basins. *Oklahoma Geol Surv Circ* 79, 60–77.
- Cathles, L.M., 1977. An analysis of the cooling of intrusives by ground-water convection which includes boiling. *Economic Geology*, 72, 804-826.
- Çetiner, L., 2004. Balçova (İzmir) BD-8 jeotermal enerji arama sondaj kuyusu bitirme raporu [Balçova (İzmir) BD-8 geothermal energy exploration drilling well completion report]. MTA Der Rap No 10674, (yayımlanmamış) MTA, Ankara, pp. 36.
- Chen W., Ghaith A., Park A., Ortoleva P., 1990. Diagenesis through coupled processes: Modeling approach, self-organization, and implications for exploration. In: Meshri, I.D., Ortoleva, P.J. (eds), *Prediction of Reservoir Quality Through Chemical Modeling*, 103-130.
- Cherubini, Y., Cacace, M., Blöcher, G., Scheck-Wenderoth, M. (2013, on line first). Impact of single inclined fault on the fluid flow and heat transport: results from 3D finite element simulations. *Environmental Earth Sciences*.
- Chouke, R.L., Van Meurs, P., Van der Poel, C., 1959. The instability of slow, immiscible, viscous liquid-liquid displacements in permeable media *Trans. AIME*, 216, 188-194.

REFERENCES

- Cimiotti, U., 1983. Zur Landschaftsentwicklung des mittleren Trave-Tales zwischen Bad Oldesloe und Schwissel, Schleswig-Holstein. Berliner Geographische Studien. TU-Berlin, Berlin.
- Clark, I.D., Fritz, P., 1997. The ^{18}O shift in geothermal water. In: Stein J (ed) Environmental Isotopes in Hydrogeology, 328.
- Clark I., Fritz P., 1997. Environmental isotopes in hydrogeology. Lewis Publishers, Boca Raton, pp 1–328.
- Claypool, G.E., Holser, W.T., Kaplan, I.R., Sakai, H., Zak, I., 1980. The age curves of sulfur and oxygen isotopes in marine sulfate and their mutual interpretation. Chem Geol 28, 199–260.
- Clayton, R.N., Friedmann, I., Graf, D.L., Mayeda, T.K., Meents, W.F., Shimp, N.F., 1966. The origin of saline formation waters. J Geophys Res 71, 3869–3882.
- Conrad, M.A., Hipfel, B., Satir, M., 1995. Chemical and stable isotopic characteristics of thermal waters from Cesme-Seferihisar Area, Izmir (W. Turkey). In: Int. Earth Science Coll. on the Aegean Region, program and abstracts, 669.
- Coumou, D., Driesner, T., Geiger, S., Heinrich, C.A., Matthäi, S., 2006. The dynamics of mid-ocean ridge hydrothermal systems: Splitting plumes and fluctuating vent temperatures. Earth and Planetary Science Letters, 245, 218-231.
- Craig, H., 1961. Isotopic variations in meteoric waters. Sci 133, 1702–1703.
- Curtis, M., Pruess, K., 1998. Layered thermohaline convection in hypersaline geothermal systems, Transport in porous media 33, 29-63.
- Demirel, Z., Sentürk, N., 1996. Geology and hydrogeology of deep thermal aquifers in Turkey. In: Al-Beirut SNAB, M.J. (ed) Integration of Information Between Oil Drilling and Hydrogeology of Deep Aquifers, The Inter-Islamic Network of Water Resources Development and Management.
- Diersch, H.J.G., Kolditz, O., 1998. Coupled groundwater flow and transport: 2. Thermohaline and 3D convection systems. Advances in Water Resources 21, 401-425.
- Diersch, H.J.G., Kolditz, O., 2002. Variable-density flow and transport in porous media: Approaches and challenges. Advances in Water Resources 25, 899-944.
- Dittmer, E., 1953. Die Grundwasserverhältnisse der schleswig-holsteinischen Marschen und deren Versalzung. Unveröff. amtl. Ber. Forschungsstelle Westküste.
- Dittmer, E., 1956. Die Versalzung des Grundwassers an der schleswig-holsteinischen Westküste. Die Küste(5), 87-102.
- Dominco, 1969. Hydrogeochemical study of the Agamemnun-Seferihisar-Urla district In: Ankara, MTA
- Domenico, P.A., Robbins, G.A., 1985. The displacement of connate water from aquifers. Geol Soc Am Bul 96, 328–335.
- Dulski, P., 1994. Interferences of oxide, hydroxide and chloride analyte species in the determination of rare earth elements in geological samples by inductively coupled plasma-mass spectrometry. Fresenius J Anal Chem 350, 194–203.
- Evans, G.E., Nunn, J.A., 1989. Free thermohaline convection in sediments surrounding a salt column. J. Geophys. Res. 94, 12413-12422.
- Drahor, M.G., Sari, C., Salk, M., 1999. Self-potential and gravity studies in the Seferihisar geothermal field J. Sci. Eng. Dokuz Eylül Univ, 1, 97-112.

REFERENCES

- Driesner, T., and Heinrich, C.A., 2007. The System H₂O-NaCl. I. Correlations for molar volume, enthalpy, and isobaric heat capacity from 0 to 1000 degrees C, 1 to 5000 bar, and 0 to 1 X-NaCl. *Geochimica et Cosmochimica Acta* 71, 4902-4919.
- Drahor, M.G., Berge, M.A., 2006. Geophysical investigations of the Seferihisar geothermal area, Western Anatolia, Turkey. *Geothermics*, 35, 302–320.
- Ercan, A., Drahor, M., Atasoy, E., 1986. Natural polarization studies at Balçova geothermal field. *Geophysical Prospecting*, 34, 475-491.
- Erdogan, B., Gungor, T., 1992. Stratigraphy and tectonic evolution of the northern margin of Menderes massive. *TPTJ Bulletin C 4/1*, Ankara, 1992, p. 1-20.
- Erdogmus, B., Toksoy, M., Ozerdem, B. Aksoy, N. 2006. Economic assessment of geothermal district heating systems: A case study of Balçova-Narlıdere, Turkey. *Energy and Buildings*, 38, 1053-1059.
- Eşder, T., 1975. Seferihisar I ve II jeotermik derin deneme sondajları kuyu bitirme raporu. In: MTA Der. Rap. No. 5495, (yayımlanmamış) Ankara, 183.
- Esder, T., Simsek, S., 1975. Geology of İzmir (Seferihisar) geothermal area, Western Anatolia of Turkey: determination of reservoirs by means of gradient drilling. In: *Proceedings of the second UN Symposium on the Development and Use of Geothermal Resources San Francisco*, 349-361.
- Eşder, T., Şimşek, S., 1977. The relationship between the temperature gradient distribution and geological structure in the İzmir-Seferihisar geothermal area, Turkey. In: *Symposium on Geothermal Energy CENTO Scientific Programme Ankara*, 93-111.
- Eşder, T., Şimşek, Ş., 1979. The relationship between the temperature gradient distribution and geological structure in the İzmir-Seferihisar geothermal area, Turkey. Paper presented at the *Alternative Energy Source II; Proceedings of the Second Miami International Conference*, University of Miami - USA, December 10-13, 1979 1979.
- Etheridge, M.A., Wall, V.J. and Vernon, R.H. 1983. The role of the fluid phase during regional metamorphism and deformation. *Journal of Metamorphic Geology*, 1, 205–226, DOI: 10.1111/j.1525-1314.1983.tb00272.x
- Evans, D.G., Nunn, J.A., 1989. Free thermohaline convection in sediments surrounding a salt column. *Journal of Geophysical Research* 94, 12, 413-412, 422.
- Evans, D.G., Nunn, J.A., Hanor, J.S., 1991. Mechanisms driving groundwater flow near salt domes. *Geophysical Research Letters*, 18(5), 927-930.
- Fairley, J.P., 2009. Modeling fluid flow in a heterogeneous, fault-controlled hydrothermal system. *Geofluids*, 9, 153-166.
- Fairley, J.P., Hinds, J. J., 2004a. Field observation of fluid circulation patterns in a normal fault system. *Geophys. Res. Lett.*, 31.
- Fairley, J.P., Hinds, J. J., 2004b. Rapid transport pathways for geothermal fluids in an active Great Basin fault zone. *Geology*, 32, 825-828.
- Fan, Y., Duffy, C.J., Oliver, D.S.Jr., 1997. Density-driven groundwater flow in closed desert basins, *Journal of Hydrology*, 196, 139–184.

REFERENCES

- Farber, E., Vengosh, A., Gavrieli, I., Marie, A., Bullen, T.D., Mayer, B., Holtzman, R., Segal, M., Shavit, U., 2004. The origin and mechanism of salinization of the Lower Jordan River. *Geochim Cosmochim Acta* 60, 1989–2006.
- Filiz, S., Gökgöz, A., Tarcan, G., 1993. Hydrogeologic comparisons of geothermal fields in the Gediz and Büyük Menderes Grabens. In: Congress of the World Hydrothermal Organisation 13-18 May 1992, Istanbul-Pamukkale, Turkey, 129-153.
- Flocks, J. G., Kindinger, J.L., Davis, J.B., Swarzenski, P., 2001. Geophysical Investigations of Upward Migrating Saline Water from the Lower to Upper Floridan Aquifer, Central Indian River Region, Florida. *Water-Resources Investigations Report 01-4011*, 135-140.
- Fontes, J.C., Matray, J.M., 1993. Geochemistry and origin of formation brines from the Paris basin, France, 1: brines associated with Triassic salts. *Chem Geol* 109, 149–175.
- Frape, S.K., Fritz, P., 1987. Geochemical trends for groundwaters from the Canadian shield. In: Fritz P, Frape S.K. (eds) *Saline water and gases in crystalline rocks*. *Geol Ass Can Spec Pap* 33, 19–38.
- Freeze R.A., Witherspoon P.A., 1967. Theoretical analysis of regional groundwater flow: 2. Effect of water-table configuration and subsurface permeability variation. *Water Resources Res.* 3, 623-634.
- Fritz P., Basharmal, G.M., Drimmie, R.J., Ibsen, J., Quereshi, R.M., 1989. Oxygen isotope exchange between sulphate and water during bacterial reduction of sulphate. *Chem Geol* 79, 99–105.
- Friedrich, P., 1902. Der Untergrund von Oldesloe nebst einer kurzen Darstellung der Geschichte der ehemaligen Saline. *Mitt. geogr. Ges. Lübeck*, 16, 1-45.
- Friedrich, P., 1917. Die Grundwasserverhältnisse der Stadt Lübeck und ihrer Umgebung. Borchers, Lübeck, 183 pp.
- Frisch, U., 1993. Stratigraphie und Gebirgsbau des Prätertiär (Paläozoikum und Mesozoikum). -. In: EHLERS, J.: *Geologische Karte von Hamburg 1:25 000, Erläuterungen zu Blatt Nr. 2526, Allermöhe: 11-27, 60-64, 72, 4 Tab., 10 Abb., 1 Schnitt*.
- Fuhrmann, J., 2002. Multiphysics systems solution by time-implicite Voronoi box finite volumes. In: *Finite Volumes in Complex Applications III: Proc. Porquerolles*, pp. 551-559, Paris (Hermes).
- Fuhrmann, J., Langmach, H., 2001. Stability and existence of solutions of time-implicit finite volume schemes for viscous nonlinear conservation laws, *Applied Numerical Mathematics*, 37(1-2), 201–230.
- Gabriel, G., Kirsch, R., Siemon, B., Wiederhold, H., 2003. Geophysical investigation of buried Pleistocene subglacial valleys in Northern Germany. *Journal of Applied Geophysics*, 53, 159– 180.
- Garven, G., 1989. A hydrogeologic model for the formation of the giant oil sands deposits of the Western Canada sedimentary basin. *Am J Sci*, 289, 105-166.
- Garven, G., 1995. Continental-scale groundwater flow and geological processes. *Annu. Rev. Earth Planet. Sci.*, 23: 89-117.
- Garven, G., Bull, S.W., Large, R.R., 2001. Hydrothermal fluid flow models of stratiform ore genesis in the McArthur Basin, Northern Territory, Australia. *Geofluids*, 1, 289-311.
- Gelhar, L.W., 1986. Stochastic subsurface hydrology from theory to applications. *Water Resour. Res.*, 22(9S), 135S-145S.

REFERENCES

- Geluk, M.C. 2005. Stratigraphy and tectonics of Permo-Triassic basins in the Netherlands and surrounding areas. In: Utrecht University, Ph.D. thesis, 171.
- Genç, S.C., Altunkaynak, S., Karacik, Z., Yazman, M., Yilmaz, Y. 2001. The Çubukludag graben, south of Izmir: its tectonic significance in the Neogene geological evolution of the western Anatolia. *Geodinamica Acta*, 14, 45-55.
- Giggenbach, W.F., 1992. Isotopic shifts in waters from geothermal and volcanic systems along convergent plate boundaries and their origin. *Earth Planet Sci Lett* 113, 495–510.
- Glander, H., Schirrmeister, L., 1975. Erfassung und Darstellung der oberen Mineralwassergrenze. *Zeitschrift für Angewandte Geologie* 21, 7, Berlin.
- Gök, I. M., Sarak, H., Onur, M., Serpen, U., Satman, A., 2005. Numerical Modeling of the Balçova-Narlıdere Geothermal Field, Turkey. *Proceedings World Geothermal Congress 2005 Antalya, Turkey*, 24-29 April 2005.
- Göktürkler, G., Salk, M., Sari, C., 2003. Numerical modeling of the conductive heat transfer in western Anatolia. *JOURNAL OF THE BALKAN GEOPHYSICAL SOCIETY*, 6, 1-15.
- Graf, T., Therrien, R., 2009. Stable-unstable flow of geothermal fluids in fractured rock. *Geofluids*, 9, 138–152.
- Graf, D.L., Meents, W.F., Friedman, I., Shimp N.F., 1966. The origin of saline formation waters III. Calcium–chloride waters. *US Geol Surv Circ* 397, 1–60.
- Grobe, M., Machel, H., 2002. Saline groundwater in the Munsterland Cretaceous Basin, Germany: clues to its origin and evolution. *Marine and Petroleum Geology* 19, 307-322.
- Grube, A., Nachtigall, K.H., Wichmann, K., 1996. Zur Grundwasserversalzung in Schleswig-Holstein. *Meyniana*, 48, 21-34.
- Grube, A., Hermsdorf, A., Lang, M., Rechlin, B., Schneider, W., Wichmann, K., 2000a. Prognose des Salzwasseraufstiegs im pleistozänen Grundwasserleiterkomplex eines geplanten Wasserwerkes im Land Brandenburg - Grundwassermodelle und hydrogeochemische Untersuchungen. *Brandenburg. Geowissenschaftl. Beiträge* 7:41-52.
- Grube, A., Wichman, K., Hahn, J., Nachtigall, K., 2000b. Geogene Grundwasserversalzung in den Porengrundwasserleitern Norddeutschlands und ihre Bedeutung für die Wasserwirtschaft. *Technologiezentrum Wasser Karlsruhe (TZW)*. Karlsruhe, pp 203.
- Grube, A., Lotz, B., 2004. Geological and numerical modeling of geogenic salinization in the area of the Lübeck Basin. *18th Salt Water Intrusion Meeting (Catagena, Spain 2004)*, 183-195.
- Gvirtzman, H., Garven, G., Gvirtzman, G., 1997. Thermal anomalies associated with forced and free ground-water convection in the Dead Sea rift valley. *Geological Society of America Bulletin*, 109, 1167-1176.
- Haneberg, W.C., 1995. Steady State Groundwater Flow Across Idealized Faults. *Water Resour. Res.*, 31, 1815-1820.
- Hannemann, M., Schirrmeister, W., 1998. Paläohydrogeologische Grundlagen der Entwicklung der Süß-/Salzwassergrenze und der Salzwasseraustritte in Brandenburg, *Brandenburgische Geowissenschaftliche Beiträge* 5, 61–72.

REFERENCES

- Hanor, J.S., 1987. Kilometre-scale thermohaline overturn of pore waters in the Louisiana Gulf Coast. *Nature* 327, 501-503.
- Hanor, J.S., 1994. Origin of saline fluids in sedimentary basins. In: Parnell J (ed) *Geofluids: origin, migration and evolution of fluids in sedimentary basins*. Geol Soc Spec Publ 151–178.
- Harcouet-Menou, V., Guillou-Frottier, L., Bonneville, A., Adler, P. M., Mourzenko, V., 2009. Hydrothermal convection in and around mineralized fault zones: insights from two- and three-dimensional numerical modeling applied to the Ashanti belt, Ghana. *Geofluids*, 9, 116-137.
- Hardie, L.A., 1990. The roles of rifting and hydrothermal CaCl₂ in the origin of potash evaporites—an hypothesis. *Am J Sci* 290, 43– 106.
- Hardie, L.A. 1991. On the Significance of Evaporites. *Annual Review of Earth and Planetary Sciences* 19, 131-168, DOI:10.1146/annurev.earth.19.050191.001023.
- Hassanizadeh, S.M., 1988. Modeling species transport by concentrated brine in aggregated porous media. *Transport in Porous Media*, 3, 299-318.
- Hayba, D.O., Ingebritsen, S.E., 1997. Multiphase groundwater flow near cooling plutons. *Journal of Geophysical Research*, 102, 12, 235-212, 252.
- Heck, H.L., 1931. Grundwasserverhältnisse und geologischer Bau im schleswig-holsteinischen Marsch- und Nordseeinselgebiet. *SBR. preuss.geol.landesanst.*, 6, 169-196.
- Heck, H.L., 1932. Das Grundwasser im Zusammenhang mit dem geologischen Bau Schleswig –Holsteins, pp. 110, 117–119, Preußische Geologische Landesanstalt, Berlin.
- Heck, H.L., 1932. Das Grundwasser in Zusammenhang mit dem geologischen Bau Schleswig-Holsteins. *Preubische Geol. Landesanstalt*, 106-133.
- Heck, H.L., 1944. Versalzungen von Grundwasser in Schleswig-Holstein, deren Umfang und Ursachen. *Germany, Reichsamt f.*
- Heck, H.L., 1948a. Grundwasseratlas von Schleswig-Holstein 1:500.000. Hamburg.
- Heck, H.L., 1948b. Die hydrogeologischen Grundlagen für die künftige Wasserwirtschaft in Schleswig-Holstein. *Gas- und Wasserfach*, 89/5, 145-151.
- Heck, H.L., 1949. Der Grundwasserschatz in Schleswig-Holstein - Ein Wegweiser zur Wassererschließung. *Cram, DeGruyter, Hamburg*, 72 pp.
- Heffner, J., Fairley, J., 2006. Using surface characteristics to infer the permeability structure of an active fault zone. *Sedimentary Geology*, 184, 255-265.
- Herbert, A.W., Jackson, C.P., Lever D.A., 1988. Coupled groundwater flow and solute transport with fluid density strongly dependent upon concentration. *Water Resources Res* 24, 1781-1795.
- Herut, B., Starinsky, A., Katz, A., Bein, A., 1990. The role of seawater freezing in the formation of subsurface brines. *Geochim Cosmochim Acta* 54, 13–21.
- Hinsch, W., 1974. Das Tertiär im Untergrund von Schleswig-Holstein (Das Nordwestdeutsche Tertiärbecken, Beitrag #5). *Geol. Jb.*, A24, 5-35.
- Hochstein, M.P., Zhongke, Y., Ehara, S., 1990. The Fuzhou Geothermal System (P.R. China): modelling study of a low temperature fracture zone system. *Geothermics*, 9, 43-60.

REFERENCES

- Hoth, P., Seibt, A., Kellner, T., Huenges, E., 1997. Geowissenschaftliche Bewertungsgrundlagen zur Nutzung hydrogeothermaler Ressourcen in Norddeutschland. -Scientific technical report ; 97, 15, 149 S, Potsdam.
- Huenges, E. 2002. Geowissenschaftliche Bewertungsgrundlagen zur Nutzung hydrogeothermaler Ressourcen in Norddeutschland, Scientific technical report; 02, 14, Potsdam.
- Hurtig, E., 1994. Land Brandenburg. Bohrungen mit kontinuierlichen Bohrlochmessungen. Bohrungen mit Maximaltemperaturen. Unveröff. Unterlagen bereitgestellt durch das Landesamt für Geowissenschaften und Rohstoffe Brandenburg.
- Ilkisik, O. M., 1995. Regional heat flow in western Anatolia using silica temperature estimates from thermal springs. *Tectonophysics*, 244, 175-184.
- Ingebritsen, S.E., Sanford, W.E., 1998. *Groundwater in Geologic Processes*. Cambridge University Press New York, pp 341.
- Jackson, M.P.A., Talbot, C.J., 1991. *A glossary of salt tectonics*. Texas, Bureau of Economic Geology.
- Johannsen, A., 1954. Die Küsten- und Untergrundversalzung in Schleswig-Holstein. *Gas- und Wasserfach.*, 95, 319-324.
- Johannsen, A., 1960. Stand und Möglichkeiten der Grundwasserversorgung im Lübecker Raum. *Gas- und Wasserfach*, 101/2, 34-39.
- Johannsen, A., 1979. Geologie und Grundwasservorkommen im Raume der Salinarstrukturen Sülfeld und Nusse (Schleswig-Holstein). *Geol Jb.*, C21, 45-97.
- Johannsen, A., 1980. Hydrogeologie von Schleswig Holstein, in *Geologisches Jahrbuch*, Series C, Vol. 28, p. 451, Bundesanstalt für Geowissenschaften und Rohstoffe und Geologische Landesämter in der Bundesrepublik Deutschland.
- Jones, G., Whitaker, F., Smart, P., Sanford, W., 2000. Numerical modelling of geothermal and reflux circulation in Enewetak Atoll: implications for dolomitization. *Journal of Geochemical Exploration* 69-70, 71-75.
- Jones, G.D., Whitaker, F.F., Smart P.L., Sanford, W.E., 2004. Numerical analysis of seawater circulation in carbonate platforms II: the dynamic interaction between geothermal and brine reflux circulation. *American Journal of Science* 304, 250-284.
- Jortzig, H., 2002. Verbreitung der Rupelfolge—Das Geopotenzial Brandenburgs. In: Stackebrandt W, Manhenke V (eds) *Atlas zur Geologie von Brandenburg*. Landesamt für Geowissenschaften und Rohstoffe Brandenburg, Kleinmachnow, vol 2, pp 72–73 .
- Kaiser, B., Cacace, M., Scheck-Wenderoth, M. (2013, on line first). 3D coupled fluid and heat transport simulations of the Northeast German Basin and their sensitivity to the spatial discretization: different sensitivities for different mechanisms of heat transport. *Environmental Earth Sciences*.
- Karakullukcu, K., 1991. Izmir - Menderes -Görece Köyü Camur Dere Göleti Mühendislik jeolojisi. In:Izmir, Doküz Eylül Üniversitesi, Master thesis.
- Katz, B.G., Plummer, L.N., Busenberg, E., Revesz, K.M., Jones, B.F., Lee , T.M., 1995. Chemical evolution of groundwater near a sinkhole lake, northern Florida. 2. Chemical patterns, mass transfer modelling, and rates of mass transfer reactions. *Water Resour Res* 31, 1565– 1584.

REFERENCES

- Kawabe, I., Ohta, A., Ishii, S., Tokumura, M., Miyauchi, K., 1999. REE partitioning between Fe–Mn oxyhydroxide precipitates and weakly acid NaCl solution: convex tetrad effect and fractionation of Y and Sc from heavy lanthanides. *Geochem J* 33, 167–179.
- Kaya, O., 1981. Miocene reference section for the coastal parts of West Anatolia. *Newsletters on Stratigraphy*, 10, 164-191.
- Kessler, D.A., Levine, H., 1986. Coalescence of Saffman-Taylor fingers: A new global instability. *Physical Review A*, 33, 3625.
- Kharaka, Y.K., Berry, F.A.F., 1973. Simultaneous flow of water and solutes through geological membranes: I. experimental investigations. *Geochim Cosmochim Acta* 37, 2577–2603.
- Klinge, H., Vogel, P., Schelkes, K., 1992. Chemical composition and origin of saline formation waters from the Konrad mine, Germany. Water rock interaction, Proceedings of the 7th international symposium on water–rock interaction/WRI-7, Park City, Utah, USA, 13–18 July, Balkema, Rotterdam pp 1117–1120.
- Kloppmann, W., Negrel, Ph., Casanova, J., Klinge, H., Schelke, K., Guerrot, C., 2001. Halite dissolution derived brines in the vicinity of a Permian salt dome (N German Basin). Evidence from boron, strontium, oxygen and hydrogen isotopes. *Geochim Cosmochim Acta* 65, 4087–4101
- Knauth, L.P., 1988. Origin and mixing history of brines, Palo Duro Basin, Texas, USA. *Appl Geochem* 3, 455–474.
- Knöller, K., Weise SM (in prep) Utilization of high temperature pyrolysis for the determination of 2H/1H and 18O/16O ratios in high salinity waters .
- Knöller, K., Vogt, C., Richnow, H-H., Weise, S.M., 2006. Sulfur and oxygen isotope fractionation during benzene, toluene, ethyl benzene, and xylene degradation by sulfate-reducing bacteria. *Environ Sci Technol* 40, 3879–3885.
- Köhler, S., Tesmer, M., Otto, R., Pekdeger, A., Lorenzen, G., Hubberten, H., 2005. Die Genese und Dynamik der Grundwasserversalzung im Raum Lübeck. In: L.f.N.u.U.d.L. Schleswig-Holstein (Editor), 72. Tagung der Arbeitsgemeinschaft Norddeutscher Geologen. Geologischer Dienst Schleswig-Holstein, Lübeck, pp. 35-36.
- Kohout, F.A., 1965 A hypothesis concerning cyclic flow of salt water related to geothermal heating in the Floridian aquifer. *New York Academy of Sciences Transactions ser. 2, v.28, no. 2, 249-271.*
- Kolditz, O., Ratke, R., Diersch, H.J.G., Zielke, W., 1998. Coupled groundwater flow and transport: 1. Verification of variable density flow and transport models. *Advances in Water Resources* 21, 27-46.
- Konikow, L.F., Reilly, T.E., Barlow, P.M., and Voss, C.I., 2006. Chapter 23: Groundwater Modeling, *in* Delleur, J., ed., *The Handbook of Groundwater Engineering*, Second Edition: Boca Raton, CRC Press, 54 p.
- Kühn, M., 1997. Geochemische Folgereaktionen bei der hydrothermalen Energiegewinnung. *Berichte aus dem Fachbereich Geowissenschaften Universität Bremen Nr. 92*, 129 S.
- Kühn, M., Dobert, F., Gessner, K., 2006. Numerical investigation of the effect of heterogeneous permeability distributions on free convection in the hydrothermal system at Mount Isa, Australia. *Earth and Planetary Science Letters*, 244, 655-671.

REFERENCES

- Lampe, C., Person, M., 2002. Advective cooling within sedimentary rift basins - Application to the Upper Rhinegraben (Germany). *Marine and Petroleum Geology* 19:361-375.
- LANU, 2002. Ideenwettbewerb zum geplanten F&E Vorhaben "Genese und Versalzung der Grundwasserleiter im Lübecker Raum (Teilprojekt des Untersuchungsprogramms zur Ermittlung des nutzbaren Grundwasserdargebots im Raum Lübeck)". In: Flintbek, LANU, 7.
- Lerman, A., 1970. Chemical equilibrium and evolution of chloride brines. 50th Anniv Symp Miner Soc Spec Pap 3, 291–306.
- Lever, D.A., Jackson, C.P., 1985. On the equations for the flow of concentrated salt solution through a porous medium. In: U.K. DOE Report No. DOE/RW/85.100.
- Lehmann, H., 1974a. Geochemie und Genesis der Tiefenwässer der Nordostdeutschen Senke, Teil 1.- Zt. für angewandte Geologie; 20/11.502-509 S.
- Lehmann, H., 1974b. Geochemie und Genesis der Tiefenwässer der Nordostdeutschen Senke, Teil 2.- Zt. für angewandte Geologie; 20/11.551-557 S.
- Lin G., Nunn, J. A., Deming., D., 2000. Thermal buffering of sedimentary basins by basement rocks: implications arising from numerical simulations. *Petroleum Geoscience*, 6, 299-307.
- Liu, H.H., Bodvarsson, G.S., Zhang, G., 2004. Scale dependency of the effective matrix diffusion coefficient. *Vadose Zone Journal*, 3, 312-314.
- Löhnert, E., 1968. Hydrogeologische und Hydrochemische Betrachtungen über die salzigen Grundwässer im Raum Bad Oldesloe. *Mitt. Geol. Staatsinst. Hamburg*, 37, 99-119.
- Löhnert, E.P., 1969. Bad Oldesloe aus hydrogeologischer Sicht. *Die Heimat*, 76(7), 209-212.
- Löhnert, E., Bauhus, W., Sonntag, C., 1986. Mechanism of groundwater salinization in the Hamburg region, F.R. Germany -facies and new findings. - In: Boekelman R.H., Van Dam, J. Evertman, M., Ten Hoorn, W. (HRSG.): Proceedings of the salt water intrusion meeting. Delft, Netherlands, 613-628.
- Lopez, D.L., Smith, L., 1995. Fluid flow in fault zones: analysis of the interplay of convective circulation and topographically driven groundwater flow. *Water Resour. Res.*, 31, 1489–1503.
- Lopez, D.L., Smith, L., 1996. Fluid Flow in Fault Zones: Influence of Hydraulic Anisotropy and Heterogeneity on the Fluid Flow and Heat Transfer Regime. *Water Resour. Res.*, 32, 3227-3235.
- Lowe, C.P., Frenkel, D., 1996. Do Hydrodynamic Dispersion Coefficients Exist? *Physical Review Letters* 77:4552 – 4555.
- Magri, F. 2004. Derivation of the coefficients of thermal expansion and compressibility for use in FEFLOW. WASY White papers III, 13-23.
- Magri, F., Bayer, U., Clausnitzer, V., Jahnke, H., Diersch, H.-J., Fuhrmann, J., Möller, P., Pekdeger, A., Tesmer, M., Voigt, H., 2005a. Deep reaching fluid flow close to convective instability in the NE german basin – results from water chemistry and numerical modeling. *Tectonophysics*, 397, 1-2, 5-20.
- Magri, F., Bayer, U., Clausnitzer, V., Jahnke, H., Diersch, H.-J., Fuhrmann, J., Möller, P., Pekdeger, A., Tesmer, M., Voigt, H., 2005b. Fluid-dynamics driving saline water in the North East German Basin. *International Journal of Earth Sciences* 94, 1056-1069.

REFERENCES

- Magri, F., 2005. Mechanisms and fluid-dynamics driving saline waters within the North East German Basin: Results from thermohaline numerical simulations. Ph.D. thesis Thesis. Fachbereich Geowissenschaften, Freie Universität Berlin, Berlin, 129 pp.
- Magri, F., Bayer, U., Tesmer, M., Möller, P., Pekdeger, A., 2008. Salinization problems in the NEGB: results from thermohaline simulations. *International Journal of Earth Sciences* 97, 5, 1075-1085.
- Magri, F., Bayer, U., Maiwald, U., Otto, R., Thomsen, C., 2009. Impact of transition zones, variable fluid viscosity and anthropogenic activities on coupled fluid-transport processes in a shallow salt-dome environment. *Geofluids*, 9, Issue 3, 182–194.
- Magri, F., 2010. Derivation of the coefficients of compressibility, thermal expansion and fluid density difference ratio for reproducing aqueous NaCl density. *WASY White papers III*, 85-92.
- Magri, F., Akar, T., Gemici, U., Pekdeger, A., 2010. Deep geothermal groundwater flow in the Seferihisar–Balçova area, Turkey: results from transient numerical simulations of coupled fluid flow and heat transport processes. *Geofluids* 10, 388–405.
- Magri, F., Akar T., Gemici, U. and Pekdeger, A., 2012. Numerical investigations of fault-induced seawater circulation in the Seferihisar-Balçova Geothermal system, Western Turkey.– *Hydrogeology Journal* 20(1),103-118
- Magri, F., Tillner E., Kempka T., Wang W., Watanabe N., Zimmermann G., 2013. 3D hydro-mechanical scenario analysis to evaluate changes of the recent stress field as a result of geological CO₂ storage. *Geophysical Research Abstracts*, Vol. xx, Abstract No: EGU2013- 2852, 07-12/04/2013, Wien, Austria
- Martens, S., 2006. Grundwassersysteme unter dem Einfluss extremer Klimabedingungen - Wirkungsanalysen und (paläo)hydrogeologische Strömungsberechnungen für den Großraum Lübeck. *Techn. Univ., Hamburg*, 158 pp.
- Maystrenko, Y., Bayer, U., Scheck-Wenderoth, M., 2005. The Glueckstadt Graben, a sedimentary record between the North and Baltic Sea in north Central Europe. *Tectonophysics*, 397, 113-126.
- Maystrenko, Y., Bayer, U., Scheck-Wenderoth, M., 2006. 3D reconstruction of salt movements within the deepest post-Permian structure of the Central European Basin System – the Glueckstadt Graben. *Netherlands Journal of Geosciences / Geologie en Mijnbou*, 85(3), 183-198.
- McKenna, J.R., Blackwell, D.D., 2004. Numerical modeling of transient Basin and Range extensional geothermal systems. *Geothermics*, 33, 457-476.
- McKibbin, R., 1986. Heat transfer in a vertically-layered porous medium heated from below. *Transport in Porous Media*, 1, 361-370.
- McLennan, S.M., 1989. Rare earth elements in sedimentary rocks: influence of provenance and sedimentary processes. In: Lipin BR, McKray GA (eds) *Geochemistry and mineralogy of rare earth elements*. Mineralogical Society of America, Washington DC, pp 169–200.
- Mercer, J.W., Pinder, G.F., 1974. Finite Element Methods in Flow Problems. In: *Finite element analysis of hydrothermal systems* (ed. Oden JT) Univ. of Alabama Press, Proc. 1st Symp., Swansea, 1974, 401-414.
- Metha, S., Fryar, A.E., Banner, J.L., 2000. Controls on the regional-scale salinization of the Ogallala aquifer, Southern High Plains, Texas USA. *Appl Geochem* 15, 849–864.

REFERENCES

- Mills, A.L., 1988. Variation in $\delta^{13}\text{C}$ of stream bicarbonate: implications for sources of alkalinity. M.S. thesis, George Washington University, Washington DC, p 160.
- Mineyuki, H., 1998. A simple model of a two-layered high-temperature liquid-dominated geothermal reservoir as a part of a large-scale hydrothermal convection system, *Transport in porous media* 33, 3-27.
- Möller, P., Rosenthal, E., Dulski, P., Geyer, S., Guttman, Y., 2003. Rare earths and yttrium hydrostratigraphy along the Lake Kinneret—Dead Sea—Arava transform fault, Israel. *Appl Geochem* 18, 1613–1628.
- Möller, P., Geyer, S., Salameh, E., Dulski, P., 2006a. Sources of mineralization of thermal groundwater of Jordan. *Acta Hydrochim Hydrobiol* 34, 86–100.
- Möller, P., Dulski, P., Salameh, E., Geyer, S., 2006b. Characterization of sources of thermal spring- and well water in Jordan by rare earth elements and yttrium distribution and stable isotopes of H_2O . *Acta Hydrochim Hydrobiol* 34, 101–116.
- Möller, P., Rosenthal, E., Geyer, S., Guttman, J., Dulski, P., Rybakov, M., Zilberbrand, M., Jahnke, C., Flexer, A., 2007. Hydrochemical processes in the lower Jordan Valley and the Dead Sea area. *Chem Geol* 239, 27–49.
- Möller P., Weise S. M., Tesmer M., Dulski P., Pekdeger A., Bayer U., Magri F., 2008. Salinization of groundwater in the North German Basin: results from conjoint investigation of major, trace element and multi-isotope distribution. *Int J Earth Sci (Geol Rundsch)* 97, 1057-1073.
- Müller, E., Papendieck, G., 1975. Zur Verteilung, Genese und Dynamik von Tiefenwässern unter besonderer Berücksichtigung des Zechsteins. *Zt. geol. Wiss.*, 3 (2), 167-196. Naumann, 2000. Salinare Tiefenwässer in Norddeutschland: Gas- und isotopengeochemische Untersuchungen zur Herkunft und geothermischen Nutzung. - Scientific technical report STR00/21/GeoForschungsZentrum, 116 S., Potsdam; 00, 21.
- Müller, A., 1993. Grundwasservorkommen von Deutschland 1:1.000.000; Blatt 2: Qualität des Grundwassers - bedeutende Vorkommen.- [Ergänzung der Karte von VIERHUFF et al. 1981 für die Neuen Länder]; Bundesanstalt für Geowissenschaften und Rohstoffe (Hannover).
- Murphy, D.H., 1979. Convective Instabilities in Vertical Fractures and Faults. *J. Geophys. Res.* 84, 6121–6130.
- Mutlu, H., Güleç, N., Hilton, D. R., 2008. Helium-carbon relationships in geothermal fluids of western Anatolia, Turkey. *Chemical Geology*, 247, 305-321.
- Neumann, E., 1975. Hydrogeologische Verhältnisse des Paläozoikums und Mesozoikums am Nordrand der Norddeutsch-Polnischen Senke und ihre Beziehungen zu den Erdöl- und Erdgasvorkommen. Dissertationsschrift an der Fakultät Mathematik und Naturwissenschaften der Bergakademie Freiberg.
- Neuzil, C.E., 1995. Abnormal pressures as hydrodynamic phenomena. *American Journal of Science* 295, 742-786.
- Nghiem, L., Sammon, P., Grabenstetter, J., Ohkuma, H., 2004. Modeling CO_2 Storage in Aquifers with a Fully-Coupled Geochemical EOS Compositional Simulator, SPE 89474.

REFERENCES

- Nield, D.A., 1968. Onset of thermohaline convection in porous medium, *Water Resour.Res.* 4(3), 553-560.
- Nield, D.A., 1974. Comments on "Effect of solute dispersion on thermal convection in a porous medium layer". *Water Resources Research* 10, 889.
- Nield, D.A., 1991. The stability of convective flows in porous media, *Convective Heat and Mass Transfer in Porous Media* 4(3), 79-122.
- Nield, D.A., 1994. Estimation of an effective Rayleigh number for convection in a vertically inhomogeneous porous medium or clear fluid. *International Journal of Heat and Fluid Flow* 15, 337-340.
- Nield, D.A., Bejan, A., 1999. *Convection in porous media*. Springer, New York, pp 1-546.
- Nordstrom, D.K., Olsson, T., 1987. Fluid inclusions as a source of dissolved salts in deep granitic groundwaters. In: Fritz P, Frape SK (eds) *Saline waters and gases in crystalline rocks*. Geol Assoc Can Spec Pap 33, 111–119.
- O'Brien, J.J., Lerche, I., 1984. The influence of salt domes on paleotemperature distributions. *Geophysics*, 49: 2032-2043.
- Ocakoğlu, N., Demirbağ, E., Kuşçu, I., 2004. Neotectonic structures in the area offshore of Alaçatı, Doğanbey and Kuşadası (western Turkey): evidence of strike-slip faulting in the Aegean extensional province. *Tectonophysics* 391, 67-83.
- Ocakoğlu N., Demirbağ, E., Kuşçu, I., 2005. Neotectonic structures in Izmir Gulf and surrounding regions (western Turkey): Evidences of strike-slip faulting with compression in the Aegean extensional regime. *Marine Geology* 219, 155–171.
- O'Sullivan, M.J., Pruess, K., Lippmann, M.J., 2001. State of the art of geothermal reservoir simulation. *Geothermics*, 30, 395-429.
- Oldenburg, C. M., Pruess, K., 1998. Layered thermohaline convection in hypersaline geothermal systems. *Transport in Porous Media* 33, 29-63.
- Oldenburg, C.M., Pruess, K., 1999. Plume separation by transient thermohaline convection in porous media. *Geophysical Research Letters* 26, 2997-3000.
- Öngür, T., 2001. Geology of Izmir Agamemnon Hot Springs-Balcova Geothermal Area and new conceptual geological model In: 24 Report for Balcova Geothermal Ltd. Izmir.
- Onur, M., Aksoy, N., Serpen, U., Satman, A., 2002. Analysis of pressure transient tests in Balcova-Narlıdere geothermal field. *Turkish Journal of Oil and Gas*, 8, 20-36.
- Onur, M., Aksoy, N., Serpen, U., Satman, A., 2005. Analysis of Well-Tests in Balcova-Narlıdere Geothermal Field, Turkey. *Proceedings World Geothermal Congress 2005 Antalya, Turkey*, 24-29 April 2005.
- Ophori, D. U., 1998. The significance of viscosity in density-dependent flow of groundwater. *Journal of Hydrology*, 204, 261-270.
- Otto, R., 2002. Ideenwettbewerb zum geplanten F&E-Vorhaben "Genese und Versalzung der Grundwasserleiter im Lübecker Raum (Teilprojekt des Untersuchungsprogramms zur Ermittlung des nutzbaren Grundwasserdargebotes im Raum Lübeck). In: Flintbeck, LANU, 7.

REFERENCES

- Patil, P.R., Vaidyanathan, G., 1982. Effect of variable viscosity on thermohaline convection in a porous medium. *Journal of Hydrology*, 57, 147-161.
- Pekdeger, A., Tesmer, M., Köhler, S., Lorenzen, G., 2006. Abschlussbericht zum F&E-Vorhaben: "Untersuchungen zur Genese und Dynamik der Grundwasserversalzung im Großraum Lübeck, Freie Universität Berlin Institut für Geologische Wissenschaften Arbeitsgruppe Hydrogeologie, Berlin.
- Person, M., Raffensperger, J.P., Ge S., Garven, G., 1996. Basin-scale hydrogeologic modeling. *Reviews of Geophysics* 34, 61-87.
- Petersen, M., 1956. Die Versalzung der schleswig-holsteinischen Marschen in wasserwirtschaftlicher Sicht. *Die Küste*(5), 146-156.
- Pinder G.F., Bredehoeft J.D., 1968. Application of the Digital Computer for Aquifer Evaluation. *Water Resour Res* 4, 1069-1093, DOI: 10.1029/WR004i005p01069.
- Potter, W., Brown, D., 1954. The volumetric properties of aqueous sodium chloride solutions from 0° to 500°C at pressures up to 2000 bars based on a regression of available data in the literature, United States Geological Survey Bulletin 1421-C.
- Quinn, K.A., Byrne, R.H., Schijf, J., 2004. Comparative scavenging of yttrium and the rare earth elements in seawater: competitive influences of solution and surface chemistry. *Aquat Chem* 100, 59–80.
- Raffensperger, J.P., Garven, G., 1995. The formation of unconformity-type uranium ore deposits 1. Coupled groundwater flow and heat transport modeling. *American Journal of Science* 295, 581-636.
- Ranganathan, V., Hanor, J.S., 1988. Density-driven groundwater flow near salt domes. *Chemical Geology* 74, 173-188.
- Rayleigh, J.W.S., 1916. On convection currents in a horizontal layer of fluid, when higher temperature is on the underside, *Philosophical Magazine and Journal of Science, Series 6*, 32, 529–546.
- Rawling, G.C., Goodwin, L.B., Wilson, J.L., 2001. Internal architecture, permeability structure, and hydrologic significance of contrasting fault-zone types. *Geology* 29(1), 43-46.
- Reese, R.S., 2003. Hydrogeology and the distribution and the origin of salinity in the Floridian aquifer system, Southeastern Florida. pp 62.
- Reuter, H.I., Nelson, A., Jarvis, A., 2007. An evaluation of void filling interpolation methods for SRTM data. *International Journal of Geographic Information Science*, 21, 983-1008.
- Rockel, W., Hoth, P., Seibt, A. 1997. Charakteristik und Aufschluss hydrogeothermaler Speicher. - *Geowissenschaften*, 15 (8), 244-252.
- Rosenberg, N.D., Spera, F.J, 1990. Role of anisotropic and/or layered permeability in hydrothermal convection. *Geophysical Research Letters* 17, 235-238.
- Rosenberg, N.D., Spera, F.J, 1992a. Convection in porous media with thermal and chemical buoyancy: a comparison of two models for solute dispersion. *Chaotic Processes in the Geological Science IMA Volume in Mathematics and Its Applications*, 319-333.
- Rosenberg, N.D., Spera FJ, 1992b. Thermohaline convection in a porous medium heated from below. *International Journal of Heat and Mass Transfer* 35: 1261-1273.

REFERENCES

- Rosenthal, E., 1997. Thermosaline water of Ca-chloride composition: diagnostics and brine evolution. *Environ Geol* 32, 245–249.
- Rowland, J.V., Sibson, R.H., 2004. Structural controls on hydrothermal flow in a segmented rift system, Taupo Volcanic Zone, New Zealand. *Geofluids*, 4, 259-283.
- Rubin, H. 1975. Effect of solute dispersion on thermal convection in a porous medium layer. *Water Resources Research* 11, 154-158.
- Rutter, S. 1988. Hydrogeologische Einschätzung des Saxons im Beckenzentrum und angrenzender Gebiete. Abschlussbericht VEB Geol. Forsch. und Erk. Halle BT Stendal.
- Saar, M.O., Manga, M., 2003. Seismicity induced by seasonal groundwater recharge at Mt. Hood, Oregon. *Earth and Planetary Science Letters* 214, 605-618, DOI: 10.1016/s0012-821x(03)00418-7.
- Saffman, P.G., Taylor, G., 1958. The Penetration of a Fluid into a Porous Medium or Hele-Shaw Cell Containing a More Viscous Liquid. *Proceedings of the Royal Society of London. Series A. Mathematical and Physical Sciences*, 245, 312-329.
- Sanford, W.E., Whitaker, F.F., Smart, P.L., Jones, G., 1998. Numerical analysis of seawater circulation in carbonate platforms; I, Geothermal convection. *Am J Sci* 298, 801-828.
- Sarkar, A., Nunn, J.A, Hanor, J.S, 1995. Free thermohaline convection beneath allochthonous salt sheets: an agent for salt dissolution and fluid flow in Gulf Coast sediments. *Journal of Geophysical Research* 100, 18, 085-18, 092.
- Sari, C., Salk, M., 2003. Heat Flow Investigations in Western Anatolia. In: *Geophysical Research Abstracts*, Nice, France, EGS-AGU-EUG Joint Assembly, Vol. 5, 08509.
- Satman, A., Serpen, U., Onur, M., 2002. Reservoir and Production Performance of Ýzmir Balçova-Narlýdere Geothermal Field. Project Report in Turkish, Balçova Jeotermal Ltd., Ýzmir.
- Satman, A., Serpen, Ü., Onur, M., 2001. İzmir Balçova-Narlýdere Jeotermal Sahasının Rezervuar ve Üretim Performansı Projesi [İzmir Balçova-Narlýdere Geothermal Field Reservoir and Production Performance Project], Cilt 1&2 Petrol ve Doğal Gaz Mühendisliđi Bölümü, İstanbul Teknik Üniversitesi, Maslak İstanbul pp. 479.
- Sayin, E., Pazi, I, Eronat, C., 2004. Investigation of Water Masses in İzmir Bay, Western Turkey. *Turkish J. Earth Sci.* 15, p. 343-372.
- Scheck, M. 1997. Dreidimensional Strukturmodellierung des Nordostdeutschen Beckens unter Einbeziehung von Krustenmodellen. Scientific Technical Report STR97/10, Geoforschungszentrum Potsdam.
- Scheck, M., Bayer, U., 1999. Evolution of the Northeast German Basin—inferences from a 3D structural model and subsidence analysis, *Tectonophysics*, 313, 145–169.
- Schenk, P., 1978. Zur Grundwasserentnahme und deren Auswirkungenauf die Grundwasserverhältnisse im Raume Lübeck. unveröffentl. Gutachten des Geologischen Landesamtes Schleswig-Holstein, 78/3.
- Schidlowski, M., Hayes, J.M., Kaplan, I.R., 1983. Isotopic inferences of ancient biochemistries: carbon, sulphur, hydrogen and nitrogen. In: Schopf JW (ed) *Earth's earliest biosphere: its origin and evolution*. Princeton University Press, Princeton, pp 149–186.

REFERENCES

- Schmidt Mumm, A., Wolfgramm, M., 2004. Fluid systems and mineralization in the north German and Polish basin. *Geofluids* 4, 315-328.
- Schirrmeister, W., 1996. Aus der Literatur überlieferte Angaben über natürliche Salzwasseraustritte an der Grundwasseroberfläche/Geländeoberfläche in Brandenburg, Brandenburgische Geowissenschaftliche Beiträge, 3, 94–96.
- Schneider, H., 1979. Geohydrologie der Elbmarsch im Raum Brunsbüttel. *Münst. Forsch. Geol. Paläont.*, 47, 91-145.
- Schoofs, S., Hansen, U., 2000. Depletion of a brine layer at the base of ridge-crest hydrothermal systems. *Earth and Planetary Science Letters*, 180, 341-353.
- Serpen, U., 2004. Hydrogeological investigations on Balçova geothermal system in Turkey. *Geothermics*, 33, 309-335.
- Sharp, J.M.J., Fenstermaker, T.R., Simmons, C.T., McKenna, T.E., Dickinson, J. K., 2001. Potential salinity-driven free convection in a shale-rich sedimentary basin: Example from the Gulf of Mexico basin in south Texas. *AAPG Bulletin*, 85, 2089–2110.
- Shewchuk, J.R., 1996. Triangle: Engineering a 2D quality mesh generator and Delaunay triangulator, *Lecture Notes in Computer Science*, 1148, 203–222, in *Applied Computational Geometry: Towards Geometric Engineering*, eds. Lin, M. C. & Manocha, D., Springer Verlag, Berlin.
- Simmons, C.T., Fenstermaker, T.R., Sharp, J.M., 2001. Variable-density groundwater flow and solute transport in heterogeneous porous media: approaches, resolutions and future challenges. *Journal of Contaminant Hydrology* 52:245-275.
- Simmons, C.T., Sharp, J.M., Jr., Nield, D.A., 2008. Modes of free convection in fractured low-permeability media. *Water Resour Res* 44.
- Simms, M.A., Garven, G., 2004. Thermal convection in faulted extensional sedimentary basins: Theoretical results from finite-element modeling. *Geofluids* 4, 109-130.
- Sofer, Z., Gat, J.R., 1972. Activities and concentrations of oxygen-18 in concentrated aqueous salt solutions: analytical and geophysical implications. *Earth Planet Sci Lett* 15m232–238.
- Sorey, M.L., 1976. Numerical modeling of liquid geothermal systems. *USGS Open File Report* 75-613.
- Spencer, D.W., 1987. Ocean chemistry—its central role in the evolution of the Earth. *Chem Int* 9/5, 196–205.
- Stackebrandt, W., Manhenke, V., 2002. Atlas zur Geologie von Brandenburg in Maßstab 1 : 1 000 000. Landesamt für Geowissenschaften und Rohstoffe Brandenburg (LGRB), Kleinmachnow, Karte 12.
- Starinsky, A., 1974. Relationship between Ca–chloride brines and sedimentary rocks in Isreal. Ph.D. thesis, Hebrew University, Jerusalem.
- Straus, J.M., Schubert, G., 1977. Thermal convection of water in a porous medium: effects of temperature and pressure dependent thermodynamic and transport properties. *Journal of Geophysical Research* 82, 325-333.
- Straus, J.M., 1979. Large amplitude convection in porous media. *Journal of Fluid Mechanic* 64, 51-63.
- Tarakci, N., 1999. Camli baraji ve cevresinin hidrojeolojisi. In: Izmir, Doküz Eylül Üniversitesi, Master thesis.

REFERENCES

- Tarcan, G., Gemici, U., 2005. Effects of the Contaminants from Turgutlu-Urganlı Thermomineral Waters on Cold Ground and Surface Waters. *Bull. Environ. Contam. Toxicol.*, 74, 485–492.
- Tarcan, G., Gemici, Ü., 2003. Water geochemistry of the Seferihisar geothermal area, Imagezmir, Turkey. *Journal of Volcanology and Geothermal Research*, 126, 225-242.
- Tarcan, G., Gemici, U., Aksoy, N., 2005. Hydrogeological and geochemical assessments of the Gediz Graben geothermal areas, western Anatolia, Turkey. *Environ Geol*, 47, 523-534.
- Tesauro, M., Kaban, M. K., Cloetingh, S.A.P.L, 2008. EuCRUST-07: A new reference model for the European crust. *Geophys. Res. Lett.*, 35.
- Tesmer, M., Otto, R., Pekdeger, A., Möller, P., Bayer, U., Magri, F., Fuhrmann, J., Enchery, G., Jahnke, C., Voigt, H.J, 2005. Migration paths and hydrochemical processes of groundwater salinization in different aquifer systems of the North German Basin. *Terra Nostra* 05/0, 123–126.
- Tesmer, M., Möller, P., Wieland, S., Jahnke, C., Voigt, H., Pekdeger, A., 2007. Deep reaching fluid flow in the North-East German Basin. Origin and processes of groundwater salinization. *Journal of Hydrology*, 15, 1431-2174.
- Tezcan, K., 1966. İzmir Agamemnon Jeofizik Etüdlerinin Jeotermik Enerji Bakımından Değerlendirilmesi. In: MTA Ege Bölge Kütüphanesi Report 98/3072 İzmir.
- Thomas, L., 1994. Hydrogeochemische Untersuchungen an Ölfeldwässern aus dem NM-Deutschland und dem Oberrheingraben und ihre Modellierung unter dem Aspekt eines Expertensystems für Fluid-Rock-Interactions (XPS Frocki).- *Berliner Geowissenschaftlichen Abhandlungen*. A-165, 167 S. ; Reimer, Berlin.
- Thornton, M.M., Wilson, A.M., 2007. Topography-driven flow versus buoyancy-driven flow in the U.S. midcontinent: implications for the residence time of brines. *Geofluids* 7, 69–78.
- Toran, L., Harris, R.F., 1989. Interpretation of sulfur and isotopes in biological and abiological sulphide oxidation. *Geochim Coschim Acta* 53, 2341–2348.
- Tóth, J. 1980. Cross-formational gravity-flow of groundwater: A mechanism of the transport and accumulation of petroleum (the generalized hydraulic theory of petroleum migration). In: *Problems of Petroleum Migration*, ed. W. H. Roberts III and R. J. Cordell. American Association of Petroleum Geologists, Studies in Geology No 10, pp. 121-167.
- Trettin, R., Haase, G., Haberdank, M., 1990. ⁸⁷Sr/⁸⁶Sr-Untersuchungen an Grundwässern des Berliner Urstromtales.-*Isotopenpraxis*, 26, 12:595-598.
- Trettin, R., Hiller, A., Wolf, M., Deibel, K., Gläßer, W., 1997. Isotopenanalytische Charakterisierung tiefliegender Grundwässer im Raum der Fürstenwalde-Gubener Störungszone.- *Grundwasser*, 2, 2:65-76, Berlin; Heidelberg.
- Tsang, C.F., 1991. Coupled hydromechanical-thermochemical processes in rock fractures. *Reviews of Geophysics* 29: 537-551.
- Uluğ, A., Duman, M., Ersoy, S., Özel, E., Avcı, M., 2005. Late Quaternary sea-level change, sedimentation and neotectonics of the Gulf of Gökova: Southeastern Aegean Sea. *Marine Geology* 221: 381-395.
- Uzel, B., Sözbilir, H., 2008. A First record of strike-slip basin in western Anatolia and its tectonic implication: The Cumaovası basin as an example. *Turkish Journal of Earth Sciences*.

REFERENCES

- Van Stempvoort, D.R., Krouse, H.R., 1994. Controls of d18O in sulphate—review of experimental data and applications to specific environments. In: Alpers CN, Blowes DW (eds) Environmental geochemistry of sulphide oxidation. Am Chem Soc Symp Ser 550, 447–480.
- Veizer, J., Ala, D., Azmy, K., Bruckschen, P., Buh, I D., Bruhn, F., Carden, G.A.F., Diener, A., Ebneith, S., Goddris, Y., Jasper, T., Korte, C., Pawellek, F., Podlaha, O.G., Strauss, H., 1999. 87Sr/86Sr, (d13C and d18O evolution of Phanerozoic seawater. Chem Geol 161, 59–88.
- Vengosh, A., Helvacl, C., Karamanderesi, I. H., 2002. Geochemical constraints for the origin of thermal waters from western Turkey. Applied Geochemistry, 17, 163-183.
- Vinck, F., 1955. Ursachen, Umfang, Bedeutung und Bekämpfung der Grundwasserversalzung in Schleswig-Holstein. Bes. Mitt. z. Dt. Gewässerkundl. Jb., 12: 45-53.
- Voigt, H., 1972. Genese und Hydrochemie mineralisierter Grundwässer. WTI Sonderheft 6, Berlin.
- Voigt, H., 1975. Zur Dynamik mineralisierter Schichtenwässer. Z. angew. Geol., 21, 4, Berlin.
- Voigt, H., 1976. Zur Geochemie der Spurenelemente Brom, Jod, Bor, Strontium und Lithium in den Mineralwässern des Nordteiles der DDR. Z. angew. Geol., 23, 8, Berlin.
- Voigt, H., 1977. Zur Geochemie der Spurenelemente Brom, Jod, Bor, Strontium und Lithium in den Mineralwässern des Nordteiles der DDR. Z. angew. Geol., 23, 8, Berlin.
- Wangen, M., 2013 Finite element modeling of hydraulic fracturing in 3D. Comput Geosci: 1-13 DOI 10.1007/s10596-013-9346-2
- Walshe, J.L., Halley, S.W., Anderson, J.A., Harrold, B.P., 1996. The interplay of groundwater and magmatic fluids in the formation of the cassiterite-sulfide deposits of western Tasmania. Ore Geology Reviews 10, 367-387, DOI 10.1016/0169-1368(95)00031-3.
- Wagner, W., Pruss, A., 2002. The IAPWS Formulation 1995 for the Thermodynamic Properties of Ordinary Water Substance for General and Scientific Use. J. Phys. Chem. Ref. Data, 31, 387-535.
- WASY-GmbH (Editor), 2002. FEFLOW finite-element subsurface flow and transport simulation system. User's Manual/Reference manual/White Papers, Release 5.2. WASY, Berlin.
- Wood, J.R., Hewett, T.A. 1982. Fluid convection and mass transport in porous limestones: A theoretical model. Geochim. Cosmochim. Acta 46, 1707-1713.
- Van der Lee, J., De Windt, L., 2001. Present state and future directions of modelling of geochemistry in hydrogeological systems. Journal of Contaminant Hydrology 47:265-282.
- Weber, H., 1977. Salzstrukturen, Erdöl und Kreidebasis in Schleswig-Holstein (Übersichtskarten zur Geologie von Schleswig-Holstein). Geol. Landesamt Schleswig-Holstein, Kiel.
- Weatherill, D., Graf, T., Simmons, C.T., Cook, P.G., Therrien, R., Reynolds, D. A., 2008. Discretizing the Fracture-Matrix Interface to Simulate Solute Transport. Ground Water, 46, 606-615.
- Wiederhold, H., Agster, G., Gabriel, G., Kirsch, R., Schenck, P. F., Scheer, W., Voss, W., 2002. Geophysikalische Erkundung eiszeitlicher Rinnen im südlichen Schleswig-Holstein. Z. Angew. Geol., 1, 13-26.
- Wiegand, B., Dietzel, M., Bieler, U., Groth, P., Nansen, B.T., 2001. 87Sr/86Sr-Verhältnisse als Tracer für geochemische Prozesse in einem Lockergesteinsaquifer (Liebenau, NW Deutschland). Acta Hydrochim Hydrobiol 29, 139–152.

REFERENCES

- Wigley, T.M.L., Plummer, L.N., Pearson, F.J., 1978. Mass transfer and carbon isotope evolution in natural water systems. *Geochim Cosmochim Acta* 42, 117–1139.
- Wisian, K.W., Blackwell, D.D., 2004. Numerical modeling of Basin and Range geothermal systems. *Geothermics*, 33, 713-741.
- Williams, M.D., Ranganathan, V., 1994. Ephemeral thermal and solute plumes formed by upwelling groundwaters near salt domes. *J. Geophys. Res.*, 99, 15, 667-615, 681.
- Wilson, A.M., 2003. The occurrence and chemical implications of geothermal convection of seawater in continental shelves. *Geophys Res Lett* 30, 2127.
- Wilson, A.M., 2005. Fresh and saline groundwater discharge to the ocean: A regional perspective. *Water Resour Res* 41: W02016.
- Wilson, A.M., Ruppel, C., 2007. Salt tectonics and shallow subseafloor fluid convection: models of coupled fluid-heat-salt transport. *Geofluids*, 7, 377-386.
- Wood, J.R., Hewett, T.A., 1982. Fluid convection and mass transfer in porous sandstones - a theoretical model. *Geochimica et Cosmochimica Acta* 46, 1707-1713.
- Yanagisawa, F., Sakai, H., 1983. Thermal decomposition of barium sulphate–vanadium pentoxide–silica glass mixtures for preparation of sulfur dioxide in sulfur isotope ratio measurements. *Anal Chem* 55, 985–987.
- Yang, J., Large, R. R., Bull, S. W., 2004. Factors controlling free thermal convection in faults in sedimentary basins: Implications for the formation of zinc-lead mineral deposits. *Geofluids*, 4, 237-247.
- Yang, J., Feng, Z., Luo, X., Chen, Y., 2009. On the role of buoyancy force in the ore genesis of SEDEX deposits: Example from Northern Australia. *Science in China Series D-Earth Sciences*, 52, 452-460.
- Yilmazer, S., 1984. İzmir Balçova jeotermal sahasında ısı üretimine yönelik değerlendirme raporu. In:(ed. MTA Der.Rap. No. 7504 y) Ankara, 18.
- Yilmazer, S., 1989. Geochemical Features of Balçova hot springs and Geothermal energy possibilities for the area. In:Isparta, Akdeniz University, Graduate School, Isparta, Turkey, PhD.
- Yu, Z., Lerche, I., Lowrie, A., 1992. Thermal impact of salt: Simulation of thermal anomalies in the gulf of Mexico. *Pure and Applied Geophysics* 138:181-192.
- Zhao, C., Hobbs, B.E., Mühlhaus, H.B., Ord, A., Lin, G., 2003. Convective instability of 3-D fluid-saturated geological fault zones heated from below. *Geophysical Journal International*, 155, 213-220.
- Zhou, Y., Wenpeng, L. 2011. A review of regional groundwater flow modeling. *Coordination Chemistry Reviews*, 2011, 2(2), 205-214, DOI: 10.1016/j.gsf.2011.03.003.
- Ziagos, J.P., Blackwell, D.D., 1986. A model for the transient temperature effects of horizontal fluid flow in geothermal systems. *Journal of Volcanology and Geothermal Research*, 27, 371-397.
- Zieschang, J., 1974. Ergebnisse und Tendenzen hydrogeologischer Forschungen in der DDR (Results and tendencies of hydrogeological research in the GDR). *Zt Angew Geol* 20, 452–458.


APPENDIX

WASY Software
FEFLOW[®]

Finite Element Subsurface Flow
& Transport Simulation System

White Papers

Vol. III

WASY
Institute for
Water Resources Planning
and Systems Research Ltd. 

Derivation of the coefficients of compressibility, thermal expansion and fluid density difference ratio for reproducing aqueous NaCl density

F. Magri

Free University of Berlin, Department of Hydrogeology, Berlin, Germany

2004

EQUATIONS AND VARIABLE DEFINITIONS

Fluid density ρ^f varies as a function of pressure (p), temperature (T) and concentration (C) of dissolved components.

In FEFLOW ρ^f is approximated by a linear form according to the following Equation of State (EOS -see Reference Manual Eq 1-77):

$$\rho^f = \rho_0^f \left(1 + \bar{\gamma}(p - p_0) - \bar{\beta}(T - T_0) + \frac{\bar{\alpha}}{C_s - C_0}(C - C_0) \right) \quad (1)$$

where

$$\bar{\gamma} \equiv \frac{1}{\rho_0^f} \frac{\partial \rho^f}{\partial p} \Bigg|_{T,C} \quad (2)$$

is the coefficient of compressibility of the fluid at constant temperature and concentration;

$$\bar{\beta} \equiv \frac{1}{\rho_0^f} \frac{\partial \rho^f}{\partial T} \Bigg|_{p,C} \quad (3)$$

is the coefficient of thermal expansion at constant pressure and concentration, and

$$\bar{\alpha} \equiv \frac{1}{\rho_0^f} \frac{\partial \rho^f}{\partial C} \Bigg|_{T,p} \quad (4)$$

introduces the effect of a density change due to the concentration of a dissolved component at constant temperature and pressure.

$\bar{\alpha}$, defined in Eq 4, is normalized by the saturation concentration of the solute, C_s (Eq. 1).

ρ^f is equal to a reference density ρ_0^f when $T = T_0$, $p = p_0$ and $C = C_0$ that is when T, p and C are respectively equal to the reference temperature T_0 , pressure p_0 and concentration C_0 .

For instance, at $p_0=100$ kPa, $T_0=0$ °C and $C_0=0$ mg/l, Eq 1 becomes:

$$\rho^f(p, T, C) = \rho_0^f \left(1 + \bar{\gamma}(p - 100) - \bar{\beta} \times T + \frac{\bar{\alpha}}{C_s} \times C \right) \quad (5)$$

with $\rho_0^f = 998.8396$ [kg/m³]

When modeling geothermal systems, wide ranges of pressure, temperature and concentration require that the coefficients $\bar{\alpha}$, $\bar{\beta}$, $\bar{\gamma}$ varies as function of p , T and C in order to correctly reproduce variable fluid density.

DATA AND POLYNOMIAL EQUATIONS

Here the coefficients $\bar{\alpha}$, $\bar{\beta}$, $\bar{\gamma}$ are derived for reproducing the fluid density of aqueous sodium chloride solution (brine) in the single liquid phase within the following ranges:

$$0.1 \leq p \leq 100 \text{ MPa}; 0 \leq T \leq 300 \text{ }^\circ\text{C}; 0 \leq C \leq 350 \text{ g l}^{-1}$$

These coefficients are of big use for the modeling of geothermal systems in which groundwater solutions are assumed to be brines. Furthermore, they can easily be implemented in FEFLOW® via the IFM (see section 3).

Data

Brine density values for different pressure, temperature and concentration have been derived by using the theoretical approach of Pitzer (1984) and Archer (1992). The resolution of the data has been set to 10 °C, 100 kPa and 7 g/l. When a (p,T,C) combination did not belong to the single fluid phase, the density values were systematically excluded from the database table. In total 159'423 densities values of the aqueous NaCl solution were generated in a p-T-C grid and used for the polynomial regression fit.

Polynomial fit

The following expression provides an approximation with an accuracy of 0.5% for ρ^f **in single liquid phase in the above mentioned range**. This accuracy is good enough for simulating hydrothermal processes (Driesner 2007).

$$\rho^f(p, T, C) = 999.843633188666 - 100^2 q_2 - 100 q_1 + (q_2 \times p^2 + q_1 \times p) + z(p, C) \times T^6 + w(p, C) \times T^5 + v(p, C) \times T^4 + u(p, C) \times T^3 + s(p, C) \times T^2 + r(p, C) \times T + (j_0 + j_1 \times p + j_2 \times p^2) \times C^2 + (h_0 + h_1 \times p + h_2 \times p^2) \times C \tag{6}$$

where

$$z(p, C) = (z_0 + z_1 \times p + z_2 \times p^2 + z_3 \times C + z_4 \times C^2)$$

$$w(p, C) = (w_0 + w_1 \times p + w_2 \times p^2 + w_3 \times C + w_4 \times C^2) \tag{7}$$

...

$$r(p, C) = (r_0 + r_1 \times p + r_2 \times p^2 + r_3 \times C + r_4 \times C^2)$$

with pressure p in kPa, temperature T in °C, and C in mg/l.

The calculated coefficients are:

Table 1. Coefficients of the polynomial fits as expressed in Eq 6 to Eq 11

h_0	0.00073104758291628	w_0	5.718374379180737E-10	u_1	-2.4220044746230556E-10
h_1	-9.422037142360847E-10	w_1	-4.996112674640022E-15	u_0	0.00003936397979529357
h_2	1.821338928754865E-15	w_2	-2.5570358684616452E-20	s_4	-7.725866104001761E-14
j_0	-3.9446778202994974E-10	w_3	-6.483691625807997E-15	s_3	3.9534845368831494E-8
j_1	7.533778133432179E-16	w_4	-5.310521468059033E-18	s_2	1.0032350032434767E-13
j_2	-2.3273323084072923E-22	v_0	-2.051960478431085E-7	s_1	2.5442857110623736E-8
q_1	0.0005257539357631474	v_1	1.58244686429457E-12	s_0	-0.0063083048607919245
q_2	-5.459359007740163E-10	v_2	8.637135897998724E-18	r_4	3.6418368120766765E-12
z_0	-6.625358276579406E-13	v_3	2.1946081669958214E-12	r_3	-2.390003668646296E-6
z_1	6.3111586728429706E-18	v_4	-5.310521468059033E-18	r_2	-3.6928765749684625E-12
z_2	2.744492639329977E-23	u_4	8.576370648910509E-16	r_1	-1.155475728462599E-6
z_3	7.513091563357645E-18	u_3	-3.7575488991610133E-10	r_0	-0.04949178536220616
z_4	-1.8936376378424672E-23	u_2	-1.4036263958416905E-15		

The coefficients in Table 1 have been derived accounting for freshwater reference condition (i.e. $C=C_0=0$ mg/l), at $p_0=100$ kPa and $T_0=0$ °C. For these reference values Eq 6 gives:

$$\rho^f(100,0,0) = \rho_0^f = 998.8396 \left[\text{kg/m}^3 \right].$$

The goal is to find the variable fluid density ratio $\bar{\alpha}$, the fluid compressibility $\bar{\gamma}$, and the coefficient of thermal expansion $\bar{\beta}$ of the fluid density function ρ^f (Eq. 5).

To do that, we consider a Taylor series expansion for the fluid density $\rho^f(p, T, C)$ expressed in Eq. 6 around $T_0=0$ and $p_0=100$ and $C_0=0$ where a 6th order approximation is used for the temperature T and a 2nd order approximation is used for both pressure and concentration dependences, viz.,

$$\begin{aligned} & 999.843633188666 + \\ & (p - 100) \left(q_1 + 200q_2 + T(r_1 + 200r_2) + T^2(s_1 + 200s_2) + T^3(u_1 + 200u_2) + T^4(v_1 + 200v_2) + \right. \\ & \left. T^5(w_1 + 200w_2) + T^6(z_1 + 200z_2) \right) + \\ & (p - 100)^2 (q_2 + T r_2 + T^2 s_2 + T^3 u_2 + T^4 v_2 + T^5 w_2 + T^6 z_2) + \\ & T \times (r_0 + 100 r_1 + 100^2 r_2) + T^2 \times (s_0 + 100 s_1 + 100^2 s_2) + T^3 \times (u_0 + 100 u_1 + 100^2 u_2) + T^4 \times (v_0 + 100 v_1 + 100^2 v_2) + \\ & T^5 \times (w_0 + 100 w_1 + 100^2 w_2) + T^6 \times (z_0 + 100 z_1 + 100^2 z_2) + \\ & C \times (h_0 + h_2(p - 100)^2 + 100h_1 + 100^2 h_2 + (p - 100)(h_1 + 200h_2) + r_3 T + s_3 T^2 + T^3 u_3 + T^4 v_3 + T^5 w_3 + T^6 z_3) + \\ & C^2 \times (j_0 + j_2(p - p_0)^2 + 100j_1 + 100^2 j_2 + (p - 100)(j_1 + 200j_2) + r_4 T + s_4 T^2 + T^3 u_4 + T^4 v_4 + T^5 w_4 + T^6 z_4) \end{aligned} \quad (8)$$

Comparing the above equation with the EOS for the fluid density (Eq 5) and reminding that $\rho_0^f = 998.8396 \left[\text{kg/m}^3 \right]$, we obtain the expression for $\bar{\alpha}(p, T, C)$, $\bar{\beta}(p, T, C)$, $\bar{\gamma}(p, T, C)$ used in Equation 1.

$$\bar{\gamma} = \frac{1}{999.843633188666} \left(q_1 + 200q_2 + T(r_1 + 200r_2) + T^2(s_1 + 200s_2) + T^3(u_1 + 200u_2) + T^4(v_1 + 200v_2) + T^5(w_1 + 200w_2) + T^6(z_1 + 200z_2) + (p - 100)(q_2 + T r_2 + T^2 s_2 + T^3 u_2 + T^4 v_2 + T^5 w_2 + T^6 z_2) \right) \quad (9)$$

$$\bar{\beta} = - \frac{1}{999.843633188666} \left((r_0 + 100 r_1 + 100^2 r_2) + T \times (s_0 + 100 s_1 + 100^2 s_2) + T^2 \times (u_0 + 100 u_1 + 100^2 u_2) + T^3 \times (v_0 + 100 v_1 + 100^2 v_2) + T^4 \times (w_0 + 100 w_1 + 100^2 w_2) + T^5 \times (z_0 + 100 z_1 + 100^2 z_2) \right) \quad (10)$$

$$\bar{\alpha} = \frac{C_i}{999.843633188666} \left(\left(h_0 + h_2(p - 100)^2 + 100h_1 + 100^2 h_2 + (p - 100)(h_1 + 200h_2) + r_3 T + s_3 T^2 + T^3 u_3 + T^4 v_3 \right) + \left(T^5 w_3 + T^6 z_3 \right) + C \times \left(j_0 + j_2(p - p_0)^2 + 100j_1 + 100^2 j_2 + (p - 100)(j_1 + 200j_2) + r_4 T + s_4 T^2 + T^3 u_4 + T^4 v_4 + T^5 w_4 + T^6 z_4 \right) \right) \quad (11)$$

where all coefficients are given in Table 1.

In the next part, the IFM source code allowing implementing these coefficients into FEFLOW is given.

IFM IMPELEMENTATION

Our goal is to incorporate in FEFLOW the following EOS

$$\rho^f(p, T, C) = \rho_0^f \left(1 + \bar{\gamma}(p - p_0) - \bar{\beta} \times T + \frac{\bar{\alpha}}{C_s} \times C \right) \quad (12)$$

with $\bar{\gamma}$, $\bar{\beta}$, $\bar{\alpha}$ expressed in Eq 9, 10, 11 and $\rho_0^f = \rho^f(100, 0, 0) = 998.8396 \text{ [kg/m}^3\text{]}$ i.e., the reference pressure, temperature and concentration are $p_0=100 \text{ kpa}$; $T_0=0 \text{ }^\circ\text{C}$, $C_0=0 \text{ mg/L}$

We remind that in FEFLOW the following EOS for the fluid density is already incorporated:

$$\rho^f(p, T, C) = \rho_0^f \left(1 - \bar{\beta}(T - T_0) + \frac{\bar{\alpha}}{C_s - C_0}(C - C_0) \right) \quad (13)$$

where $\bar{\beta}$ and $\bar{\alpha}$ are defined by the user.

How to implement the equations?

The implementation of $\bar{\beta}$ and $\bar{\alpha}$ can be done directly by the use of the IFM through the API "IfmSetMatFlowExpansionCoeff" and IfmSetMatFlowDensityRatio. On the other hand, no related API interface exists for the coefficient of compressibility $\bar{\gamma}$.

To make up for this lack, we have to use a little trick:

Let's consider the EOS for the fluid density that we want to incorporate into FEFLOW (Eq. 1) and apply a simple factorisation in the following way:

$$\begin{aligned} \rho^f(p, T, C) &= \rho_0^f \left(1 + \bar{\gamma}(p - p_0) - \bar{\beta} \times T + \frac{\bar{\alpha}}{C_s} \times C \right) \\ &= \rho_0^f \left(1 - \left(\bar{\beta} - \bar{\gamma} \frac{(p - p_0)}{T} \right) T + \frac{\bar{\alpha}}{C_s} \times C \right) \\ &= \rho_0^f \left(1 - \bar{\beta}^* \times T + \frac{\bar{\alpha}}{C_s} \times C \right) \end{aligned} \quad (14)$$

$$\text{with } \bar{\beta}^* = \begin{pmatrix} \bar{\beta} & + & \underbrace{-\bar{\gamma} \times \frac{(p - p_0)}{T}} \\ \text{Defined as BETASTAR} & & \text{Defined as GAMMASTAR} \\ \text{in the source code} & & \text{in the source code} \end{pmatrix} \quad T \neq T_0 \quad (15)$$

and $\bar{\gamma}$, $\bar{\beta}$ expressed in Eq 9 and Eq 10 respectively.

In this way, the effects due to the compressibility on the brine density are implicitly expressed in the new variable $\bar{\beta}$. $\bar{\beta}$ can then be implemented into FEFLOW by use of the API "IfmSetMatFlowExpansionCoeff".

Description of the source code brine_dens.C

The input data required are the pressure (p), temperature (T), and the concentration (C) for each element of the FE mesh. These values can be retrieved by the use of the API functions "IfmGetResultsFlowPressureValue" "IfmGetResultsTransportHeatValue" "IfmGetResultsTransportMassValue"

which respectively load the nodal values of the pressure (kPa), temperature (°C) and concentration (mg/l) calculated during the simulations. Once the mean values of these parameters are calculated, they can be used as input for calculating, $\bar{\beta}$ and $\bar{\alpha}$ by use of the polynomial fit (Eq. 9, Eq. 10, Eq. 11)

The returned values are then stored into the API function "IfmSetMatFlowExpansionCoeff" and "IfmSetMatFlowExpansionCoeff". Below is attached the complete source code brine_dens.C. The code is programmed in C++ language through the IFM tool in the "Simulation" interface under the callback function "PostTimeStep".

IMPORTANT NOTICE:

For correctly fitting the brine density, the user must set the following reference values for temperature and concentration in the "heat and mass transport properties" of FEFLOW:

$T_0=0$; $C_0=0$; $C_s = 350000$ mg/l (considered as brine concentration at saturation state)

```
static void PostTimeStep (IfmDocument pDoc)
{
    int e, i;
    double T, p, C;
    double beta, gamma, alpha, BETASTAR, gammastar, ALPHASTAR;
    double alph, alph1, gam, gam1;

    /* Coefficients for the fitting and its derivatives */

    double p0 = 100.;
    double z2=2.744492639329977e-23;
    double z1=6.3111586728429706e-18;
    double z0=-6.625358276579406e-13;
    double w2=-2.5570358684616452e-20;
    double w1=-4.996112674640022e-15;
    double w0=5.718374379180737e-10;
    double v2=8.637135897998724e-18;
    double v1=1.58244686429457e-12;
    double v0=-2.051960478431085e-7;
    double u2=-1.4036263958416905e-15;
    double u1=-2.4220044746230556e-10;
```

```

double u0=0.00003936397979529357;
double s2=1.0032350032434767e-13;
double s1=2.5442857110623736e-8;
double s0=-0.0063083048607919245;
double r2=-3.6928765749684625e-12;
double r1=-1.155475728462599e-6;
double r0=-0.04949178536220616;
double q2=-5.459359007740163e-10;
double q1=0.0005257539357631474;
double h0=0.00073104758291628;
double h1=-9.422037142360847e-10;
double h2=1.821338928754865e-15;
double r3=-2.390003668646296e-6;
double s3=3.9534845368831494e-8;
double u3=-3.7575488991610133e-10;
double v3=2.1946081669958214e-12;
double w3=-6.483691625807997e-15;
double z3=7.513091563357645e-18;
double j0=-3.9446778202994974e-10;
double j1=7.533778133432179e-16;
double j2=-2.3273323084072923e-22;
double r4=3.6418368120766765e-12;
double s4=-7.725866104001761e-14;
double u4=8.576370648910509e-16;
double v4=-5.310521468059033e-18;
double w4=1.6153538522556503e-20;
double z4=-1.8936376378424672e-23;
double bet=r0+100*r1+10000*r2;
double bet1=s0+100*s1+10000*s2;
double bet2=u0+100*u1+10000*u2;
double bet3=v0+100*v1+10000*v2;
double bet4=w0+100*w1+10000*w2;
double bet5=z0+100*z1+10000*z2;

/* Number of elements and number of nodes */
int nElements = IfmGetNumberOfElements(pDoc);
int nNodes = IfmGetNumberOfNodesPerElement(pDoc);

/* Loop through all elements */
for (e = 0; e < nElements; e++)
{
    T = 0.;
    p = 0.;
    C = 0.;
    /* loop locally through all nodes of this element */
    for (i = 0; i < nNodes; i++)
    {
        /* Get global node index */
        int indNode = IfmGetNode(pDoc, e, i);

        T +=IfmGetResultsTransportHeatValue(pDoc,indNode);
        p +=IfmGetResultsFlowPressureValue(pDoc,indNode);
        C +=IfmGetResultsTransportMassValue(pDoc,indNode);
    }
}

```

```

        /* Solving the average physical properties (T and p) of this element
*/
    T /=(double) nNodes;
    p /=(double) nNodes;
    C /=(double) nNodes;

    if (p < 100) p=100.;

    alph=h0+h2*(p-p0)*(p-p0)+100*h1+10000*h2+(p-
100)*(h1+200*h2)+(r3+(s3+(u3+(v3+(w3+z3*T)*T)*T)*T)*T)*T;
    alph1=j0+j2*(p-p0)*(p-p0)+100*j1+10000*j2+(p-
100)*(j1+200*j2)+(r4+(s4+(u4+(v4+(w4+z4*T)*T)*T)*T)*T)*T;
    gam=gam=q1+200*q2+((r1+200*r2)+((s1+200*s2)+((u1+200*u2)+((v1+200*v2)+((w1+200*w
2)+(z1+200*z2)*T)*T)*T)*T)*T)*T;
    gam1=q2+(r2+(s2+(u2+(v2+(w2+z2*T)*T)*T)*T)*T)*T)*T;
    /* Set ALPHA */
    alpha=(1/999.843633188666)*(alph+alph1*C);
    /* Set BETA */
    beta=
(1/999.843633188666)*(bet+(bet1+(bet2+(bet3+(bet4+bet5*T)*T)*T)*T)*T);
    /* Set GAMMA */
    gamma=(1/999.843633188666)*(gam+gam1*(p-p0));
    /* Set Gammastar */
    gammastar=-gamma*(p-p0)/(T+.01);
    /* Set BETASTAR */
    BETASTAR=beta+gammastar;
    fmSetMatFlowExpansionCoeff(pDoc, e, BETASTAR);
    /* Set ALPHASTAR by multiplying ALPHA time Cs=350000 mg/L*/
    ALPHASTAR=alpha*350000;
    IfmSetMatFlowDensityRatio(pDoc, e, ALPHASTAR);
    }
}

```

ACKNOWLEDGEMENTS

Dr. Driesner from ETH, Zurich is greatly acknowledged for sharing his expertise in thermodynamic properties of fluids. I thank Prof. Diersch, Dr. Clausnitzer and Dr. Schaetzel from WASY for the support in developing the IFM code.

References

- Archer, D.G., 1992. Thermodynamic Properties of the NaCl+H₂O System. II. Thermodynamic Properties of NaCl(aq), NaCl 2HO(cr), and Phase Equilibria. *Journal of Physical and Chemical Reference Data* 21, 793-829.
- Driesner, T., 2007. The system H₂O-NaCl. Part II: Correlations for molar volume, enthalpy, and isobaric heat capacity from 0 to 1000 [degree sign]C, 1 to 5000 bar, and 0 to 1 XNaCl. *Geochimica et Cosmochimica Acta* 71, 4902-4919.
- Pitzer, K.S., Peiper, J.C., Busey, R.H., 1984. Thermodynamic Properties of Aqueous Sodium Chloride Solutions. *Journal of Physical and Chemical Reference Data* 13, 1-102.

Governing equations

The governing equations of thermohaline convection in a saturated porous media are derived from the conservation principles for linear momentum, mass and energy (e.g. Bear 1991; Kolditz et al. 1998; Nield and Bejan 1999). The resulting system is fully implemented in FEFLOW® (Reference manual, p.51) and is briefly reported here by the following set of differential equations:

$$S_0 \frac{\partial \varphi}{\partial t} + \text{div}(\mathbf{q}) = Q_{\text{Boussinesq}} \quad (1)$$

$$\mathbf{q} = -\mathbf{K} \left[\mathbf{grad}(\varphi) + \frac{\rho_f - \rho_{0f}}{\rho_{0f}} \right] \quad (2)$$

$$\frac{\partial \phi C}{\partial t} + \text{div}(\mathbf{q}C) - \text{div}(\mathbf{D} \mathbf{grad}(C)) = Q_c \quad (3)$$

$$\frac{\partial}{\partial t} \left((\phi \rho_f c_f + (1 - \phi) \rho_s c_s) T \right) + \text{div}(\rho_f c_f T \mathbf{q}) - \text{div}(\lambda \mathbf{grad}(T)) = Q^T \quad (4)$$

Eq.(1) is the equation of fluid mass conservation. S_0 is the medium storativity, φ is the hydraulic head. \mathbf{q} is the Darcy (or volumetric flux density) velocity defining the specific discharge of the fluid. $Q_{\text{Boussinesq}}$ is the Boussinesq term which incorporates first order derivatives of mass-dependent and temperature dependent compression effects. The Darcy's law is expressed by Eq. 2 where \mathbf{K} is the hydraulic conductivity tensor. Eq. 3 is the equation of solute mass conservation where ϕ is the porosity of the porous medium, C is the mass concentration, \mathbf{D} is the tensor of hydrodynamic dispersion and Q^c is a mass supply. $\frac{\rho_f - \rho_{0f}}{\rho_{0f}}$ is the buoyancy force induced by density variation where ρ_f and ρ_{0f} denote the fluid density and its reference value, respectively. Eq. 4 is the energy balance equation of the fluid and the porous media. c_f and c_s is the heat capacity of the fluid and solid respectively, T is the temperature, λ is the thermal conductivity of the saturated porous medium as a whole.

Constitutive and phenomenological relations of the different physical parameters involved in the equations are needed to close this coupled system. Here the hydraulic conductivity relation and the Equation Of State (EOS) for the fluid density are recalled:

$$\rho^f = \rho_0^f \left(1 - \bar{\beta}(T, p)(T - T_0) + \bar{\gamma}(T, p)(p - p_0) + \frac{\bar{\alpha}}{C_s - C_0}(C - C_0) \right) \quad (5)$$

$$\mathbf{K} = \frac{\mathbf{k} \rho_{0f} g}{\mu_f(C, T)} \quad (6)$$

Eq. 6 is expressed in terms of reference values for density, temperature, pressure and concentration (T_0 , p_0 and C_0). $\bar{\alpha}(T, p)$ denotes the mass concentration ratio, $\bar{\beta}(T, p)$ the coefficient of thermal expansion and $\bar{\gamma}(T, p)$ the coefficient of compressibility.

The flow and transport equations (Equations 2, 3 and 4) for thermohaline convection are non-linear and strongly coupled since temperature and salinity control the fluid density ρ^f and dynamic viscosity μ_f .

Eq. 6 has been approximated by mean of a polynomial expression in order to fit liquid brine density values within the following ranges: $0.1 \leq p \leq 100$ MPa; $0 \leq T \leq 300$ °C; $0 \leq C \leq 350$ g l^{-1} as explained in the next white paper published in the FEFLOW manuals